Investigating and Targeting Folate Metabolism in Chronic Myeloid Leukaemia

Martha-Maria Zarou BSc

Thesis submitted to the University of Glasgow in accordance with the requirements for the degree of Doctor of Philosophy

Institute of Cancer Sciences
College of Medical, Veterinary and Life Sciences
University of Glasgow
January,2022

Abstract

Chronic myeloid leukaemia (CML) is myeloproliferative disease that arises due to the formation of the fusion oncogene, BCR-ABL, in a haematopoietic stem cell (HSC). BCR-ABL oncogene has a constitutive tyrosine kinase activity and drives myeloid expansion and accumulation of mature blood cells. Due to the introduction of imatinib, a specific tyrosine kinase inhibitor (TKI), treatment of the disease has drastically improved the last 20 years. Nevertheless, imatinib and second/third generation TKIs do not eradicate leukaemic stem cells (LSCs), This population of cells persists and is therapy resistant. Thus, current research is focused on the identification of novel targets to target CML LSCs and ultimately, cure the disease.

Recent work from our lab has demonstrated that CML LSCs have high mitochondrial mass and activity and that they rely on oxidative phosphorylation (OXPHOS) when compared to patient matched progenitor cells or normal HSCs. Folate-mediated one carbon (1C) metabolism plays a crucial role in nucleotide synthesis, energy homeostasis and redox defence. Furthermore, folate metabolism is a metabolic vulnerability for various haematological malignancies. As the role of folate metabolism in CML remains unknown, we aimed to investigate the importance of 1C metabolism in CML as a model of LSC-driven haematological malignancies.

By using publicly available microarray datasets we established that folate metabolism associated genes are upregulated in LSCs compared to normal counterparts. Furthermore, we discovered that expression of those genes does not change in CML stem cell enriched (CD34+) primary cells following a 7-day imatinib treatment. In addition, we revealed that the activity of the pathway is significantly upregulated in CML CD34+ cells when compared to normal CD34+ cells.

We also uncovered that genetic inhibition of the pathway following loss of the mitochondrial serine hydroxymethyl transferase 2 (SHMT2), leads to decreased cell growth and cell cycle arrest of K562 cells. Furthermore, loss of SHMT2 significantly impaired tumour xenograft formation of KCL22 cells.

Metabolically, genetic or pharmacological (SHIN1; SHMT1/2 inhibitor) inhibition of 1C metabolism resulted in decreased *de novo* purine synthesis and glycolysis. Besides this, inhibition of the folate pathway led to AMPK activation, mTORC1 suppression and autophagy induction. Inhibition of the pathway also altered mitochondrial homeostasis by decreasing mitochondrial reactive oxygen species (ROS), causing hyperpolarisation of the mitochondrial membrane and accumulation of the mitochondrial fission related protein DRP1 and mitophagy receptor NIX. Of note, formate (1C unit donor independent from SHMT1/2 activity) supplementation was sufficient to reverse changes caused by folate metabolism inhibition.

Phenotypically, inhibition of 1C metabolism induced the expression of erythropoiesis markers CD71 and Glycophorin A in K562 cells, which was reversed following formate supplementation. Similar results were obtained in CML $CD34^+$ cells when challenged with erythropoietin (EPO). Furthermore, we uncovered that promotion of maturation of CML cells was AMPK-independent, but autophagy dependent.

Of clinical relevance, pharmacological inhibition of 1C metabolism resulted in impaired cell proliferation and short-term colony formation potential of CML $CD34^+$ cells, with minimum effect on normal counterparts. Lastly, combination treatment of SHIN1 with imatinib significantly increased the sensitivity of primary CML cells to imatinib.

In conclusion, these results describe a novel role of folate metabolism in CML, indicating that the pathway can be a metabolic vulnerability for LSCs and sensitise this population to traditional therapeutic approaches.

Table of Contents

List of Figures

List of Tables

Acknowledgements

I would like to first thank my supervisor Dr Vignir Helgason for giving me the opportunity to undertake a PhD in his group. I would also like to thank him for his support, guidance, and encouragement throughout the last 4 years, and for always being available to chat and listen to my new scientific curiosities. This has been a great experience which has allowed me to develop both scientifically and professionally. I would also like to thank my second supervisor Dr Alexei Vazquez for all the conversations on folate metabolism and his valuable suggestions.

A special thanks goes to all the members of Vignir's group for all the helpful scientific discussions and great moments shared together. I would like to give a special thank you to Kevin for the great time working together and his "funny" jokes and to Angela, for being my older sister in the lab, and for all our late-night scientific discussions. I would also like to thank all the people on Level 3 at WWCRC for the great environment and the nice memories.

I would also like to thank and acknowledge all people who have made this work possible. The Beatson metabolomic team for running LC-MS and bioanalyser samples. Ms Karen Dunn for her support and expertise with the *in vivo* models. Prof Mhairi Copland and Dr Alan Hair for looking after the biobank and the NHS Biorepository Research Department for providing all the normal samples.

I would like to thank all the amazing people that I met during this journey and have been a valuable part of my life. Marti, for the support and for being the smallest "giant" rock to lean on. Francesca for being a fantastic friend and cook! Chris and Marco for all the adventures.

Lastly, I would like to thank my family and, especially, my parents. I would have not been able to achieve any of this without their love and support.

Finally, I would like to dedicate this work to my grandmother, who was my biggest supporter throughout all these years.

Author's Declaration

I hereby declare that the work presented in this thesis is my own, unless specific reference is made to the contribution of others. This work has not been submitted for any other degree.

Martha-Maria Zarou

Abbreviations

18S	18S ribosomal RNA
2DG	2-Deoxyglucose
7-ADD	7-Aminoactinomycin D
ABCC1-4	ATP Binding Cassette Subfamily C Member 1-4
ABCG2	ATP Binding Cassette Subfamily G Member 2
ABL	ABL Proto-Oncogene 1, Non-Receptor Tyrosine Kinase
ADP	Adenosine diphosphate
AF9	MLLT3 Super Elongation Complex Subunit
AICAR	5-aminoimidazole-4-carboxamide-1-ß-D-ribofuranoside
AKT	Protein kinase B
ALDH1L1	Aldehyde Dehydrogenase 1 Family Member L1
ALDH1L2	Aldehyde Dehydrogenase 1 Family Member L2
ALL	Acute lymphoblastic leukaemia
AML	Acute myeloid leukemia
AMP	Adenosine monophosphate
AMPK	AMP-activated protein kinase
ATG12	Autophagy related protein 12
ATG13	Autophagy related protein 13
ATG5	Autophagy related protein 5
ATG7	Autophagy related protein 7
ATP	Adenosine triphosphate
BCA	Bicinchoninic acid
BCR	Breakpoint cluster region
BIT	BSA insulin and transferrin
BM	Bone Marrow
BNIP3	BCL2 Interacting Protein 3
BSA	Bovine serum albumin
CaCl2	Calcium chloride
CAIR	5'-Phosphoribosyl-4-carboxy-5-aminoimidazole
CCCP	Carbonyl cyanide m-chlorophenyl hydrazone
CD11b	Integrin alpha M
CD133	Prominin-1
CD235a	Glycophorin A
CD34	Cluster of differentiation 34
CD38	cyclic ADP ribose hydrolase
CD45RA	Protein Tyrosine Phosphatase Receptor Type C
CD71	Transferrin receptor 1
CD90	Cluster of Differentiation 90
cDNA	Complementary DNA
CDP	Cytidine diphosphate
CFU	Colony forming unit
CFU-E	Colony Forming Unit-Erythroid
c-Kit	Stem cell factor receptor

CLP	common lymphoid progenitor
CML	Chronic myeloid leukaemia
CML-BP	Chronic myeloid leukaemia blastic phase
CML-CP	Chronic myeloid leukaemia chronic phase
CMP	common myeloid progenitor
CNS	Central nervous system
CO_2	Carbon dioxide
CoA	Coenzyme A
CFC	Colony forming cell
CT	Cycle threshold
CTP	Cytidine triphosphate
CTV	CellTrace Violet
dADP	Deoxyadenosine diphosphate
dAMP	Deoxyadenosine monophosphate
dATP	Deoxyadenosine triphosphate
dCDP	Deoxycytidine diphosphate
dCMP	Deoxycytidine monophosphate
dGDP	Deoxyguanosine diphosphate
dGTP	Deoxyguanosine triphosphate
DHF	Dihydrofolic acid
DHFR	Dihydrofolate Reductase
DMEM	Dulbecco's Modified Eagle Medium
DMSO	Dimethyl sulfoxide
DNA	Deoxyribonucleic acid
DPBS	Dulbecco's phosphate-buffered saline
DRP1	dynamin-related protein 1
DTG	Double transgenic
dTMP	Deoxythymidine monophosphate
dTTP	Deoxythymidine triphosphate
dUMP	Deoxyuridine monophosphate
ECAR	Extracellular acidification rate
ECL	Enhanced Chemiluminescence
EDTA	Ethylenediaminetetraacetic acid
Epo	Erythropoietin
ER	Endoplasmic reticulum
ETC	Electron transport chain
FACS	Fluorescence-activated cell sorting
FAD+	Flavin adenine dinucleotide
FADH	Reduced FAD
FAM	Fluorescein amidites
FAO	Fatty acid oxidation
FBS	Fetal bovine serum
FC	Fold change
FGAR	Phosphoribosyl-N-formylglycineamide
FIS1	Mitochondrial fission 1 protein
FLT3-ITD	FMS-like tyrosine kinase 3-internal tandem duplication

FOXO3	Forkhead box O3
FPSG	Folypolyglutamate synthase
G6PDH	Glucose-6-phosphate dehydrogenase
GAB2	GRB2 Associated Binding Protein 2
GAPDH	Glyceraldehyde 3-phosphate dehydrogenase
GART/ATIC	Phosphoribosylglycinamide formyltransferase/ AICAR transformylase IMP cyclohydrolase
GC	Gass chromatography
G-CSF	Granulocyte-colony stimulating factor
GDP	Guanosine diphosphate
GlyA	Glychophorin A
GM-CSF	Granulocyte-macrophage colony-stimulating factor
GMP	Granulocyte monocyte progenitor
GMP	Guanosine monophosphate
GRB2	Growth factor receptor-bound protein 2
GTP	Guanosine triphosphate
HBSS	Hanks' Balanced Salt Solution
HCQ	Hydroxychloroquine
HEPES	4-(2-hydroxyethyl)-1-piperazineethanesulfonic acid
HIF-1α	Hypoxia-inducible factor 1-alpha
HIF-1β	Hypoxia-inducible factor 1-beta
HPLC	High-performance liquid chromatography
HRP	Horseradish Peroxidase
HSC	Haematopoietic stem cell
HSP90	Heat shock protein 90
HT	Hypoxanthine thymidine
IgG	Immunoglobulin G
IL-2	Interleukin 2
IL-6	Interleukin 6
IMDM	Iscove's Modified Dulbecco's Medium
IMP	Inosine monophosphate
JAK	Janus kinase
JC-1	1,1',3,3'-tetraethylbenzimi-dazoylcarbocyanine iodide
KCl	Potassium chloride
LB	Lysogeny broth
LC3B	Microtubule-associated proteins 1A/1B light chain 3B
LIC	Leukaemia initiating cell
LIF	Leukaemia inhibitory factor
Lin	Lineage
LSC	Leukaemic stem cell
LSK	Lin- Sca-1+ c-kit+
LTC-IC	Long term colony initiating capacity
LT-HSC	Long term haematopoietic stem cell
LTX	Lometrexol
MCF	Methyl chloroformate
MegEs	Megakaryocyte Erythroid

MEP	Megakaryocyte–erythroid progenitor
MFN2	Mitofusin 2
MIP-1a	Macrophage Inflammatory Proteins 1-alpha
MLL	Mixed lineage leukaemia
MM	Multiple myeloma
MPP	Multipotent progenitor
MPP1	Multipotent progenitor 1
MPP2	Multipotent progenitor 2
MPP3	Multipotent progenitor 3
MPP4	Multipotent progenitor 4
MS	Mass spectrometry
MR	Molecular response
MTBE	Methyl tert -butyl ether
MTG	Mitotracker green
MTHFD1	Methylene-tetrahydrofolate dehydrogenase 1
MTHFD1L	Methylene-tetrahydrofolate dehydrogenase 1 like
MTHFD2	Methylene-tetrahydrofolate dehydrogenase 2
MTHFD2L	Methylene-tetrahydrofolate dehydrogenase 2 like
mTOR	Mechanistic target of rapamycin
MTX	Methotrexate
$MTX(Glu)_n$	Methotrexate polyglutamates
Na2HPO4 2H2O	Sodium phosphate dibasic dihydrate
NAC	N-Acetylcysteine
NaCl	Sodium chloride
NAD+	Nicotinamide adenine dinucleotide
NADH	Nicotinamide adenine dinucleotide hydrogen
NaHCO3	Sodium bicarbonate
NES	Normalised enrichment score
NF-κB	Nuclear factor kappa B
NIX (BNIP3L)	BCL2/Adenovirus E1B 19 kDa protein-interacting protein 3-like
NK	Natural killer
NRF2	Nuclear factor erythroid-derived 2-like 2
NRGW	NOD.Cg- $Rag1^{tm1Mom}$ $KitW^{-41J}$ $Il2rg^{tm1Wjl}$/EavJ
OXPHOS	Oxidative phosphorylation
p62 (SQSTM1)	Sequestosome 1
PARK2	Parkinson disease 2
PC	Pyruvate carboxylase
PDGF	Platelet-derived growth factor
PDH	Pyruvate dehydrogenase
PDK2	Pyruvate dehydrogenase kinase isoform 2
PDK4	Pyruvate dehydrogenase kinase isoform 4
PDX	Pralatrexate
PFKFB3	6-phosphofructo-2-kinase/fructose-2,6-biphosphatase 3

PGC-1α	Peroxisome proliferator-activated receptor-gamma coactivator -1 alpha
Ph	Philadelphia chromosome
PI	Propidium iodide
PI3K	Phosphoinositide 3-kinase
PINK1	PTEN-induced putative kinase protein 1
PPAR	Peroxisome proliferator-activated receptor
PPP	Pentose phosphate pathway
PRPP	Phosphoribosyl Pyrophosphate
PTX	Pralatrexate
Rag	Recombination-activating genes
RAPTOR	Regulatory-associated protein of mTOR
RAS	Rat sarcoma virus
RBC	Red blood cell
RFC-1	Reduced folate carrier 1
RIPA	Radioimmunoprecipitation assay
RNA	Ribonucleic acid
ROS	Reactive oxygen species
RPMI	Roswell Park Memorial Institute
Sca1	Stem cell antigen 1
SCF	Stem cell factor
SCL	Stem cell leukaemia
SDS	Sodium dodecyl sulphate
SFM	Serum free media
SHIN1	Serine hydroxymethyl transferase inhibitor 1
SHMT1	Serine hydroxymethyl transferase 1
SHMT2	Serine hydroxymethyl transferase 2
SIRT1	Sirtuin 1
SL-MkPs	Stem-like megakaryocyte committed progenitors
SOS	Son of Sevenless
STAT3	Signal transducer and activator of transcription 3
STAT5	Signal transducer and activator of transcription 5
ST-HSC	Short term haematopoietic stem cell
TBS	Tris buffer saline
TBST	Tris buffer saline with Tween 20
TCA	Tricarboxylic acid cycle
TGFβ	Transforming growth factor beta
THF	Tetrahydrofolate
Tie2	Tyrosine-Protein Kinase Receptor
TKI	Tyrosine kinase inhibitor
TNF-α	Tumour necrosis factor alpha
tRNA	Transfer ribonucleic acid
TSC1	Tuberous sclerosis 1
TSC2	Tuberous sclerosis 2
TYMS	Thymidylate synthase
UDP	Uridine diphosphate

ULK1	Unc-51 like autophagy activating kinase 1
UMP	Uridine monophosphate
UQCRFS1	Ubiquinol-Cytochrome C Reductase, Rieske Iron-Sulfur Polypeptide 1
UTP	Uridine triphosphate
γGH	gamma-glutamyl hydrolase

Chapter 1 Introduction

Part of the introduction was taken or adapted from our review article entitled *"Folate metabolism: a re-emerging therapeutic target in haematological cancers"* (published in Leukemia, March 2021).

1.1 Haematopoiesis and the haematopoietic stem cell

1.1.1 A brief history of haematopoiesis

Haematopoiesis deriving from the Greek "haema", blood, and "poiesis", to create, is the tightly regulated process that leads to the generations of the various components of the blood. More than $2x10^{11}$ haematopoietic cells are daily produced in humans from a small pool of adult haematopoietic stem cells (HSCs)[1]. The concept of "stem cell" and the first *in vivo* evidence for its existence were described by Till and McCulloch in the early 60s. During their pioneering studies of the regeneration of the blood system, they observed the formation of splenic colonies after transplantation of haematopoietic cells in lethally irradiated mice. They further demonstrated that those cells had the ability to give rise to multiple types of myeloerythroid cells and the ability to self-renew[2-4]. These observations introduced the two defining criteria of HSCs, multi-potent differentiation, and self-renewal.

1.1.2 Haematopoietic differentiation tree: A reconciled model for HSC differentiation

In the classical model of haematopoietic hierarchy HSCs are divided into long-term (LT)-HSCs and short-term (ST)-HSCs.LT-HSCs are a rare, quiescent population that has a full long-term reconstitution capacity and can subsequently differentiate to ST-HSCs with a more limited self-renewal capacity. This rare population of HSC can reversibly switch between quiescence and self-renewal under conditions of haematopoietic stress. ST-HSCs can then give rise to multipotent progenitors (MPPs), which no longer carry self-renewal ability. MPPs give rise to myeloid and lymphoid lineages through lineage-committed progenitors. The common myeloid progenitor (CMP) gives rise to all myeloid cells through a megakaryocyte-erythroid progenitor (MEP) and a granulocyte-macrophage progenitor (GMP). Whereas the common lymphoid progenitor (CLP) can differentiate into B and T lymphocytes and natural killer (NK) cells.

However, this model oversimplifies the complexity of HSCs and progenitor cells, and it is only based on the surface markers and transplantation using bulk cells.

Studies of the last two decades have pointed out towards a heterogeneity in the MPP compartment. More specifically the MPP population has been divided immunophenotypically into MPP1, MPP2, MPP3 and MPP4. MPP1 has been identified to be a metabolically active subset of HSCs, similar to ST-HSCs, whereas MPP2/3/4 lack self-renewal ability and only exhibit a short-term myeloid reconstitution ability. MMP2 is a megakaryocyte-biased MPP subset, while MPP3 is a myeloid-based subset. MPP4 is a functionally distinct population that is lymphoid-primed. HSCs firstly produce MPP1/2 to quickly establish the myeloid compartment and then they establish the lymphoid compartment (**Figure** 1-1)[5-8].

Furthermore, Pronk *et al*. provided new insights into progenitor subpopulations. They characterised four newly defined subpopulations including pre (megakaryocyte erythroid) MegEs, pre GMs, pre (colony forming unit- erythroid) CFU-Es and CFU-Es. Pre MegEs can further differentiate to erythroid, megakaryocyte cells, while pre CFU-Es can produce almost exclusively erythroid colonies (CFU-Es). Pre GMs lie upstream of GMPs and have similar clonal lineage output (**Figure** 1-1)[9]. Paul *et al*. suggested that MEPs might not be the true precursor of megakaryocytes. Transcriptomic analysis of single cell MEPs revealed that those cells do not express any megakaryocyte markers nor transcriptional factors[10]. Another study reported that the HSC compartment contains stem-like megakaryocyte committed progenitors (SL-MkPs), a population similar to HSCs[11]

It is also worth mentioning that more and more studies support a continuous hematopoietic differentiation model, where there is no apparent boundary among HSC and progenitors. While the traditional discrete differentiation model suggests that HSCs differentiation is a step-wise process with a tree-like hierarchy, the new continuous model proposes that individual HSCs acquire lineage biases without any major transition through discrete hierarchically organised progenitors[12]

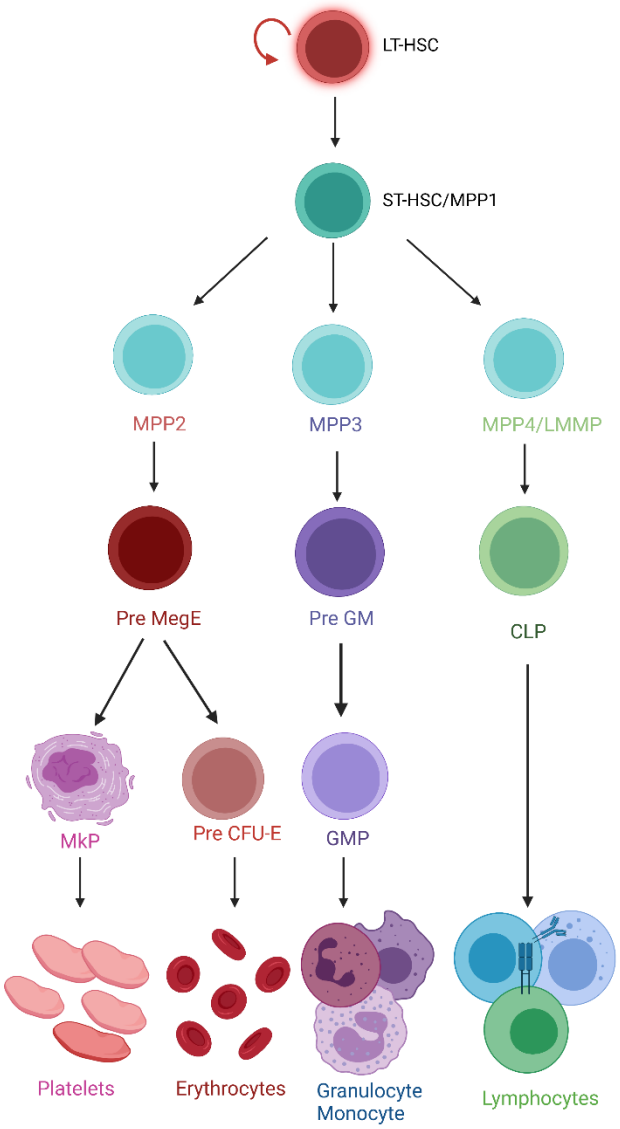

Figure 1-1: Schematic representation of haematopoiesis. In this reconciled model of HSC differentiation, LT-HSCs first give rise to ST-HSC1/MPP1, then to MPP2, MPP3, lymphoid MPP4 (LMPP). MMP2 generate pre MegE, which differentiate to platelets through a megakaryocyte progenitor (MkP) and to erythrocytes through Pre CFU-E. MPP3 mostly differentiated to granulocytes/monocytes through GMPs. LMPPs mainly contribute to lymphocytes. Generated with BioRender.com

1.1.3 Cell surface markers to define HSCs

Cell surface markers and fluorescence-activated cell sorting (FACS) has enabled separation and isolation of HSCs. One of the most famous cell surface markers associated with HSCs is CD34. CD34 plays an important role in localisation and maintenance of HSCs in the bone marrow (BM) niche[13]. However, Baum *et al*. demonstrated that CD34 expressing cells are a heterogeneous population. They suggested that the $CD34^{+}CD90^{+}Lineage(Lin)^{-}$ subset is more enriched in HSC as it can differentiate into myeloid and lymphoid lineages when transplanted into immunodeficient mice[14]. Another cell surface marker that has been linked to HSCs is CD38, which is essential for the regulation of intracellular calcium metabolism[15]. Extended long-term culture of HSCs revealed that $CD34^{+}CD38^{-}$ cells represent a population enriched in LT-HSCs[16]. Overall, it has been established that the most primitive haematopoietic progenitor cell populations harbour $Lin^{-}CD34^{+}CD38^{-}CD90^{+}CD45RA^{-}$surface markers[17].

1.1.4 HSCs regulation: How mitochondria control HSC homeostasis

1.1.4.1 Mitochondria and Reactive Oxygen Species (ROS)

HSCs reside in a hypoxic bone marrow (BM) niche with limited oxygen levels and low levels of ROS (**Figure** 1-2). ROS arises from the one-electron reduction of molecular oxygen, a common by-product during mitochondrial oxidative phosphorylation (OXPHOS). HSCs rely on anaerobic glycolysis and this dependence is due to their position on the hypoxic BM niche, the low energy requirements of quiescence and their need to minimise oxidative stress caused by mitochondrial ROS[18, 19]. Elevated ROS, increased mitochondrial biogenesis and increased oxidative phosphorylation is associated with HSC differentiation.

A key player in HSC metabolism is the hypoxia-inducible factor 1(HIF1), a transcriptional factor essential in cellular response to oxygen levels. HIF1 is a heterodimer that is composed of two components: HIF-1α, whose expression is stabilised by hypoxia, and HIF-1ß, which is constitutively expressed. When HIF-1α and HIF-1ß associate, they form a transcriptional factor that promotes expression of multiple glycolytic genes[20]. Furthermore, HIF-1α promotes expression of pyruvate dehydrogenase kinase 2 and 4 (PDK2 and PDK4), which

prevent pyruvate from entering the tricarboxylic acid cycle (TCA) (**Figure** 1-2). Depletion of *HIF-1a* causes increase in ROS and OXPHOS, that ultimately leads to lose of quiescence, while overexpression of *PDK2* and *PDK4* can rescue such phenotype[21].

Simsek *et al*. and Vanini *et al*. suggested that LT-HSCs contain mitochondria with low activity levels, demonstrated by low mitochondrial potential. They described that $Lin^{-}Sca1^{+}c\text{-}Kit^{+}$ (LSK) cells with low mitochondrial potential induce significantly higher long-term multi-lineage reconstitution levels and the majority of LT-HSCs (89%) were expressing HIF-1α, compared to just 30% of the whole BM. Thus, linking mitochondria potential and activity with ROS response [22, 23].

Studies investigating the role of mechanistic target of rapamycin (mTOR) in adult HSCs have highlighted the key role of ROS in the maintenance of quiescence. mTOR is a key regulator of cellular metabolism that controls protein synthesis, autophagy, and nutrient uptake[24]. Schieke *et al*. described that inhibition of mTOR through rapamycin treatment lowered mitochondrial potential and oxygen consumption in Jurkat T cells[25]. Furthermore, upregulation of mTOR activity results in higher levels of ROS in HSCs[18]. Both lines of evidence hinting on a role of the pathway in HSC function. Ultimately, Chen *et al* demonstrated that deletion of tuberous sclerosis complex (*TSC1*), a negative regulator of mTOR activity, caused accumulation of ROS, increase of mitochondrial biogenesis, loss of long-term functions of HSCs, as well as loss of quiescence. Additionally, they confirmed that *N*-acetylcysteine (NAC), an antagonist of ROS, could rescue HSC defects, suggesting that TSC1-mTOR control quiescence and function of HSCs by repressing ROS[26].

Interestingly, Rimmelé *et al*. highlighted the importance of maintenance of mitochondrial metabolism for HSC homeostasis[27]. FOXO3, member of the forkhead family of transcriptional factors, has been shown to be critical for the self-renewal of HSCs. Deletion of *FOXO3* results in reduction of colony-forming cells in long-term cocultures and also in impairment of reconstitution of haematopoiesis *in vivo*[28]. Rimmelé *et al*. demonstrated that loss of *FOXO3* repressed mitochondrial metabolism in HSC. More specifically, they observed a decrease in OXPHOS, decrease in ATP content and an increase of mitochondrial

fragmentation. Surprisingly, this was accompanied by an elevation of ROS and increase in mitochondrial potential. Furthermore, modulation of ROS with NAC did not rescue the phenotype caused by deletion of *FOXO3*, suggesting that loss of self-renewal of HSCs might not be ROS-dependent, but dependent on the mitochondrial metabolism of those cells. In support of this, Ansó and colleagues revealed that loss of the Rieske iron-sulphur protein (RISP), a component of the electron transport chain (ETC) complex III, suppressed OXPHOS which resulted in impaired differentiation, loss of quiescence, increased apoptosis and increased DNA damage in adult HSCs[29], highlighting the importance of mitochondrial respiration in HSC maintenance.

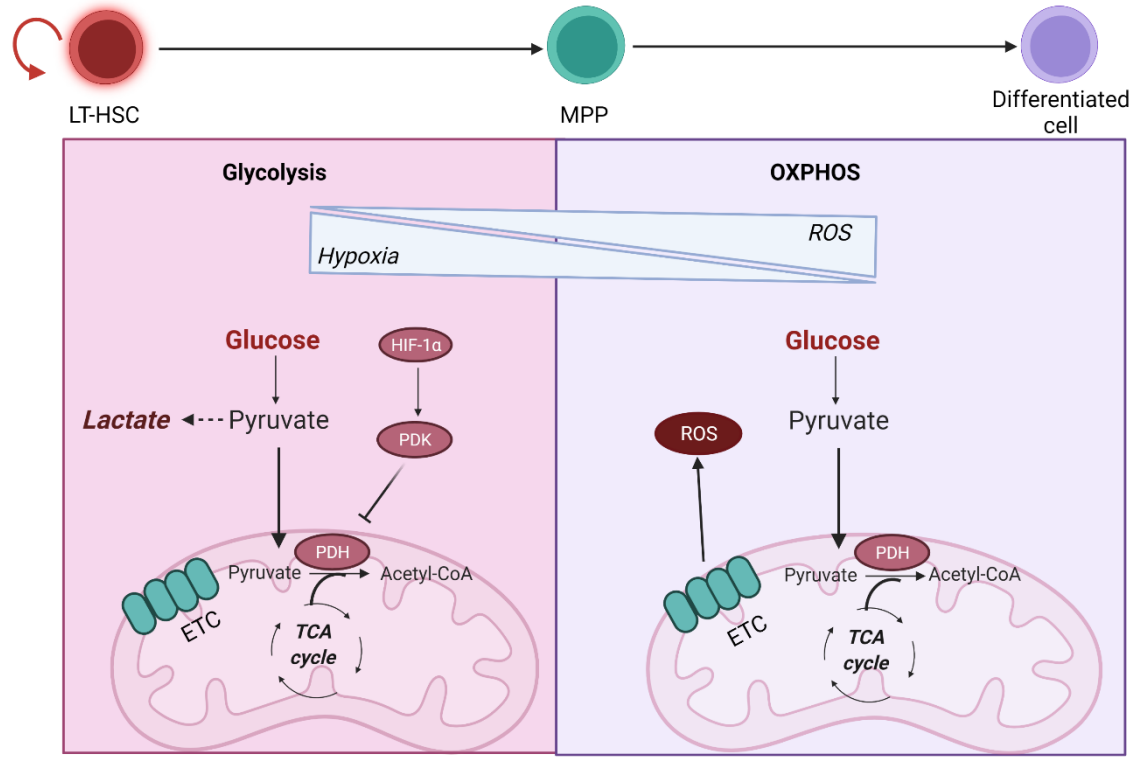

Figure 1-2: Transition from glycolysis to OXPHOS during HSC differentiation. HSC are known to reside in a hypoxic bone marrow niche and to rely on anaerobic glycolysis. Hypoxic conditions activate hypoxia-inducible factor 1α (HIF-1α), which promotes activation of pyruvate dehydrogenase kinase (PDK). PDK in turns prevents pyruvate entry to the tricarboxylic acid cycle (TCA) by inhibiting pyruvate dehydrogenase (PDH). HSC differentiation is associated with elevation of ROS due to a metabolic switch towards oxidative phosphorylation (OXPHOS) and increased oxygen consumption. ETC, electron transport chain. Generated with Biorender.com

1.1.4.2 Autophagy: The quality control of mitochondrial health in HSCs

Autophagy is an essential stress response mechanism that maintains cellular health by regulating the quantity and quality of organelles e.g., mitochondria, through lysosomal degradation to generate energy and allow survival in response to nutrient deprivation and other stressors[30]. Mortensen and colleagues demonstrated that deletion of autophagy related gene 7 (*Atg7*) in the haematopoietic system of mice resulted in loss of normal HSC function. HSCs from Vav-iCre^{+}; Atg7$^{Flox/Flox}$ BM were unable to reconstitute the haematopoietic system of lethally irradiated mice. Furthermore, *Atg7*-deficient LSK displayed increase in mitochondrial ROS and mitochondrial number[31]. In addition, autophagy inhibition by deletion of the autophagy related gene 12 (*ATG12*) was described to lead to loss of quiescence and pro-myeloid differentiation, altering HSC fate. Furthermore, it increased mitochondrial membrane potential, OXPHOS and ROS, suggesting that autophagy might be regulating mitochondrial content in HSCs[32].

Mitophagy, a selective form of autophagy for the clearance of mitochondria, has also been implicated in HSC maintenance. Mitophagy requires the stabilisation of PTEN-induced putative kinase 1 (PINK1) at the mitochondrial outer membrane to initiate clearance of damaged mitochondria. PINK1 then recruits and phosphorylates a cytosolic E3 ubiquitin ligase encoded by PARK2, PARKIN. Tie2^{+} mouse HSCs, where Tie2 is a tyrosine kinase receptor that marks the most primitive HSCs, undergo PINK1-PARKIN-dependent-mitophagy which plays an important role for their self-renewal and expansion. In this case mitophagy seems to be regulated by the fatty acid oxidation (FAO) pathway. Activation of the PPAR (peroxisome proliferator–activated receptor)–FAO pathway promoted expansion of Tie2^{+} HSCs through enhanced parkin recruitment in mitochondria. Additionally, silencing of *PARK2* or *PINK1*, decreased mitophagy flux and impaired reconstitution capacity of Tie2^{+} HSCs. Therefore, PINK1-PARKIN-dependent mitophagy can help to maintain self-renewal capacity of this primitive population due to high mitochondrial clearance[33].

Furthermore, recent studies have highlighted the importance of mitophagy during erythroid maturation. NIX, a BH3-only member of the Bcl-2 family, is an outer mitochondrial membrane protein that has been found to be upregulated

during terminal erythroid differentiation. NIX was shown to target mitochondria to autophagosome-like structures and its absence caused a mild, nonlethal anaemia[34]. Additionally, loss of the autophagy activating kinase ULK1 also caused a mild anaemia, which was a result of a delay in the clearance of mitochondria and ribosomes in reticulocytes[35].

1.1.5 Erythroid maturation

Erythropoiesis is a tightly regulated process that takes place in the BM and gives rise to mature erythrocytes. CFU-Es go through a number of differentiation steps which ultimately lead to mature red blood cells. This is a finely regulated process, involving several cell division steps, removal of intracellular compartments and acquisition of a red phenotype due to increasing concentration of haemoglobin. During erythroid maturation, there is a gradual decrease in ribosome and mitochondria numbers, which supports the idea that autophagy/mitophagy play a crucial role in the process. There is a number of growth factors known to participate in the regulation of erythropoiesis, however, erythropoietin (Epo) has been identified as the master regulator of RBC production.

The CML cell line K562 has been proposed as a useful *in vitro* model to study erythropoiesis, as these cells undergo erythroid differentiation when treated with a variety of compounds[36].

Erythroid maturation is a concept that we will further explore during the result chapters of this thesis (**4.4**).

1.2 Chronic Myeloid Leukaemia

1.2.1 Introduction

CML is a clonal, myeloproliferative disease that originates in a single HSC with a chromosomal translocation t(9;22) that gives rise to the Philadelphia chromosome (Ph) and the BCR-ABL oncoprotein[37-39].The BCR-ABL oncoprotein is a constitutively active tyrosine kinase, which promotes cell survival and proliferation and is a target of therapeutic interventions[40].

CML affects 0.7-1.0 per 100,000 individuals in Europe, with a median age at diagnosis of 57-60 years and a higher incidence in males than females[41].Terms like leukaemic stem cell (LSC) and leukaemia-initiating cell (LIC) have been used to describe the cell able to reconstitute leukaemic haematopoiesis. A different number of immature progenitors, also known as blast cells, defines different stages of the disease. CML begins with a chronic phase (CML-CP) which is characterised by an abundance of fully differentiated and functional myeloid cells and between 0-15% blast cells. The expansion of myeloid cells is associated with splenomegaly and anaemia. Without effective therapy, CML progresses to accelerated and then blastic phase (CML-BP), characterised by a differentiation arrest (has >30% of GMP blasts), and ultimately death within 5-7 years[42].

1.2.2 BCR-ABL molecular pathways

In physiological conditions, ABL protein shuffles between the nucleus and cytoplasm, however, when fused with BCR, ABL loses this property, and it is mainly retained in the cytoplasm. The BCR-ABL fusion favours dimerization or tetramerization and subsequent autophosphorylation of the consequently active kinase, increasing the number of phosphotyrosines in the BCR-ABL and potential binding sites for the SH2 domains of other proteins (**Figure** 1-3). The N-terminal domain of BCR-ABL binds to the SH2 domain of the adaptor protein GRB2, to then recruit Son of Sevenless (SOS) and the scaffold adapter GRB2-associated binding protein 2 (GAB2) forming the GRB2/GAB2/SOS complex[43]. The GRB2/GAB2/SOS complex causes consequent activation of the RAS downstream pathway, and ultimately activating the MAP kinase (MAPK) pathway, which promotes cellular growth and proliferation[44, 45]. Furthermore, the GRB2/GAB2/SOS complex recruits phosphatidylinositol 3-kinase (PI3K) to activate the PI3K/AKT pathway that promotes survival by suppressing the activity of FOXO and promoting the activity of mTOR[46-48]. Moreover, a critical outlet of BCR-ABL is activation of the signal transducer and activator of transcription 5 (STAT5) that is indispensable for CML maintenance and progression[49]. Lastly, MYC is another target of BCR-ABL whose activity has been linked to leukaemia progression[50].

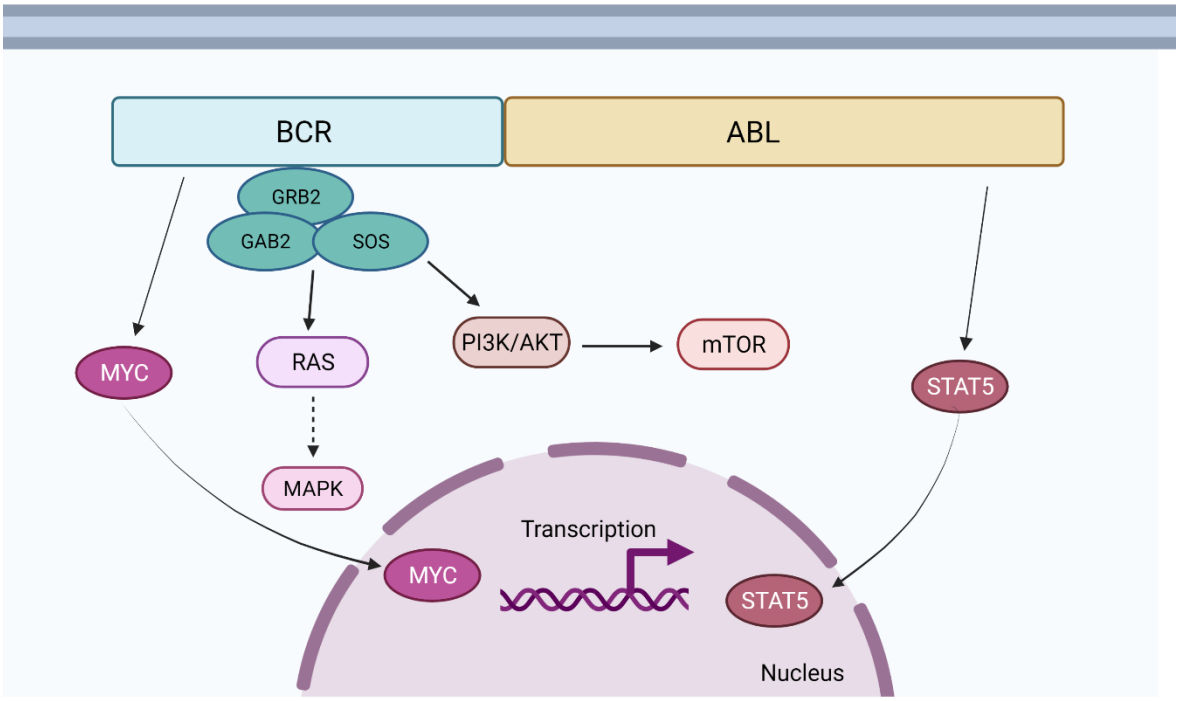

Figure 1-3: Schematic representation of the molecular pathway activated by BCR-ABL. BCR-ABL forms a complex with GRB2, Son of Sevenless (SOS) and the scaffold adapter GRB2 to ultimately activate RAS and MAPK pathway and the phosphatidylinositol 3-kinase (PI3K)/AKT pathway. It also activates MYC and the signal transducer and activator of transcription 5 (STAT5), both entering the nucleus and regulating transcription. Generated with Biorender.com

1.2.3 Tyrosine kinase inhibitors in CML therapy

The introduction of tyrosine kinase inhibitors (TKI), and more specifically imatinib, targeting the tyrosine kinase activity of ABL, revolutionised CML therapy. Imatinib is a highly selective competitive inhibitor that binds to the ATP binding-pocket of the ABL kinase domain, therefore impairing its tyrosine kinase activity and preventing phosphorylation of its key downstream substrates[51]. However, it shows affinity for other tyrosine kinases such as the platelet-derived growth factor (PDGF) and c-KIT receptors[52]. Following successful clinical trials where imatinib showed a 76% complete cytogenetic response, compared to just 14% with previous standard of care, imatinib was introduced as the first line treatment of CP-CML[53].

Nonetheless, imatinib is not perfect; drug intolerance, adverse effects and drug resistance are some of the issues that have been reported in patients[54]. This led to the development of second and third generation TKIs, including nilotinib, dasatinib, bosutinib and finally ponatinib, which are efficient rescue therapies for patients experiencing imatinib resistance or intolerance. However, despite the success of 1-3rd generation TKIs, TKI treatment does not cure CML. TKI discontinuation studies in patients with stable molecular response 4.5 ($MR^{4.5}$) have suggested that molecular relapse rates within the first six months of imatinib discontinuation are about 60%[55]. Similar results were obtained in discontinuation trials of nilotinib and dasatinib[56], suggesting that the majority of patients are required to remain in lifelong TKI therapy, which is associated with significant side effects and large economic burden.

1.2.4 LSCs persistence during TKI therapy

As previously mentioned, CML is a clonal stem cell-driven disease and the initiator cell which drives malignant haematopoiesis is known as LSC or LIC. First evidence on the stem cell origin of CML came in the late 70s by Fialkow and colleagues. They demonstrated that myeloid erythroid cells of eight female CML patients with heterozygous X-linked glucose-6-phosphate dehydrogenase (G6PDH) had the same enzyme type of G6PDH and did not experience any heterogeneity[57]. Furthermore, it has been shown that BCR-ABL is present in all haematological lineages indicating that the initial chromosomal translocation

occurs in a pluripotent HSC[58]. Lastly, expression of *BCR-ABL* fails to confer self-renewal capacity to committed progenitors, suggesting that CML originates from a cell with intrinsic self-renewal capacity[59].

Similarly to HSCs, LSCs were shown to be quiescent, and their quiescent state has been linked to TKI resistance and disease persistence[60-62]. Interestingly, Corbin *et al*. demonstrated that LSCs are able to maintain their viability using BCR-ABL independent survival signals when treated with imatinib[63]. Reinforcing these findings, Hamilton *et al*. showed that a combination of dasatinib treatment and growth factor withdrawal is not sufficient to target primitive LSCs despite complete inhibition of BCR-ABL kinase activity[64].

In summary, these data demonstrate that LSC do not rely on BCR-ABL for their survival, turning the main focus of current CML research on identifying targetable vulnerabilities of CML LSCs that could sensitise this quiescent population to traditional TKI therapy and potentially, cure the disease. Bellodi and colleagues demonstrated that autophagy might provide a survival mechanism to TKI treated LSCs. They described that TKI therapy causes induction of autophagy in LSCs and its inhibition, either pharmacological or genetic, can sensitise them to TKIs[65]. More recent studies have further characterised this protective autophagy phenotype observed in TKI-treated LSCs. It has been shown that inhibition of autophagy promotes ROS induced differentiation of LSCs and sensitises them to TKI therapy[66, 67].

Giustacchini *et al*. elegantly used a combination of mutation detection and RNA sequencing (RNAseq) to reveal that TKI-resistant BCR-ABL$^+$ LSCs overexpress TNF-α, Wnt/β-catenin-pathway-associated genes, TGFβ-pathway gene *SKIL*, regulators of NF-κB and HIF-1α in comparison with normal HSCs. Furthermore, elevated TNF-α and TGFβ correlated with poor response to TKI therapy. Lastly, when culturing single normal HSCs and LSCs in the presence of TNF-α or TGFβ authors noticed that TGFβ more strongly influenced cell division rate and induced quiescence in LSCs compared to normal counterparts[68]. Thus, targeting such inflammatory pathways might be of therapeutic value.

1.2.5 LSCs and mitochondrial metabolism: Targeting metabolic vulnerabilities

1.2.5.1 Metabolic reprogramming of cancer cells

Cancer cells undergo metabolic changes to harness nutrients and support their rapid growth and proliferation. Such metabolic reprogramming has been extensively studied. During the early 20th century, Otto Warburg observed the first evidence for changes in cancer metabolism. Warburg described an increase in aerobic glycolysis, "Warburg effect", where cancer cells took up and fermented glucose to lactate in the presence of oxygen (**Figure** 1-4)[69]. Metabolic alterations have been exploited by researchers ever since, to understand tumour growth and metastatic dissemination.

Much of recent research has focused on determining why the Warburg effect might be advantageous for tumour growth. Vander Heiden and colleagues described that anaerobic glycolysis is a mean to synthesise anabolic molecules (lipids, amino acids, nucleotides) to support cell proliferation[70]. However, in the past decade, mitochondrial respiration (comprising of the TCA cycle and OXPHOS) has re-emerged as a key anabolic hub supporting tumour growth. This key function of mitochondrial respiration is not solemnly attributed to ATP synthesis and to fulfilment of energetic needs of the cell. Several studies have demonstrated that mitochondrial respiration is necessary for aspartate biosynthesis in cancer cells (**Figure** 1-4). More specifically, aspartate is a biosynthetic precursor and it contributes to nucleotide synthesis, essential for a rapidly proliferating cancer cell. Furthermore, ETC inhibition leads to asparagine depletion and impaired mTOR signalling, linking mitochondrial metabolism to cellular signalling pathways[71-73]. Additionally, it has been recently shown that when disrupting the ETC-linked generation of ATP via OXPHOS, cancer cells can still survive as long as the ETC-linked TCA cycle function is intact[74].This indicates that ATP derived from glycolysis can support tumour growth, reinforcing the idea that mitochondrial respiration supports tumour growth by supporting anabolic processes.

Overall, aerobic glycolysis likely does not replace mitochondrial respiration, but rather, in proliferating cells these processes occur in parallel to fulfil the energetic and biosynthetic needs of the cell.

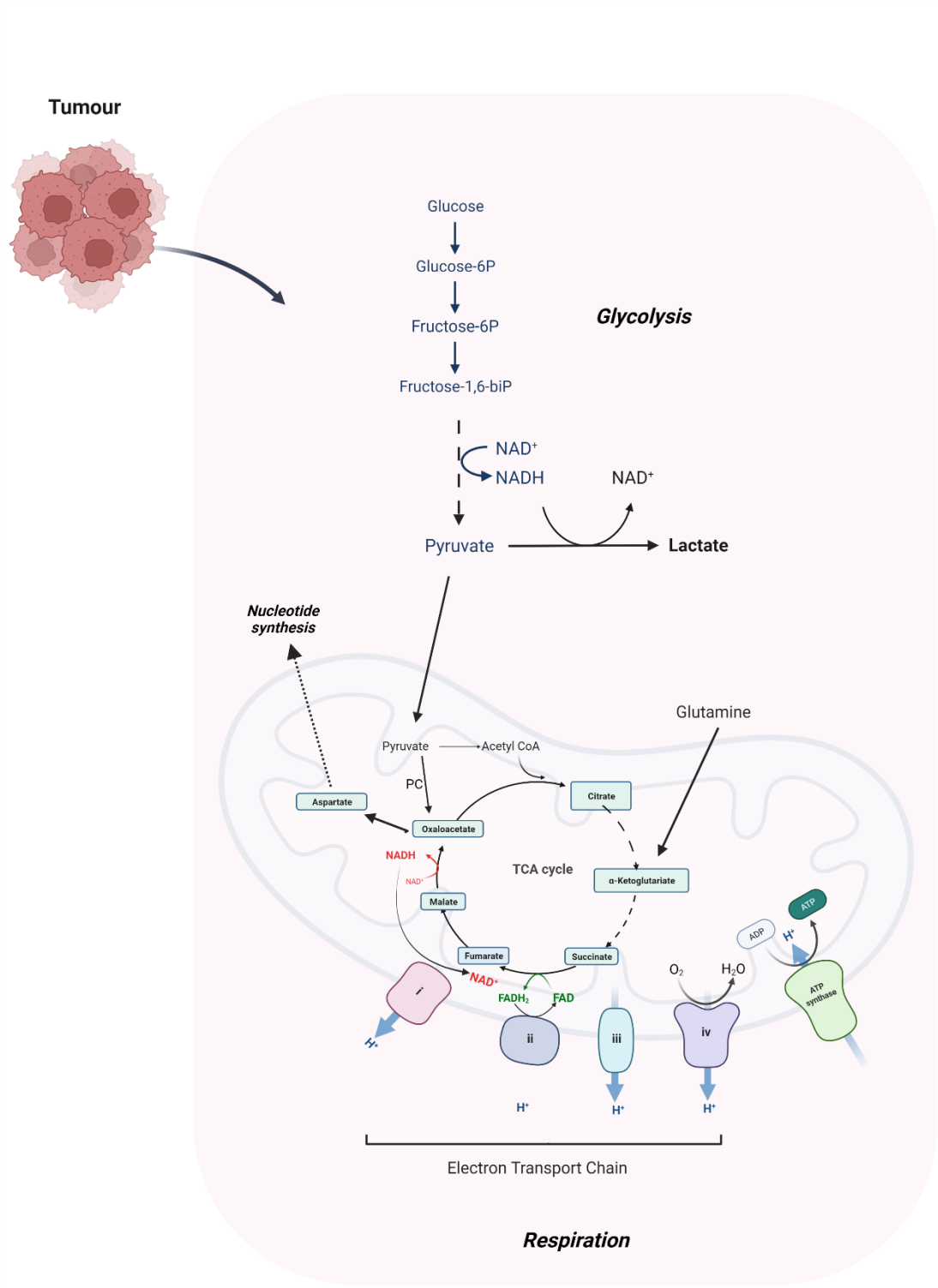

Figure 1-4: Overview of energy metabolism in a cancer cell. Cancer cells are using both glycolysis and mitochondrial respiration in parallel. Mitochondrial respiration and oxidative anaplerosis,that converts pyruvate to oxaloacetate with the help of pyruvate carboxylase (PC) leads to aspartate biosynthesis. Aspartate contributes to nucleotide synthesis and cancer cell proliferation. Generated with Biorender.com

1.2.5.2 Metabolic rewiring of LSCs

Recent studies have shed light on the energetic needs of LSCs. One of the most compelling observations was that unlike primitive HSCs that rely on glycolysis to maintain their quiescent, primitive LSCs rely on mitochondrial respiration compared to HSCs and more differentiated CML cells. Furthermore, Kuntz and colleagues demonstrated that CML LSCs have a higher mitochondrial mass and activity compared to normal counterparts. Interestingly, compared to normal HSCs, they display an increased oxidative anaplerotic metabolism, where pyruvate gets converted to oxaloacetate (a reaction catalysed by pyruvate carboxylase; **Figure** 1-4) and this leads to increased aspartate biosynthesis. Additionally, authors demonstrated that tigecycline, an antibiotic that impairs ETC by inhibiting mitochondrial protein synthesis, can sensitise LSCs to imatinib *in vitro* and *in vivo*[75]. Given that ETC inhibition impairs nucleotide synthesis by suppressing aspartate biosynthesis, it would be interesting to see if this is the case in the context of LSCs and whether their dependency on mitochondrial respiration is due to the need for robust nucleotide production.

Guistacchini *et al*. demonstrated that BCR-ABL$^+$ LSCs display upregulation of genes related to OXPHOS when compared to normal HSCs of the same patient, reinforcing that targeting OXPHOS might be selectively targeting LSCs. Abraham and colleagues recently described that upregulated mitochondrial respiration was partially regulated by the NAD-dependent deacetylase sirtuin-1 (SIRT1)[76]. Previous work from the same lab had described that SIRT1 overexpression in CML LSCs leads to p53 deacetylation and inhibition, that ultimately leads to LSC survival and resistance to TKI therapy[77]. With regards to SIRT1 and its role in mitochondrial metabolism, authors described that SIRT1 promotes mitochondrial biogenesis and activity through PGC-1α. Its effect on PGC-1α can be either direct or through the AMP-dependant protein kinase (AMPK). However, although direct inhibition of PGC-1α reduced mitochondrial OXPHOS, it did not fully inhibit CML pathogenesis *in vivo*, suggesting that additional SIRT1-dependent mechanisms promote LSCs survival[76].

Altogether, these studies highlight the importance of mitochondrial respiration and activity in LSCs and how targeting OXPHOS might sensitise resistant LSCs to TKI therapy.

1.3 Folate-mediated one-carbon metabolism

1.3.1 Introduction

Folate metabolism, considered the core of a broader set of transformations known as one-carbon (1C) metabolism, allows the transfer of 1C units for biosynthetic purposes such as *de novo* synthesis of adenosine, guanosine and thymidylate, and for methylation reactions that support the methionine cycle. As animals cannot synthesize folate, insufficient dietary intake can cause neural tube defects in developing foetuses and anaemia[78-80].

With regards to the association of the folate metabolism to blood cancers, the idea that antagonists of folates could reduce the proliferation of malignant cells in paediatric leukaemia gave rise to modern cancer therapy and a class of drugs known as antifolates[81]. Since then, methotrexate (MTX), likely the most well-known antifolate, has been used to treat a variety of neoplastic and inflammatory diseases.

1.3.2 Folate cycle and compartmentalisation

Folate metabolism occurs in two parallel and complementary pathways, localized in the cytosol and mitochondria (**Figure** 1-5). New 1C units are donated from amino acids such as serine (the primary source of 1C units), glycine (through the glycine cleavage system) and the choline degradation products dimethylglycine and methylglycine (sarcosine), while folate molecules function as 1C unit carriers. In brief, the first step of the reaction is catalysed by serine hydroxymethyl transferase, SHMT1 (cytoplasmic) and SHMT2 (mitochondrial), where serine gets converted to glycine and its 1C unit is donated to tetrahydrofolate (THF) to give rise to 5,10-methylene-THF. In the cytosol, 5,10-methylene-THF contributes to thymidylate synthesis and the methionine cycle. Interestingly, SHMT2 was found to contribute to mitochondrial translation by providing methyl donors for the taurinomethyluridine synthesis [82]. 5,10-methylene-THF is then converted to the most oxidized form of folate carbon, 10-formyl-THF. In the cytosol, this conversion is carried out by the trifunctional enzyme methylene-THF dehydrogenase 1 (MTHFD1) with a 5,10-methylene-THF dehydrogenase, 5,10-methenyl-THF cyclohydrolase and 10-formyl-THF synthase activity. Whereas in the mitochondria, it is the bifunctional methylene-THF

dehydrogenase 2 (MTHFD2) or 2 like (MTHFD2L) with dehydrogenase and cyclohydrolase activity that catalyses the conversion. Nilsson *et al.* demonstrated that normal and cancer cells express both enzymes, even though MTHFD2 exhibits a higher baseline expression. Surprisingly, MTHFD2L exhibited a greater increase in cancer tissue versus normal tissue in AML compared to MTHFD2, even though they do not clarify what tissues were used to make this comparison. In general, MTHFD2L was unable to compensate for the loss of *MTHFD2* and it did not show any association with proliferation or response to growth factors[83]. Cytosolic 10- formyl-THF is essential for *de novo* purine synthesis. More specifically, for every newly synthesized DNA or RNA base, one molecule of 10-formyl-THF is required[84, 85]. Mitochondrial 10-formyl-THF is used to initiate mitochondrial translation by producing formyl-methionine tRNA. Additionally, as 10-formyl-THF cannot cross the mitochondrial membrane, it first gets hydrolysed to formate by the MTHFD1-like (MTHFD1L) enzyme. Lastly, 10-formyl-THF can be fully oxidized to CO_2, a reaction catalysed by 10-formyltetrahydrofolate dehydrogenase 1 (ALDH1L1) or 2 (ALDH1L2) in the cytosol or mitochondria respectively, leading to its terminal elimination.

The presence of these two parallel pathways allows for a complete oxidative/reductive cycle, where serine gets catabolized in the mitochondria and then synthesized in the cytosol. Interestingly, studies have revealed that this subcellular compartmentalisation is conserved from yeast to mammalian cells[86]. Ducker *et al.* using a serine tracer that was developed to distinguish the mitochondrial-derived serine contribution versus the cytosolic[87-89], demonstrated that most cultured cell lines generate 1C units exclusively in the mitochondria and that mitochondrial-released formate directly contributes to nucleotide and serine synthesis. Interestingly, the same and consecutive studies have shown that genetic inhibition of mitochondrial 1C enzymes induces a rewiring of the flux, where the cytosolic pathway switches from serine synthesis to serine catabolism[89, 90]. Cells end up becoming glycine auxotrophs, depending on extracellular glycine, as the cytosolic pathway cannot compensate for the loss of mitochondrial glycine production[91]. Labuschagne *et al.* showed that in the absence of serine, exogenous glycine is unable to support nucleotide synthesis as cells start using glycine for serine synthesis[92].

Several studies have tried to shed light on the compartmentalisation and directionality of folate metabolism. Conversion of 5, 10-methylene-THF to 5, 10-methenyl-THF by MTHFD2 is accompanied by mitochondrial NAD(P)H production. Whereas the reverse reaction catalysed by MTHFD1 in the cytosol proceeds in a NADPH-consuming direction[89, 93, 94]. The difference in electrochemical potential between NADH and NADPH explains the directionality of folate metabolism, where mitochondrial formate gets shuttled to the cytosol. With regards to why there should be a mitochondrial compartment in the first place, Zheng *et al.* conclude that the existence of the mitochondrial compartment provides the necessary flexibility to balance cellular demands for glycine and 1C units. Whereas, a single cytosolic compartment would probably overwhelm the cell, as it would require multiple complex regulatory mechanisms (similar to *E.coli* where there is a single compartment)[95]. Additionally, Ducker and Rabinowitz suggest that most of serine catabolism is localized in the mitochondria to separate 1C metabolism from glycolysis that happens in the cytosol. They argue that NADH production from the conversion of 5,10-methylene-THF to 5,10-methenyl-THF could deplete the cytosolic NAD^+ pool needed for glycolysis. Overall, it seems that nature and evolution have enabled this compartmentalisation to maximize efficiency[84].

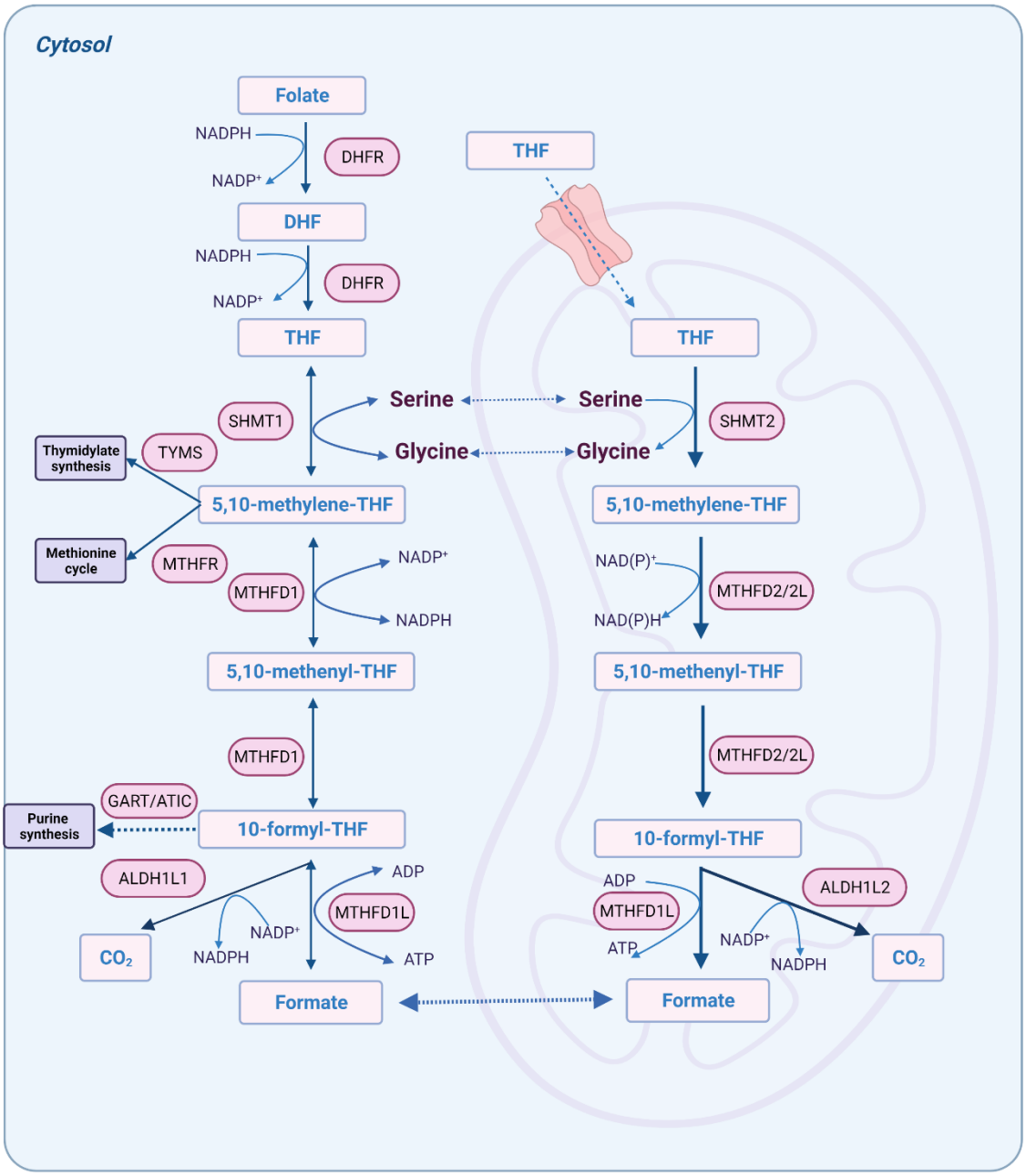

Figure 1-5: An overview of folate-mediated 1C metabolism and its compartmentalisation. From yeast to mammalian cells 1C units tend to flow clockwise allowing for a complete oxidative/reductive cycle where serine gets oxidized in the mitochondrial compartment and formate gets reduced in the cytosol. Through this intercompartmental cycle folate metabolism supports anabolic reactions such as purine and thymidylate synthesis as well as the methionine cycle. DHF, dihydrofolate; THF, tetrahydrofolate; DHFR, dihydrofolate reductase; SHTMT1/2, serine hydroxymethyl transferase, cytosolic (1)/ mitochondrial (2); MTHFD1, methylenetetrahydrofolate dehydrogenase 1; MTHFD2(L), methylenetetrahydrofolate dehydrogenase 2 (2-like); MTHFD1L, monofunctional tetrahydrofolate synthase; TYMS, thymidylate synthetase; MTHFR, methylenetetrahydrofolate reductase; GART, phosphoribosylglycinamide formyltransferase; ATIC, 5-aminoimidazole-4-carboxamide ribonucleotide formyltransferase/IMP cyclohydrolase; ALDH1L1/2, 10-formyltetrahydrofolate dehydrogenase cytosolic (1)/mitochondrial (2). Generated with Biorender.com

1.3.3 Formate overflow and its implications

Several studies have reported that formate production through serine catabolism exceeds the 1C demands for nucleotide synthesis. This excess of formate, also known as formate overflow, depends on the expression of mitochondrial folate enzymes and the OXPHOS status of the cells[89, 90, 96, 97]. Meiser *et al*. demonstrated that tumours with an active and robust oxidative metabolism are formate overflow positive, describing this formate overflow as a hallmark of oxidative cancers. Additionally, the authors revealed that cancer tissues exhibit significantly higher serine catabolism to formate compared to normal adjacent tissue and other non-tumour-bearing organs. Plasma formate levels were found to be significantly higher in tumour bearing mice compared to wild-type mice[97].

There are various hypotheses for the selective advantage of formate overflow, but it is still difficult to make solid conclusions. When Meiser *et al*. demonstrated that formate overflow is a hallmark of oxidative tumours they also showed that the excess formate that was being released from cancer cells promoted invasion *in vitro*. Here it is tempting to hypothesize that increased mitochondrial 1C metabolism and consequently formate overflow, might be advantageous for cancer development as it promotes invasion. Furthermore, Oizel *et al*. concludes that formate overflow induces a metabolic switch to a cellular state with high purine and pyrimidine nucleotide levels and an increased rate of glycolysis. The increase in purine synthesis links formate overflow with cell signalling. In the process of increasing purine synthesis, there is a dramatic reduction of intracellular 1-(5'-Phosphoribosyl)-5-aminoimidazole-4-carboxamide ribotide (AICAR), the phosphorylated variant of the AMPK activating drug acadesine. The decrease in AICAR then results in a reduction of AMPK activity[98]. Concomitantly, the increase in purine levels promotes an increase in the mTOR kinase activity[99]. Ultimately, what they hypothesize is that serine catabolism to formate is required to trigger this metabolic switch, which potentially serves as a selective advantage for the existence of the mitochondrial branch of folate metabolism[98].

1.3.4 Folate cycle role in nucleotide synthesis

As we previously mentioned, folate metabolism fulfils the 1C demand for purine and thymidylate synthesis. Purines are required for the synthesis of RNA, DNA and the free ATP pool and they represent the major biosynthetic demand for 1C units in proliferating cells. Apart from 1C units, purine synthesis also requires glycine, another important product of folate metabolism (**Figure** 1-6). On the other hand, thymidylate synthesis represents a smaller but important demand for 1C units. Folate-derived 1C units are required for the conversion of deoxyuridine monophosphate (dUMP) to deoxythymidine monophosphate (dTMP), which is ultimately converted to deoxythymidine triphosphate (dTTP).

Interestingly, besides the direct role of 1C units for thymidylate synthesis, folate metabolism has been recently implicated with earlier steps of pyrimidine synthesis. Oizel and colleagues demonstrated that dihydroorotate and orotate, two early intermediates in pyrimidine synthesis, are depleted upon genetic inhibition of 1C metabolism. A gradual decrease was observed also for uridine monophosphate (UMP)[98]. The same group recently described that formate induces pyrimidine synthesis through mTORC1 activation. They also demonstrated that this is dependent on purine availability[99]. This represents a direct link between purine and pyrimidine synthesis through folate metabolism.

Purine and pyrimidine biosynthesis will also be further discussed in this thesis, as the majority of the changes we observed following 1C inhibition were rescued by reconstitution of *de novo* purine and thymidylate synthesis.

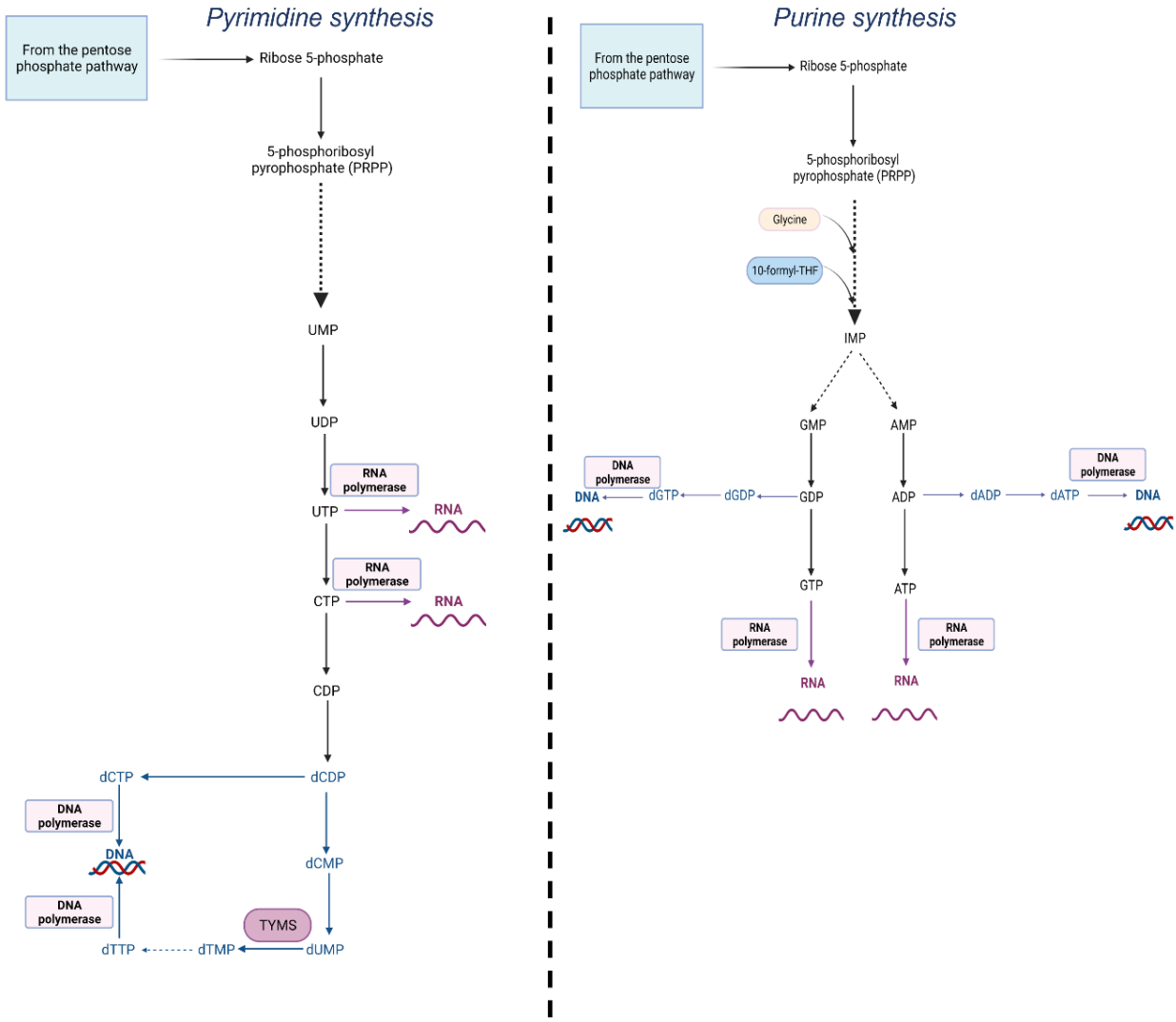

Figure 1-6: A graphical representation of pyrimidines and purine synthesis. *De novo* pyrimidine and purine synthesis require 1C units from the folate pool. Purine biosynthesis requires glycine, another product of 1C metabolism. Ultimately, deoxy-ribonucleotides (dCTP, dTTP, dATP, dGTP) are used for DNA synthesis, while UTP, CTP, ATP, GTP are used for RNA synthesis. UMP, uridine monophosphate; UDP, uridine diphosphate; UTP, uridine triphosphate; CTP, cytidine triphosphate; CDP, cytidine diphosphate; dTMP, deoxythymidine monophosphate; dTTP, deoxythymidine triphosphate; IMP, inosine monophosphate; AMP, adenosine monophosphate; ADP, adenosine diphosphate; ATP, adenosine triphosphate; GMP, guanosine monophosphate; GDP, guanosine diphosphate; GTP, guanosine triphosphate. Generated with BioRender.com

1.3.5 Folate cycle by-products and their cellular roles

Undeniably, the major role of folate metabolism is its contribution to nucleotide synthesis. However, more and more evidence suggest that it is not just nucleotide contribution that might have important implications on a cellular level. Similar to formate overflow, and its role in energy metabolism (as a metabolic switch) and invasion, there is increasing evidence that other by-products of the folate pathway have important cellular roles, linking folate metabolism to cellular respiration and antioxidant defence.

1.3.5.1 NADH and mitochondrial respiration

NADH production by the mitochondrial MTHFD2 links 1C metabolism to OXPHOS. NADH is subsequently oxidized while its electrons are transferred to the ETC complexes. This, ultimately, contributes to energy production in the form of ATP. Remarkably, Ducker *et al*. demonstrated that serine catabolism contributes to up to 7% of the NADH pool[89]. Additionally, formate production correlates with the respiration status of the cell, where ETC impairment upon treatment with ETC inhibitors (i.e. rotenone, metformin) or mitochondrial DNA depletion, causes a reduction of formate release from the cells[90, 91, 96]. Interestingly, Bao *et al*. showed that respiration chain dysfunction induces an adaptive response to increase serine synthesis (1C donor) to feed the mitochondrial 1C pathway[96]. Furthermore, Yang *et al*. described that upon respiration impairment, serine catabolism becomes a major source of NADH, whereas the other NADH sources like glutamine, FAO and lactate are blocked. This persistence of serine catabolism contributes to an accumulation of NADH that can be toxic. Inhibition of serine catabolism in the context of impaired respiration can normalize NADH levels and facilitate cell growth[100]. However, previous studies have reported a synergistic effect in growth inhibition when 1C metabolism (via serine deprivation) and ETC are impaired[101, 102]. What one can say with certainty is that there is a definitive link between cellular respiration and 1C metabolism and it is worth of further investigation.

1.3.5.2 NADPH and antioxidant defence

The oxidation step of methylene-THF to 10-formyl-THF is coupled to the production of NADPH. Additionally, full oxidation of 10-formyl-THF to CO_2 also

contributes to NADPH[93, 94]. NADPH is primarily synthetized through the pentose phosphate pathway (PPP) and provides high-energy electrons for antioxidant defence and reductive biosynthesis such as fatty acid and proline synthesis. Interestingly, to date there are two connections of folate metabolism to NADPH. The first connection is the production of NADPH via 1C metabolism and the second is that NADPH production through the PPP supports the folate pathway via regulation of the dihydrofolate reductase (DHFR) activity[103]. In a cancer context, evidence suggests that upregulation of mitochondrial 1C metabolism contributes to cancer progression by supporting antioxidant defence. Ye *et al.* described that in MYC amplified cancer cell lines and neuroblastoma patient samples, SHMT2 gets induced to produce NADPH (by initiating the degradation of serine to CO_2) and to maintain redox balance under hypoxic conditions[104]. Ducker *et al.* also demonstrated that cell lines deficient in MTHFD2 and ALDH1L2 were sensitized to hydrogen peroxide, a form of oxidative stress[89]. Piskounova *et al.* showed that folate pathway inhibition by MTX, ALDH1L2 knockdown or MTHFD1 knockdown inhibited tumour metastasis, concluding that ALDH1L2 counteracts oxidative stress and promotes metastasis[105]. On that note, it was recently shown that cybrid cells (cells produced by combining cytoplasm of nucleated cells with non-nucleated cells or cytoplasts) with a mutation in a gene encoding an integral component of Complex I subunit of the ETC display a reduction in serine catabolism and NADPH production that leads to oxidative stress, inflammation and, ultimately, cell death[106]. While in HCT116 cells, both *ALDH1L1* and *ALDH1L2* expression is minimal, suggesting that the folate pathway does not contribute substantially to NADPH, *ALDH1L2* expression is found to be upregulated in several tumour types[107]. It would be interesting to gain a better insight into this upregulation that suggests that specific tumours would require NADPH for an antioxidant response, therefore making them more vulnerable to oxidative stress.

1.3.6 Targeting folate metabolism in haematological malignancies

Since the late 40s when Sydney Farber administered a newly synthesized folate analogue (aminopterin) to children with ALL, antifolates targeting 1C metabolism have been used to treat a wide range of cancers including haematological malignancies. MTX, the most frequently used antifolate, has been approved for the prophylaxis of meningeal leukaemia and it is also used in

maintenance therapy with other chemotherapeutic drugs in patients with ALL[108] MTX followed by whole-brain radiotherapy is the mostly commonly used approach for patients diagnosed with a rare form of non-Hodgkin lymphoma, central nervous system (CNS) lymphoma[109]. Such treatment results in a 5-year survival for 20-35% of patients[110].

1.3.6.1 Mechanism of action of MTX

MTX enters the cell via the reduced folate carrier (RFC-1), a protein found predominantly in the cell membranes of foetal and cancer cells (**Figure** 1-7). Once in the cytosol, it gets polyglutamylated by folylpolyglutamate synthetase (FPSG). Polyglutamylation is a time- and concentration- dependent process that ultimately enhances the action of MTX. Polyglutamates (up to 5 additional glutamates) of MTX are retained longer in the cell, thus the amount accumulated and the length of the chain of MTX polyglutamates are key determinants of antifolate-mediated cytotoxicity. MTX and its polyglutamates inhibit DHFR, that catalyses the conversion of dihydrofolate (DHF) to THF. Additionally, polyglutamation alters the cellular effects of MTX, as studies have shown that MTX polyglutamates are more potent inhibitors of other folate-dependent enzymes such as thymidylate synthase (TYMS) and 5-aminoimidazole-4-carboxyamide ribonucleotide formyltransferase (ATIC), ultimately blocking both thymidylate and purine syntheses[108, 111-113]. MTX polyglutamates with chains longer than three glutamate residues cannot be exported out of the cell; therefore, they need to be deglutamated, a reaction catalysed by the lysosomal γ-glutamyl hydrolase (γGH). The balance between polyglutamation and deglutamation generates a steady state level of intracellular MTX. Lastly, MTX gets exported from the cell by the ATP-binding cassette proteins (ABCC1-4 and ABCG2). Overexpression of these efflux transporters has been associated with antifolate resistance[114].

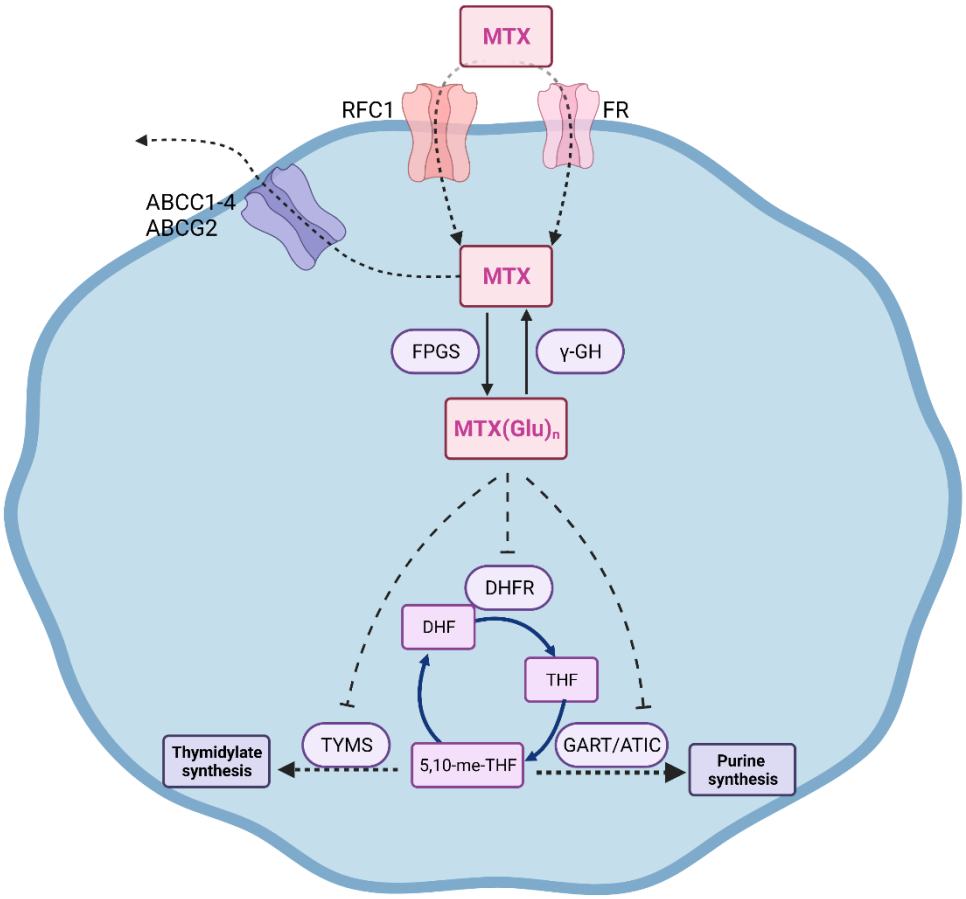

Figure 1-7: Mechanism of action of MTX. Methotrexate (MTX) enters the cell mainly through the reduced folate carrier (RFC-1) and to a lesser extend through receptor-mediated endocytosis via a folate receptor (FR). Upon entry, MTX gets polyglutamated ($MTX(Glu)_n$) by folylpolyglutamate synthase (FPGS). Polyglutamates of MTX are a superior antifolate agent compared to MTX, capable of highly potent irreversible inhibition of DHFR. Furthermore, MTX induces inhibition of other enzymes like TYMS and GART/ATIC, ultimately blocking *de novo* thymidylate and purine syntheses. γ-glutamyl hydrolase (γ-GH) (compartmentalized in lysosomes) removes glutamate residues from MTX, while ATP-binding cassette (ABC) transporters assist in the excretion of MTX from the cell. Generated with Biorender.com

1.3.6.2 Impact of MTX on cellular homeostasis

A number of studies have aimed to further describe the mechanism of action of MTX. MTX treatment causes accumulation of AICAR leading to activation of AMPK in breast and prostate cancer cell lines[115]. Induction of AMPK through MTX was found to promote glucose uptake and lipid oxidation, as well as inhibiting protein synthesis, linking the anti-proliferative effects of MTX to AMPK activation[115-117]. Sengupta *et al*. while investigating the effect of AICAR in ALL cell lines, found that AICAR-mediates AMPK activation inhibits cell proliferation, induces cell cycle arrest and apoptosis. In addition, cells treated with AICAR exhibit activation of PI3K/Akt signalling pathway, potentially as a compensatory survival mechanism against AICAR mediated cytotoxicity, and inhibition of mTOR[118]. Beckers *et al*. suggested that MTX enhances the antianabolic and antiproliferative effects of cell permeable AICAR treatment, where MTX and AICAR were found to have a synergistic effect[119]. Similarly, Kuznetsov *et al*. demonstrated that AICAR potentiates MTX-induced ROS accumulation and consequently endoplasmatic reticulum (ER) stress. They hypothesize that AICAR in combination with MTX and in conjugation with the upregulation of PI3K/Akt pathway that inhibits AMPK, leads to prolonged cellular ER stress that ultimately results in cell death. While PI3K/Akt pathway normally exhibits a pro-oncogenic role, in this model it seems to play a proapoptotic role[120]. Furthermore, mTOR inhibitors have been found to downregulate DHFR expression and increase sensitivity to MTX both *in vitro* and *in vivo*. These findings also led to a pilot clinical trial that aimed to investigate such combination treatment in adults with relapsed ALL[121].

Papadopoli *et al*. demonstrated a similar effect when MTX was combined with biguanides (metformin, phenformin; display AMPK-dependent anti-tumourigenic effects), stimulating discussion on how biguanides can be used to improve chemotherapeutic response to antifolates. Indeed, there has been increasing interest in repurposing biguanides for cancer treatment. Interestingly, at clinically relevant concentrations, metformin was found to induce folate cofactors to become trapped as 5-formimino-THF, a cofactor that cells seem to be unable to use for 1C units, ultimately blocking DNA and RNA synthesis[122]. This antifolate behaviour of metformin can potentially present a major mechanism of its anticancer effect, linked to an AMPK-dependent anti-neoplastic response[123].

The fact that metformin behaves as an antifolate and activates AMPK might explain why it synergizes with MTX and it potentiates its effect. In addition to its antitumour activity, metformin was found to ameliorate MTX-induced hepatorenal toxicity in an *in vivo* model. Kanarek *et al*. suggested that the histidine degradation pathway also influences the sensitivity to MTX in leukaemia xenografts, suggesting that histidine dietary intervention could potentially be exploited to improve efficacy[124].

1.3.6.3 MTX and its deleterious side effects

It is worth mentioning that usually patients with ALL and lymphoma receive intravenously delivered MTX doses of 500mg/m^2 or higher, known as high-dose MTX. Such dosages are routinely used to treat CNS ALL, where conventional doses of MTX fail to protect against CNS relapse. Doses of up to 33.6g are being utilised to provide significant MTX exposure in sites like CNS[125-128]. High-dose MTX and can have adverse effects in patients, leading to significant morbidity and even mortality[129]. Toxicity is primarily caused by delayed MTX excretion and persistent high plasma MTX levels as a result of MTX-induced renal dysfunction[130]. Gastrointestinal mucosal injury, BM suppression, renal or liver impairment are some of the adverse effects caused by high-dose MTX[131, 132]. Nilsson and colleagues showed that DHFR and TYMS are expressed in many proliferating tissues, in which the adverse effects of MTX are observed[133]. In agreement with the DHFR and TYMS expression pattern, MTX has been shown to accumulate in BM cells and intestinal mucosa both *in vitro* and *in vivo*. Even though malignant cell lines have shown a markedly greater capacity to convert MTX to polyglutamates, emergence of MTX polyglutamates is dose and time dependent, thus making highly replicating cells, with high demands of purine and thymidylate synthesis susceptible to MTX toxicity[134-137]. Furthermore, Barredo and Moran described that FPGS activity is linked to proliferation rate and differentiation stage. In other words, highly proliferating tissues and immature cells exhibit an increased activity of FPGS[138]. These findings can give some clues about the susceptibility of these tissues to antifolates; however, it would be interesting to further assess differences of FPGS, FPGH activity, expression of MTX influx and efflux transporters between malignant cells and other highly proliferating cells.

1.3.6.4 Resistance to MTX

Another issue that arises with MTX treatment is drug resistance. Mutations in RFC-1, amplification, or mutation of DHFR, and loss of polyglutamation have been shown to contribute to the loss of efficacy[113, 139, 140]. Apart from acquired resistance to MTX, frequently associated with mutations to RFC-1 or amplification of DHFR, an interesting aspect is the intrinsic resistance. Even though AML cell lines show high sensitivity to MTX blast cells from patients with AML appear to be less able to form long-chain polyglutamates compared to blast cells from ALL patients, making them unable to retain substantial amounts of MTX[141]. This inability to form long-chain polyglutamates has been linked to increased expression of ABC efflux transporters, low activity of FPGS and high activity of γ-GH, responsible for the degradation of the glutamate side chain[142-144]. Interestingly, a number of studies have described that even though AML blasts exhibit poor intracellular MTX polyglutamylation, MTX polyglutamylation in samples from acute monocytic leukaemia patients (AML-M5) and acute megakaryocytic leukaemia (AML-M7) patients is comparable to paediatric B-ALL patient samples[145, 146]. Rots *et al*. observed poor MTX polyglutamylation in AML-M5 samples, but an increased sensitivity to MTX compared to AML-nonM5[147]. Further investigation with regards to MTX polyglutamylation in AML-M5 is required to evaluate the possible use of MTX as a treatment. However, intrinsic resistance is a noteworthy issue, as it points to the critical need of new ways to target 1C metabolism that could potentially overcome the need for intracellular polyglutamylation. Pralatrexate (PDX), a MTX analogue, was designed to have improved cellular transport via RFC-1 and enhanced formation of polyglutamates, resulting in greater intracellular retention[148]. In 2009, PDX was approved for the treatment of relapsed or refractory T-cell lymphoma and in a recent study it was shown to have anti-tumour activity in preclinical models of multiple myeloma (MM)[149]. Additionally, pemetrexed, another anti-folate that shows high affinity for both DHFR and TYMS, was described to cause cell cycle blockage and consequently apoptosis in MM cells *in vitro* and also in animal models *in vivo*[150]. However, pemetrexed and pralatrexate target predominantly DHFR implying that they can have similar limitations regarding toxicity in normal tissues and drug resistance as MTX.

1.3.6.5 Novel strategies to target folate metabolism

A number of recent studies have tried to reveal novel strategies to target 1C metabolism. Nilsson *et al*. demonstrated that among 1,454 metabolic enzymes examined, MTHFD2 is the most consistently overexpressed in tumours, while SHMT2 is the fifth[133]. Vazquez and colleagues proposed that expression of mitochondrial 1C metabolism enzymes determine the response to MTX[151]. On that note, García-Cañaveras *et al*. showed that a dual inhibitor of SHMT1/2, synergizes with MTX both *in vitro* and *in vivo*. More specifically, as a single agent it inhibited the proliferation of T-ALL cell lines and increased survival in NOTCH1-driven mouse T-ALL models. Furthermore, it sensitized MTX-resistant human T-ALL cells[152]. In support of this study, Pikman *et al*. showed that T-ALL cell lines that had developed resistance to MTX, remain sensitive to dual inhibition of SHMT1/2. The authors also demonstrated that loss of both SHMT1 and SHMT2 activity was required for the anti-proliferative effect that was observed, whereas repression of each enzyme alone was not enough to elicit such an effect[153]. The findings reported reinforce the idea that there is a redundancy between SHMT1 and SHMT2 and one can compensate for the loss of the other. Thus, to block production of 1C units from serine, simultaneous inhibition of both enzymes is necessary. The synergistic effect of MTX with SHMT inhibitors could be a result of the depletion of THF (SHMT substrate) by MTX, therefore sensitizing cells to SHMT inhibition. In MTX resistant cells, decrease of MTX polyglutamates due to decreased RFC1 or FPGS activity or increased γ-GH would result in decrease of THF-polyglutamates, as folate has a similar influx mechanism and polyglutamation pattern. Therefore, a decrease in THF-polyglutamates due to the MTX resistance would deplete the substrate of the SHMT reaction and make cells sensitive to SHMT inhibitors.

In the context of lymphoma, diffuse large B-cell lymphoma was shown to have a defective glycine import, making it sensitive to pharmacological SHMT inhibition[154]. This effect is explained by the fact that inhibition of mitochondrial metabolism makes cells glycine auxotrophs, depending on extracellular glycine uptake. In such circumstances, inhibition of the mitochondrial compartment would be enough to sensitize cells, as the cytosolic compartment cannot compensate for the lack of mitochondrial glycine production, as we previously mentioned. Lometrexol, an antifolate that targets GART, was found to have high

affinity for SHMT2[155]. Selective SHMT2 inhibitors could be useful for the treatment of malignancies like diffuse large B-cell lymphoma where glycine uptake is impaired and cancer cells are solemnly depending on mitochondrial 1C metabolism for glycine production. Lastly, it was reported that loss of MTHFD2 impairs growth and induces differentiation in AML cell lines and primary AML blasts, while it decreases leukaemia burden in human xenograft and MLL-AF9 mouse leukaemia models. In the same study authors described that AML cell lines characterized by a FMS-like tyrosine kinase 3 internal tandem duplication (FLT3-ITD) mutation are more sensitive to loss of MTHFD2[156].

The cancer cell's response to SHMT1/2 inhibitors exhibits a metabolic pattern with many similarities to what observed for MTX. By depriving cells from 1C units and glycine, SHMT inhibitors block purine and thymidylate synthesis. SHMT inhibitors also induce an increase in AICAR and activation of AMPK, as observed for MTX[98]. This evidence suggests that SHMT inhibitors have a mechanism of action similar to traditional antifolates. Yet, by acting on a different enzyme and being independent of folate transporters, SHMT inhibitors may help to overcome resistance to MTX.

1.4 Aims of the thesis

As targeting folate metabolism has proven beneficial in several haematological malignancies, firstly, we wanted to assess the activity of the pathway in CML LSCs and whether the pathway could serve as a potential metabolic vulnerability.

Secondary, we aimed to uncover the cellular effects elicited by inhibition of the pathway by using both pharmacological and genetic approaches.

Thirdly, we aimed to investigate whether inhibition of the pathway could sensitise leukaemic cells to TKI treatment.

Overall, the aim of this investigation was to provide further insight into the importance of 1C metabolism in cancer cells using CML as a model of LSC-driven haematological malignancies and how targeting this pathway can improve traditional chemotherapeutic approaches.

Chapter 2 Materials and Methods

2.1 Materials

2.1.1 General Reagents

Product	Manufacturer	Catalogue Number
^{13}C,^{2}H-Sodium formate	Merck	1215684-17-5
2-Mercarptoethanol	Life Technologies	21985023
10x Tris/Glycine Buffer for Western Blots	Bio-Rad	1610734
Acetonitrile	VWR International Ltd	83639.32
AICAR	Stratech (ApexBio)	A8184-APE-50mg
AlbuMAX II Lipid-Rich Bovine Serum Albumin (BSA)	Gibco	11021045
Ampicillin	Sigma Aldrich	A5354-10ML
Antimycin A	Sigma Aldrich	A8674
Benzyl Alcohol	Merck	100-51-6
Blasticidin S hydrochloride	Fisher Scientific	10658203
BSA insulin and transferrin (BIT) 9500 Serum Substitute	Stem Cell Technologies	9500
BsmBI Enzyme	New England BioLabs	R0580
Calcium chloride (CaCl2)	Sigma Aldrich	1023780500
Carbonyl cyanide 3-chlorophenylhydrazone (CCCP)	Sigma Aldrich	C2759
CD34 MicroBead Kit	Miltenyi Biotech	130-046-702
Cell Tak	Fisher Scientific	354240
Cell trace Violet	Life Technologies	C34557
Compensation beads	Thermo Fisher	01-2222-42
Dimethyl Sulfoxide (DMSO)	Sigma Aldrich	D2660
Dialyzed Foeatal Bovine Serum (FBS)	Gibco	A3382001
Dulbecco's Modified Eagle Medium (DMEM)	Gibco	21969-035
DNase I	Sigma Aldrich	11284923001
DNase Set - RNase free	Qiagen	79254
Dounce homogeniser	Scientific Laboratory Supplies	HOM2570
Dulbecco’s Phosphate Buffered Saline (DPBS)	Gibco	14190-094
FBS	Gibco	10500064
ECL Western Blotting substrate	Fisher Scientific	10005943
Glucose	Sigma Aldrich	G7021

Hank's Balanced Salt Solution (HBSS) (10X), calcium, magnesium, no phenol red	Gibco	14065049
HEPES	Sigma Aldrich	H3375-100G
High-Capacity cDNA Reverse Transcription Kit	Thermo Fisher Scientific	4387406
Histopaque 1119	Sigma Aldrich	11191
Human erythropoietin (EPO)	PeproTech	100-64
Human Flt3-Ligand	PeproTech	300-19
Human granulocyte colony-stimulating factor (G-CSF)	PeproTech	300-23
Human granulocyte-macrophage CSF (GM-SCF)	PeproTech	300-03
Human insulin solution	Sigma Aldrich	I9278-5ML
Human interleukin-6 (IL-6)	PeproTech	200-06
Human leukemia inhibitory factor (LIF)	PeproTech	300-05
Human macrophage inflammatory protein α (MIP-1α)	PeproTech	300-08
Human stem cell factor (SCF)	PeproTech	300-07
Human Serum Albumin	National Blood Transfusion Service	
Hydroxychloroquine Sulfate	Merck	PHR1782-1G
Hypoxanthine and thymidine (HT) Supplement (100X)	Thermo Fisher Scientific	11067030
Imatinib Mesylate	LC Laboratories	I-5508
Iscove's Modified Dulbecco's Medium (IMDM)	Gibco	21980
JC-1 Mitochondrial Membrane Potential Dye	Thermo Fisher Scientific	65-0851-38
L-Glutamine	Life Technologies	25030-024
Low density lipoprotein	Sigma Aldrich	L4646
Luciferin Monopotassium Salt	Fisher Scientific	15225733
Magnesium chloride	Sigma Aldrich	208337
Methanol	Fisher Scientific	M/4056/17
Methanol (HPLC grade)	Fisher Scientific	67-56-1
MethoCult™ H4034	Stem Cell Technologies	4034
Methyl chloroformate (MCF)	Sigma Aldrich	79-22-1
Methyl tert-butyl ether (MTBE)	Sigma Aldrich	306975-250ML

Mitochondria Isolation Kit	Thermo Fisher Scientific	89874
MitoSOX™ Red Mitochondrial Superoxide Indicator	Life Technologies	M36008
MitoTracker™ Green	Life Technologies	M46750
N-acetyl-L-cysteine (NAC)	Sigma Aldrich	A9165-25G
NuPAGE™ 4-12% Bis-Tris Protein Gels, 1.0 mm, 10-well	Life Technologies	NP0321BOX
NuPAGE™ LDS Sample Buffer (4X)	Life Technologies	NP0007
NuPAGE™ MES running buffer	Life Technologies	NP0002
Oligomycin	Sigma Aldrich	O4876-5MG
One Shot™ Stbl3™ Chemically Competent E. coli	Thermo Fisher Scientific	C737303
PageRuler™ Plus Prestained Protein Ladder	Thermo Fisher Scientific	26619
Penicillin Streptomycin	Life Technologies	15140-122
Pierce™ BCA Protein Assay Kit	Thermo Fischer Scientific	23225
Pierce™ BSA Standard Ampules, 2 mg/mL	Thermo Fischer Scientific	23209
PhosSTOP (phosphatase inhibitors)	Roche	4906845001
Polybrene Transfection Reagent	Merck	TR-1003-G
Potassium Chloride (KCl)	Thermo Fisher Scientific	10684732
Power SYBR Green Master Mix	Thermo Fisher Scientific	4368577
Pre-Separation Filters (30 µm)	Miltenyi Biotec	130-041-407
Protease inhibitors cocktail	Sigma	P8340
Puromycin Dihydrochloride	Life Technologies	12122530
PVDF Transfer Membrane	Thermo Fisher Scientific	88520
Pyridine	Sigma Aldrich	360570
QIAquick Gel Extraction Kit	Qiagen	28704
Quick Ligation™ Kit	New England BioLabs	M2200S
Rapamycin	LC Laboratories	R-5000
RNase Inhibitor	Thermo Fisher Scientific	N8080119
RNeasy Mini Kit	Qiagen	74104
Rotenone	Sigma Aldrich	R8875
Roswell Park Memorial Institute media (RPMI) 1640	Gibco	31870-025

Seahorse XF Base Medium	Agilent Technologies	102353
Separation columns	Miltenyi Biotec	130-042-401
Sigma 7-9 (Trizma® base, Tris base)	Sigma Aldrich	T1378
SHIN1	Cambridge Biosciences	HY-112066-5mg
Sodium bicarbonate (NaHCO3)	Sigma Aldrich	S5761
Sodium cloride (NaCl)	Sigma Aldrich	S5886
Sodium dodecyl sulfate (SDS)	Sigma Aldrich	L5750
Sodium formate	Sigma Aldrich	247596-500G
Sodium hydroxide (NaOH)	Sigma Aldrich	S0899
Sodium phosphate dibasic dihydrate (Na2HPO4 · 2H2O)	Sigma Aldrich	10028-24-7
Sodium pyruvate	Gibco	11360070
SuperSignal™ West Femto Maximum Sensitivity Substrate	Thermo Fisher Scientific	34094
SYBR™ Safe DNA Gel Stain	Thermo Fisher Scientific	S33102
T4 Polynucleotide Kinase	New England Biolabs	M0201S
TaqMan™ Fast Advanced Master Mix, no UNG	Thermo Fisher Scientific	A44360
Trypsin-EDTA (0.05%), phenol red	Thermo Fisher Scientific	25300054
Tween 20	Sigma Aldrich	P9416-100ML
Seahorse XFe96 FluxPak (includes calibrant)	Agilent Technologies	102416-100
Transferrin	Sigma Aldrich	T4132-100MG

2.1.2 Western Blot Antibodies

Product	Manufacturer	Catalogue Number
Primary antibodies		
ß-tubulin	Cell Signaling Technology	2146S
ACC	Cell Signaling Technology	3662S
AMPKα	Cell Signaling Technology	2535S
ATG13	Cell Signaling Technology	13468S

ATG7	Cell Signaling Technology	8558S
DRP1	Cell Signaling Technology	5391S
GAPDH	Cell Signaling Technology	5174S
HSP90	Proteintech	60318-1-Ig
LC3B	Cell Signaling Technology	2775S
MFN2	Cell Signaling Technology	11925S
MTOR	Cell Signaling Technology	2983S
NIX	Cell Signaling Technology	12396S
P62	BD Biosciences	610833
p-ACC^{Ser79}	Cell Signaling Technology	3661S
p-AMPKα^{Tyr172}	Cell Signaling Technology	2531S
p-ATG13^{Ser355}	Cell Signaling Technology	46329S
p-MTOR^{Ser2448}	Cell Signaling Technology	2971S
p-S6$^{Ser240/244}$	Cell Signaling Technology	5364S
p-ULK1^{Ser555}	Cell Signaling Technology	5869S
p-ULK1^{Ser757}	Cell Signaling Technology	6888S
S6	Cell Signaling Technology	2317S
SHMT2	Cell Signaling Technology	33443S
ULK1	Cell Signaling Technology	8054S
UQCRFS1	Proteintech	18443-1-AP
Secondary antibodies		
Anti-mouse IgG, HRP-linked	Cell Signaling Technology	7076S
Anti-rabbit IgG, HRP-linked	Cell Signaling Technology	7074S

2.1.3 Flow Cytometry Antibodies

Product	Manufacturer	Catalogue Number
7-ADD	BD Biosciences	559925
APC Anti-Human Annexin V	BD Biosciences	550475
APC Anti-Human CD34	BD Biosciences	555824
APC Anti-Human CD71	Biolegend	334108
FITC Annexin V	BioLegend	640906
PE Anti-Human CD11b	BioLegend	301306
PE Anti-Human CD133	Milteney Biotec	130-113-108
PE Anti-Human CD235a (Glycophorin A)	BioLegend	349106
PE Anti-Human CD71	BD Biosciences	555537
PerCP/Cy5.5 Anti-Human CD235a (Glycophorin A)	BioLegend	349110

2.1.4 Quantitative polymerase chain reaction (PCR) primers

Name of gene	Supplier	Catalogue Number
Human ACTIN	Thermo Fisher Scientific	Hs99999903_m1
Human ATG5	Thermo Fisher Scientific	Hs00355494_m1
Human ATG7	Thermo Fisher Scientific	Hs00197348_m1
Human BNIP3	Thermo Fisher Scientific	Hs00969291_m1
Human NIX/BNIP3L	Thermo Fisher Scientific	Hs01087963_m1
Human SQSTM1/P62	Thermo Fisher Scientific	Hs00177654_m1
Human ULK1	Thermo Fisher Scientific	Hs00177504_m1
Eukaryotic 18S	Thermo Fisher Scientific	4333760T

2.1.5 CRISPR Guides

Gene	Targeting Sequence
AMPKα1	5′-GAAGATCGGCCACTACATTC-3′
AMPKα2	5′-GAAGATCGGACACTACGTGC-3′
ATG7	5′-GAAGCTGAACGAGTATCGGC-3′
SHMT2	5′-GGACAGGCAGTGTCGTGGCC-3′
ULK1	5′-AGCAGATCGCGGGCGCCATG-3′

Of note, targeting sequences for AMPKα1 and AMPKα2 were adapted from Toyama and colleagues[157]. Targeting sequence for SHMT2 was firstly described by Ducker and colleagues[89]. Targeting sequences for ATG7 and ULK1 were designed and generated by Dr Angela Ianniciello using the optimised tool https://zlab.bio/guide-design-resources.

2.1.6 Cell lines

All cell lines (K562, KCL22, THP1, MOLM12 and HEK293FT) were available in-house. All cell lines were routinely tested for mycoplasma contamination.

2.1.7 Primary Cells

Sample ID	BCR-ABL Status	Disease State	Text/figure reference
CML 340	+	Chronic Phase	CML #1
CML 343	+	Chronic Phase	CML #2
CML 399	+	Chronic Phase	CML #3
CML 480	+	Chronic Phase	CML #4
CML 484	+	Chronic Phase	CML #5
HIP 7	-	N/A	Normal #1

HIP 9	-	N/A	Normal #2
HIP 14	-	N/A	Normal #3

2.1.8 Equipment

Name	Supplier
7000 Series Triple Quadrupole MS System	Agilent
7890A GC system	Agilent
Biochemistry Analyser	YSI
CASY Cell Counter and Analyser	Roche
CFX96 Touch Real-Time PCR Machine	Bio-Rad
FACS Verse	BD Biosciences
Infinite M200 Pro Plate Reader	Tecan
IVIS Spectrum In Vivo Imaging System	Perkin Elmer
Nanodrop 2000	Thermo Fisher Scientific
Odyssey FC	LiCor
Peltier Thermal Cycler PTC 225	MJ Research
Q Exactive Orbitrap MS sysytem	Thermo Fisher Scientific
Seahorse XFe96 Analyser	Agilent
Ultimate 3000 HPLC System	Thermo Fisher Scientific

2.2 Composition of Buffers and Cell Culture Media

Complete RPMI

Name	Final concentration
RPMI 1640	N/A
FBS, heat inactivated	10%
L-Glutamine	2mM
Penicillin-Streptomycin (Pen/Strep)	100 IU/mL

Complete DMEM

Name	Final concentration
DMEM 1X With sodium pyruvate	N/A
FBS, heat inactivated	10%
L-Glutamine	2mM
Pen/Strep	100 IU/mL

Serum free media (SFM)

Name	Final concentration
IMDM	N/A
BIT (BSA/Insulin/Transferrin)	20%
2-Mercaptoethanol	0.2%
Low Density Lipoprotein	40µg/ml
L-Glutamine	2mM
Pen/Strep	100 IU/mL

SFM supplemented with physiological growth factors (φGF)

Name	Final concentration
SFM	N/A
SCF	0.2ng/ml
IL-6	1ng/ml
G-CSF	1ng/ml
GM-CSF	0.2ng/ml
MIP-a	1ng/ml
LIF	0.05ng/ml

DAMP solution

Name	Final concentration
DPBS	N/A
Magnesium Chloride	1M
Trisodium Citrate	0.155M
Human Serum Albumin	0.2
DNase I	2500U/ml

Plasmax (primary cells)

On the day of the experiment, glucose-free Earle's Balanced Salt Solution (EBSS) was supplemented with amino acids, vitamins, salts, trace elements and uric acid to obtain Plasmax as described by Vourde *et al*[158]. Plasmax was further supplemented as follows:

Name	Final concentration
Plasmax base media	N/A
L-Glutamine	0.65mM

Pyruvate	100µM
Pen/Strep	100IU/mL
AlbuMAX II Lipid-Rich BSA	0.50%
Insulin	10µg/mL
Transferrin	7.5µg/mL
2-Mercaptoethanol	0.2%
φGF cocktail	as described

Seahorse XF Media (Mito Stress Test)

Name	Final concentration
XF Seahorse Base Media	N/A
Glucose	11.1 mM
L-Glutamine	2mM

Seahorse XF Media (Glyco Stress Test)

Name	Final concentration
XF Seahorse Base Media	N/A
L-Glutamine	2mM

Protein Lysis Buffer

Name	Final concentration
RIPA Buffer	N/A
PhosphoSTOP	10%
Protease Inhibitor	10%
SDS	10%

10x TBS (pH=7.5)

Name	Recipe for 1L
H_2O	1L
Tris	60.5g
NaCl	87.6g

TBST

Name	Recipe for 1L
H_2O	900ml
10x TBS	100ml
Tween20	1ml

Blocking buffer

Name	Final concentration
TBST	N/A
BSA	2%

2X HEPES-Buffered Saline (HBS) (pH=7.0-7.1)

Name	Recipe for 500ml
H_2O 480ml	480ml
NaCl 8g	8g
KCl	0.37g
Glucose	1g
HEPES	5g
$Na_2HPO_4*7H_2O$ (100x)	500µl

2x $CaCl_2$

Name	Recipe for 500ml
H_2O	500ml
$CaCl_2*2H_2O$	147g

2.3 Methods

2.3.1 Primary samples

2.3.1.1 Primary samples origin

All patient samples were kindly donated with ethical approval and informed consent (REC 10/S0704/60 & REC 15/WS/0077). CML samples were obtained from CP-CML patients (Ph+) and were products of leukaepheresis at the time of diagnosis, before TKI treatment. Normal samples were surplus cells collected from femoral head BM, surgically removed from patients undergoing hip replacement.

2.3.1.2 Histopaque separation of human BM cells

Surplus normal femoral head BM was prepared by crushing in PBS and passed through a 0.2μm cell strainer to remove any cartilage. The suspension was centrifuged at 400xg for 10min. The pellet was suspended in 7ml PBS and transferred into a falcon tube containing 8ml of histopaque. To isolate white blood cells, the BM was separated in a histopaque density gradient by centrifuging for 30min at 400xg, with the brake removed. The mononuclear cell layer was then transferred into a new falcon tube, topped up with PBS and centrifuged for 10min at 400xg.

2.3.1.3 Isolation of $CD34^+$ cells

Isolation of $CD34^+$ cells from CML samples was performed by Dr Alan Hair, while isolation of normal $CD34^+$ was performed in Helgason lab. CD34 Microbead Kit (**2.1.1**) was used to isolate $CD34^+$ on both occasions. In brief, after centrifuging mononuclear cell layer for 10min at 400g (**2.3.1.2**), cells were resuspended in 300μL PBS and 100 μl FcR blocking reagent. 100μL of CD34 Microbeads were added to the mixture, which was left for 30min at 4°C. Cells were washed in PBS, centrifuged for 10min at 300g and resuspended in 500μL of PBS. Freshly resuspended cells were added to the magnetic column for separation. After three washes, the magnetically labelled cells were collected by pushing the plunger into the column.

2.3.2 Cell culture

2.3.2.1 Cell lines and primary cells maintenance in culture

CML (K562 and KCL22) and AML (THP1, MOLM13) cell lines were cultures in complete RPMI (**2.2**) at 5% CO_2, 37°C. Cells were passaged every 2 days and maintained at 0.2-0.3x10^6 cells/ml. K562 and KCL22 SHMT2 KO cells were cultures in RPMI supplemented in 1% hypoxanthine and thymidine (HT) supplement. Supplement was removed prior to any experimental procedures. HEK293FT were cultures in complete DMEM (**2.2**). They were passaged every 2 days with the addition of trypsin-EDTA to detach cells from plastic and maintained at 0.5x10^6 cells/ml. Primary normal/CML $CD34^+$ cells were cultured in SFM+φGFs (2.2) in non-adherent tissue culture flasks. Primary cells were seeded at concentration of 1.0x10^6 cells/ml for overnight recovery after thawing.

2.3.2.2 Cryopreservation of cell lines and primary cells

Cell lines were cryopreserved by suspending cell pellets in a freezing medium containing 90% FBS with 10% DMSO. Primary cells were suspended in a medium containing 50% FBS, 40% IMDM and 10% DMSO. The cell suspensions were transferred to cryopreservation vials and quickly transferred to -80°C. After 24hours (h), cryovials were transfer into liquid nitrogen containers.

2.3.2.3 Recovery of cell lines and primary cells

Cell lines were recovered by being placed in a 37°C water bath for approximately one minute. Cells were then washed in pre-warmed complete media (**2.2**) to remove DMSO and then allowed to recover in culture overnight.

Frozen human primary cells were similarly placed in a 37°C to remove ice crystals and then washed with DAMP solution (**2.2**). 10ml DAMP solution was added in a dropwise manner over 20min. Cells were than centrifuged and the dropwise addition of DAMP was repeated 2x. DAMP solution was removed by centrifugation at 300xg for 10min. Cells were then suspended in SFM+φGFs (**2.2**) and left to recover overnight.

2.3.2.4 Drug preparation

SHIN1, the 1C metabolism inhibitor, was dissolved in DMSO at a concentration of 5mM and the stock solution was stored at -20°C for a maximum of 3 months. Formate was dissolved in water at a concentration of 1M and was stored at 4°C for a maximum of one month. AICAR was dissolved in water at a concentration of 50mM and stored at -20°C for a maximum of 3 months. Stock of imatinib was prepared in water at a concentration of 1mM and was stored at 4°C for a maximum of 3 months.

2.3.2.5 Cell line growth rate

K562, K562 SHMT2 KO +/- 1% HT supplement were plated at $5x10^4$ cells/ml in 3ml of RPMI and cultured for 72hr.Cell counts were obtained at 24h intervals using the CASY automated cell counter.

2.3.3 Flow cytometry

2.3.3.1 Cell cycle analysis

Propidium iodide (PI) was used to assess DNA content and deduce the cell cycle stage the cells were at prior to fixing. In brief, PI is a membrane impermeant dye that binds in proportion to the amount of DNA present in the cell. For example, cells in the S phase have more DNA content than cells in G1 phase, therefore, they will take up proportionally more dye and will fluoresce more brightly. Cell in G2 phase will have doubled their DNA content and will be approximately twice as bright as cells in G1.

Cells were washed in PBS and fixed by adding 70% ice-cold ethanol dropwise while gently vortexing. Vortexing is necessary to prevent cell clumping. Fixed cells were left for a minimum of 30min at 4°C. Cells were then washed twice in PBS and spinned at 400g for 5min. As PI is capable of staining RNA, to ensure that only DNA was stained, cells were treated with 2µl of 100µg/ml RNase. Lastly, 200µL of PI (50µg/ml) were added to the cells and then cells were analyses using the FACS Verse.

Cell cycle analysis was done using FlowJo V10.7. To determine each cell cycle phase accurately, the geometrical mean intensity of the PI dye was used (**Figure** 2-1). G2/M phase was calculated to be with almost double the geometrical mean intensity of G0/G1.

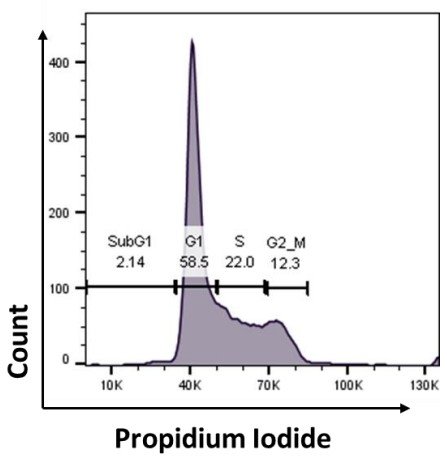

Figure 2-1: Propidium iodide (PI) gating strategy to assess cell cycle. Geometrical mean intensity of PI dye was calculated to separate different cell cycle phases.

2.3.3.2 Apoptosis assay

Translocation of phosphatidylserine to the outer cell membrane is an early indicator of apoptosis. This can be measured by annexin V, a calcium-dependent phospholipid-binding protein that has a high affinity for phosphatidylserine. Annexin V staining combined with a cell impermeable viability dye, 7-ADD, allows for staining of apoptotic cells. Annexin V^+ 7-ADD^+ cells are considered to be in late apoptosis, while Annexin V^+ 7-ADD^- cells are considered to be in early apoptosis.

Apoptosis was assessed in both cell lines and CML $CD34^+$ cells. For cell lines, $2x10^5$ cells were washed twice with PBS and then 3µl of 7-ADD and 3µl Annexin V (APC) were added in a total volume of 50µl of HBSS $Ca2^+$ $Mg2^+$. For primary cells, 5µl of 7-ADD and 5µl Annexin V (FITC) were used to stain $2x10^5$ cells in a total volume of 50µl HBSS $Ca2^+$ $Mg2^+$. Staining was conducted in the dark, at room temperature (RT) for 15-20min. Following staining, an additional 200µl HBSS was added to each sample and subjected immediately to flow cytometry analysis.

2.3.3.3 Erythroid maturation analysis

Expression of erythroid maturation markers was assessed in K562 cells and CML $CD34^+$ cells. K562 cells tend to undergo erythroid differentiation when treated with a variety of compounds and are considered to be a useful *in vitro* model to study erythropoiesis. CML $CD34^+$cells were cultured in SFM media with the addition of low units of EPO (3U/ml) to sensitise cells to erythroid differentiation. To assess erythroid differentiation glycophorin A (GlyA) and CD71 markers were used. Both GlyA and CD71 are well-known erythroid markers.

K562 ($2x10^5$ cells) cells were washed twice with PBS and then stained with 3µL of CD71 (PE) and 3µL of GlyA (PerCP/Cy5.5) in a total volume of 50µL PBS. For CML $CD34^+$cells, 3µL of CD71 (APC) and 3µL of GlyA (PE) were used to stain $2x10^5$ cells in 50µL PBS. Staining was conducted in the dark, at RT for 20min.Cells were then washed in 1ml of PBS ensure removal of the fluorescent probes and then resuspended in 300µL of PBS prior to flow cytometry analysis.

2.3.3.4 Myeloid maturation analysis

Expression of the monocytic cell surface marker CD11b was assessed in AML cell lines THP1 and MOLM13. Increased expression of CD11b correlates with differentiation into the myeloid lineage. $2x10^5$ THP1 and MOLM13 cells were stained with 3µL of CD11b (PE) in 50µL of PBS for 20min in RT in the dark. Cells were washed with PBS and suspended in 300µL of PBS prior to being analysed with the FACS Verse.

2.3.3.5 Mitochondrial ROS

MITOSOX Red was used to assess mitochondrial ROS levels in K562 cells. MitoSOX Red is a permeable dye that selectively targets mitochondria due to the presence of a triphenylphosphonium cation. Its oxidation due to the presence of superoxide in the mitochondria produces red fluorescence.

Approximately $3x10^5$ K562 cells were stained with 5µM MITOSOX Red in 1ml of PBS. Cells were incubated for 30min at 37°C and 5% CO_2, in the dark. Cells were then washed with PBS and suspended in 300µL PBS and analysed using the FACS Verse flow cytometer.

2.3.3.6 Mitochondrial content

Mitotracker Green is a cell-permeant dye that accumulates selectively in mitochondria. Its fluorescence correlates directly to the mitochondrial content of the cell.

To assess mitochondrial content in K562 cells, approximately $3x10^5$ cells were stained with 100nM of mitotracker green and were incubated for 30min at 37°C and 5% CO_2, in the dark. Cells were then washed with PBS and suspended in 300µL PBS. The cell suspension was then immediately subjected to flow cytometry analysis.

2.3.3.7 Mitochondrial membrane potential

To assess mitochondrial membrane potential, a potential-dependent dye, JC-1, was used. The monomeric version of the probe exhibits green fluorescence emission, while when JC-1 aggregates are formed, the emission shifts to red. The ratio of red/green fluorescence intensity can give indications about the status of the mitochondrial membrane potential.

K562 cells were stained with 2µM of the JC-1 probe and were incubated at 37°C, 5% CO_2, for 20-30min. Cells were washed and resuspended in 300µL PBS. Cell suspension was analysed using the FACS Verse flow cytometer.

2.3.3.8 Cell trace violet (CTV) proliferation assay

CTV is a fluorescent dye that covalently binds intracellular amino acid residues. CTV can be retained for long periods and is not transferred during cellular division. Thus, every time a population of cells divide, there will be a loss of the dye, and hence fluorescence, which can be monitored by flow cytometry.

At day 0, CML $CD34^+$ cells were stained with 1µM of CTV dye for 30min at 37°C. The reaction was quenched by adding cell culture media containing 10% FBS and cells were subjected to flow cytometry analysis. This measurement was considered as CTV^{max}. Cells were then washed and suspended in Plasmax media (**2.2**). The number of $CD34^+$ cells used to establish each culture were recorded. After the 72h culture period, the total number of cells harvested from each

culture condition was also recorded. Fluorescence was analysed by flow cytometry, as measured by sequential dilution of the CTV dye. CTV analysis was conducted using FloJo 10.7. Each division was gated using the geometric mean fluorescence intensity to determine the divisions, with each subsequent division having half the fluorescent intensity of the previous division (**Figure** 2-2). Percentage recovery of input cells in each peak was then calculated by dividing the absolute number of total cells in each peak on day 3, corrected for cell division, by the total number of input CD34+ cells and multiplying by 100% (**Table 1**).

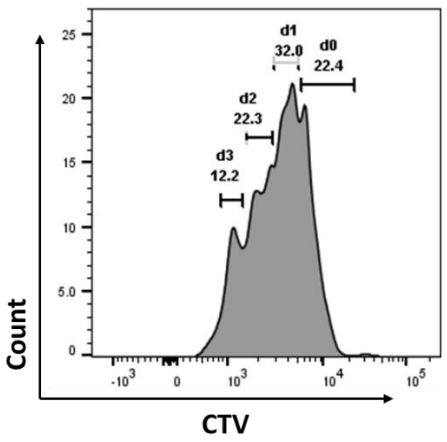

Figure 2-2: CTV gaiting strategy to assess proliferation of CML CD34$^+$ cells. Division 0 to Division 3 (D0-D3) measured as dilution of the fluorescence intensity of the CTV dye.

Input (Day 0)	Output (Day 3)	% of UD CD34$^+$	% of Div 1 CD34$^+$	% of Div 2 CD34$^+$	% of Div 3 CD34$^+$
CD34$^+$ Cell no. (x 10 ^{5})	CD34$^+$ Cell no. (x 10 ^{5})				
1.5	5	11	22	35	10.1
	Calculate how many cells in each division (x10 ^{5})	0.55	1.1	1.75	0.505
	Correct for cell division (eg if 1 cell has divided twice the CTV die has been diluted 4 times)	0.55	0.55	0.4375	0.063125
	% of recovery of input	36.66666667	36.66666667	29.16666667	4.208333333

Table 1: Example of calculations for the percentage recovery of input.

2.3.3.9 Expression of stem cell markers in primary cells

Expression of stem cell markers CD34 and CD133 was assessed in CML samples. For isolation and quantification of rare CML LSCs we interchangeably use the accepted stem cell markers CD38 and CD133, in combination with CD34. In our experience, the drawback of using CD38 as a stem cell marker is that its expression ranges from low to high (making clear separation challenging) and the

expression levels rapidly diminish in cell culture. Therefore, our preferred option is to use CD133, in combination with CD34, which we have shown to be highly enriched in the quiescent cell population[66]. Importantly, $CD34^{+}CD133^{+}$ CML cells have been shown to be enriched following TKI therapy[64, 67]. CML cells ($2x10^5$ cells) were stained with 3µL of CD34 (APC) and 3µL of CD133 (PE) in a total of 50µL PBS. Cells were stained at RT for 20min in the dark. Following staining, cells were washed and resuspended in 300µl PBS. Samples were subjected immediately to flow cytometry analysis.

2.3.4 Western blotting

2.3.4.1 Mitochondrial Isolation

Isolation of mitochondrial-enriched fractions from K562 cells was performed with the Thermo Mitochondrial Isolation Kit (**2.1.1**). In brief, 800µL of the mitochondria isolation reagent A containing protease inhibitors was added to $20x10^6$ pelleted cells. Cells were then homogenised on ice using a dounce homogeniser (2.1.22.1.1). 60-80 strokes were performed to ensure effective lysis of the cells. Lysed cells were returned to a 2ml tube and 800µL of mitochondria isolation reagent C containing protease inhibitors was added. Tubes were centrifuged at 700xg for 10min at 4°C. The supernatant was transferred to a new 2mL tube and centrifuged at 3000xg for 15min at 4°C. The supernatant (cytosol-enriched fraction) was transferred to a new tube, while the pellet containing the mitochondrial-enriched fraction was centrifuged at 12,000xg for 5min at 4°C. The supernatant was discarded, and the pelleted mitochondrial-enriched fraction was kept on ice for downstream processing.

2.3.4.2 Protein lysis with RIPA buffer

Cells from different conditions were counted and collected in falcon tubes. They were washed once with ice-cold PBS and transferred to 1.5mL Eppendorf tubes for a second wash with ice-cold PBS. Cell pellets and mitochondrial-enriched fractions (**2.3.4.1**) were thoroughly suspended in RIPA lysis buffer (**2.2**) to achieve a concentration of lysed cells of 2.5-5 x 10^6 cells/ml. Tubes were kept on ice for a minimum of 15min to ensure proper lysis of the cells and were centrifuged at 16,000xg for 15min at 4°C. The supernatant was collected and stored at -80°C until further use.

2.3.4.3 Protein quantification

Proteins were quantified using the bicinchoninic acid (BCA) assay. The BCA assay works on the principle that amino acid residues result in the reduction of Cu^{2+} to Cu^{1+} in the presence of alkaline solution. More specifically, a complex between Cu^{2+} and proteins including the amino acids cysteine, cystine, tyrosine and tryptophan will be firstly formed. In an alkaline environment, Cu^{2+} is reduced in Cu^{+}. The chelation of Cu^{1+} with BCA results in the formation of purple colour that can be read at 562nm wavelength. The intensity of the colour is proportional to the protein quantity in the sample.

For quantification, a BSA standard curve at 2μg to 0μg was generated by 1:2 serial dilution in water.10μl of each standard were plated in duplicate per well of a flat-bottomed 96-well plate. For protein samples, 2μL of lysate was plated in duplicate. The BCA solution was prepared according to manufacturer's instructions (**2.1.1**) by mixing 98% (v/v) solution A with 2% (v/v) solution B. 200μL of this solution was distributed to the 96-well plate. The plate was then incubated at 37ºC for 30min. The absorbance was then measured at 562nm using a spectrophotometer plate reader. The quantity of protein was determined by interpolating their absorbance values with the standard curve.

2.3.4.4 Sodium dodecyl sulfate polyacrylamide gel electrophoresis (SDS-PAGE)

Equal amounts of protein (10-20μg) were prepared with 4xLDS sample buffer and H_2O to a total volume of 30μL. Samples were then boiled at 95ºC for 10min to ensure protein denaturation. Samples were loaded into a pre-cast 4-12%. To estimate the molecular weight of sample proteins, 4μL of a protein molecular weight ladder from 10-250kDa was loaded into the first well of the gel. Gels were run with 1X running buffer (Thermo Fisher Scientific) at 120V until desired separation was achieved in a mini-cell electrophoresis system.

2.3.4.5 PVDF transfer

Following the SDS-PAGE, proteins were transferred to a PVDF membrane using a "sandwich" wet transfer system. PVDF membrane was firstly activated in methanol for 5min at RT and then a "sandwich" was assembled as follows: from

cathode (-) - 1 sponge – 2 paper Whatman – polyacrylamide gel – PVDF membrane – 2 paper Whatman – 1 sponge – anode (+). The sandwich was placed in the transfer tank with 1X Bio-Rad transfer buffer and proteins were transferred from the gel to the membrane at 400mA for 1h and 30min.

2.3.4.6 Immunoblotting

The membrane was blocked in 2% BSA solution (**2.2**) for 1h with gentle rocking. The membrane was then incubated overnight with primary antibodies diluted in blocking buffer at 4ºC. The following day, the membrane was washed 3x 5min with TBST (**2.2**) and incubated for 1h with the appropriate HRP-linked secondary antibody (1:5000 dilution). The membrane was washed a further 3 times to remove any unbound secondary antibody conjugate. Membrane was incubated with equal volumes of the luminol-enhancer and peroxide solute of the SuperSignal™ West Femto Maximum Sensitivity Substrate (Thermo Fisher Scientific) and developed using the Odyssey FC imaging system.

2.3.5 Quantitative PCR

2.3.5.1 RNA extraction from cell lines

RNA was isolated from $1x10^6$ cells using the RNeasy RNA extraction kit (Qiagen). The isolation was performed according to kit instructions. Briefly, cell pellets were lysed using the RLT lysis buffer. Consequently, lysates were mixed 1:1 with 70% ethanol, loaded to Qiagen RNA extraction columns, and centrifuged at 8000xg for 15s. The flow-through was discarded, and the columns were washed once using 350μL of RW1 washing buffer. Following the wash, DNAse digestion was performed by adding 80μL of DNAse in RDD Buffer (Qiagen) and leaving the columns for 15min at RT. After 2x washes with RPE buffer, RNA was extracted from columns by adding 30μL of nuclease free water followed by a centrifugation step at 8000xg for 1min. Finally, RNA concentration was measured with the NanoDrop 2000 Spectrophotometer (Thermo Fisher Scientific) and the RNA was stored at -80ºC until further use

2.3.5.2 Reverse transcription

cDNA was synthesised from RNA with the High-Capacity cDNA Reverse Transcription Kit (Thermo Fisher Scientific) according to manufacturer's instructions. Briefly, 1µg of RNA was mixed with random primers, dNTPs, RT buffer, RNase inhibitor, PCR-grade water and reverse transcriptase to a final volume of 20µL. Reverse transcription was performed using a thermal cycler.

2.3.5.3 Quantitative PCR

cDNA, the TaqMan advanced master mix, the primer/probe FAM set and PCR grade water were combined to a final well volume of 10µL. The PCR was performed with the following steps:

50°C 2m
95°C 10m
95°C 15s } 40X
60°C 30s
4°C ∞

Transcript levels were calculated using the –ΔCT method. –ΔCT was calculated by subtracting the threshold cycle (CT) (in technical triplicate) of the transcript of interest from the CT of the reference gene used (*18S* or *ACTIN*).

2.3.6 Generation of CRISPR-Cas9 KO cell lines

2.3.6.1 Cloning of guide RNA sequence into LentiCRISPR plasmid

Cloning of gRNA into LentiCRISPR v2 was adapted from O'Prey and colleagues[159]. LentiCRISPR v2 including either a puromycin-resistance marker (**Figure** 2-3) or a blasticidin-resistance marker (**Figure** 2-4) was digested for 2h at 37°C as indicated below:

5µg	LentiCRISPR v2
2µL	BsmBI enzyme (NEB)
5µL	10× buffer 3.1 (NEB)
XµL	deionised H2O
50µL	Total reaction volume

Digested plasmid was run in a 2% agarose gel. Digested fraction (~11kb) was gel-purified using the QIAquick Gel Extraction Kit (Qiagen). Purified product was quantified using the NanoDrop 2000 Spectrophotometer (Thermo Fisher Scientific).

Each pair of oligos (**2.1.5**) was phosphorylated and annealed as described below:

1µL	gRNA oligo forward (100 µM)
1µL	gRNA oligo reverse (100 µM)
1µL	10X T4 Ligation Buffer (NEB)
0.5µL	T4 polynucleotide kinase (NEB)
6.5µL	deionised H2O

The annealing reaction was performed in a thermal cycler (**2.1.8**).

Step 1	37ºC 30min
Step 2	95ºC 5min
	and then ramp down to 25ºC at 5ºC/min

Annealed oligos were diluted in deionised H_2O at 1:200 dilution. Digested lentiCRISPR v2 was then ligated with annealed oligos for 15min at RT as indicated below:

50ng	BsmBI digested LentiCRISPR v2
1µL	Diluted duplex oligos
5µL	2X Quick Ligase Buffer (NEB)
1µL	Quick Ligase (NEB)
XµL	deionised H_20 to reach 10µL total volume

It should be noted that to generate an AMPKα1α2 KO cell line, AMPKα1 targeting sequence was ligated with digested lentiCRISPR v2 containing puromycin-resistance marker and AMPKα2 targeting sequence was ligated with digested lentiCRISPR v2 containing blasticidin-resistance marker.

Ligation product was transformed into Stbl3 competent bacteria cells (**2.1.1**) and cultured overnight at 37°C into ampicillin-containing agar plates. Colonies

were picked and bacteria amplified by growing in 200ml lysogeny broth (LB) at 37ºC, with agitation at 225rpm, for 24h. The plasmid DNA was then isolated by using a Maxiprep kit (Qiagen).

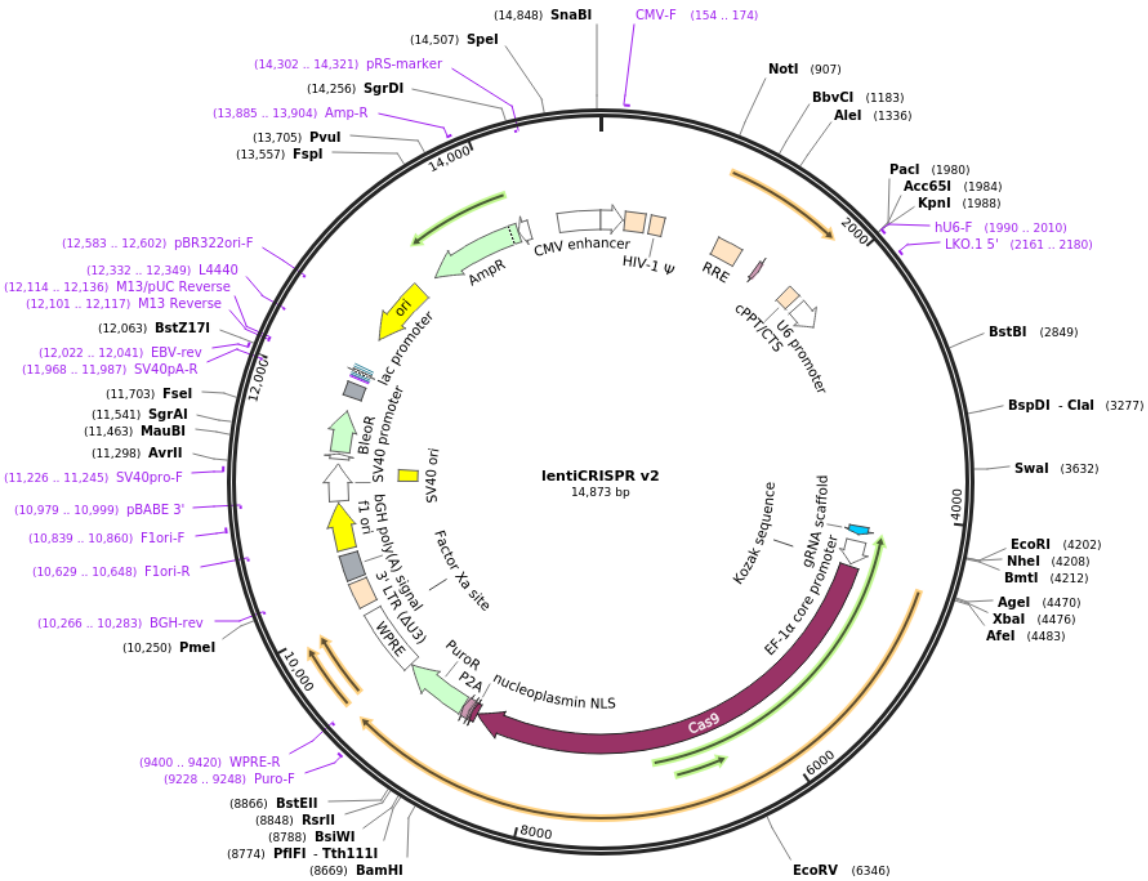

Figure 2-3:Vector map of LentiCRISPR v2 plasmid including puromycin-resistance marker (Addgene Plasmid #52961)

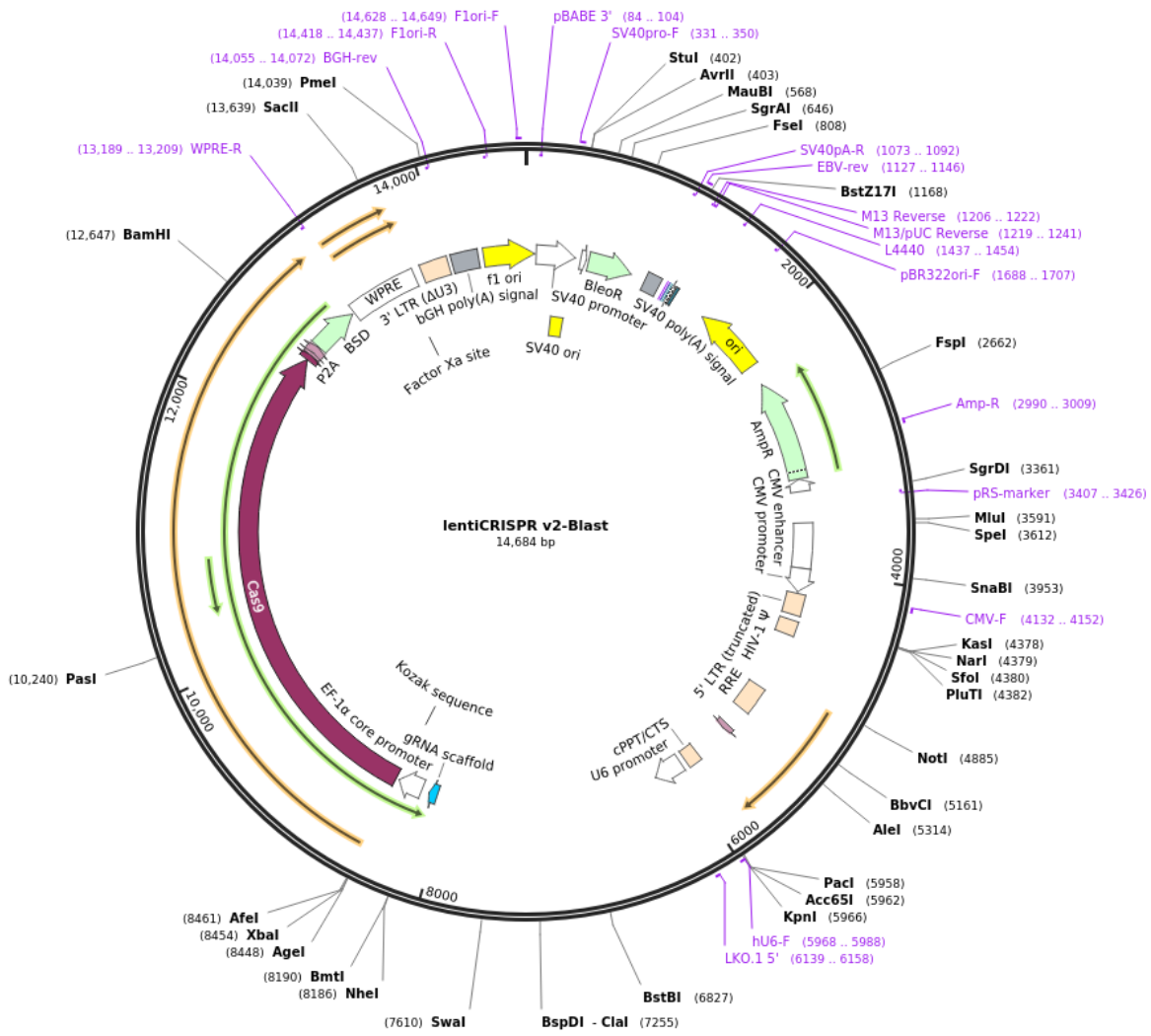

Figure 2-4: Vector map of LentiCRISPR v2 plasmid including a blasticidin resistance marker (Addgene Plasmid # 83480).

2.3.6.2 Viral production and infection of CML cells

A total of $0.5x10^6$ HEK293FT cells were plated in a $10cm^2$

cell culture petri dish and cultured for 72hr. Once cells had reached 70-80% confluency, 8.5ml DMEM was added to the cells and placed at 37ºC to incubate. At the same time, a DNA plasmid mixture was prepared in distilled water as described in **Table 2**. To the DNA mix, 183µl of $CaCl_2$ (**2.2**)was added dropwise. The solution was then vigorously mixed and 1.5ml of 2xHBS (**2.2**) added dropwise, ensuring that no crystals were formed. The solution was incubated for 30min at 37ºC.

Lentivector	14.2µg
Packaging plasmid	12.45µg
Envelope plasmid (pVSVg)	4.5µg
Distilled Water	Make up to 1317µl

Table 2: DNA mix

The DNA solution was added to the HEK293FT cells in a dropwise manner. Cells were incubated with the mix for 6-7h at 37ºC. Following incubation, medium was carefully removed and replaced with 10mL fresh DMEM medium. Medium was refreshed the following day and 48h later the medium was harvested and filtered using a 0.45µm filter. Virus particles were added to $0.5x10^6$ CML cells. The viral medium was removed by centrifugation after 24h. Cells were left to recover for 48h and then selection of CML cells with either puromycin or blasticidin was started. KO was confirmed via western blot.

2.3.7 Metabolomics

2.3.7.1 Intracellular metabolite extraction

At Day 0, CML cells were plated in different experimental condition at a concentration of $3x10^5$ cells/ml. At Day 1, cells concentration was measured with the CASY automated cell counter and cells were washed 2x with ice-cold PBS and extracted with ice-cold extraction solvent (Acetonitrile/MeOH/H_2O (30/50/20)), shaken for 5min at 4ºC, transferred into microcentrifuge tubes and then centrifuged at 18,000g for 5min. The supernatant was transferred in LC-MS

(Liquid Chromatography-Mass Spectrometry) glass vials and kept at -80ºC until measurements were performed.

2.3.7.2 LC-MS analysis

Intracellular metabolites samples were analysed by LC-MS as previously described[160]. The LC-MS set-up consisted of a Thermo Ultimate 3000 High pressure liquid chromatography (HPLC) system (Thermo Scientific) and a Q Exactive Orbitrap mass spectrometer (Thermo Scientific). The HPLC system consisted of a ZIC-pHILIC column (SeQuant, 150 x 2.1mm, 5µm, Merck KGaA), with a ZIC-pHILIC guard column (SeQuant, 20 x 2.1mm) and an initial mobile phase of 20% 20mM ammonium carbonate, pH 9.4, and 80% acetonitrile. Metabolite extracts (5µL) were injected into the system, and metabolites were separated over a 15min mobile phase gradient decreasing the acetonitrile content to 20%, at a flow rate of 200µl/min and a column temperature of 45ºC. Metabolites were then detected using the mass spectrometer with electrospray ionization and polarity switching. All metabolites were detected across a mass range of 75 - 1000m/z at a resolution of 35,000 (at 200m/z), and with a mass accuracy below 5ppm. Data were acquired using Thermo Xcalibur software. The peak areas of different metabolites were determined using the Thermo TraceFinder software. Peak areas were normalised to cell number and volume measured prior to metabolite extraction.

2.3.7.3 Formate derivatisation

Media samples from CML cells (40µL) were added in 1.5ml Eppendorf tubes, followed by 20µl of 50µM internal standard sodium $^{13}C,^{2}H$-formate (M^{+2}), 10µl of 1M sodium hydroxide, 5µl of benzyl alcohol and 50µl of pyridine. Following a 5min incubation on ice, derivatisation of formate was commenced by the addition of 20µl of methyl chloroformate (in a fume hood as gases are produced during the reaction). 200µl of H_20 and 100µl of methyl tertiary butyl ether were then added, and the sample was vortexed for 20s and centrifuged at 10,000xg for 5min. 50µl of the resulting upper layer containing formate derivative (benzyl formate) was transferred to a GC (Gas Chromatography) glass vial and stored at −80ºC until analysis. Formate standards and blank samples (water) were prepared in the same manner and analysed with the experimental samples.

2.3.7.4 GC-MS measurements

Derivatized formate samples were analyzed with an Agilent 7890B GC system coupled to a 7000 triple quadrupole MS system[160]. The column was a Phenomenex ZB-1701 column (30m × 0.25mm × 0.25µm). Samples (2µl) were injected into the GC-MS using split mode [0.5 bars; split flow (25ml/min)]. Gas flow through the column was held constant at 1.0ml of He per minute. The temperature of the inlet was 280ºC, the interface temperature was 230ºC, and the quadrupole temperature was 200ºC. Reduced electron energy (60eV) was used for analyte ionization. The column was equilibrated for 3min before each analysis. The mass spectrometer was operated in selected ion monitoring (SIM) mode between 3.0 and 4.3min with SIM masses of 136, 137, and 138 for M0, M^{+1}, and M^{+2} (internal standard) formate, respectively. MassHunter Quantitative analysis software was used to extract and process the peak areas for formate, M^{+1} formate and M^{+2} formate. After correction for background signals using formate standards and blank samples, quantification was performed by comparing the peak area of formate (m/z of 136) and of M^{+1} formate (m/z of 137) against that of M^{+2} formate (m/z of 138). To calculate the formate exchange rate integrated peak areas were normalised to proliferation rate prior to metabolite extraction. Calculations of formate concentration were conducted using media only samples as baseline. Analysis was conducted by Dr Alexei Vazquez.

2.3.7.5 Quantitative analysis of extracellular metabolites

To measure the total level of extracellular metabolites, CML cells were counted, pelleted and media was collected in Eppendorf tubes. Tubes were centrifuged at 400xg at 4ºC for 5min. Supernatant was transferred in fresh tubes. Tubes were stored at -80ºC. On the day of the analysis, 300µl of each sample were transferred to a 96-well plate. Quantity of extracellular metabolites was determined using a Biochemistry Analyzer. The Biochemistry Analyzer uses an enzyme sensor technology. When a sample is injected into the sample chamber, immobilised oxidase enzymes rapidly catalyse the oxidation of different metabolites into hydrogen peroxide. The hydrogen peroxide is amperometrically detected at the platinum electrode surface. The current flow at the electrode is directly proportional to the hydrogen peroxide concentration and hence to the

metabolite concentration. Finally, metabolite concentrations were calculated relative to media only samples (baseline) and were normalised to cell growth.

2.3.8 Seahorse metabolic assays

Seahorse XFe96 analyser (Agilent) was used to perform several live cell metabolic assays. The Seahorse analyser is instrument that can measure two parameters in the media: oxygen consumption rate (OCR) and extracellular acidification rate (ECAR). OCR is used as a readout for the cells' OXPHOS activity, while ECAR IS used as a readout for the cells' glycolytic activity.

Procedure: At Day 0, Seahorse 96 well cell plate was coated with Cell-Tak. In brief, a Cell-Tak solution at 0.02mg/mL was prepared in $NaHCO_3$, pH was adjusted to 7.4 with NaOH and 25µL of solution was added to each well. After a 30min incubation, the Cell-Tak solution was discarded, the wells were washed 2x with deionised H_20 and left to air dry at RT.

The XF96 sensor cartridge was hydrated overnight with the addition of 200µl calibrant solution to the 96-well utility plate. The cartridge was incubated at 37ºC overnight, wrapped in parafilm to prevent evaporation.

At Day 1, seahorse medium was prepared (**2.2**) and pH was adjusted to 7.4 with HCL. Cells were counted and suspended in seahorse medium for plating at 80,000 – 100,000 cells per well. Cell concentration was measured just before seeding, to allow for normalisation of the assay's results. To help cells to adhere, the plate was centrifuged at 200xg for 2min without brakes. Cells were incubated at 37ºC in a CO_2-free incubator for 30min.

To evaluate OCR, oligomycin (1µM), CCCP (1µM), rotenone (1µM) and antimycin A (1µM) were injected subsequently as illustrated in **Figure** 2-5**.** To measure ECAR, glucose (10mM), oligomycin (1µM) and 2-deoxy-glucose (2DG, 50mM) were added subsequently (**Figure** 2-6). Drugs were prepared in seahorse medium and transferred into the sensor cartridge. The sensor cartridge was loaded on the XF Instrument for calibration, followed by the cell plate for cell readings. The data obtained was then analysed using the Seahorse desktop software Wave (Agilent).

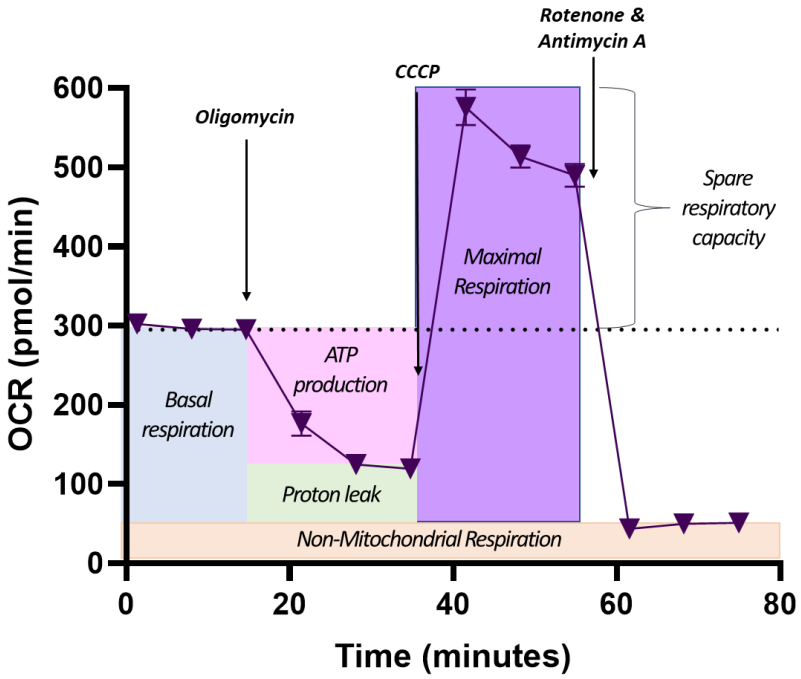

Figure 2-5: Seahorse Mito Stress Test profile. Oxygen consumption rate (OCR) of cells is measured throughout a series of injections of oligomycin to inhibit complex V of the electron transport chain, CCCP to disrupt the proton gradient and mitochondrial membrane potential followed by Rotenone and Antimycin A to inhibit complex I and III respectively.

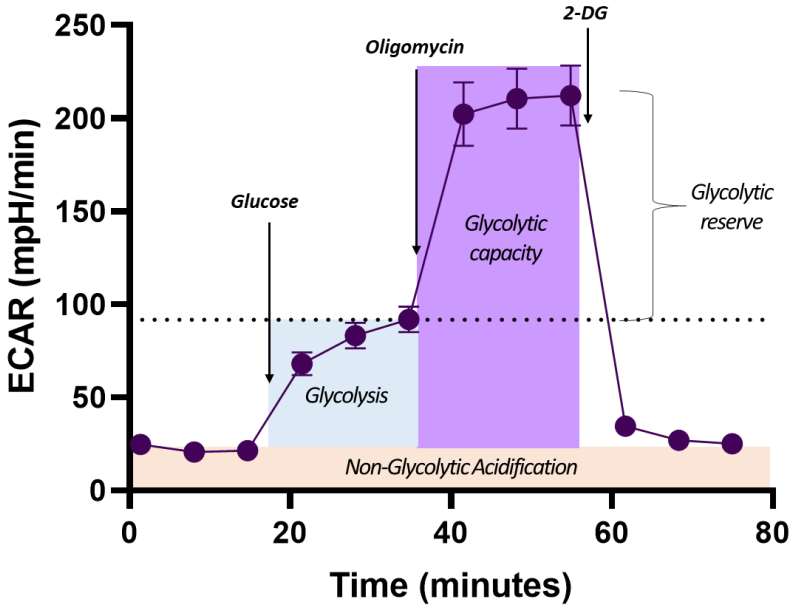

Figure 2-6: Seahorse Glyco Stress Test profile. Extracellular acidification rate (ECAR) of cells is measured throughout a series of injections of glucose to promote glycolysis, oligomycin to inhibit complex V of the electron transport chain and further promote glycolysis and 2-deoxy-glucose (2-DG), a glucose analogue, which inhibits glycolysis through competitive binding to glucose hexokinase.

2.3.9 Colony forming cell (CFC) assay

CFC assay is an *in vitro* assay commonly used in the field of haematology to assess the ability of progenitor cells to proliferate and differentiate into colonies in a semi-solid medium in response to cytokine stimulation. The number of colonies at end-point reflects the number of viable progenitors.

Primary CML and normal $CD34^+$ cells were seeded at a concentration of $3x10^5$ cells/ml in Plasmax (**2.2**) in the presence of indicated drugs. Following 72h incubation, cells from each condition were counted and 3,000 cells transferred in 1.5ml of methylcellulose-based medium and vortexed for 10sec. The methylcellulose mixture was transferred into a 6-well dish and incubated for 12-14 days at 37ºC, 5% CO_2. Colonies were then manually scored.

2.3.10 Animal work

All animal experiments were conducted in accordance with the regulations outlined by the Animals Scientific Procedures Act 1986 and UK Home Office regulations. All experiments were conducted using personal licence number I1F599357 and project licence PP2518370 held by Dr Vignir Helgason. Animals of both sexes were housed in a pathogen-free facility and kept in day/night cycles (12 hours each). Mice were fed with *ad libitum* with food and water.

2.3.10.1 NRGW^{41} mouse model

NOD.Cg- *Rag1*^{tm1Mom} *Kit*$^{W-41J}$ *Il2rg*^{tm1Wjl}/EavJ (NRGW^{41}) is an immunocompromised mouse model was established by the Eaves lab[161]. These mice do not carry the *Prkdc*^{scid} allele which increases sensitivity to ionizing radiation. These mice lack the stem cell growth factor receptor KIT, resulting in high levels of human chimerism. Lack of interleukin-2 (IL2) receptor gamma chain and recombination activating gene 1 (Rag1) results in impairment of T and B cell maturation.

2.3.10.2 KCL22-luciferase experiment

KCL22 cells were transfected by Dr Kevin Rattigan with a lentiviral plasmid carrying a firefly luciferase reporter gene and were subsequently selected using

blasticidin. CRISPR-Cas9 technology was used to generate a KCL22 luciferase$^+$ SHMT2 KO cell line. 4x10^6 KCL22 luciferase$^+$ vector control and SHMT2 KO cells were suspended in 200µL of PBS/0.5% FBS and were transplanted tail vein injection into female NRGW^{41} mice aged 8-12 weeks. To measure the efficacy of the transplantation, mice were injected with D-luciferin subcutaneously and analysed by luciferase bioimaging via the IVIS Spectrum In Vivo Imaging System (Perkin Emer) 30min after injection of the cells. In brief, firefly luciferase catalyses the oxidation of D-luciferin that is accompanied by bioluminescence emission. Tumour growth was monitored weekly using the IVIS imaging system until tumour burden reached the experimental threshold and animals were sacrificed.

2.3.11 Microarray data analysis

Publicly available microarray datasets were analysed by Mr Daniele Sarnello and Dr Zuzana Brabcova using the R software.

2.3.12 Graphical representation and statistical analysis

Data were plotted and analysed using GraphPad Prism (GraphPad Software 9.3.0). We did not use any statistical method to predetermine sample size. Data distribution was assessed using Shapiro-Wilk test. Statistical tests employed are described in figure legends. Results were considered statically different when p values ≤ 0.05.

Chapter 3 Folate metabolism is a metabolic vulnerability for LSCs

3.1 Introduction

As previously mentioned, the role of folate metabolism in CML and, more specifically, LSCs remains unknown. Work from our lab has shown that CML $CD34^+CD38^-$ stem cells have a high mitochondrial mass and activity and that they rely on OXPHOS when compared to patient matched $CD34^+CD38^+$ progenitor cells or normal HSCs[75]. Folate metabolism plays an important role in nucleotide biosynthesis, energy homeostasis and redox defence. Furthermore, several folate metabolism enzymes such as DHFR, SHMT2, SHMT1, MTHFD2 are targets of the transcriptional regulator MYC[151]. MYC is a target of BCR-ABL, and its activation has been linked to leukaemia progression. Besides this, literature has shown that folate metabolism is a metabolic vulnerability in various malignancies, including several haematological cancers. All these data are hinting on a potential role of folate metabolism in LSCs and their maintenance.

To gain a better insight into its role in LSCs, we firstly used a transcriptomic approach where we compared expression of folate associated enzymes in LSCs and HSCs, using publicly available datasets. Secondly, we assessed how their expression changes when CML cells are treated with imatinib. In addition, we used formate exchange rate and formate secretion as a measure of the activity of the pathway in patient-derived CML $CD34^+$ cells and compared to normal counterparts.

To support our *in-silico* findings, we decided to use an *in vitro* approach, and inhibit folate metabolism in K562 CML cells. Taking advantage of the CRISPR-Cas9 technology we knocked out the mitochondrial enzyme responsible for the serine to glycine conversion, SHMT2. We assessed cell proliferation and cell death of K562 cells upon loss of SHMT2. Secondly, we investigated the impact of loss of SHMT2 in an *in vivo* setting, by assessing xenograft formation. Lastly, we investigated metabolic changes following inhibition of 1C metabolism using LC-MS.

3.2 Folate metabolism associated genes are upregulated in LSCs

3.2.1 Folate metabolism is enriched in LSCs compared to HSCs

To get an insight into expression of folate metabolism associated enzymes in LSCs, we performed a computational analysis on a publicly available microarray dataset (E-MTAB-2581), containing HSCs ($CD34^+CD38^-$), normal progenitor cells (HPCs; $CD34^+CD38^+$), LSCs ($CD34^+CD38^-$) and leukaemic progenitor cells (LPCs; $CD34^+CD38^+$). LSCs and LPCs were obtained from CP-CML patients, while HSCs and HPCs from non-CML patients (patients with other haematological malignancies where the $CD34^+$ cell population is not affected), which will be referred as normal. When comparing transcriptional signatures of LSCs to HSCs, gene set enrichment analysis (GSEA) revealed that MYC targets, mTORC1 signalling, OXPHOS and fatty acid metabolism are significantly upregulated in LSCs with an normalised enrichment score (NES) between 1.7-2.0, when compared to HSCs **(Figure** 3-1**a**). Upregulation of such processes reinforces the idea that LSCs are more metabolically active than HSCs. As we mentioned in the **Introduction** of this chapter, enzymes of the folate pathway are transcriptionally regulated by MYC. Indeed, when taking a closer look to pathways upregulated in LSCs, folate metabolism was found to be significantly upregulated with a NES of 1.7 (**Figure** 3-1**b&c**). Of note, other pathways found to be upregulated were DNA replication, DNA damage response, DNA repair pathways and amino acid metabolism. Due to its contribution to purine and pyrimidine synthesis and to serine catabolism and anabolism, folate metabolisms is, therefore, linked to other pathways found to be upregulated in LSCs.

When taking a closer look to gene signatures that contribute to upregulation of folate metabolism in LSCs, *MTHFD1L* ($log_2FC=0.82$), *MTHFD1* ($log_2FC=0.97$), *ALDH1L2* ($log_2FC=0.98$), *SHMT2* ($log_2FC=1.06$), *DHFR* ($log_2FC=1.18$) and *MTHFD2* ($log_2FC=1.53$), were found to be significantly upregulated compared to normal counterparts (**Figure** 3-2**a&b**). It is worth noting that two of the three top hits are genes that encode folate metabolism enzymes that compartmentalise into the mitochondria, namely SHMT2 and MTHFD2. Surprisingly, the cytosolic counterpart of SHMT2, SHMT1 was not found to be significantly upregulated

(log_2FC=0.33). Of interest, ALDH1L2, which was found to be upregulated in LSCs, is linked to antioxidant defence through NADPH production.

3.2.2 Expression of folate metabolism genes remains unchanged in LPCs

Following the observed upregulation of folate metabolism genes in LSCs when compared to normal counterparts, we wanted to investigate whether there are any changes in expression of those genes when comparing LSCs to more differentiated CML cells, LPCs. This comparison could give some indications wherever upregulation of folate metabolism genes is only specific to LSCs or if it is a general feature of both stem and more differentiated leukaemic cells. Expression of *SHMT2*, *MTHFD2*, *ALDH1L2* remained unchanged in LPCs compared to LSCs (**Figure** 3-3). Interestingly, there was a trend of increased *SHMT1* and *MTHFD1* expression in LPCs, however this increase was not statistically significant. On the other hand, there was a two-fold increase in *DHFR* expression in the more differentiated population of leukaemic cells.

3.2.3 Folate metabolism genes are upregulated in HPCs compared to HSCs

Given that expression of 1C metabolism associated genes remains predominantly unchanged in CML $CD34^+CD38^+$ cells, when compared to CML $CD34^+CD38^-$ cells, we wondered if there would be any transcriptional changes when comparing expression of folate metabolism genes between LPCs and normal counterparts (HPCs). Overall, expression was similar when comparing LPCS to HPCs (**Figure** 3-4). We observed a trend of increased *DHFR*, *MTHFD1* and *ALDH1L2* expression, however this was not statistically significant. Therefore, we hypothesised that 1C metabolism genes might be upregulated during normal cell fate decisions (HSCs → HPCs). This would explain why expression of these genes is similar between LPCs and HPCs. Indeed, we observed a 2-fold increase in expression of *MTHFD1*, *SHMT2*, *MTHFD2* and a 3-fold increase in expression of *DHFR*, implying that cell fate decisions from HSCs to HPCs lead to increased expression of folate metabolism associated genes (**Figure** 3-5). If this also correlated with increased activity of 1C metabolism in HPCs compared to normal stem cells, remains to be discovered.

Overall, these data demonstrate that expression of enzymes involved in folate metabolism are upregulated in LSCs compared to HSCs. In addition, expression remains unchanged in LPCs compared to LSCs, with a single exception, DHFR; its expression is 2-fold higher in LPCs. On the contrary, during normal cell fate decisions expression of folate metabolism associated genes is significantly increased.

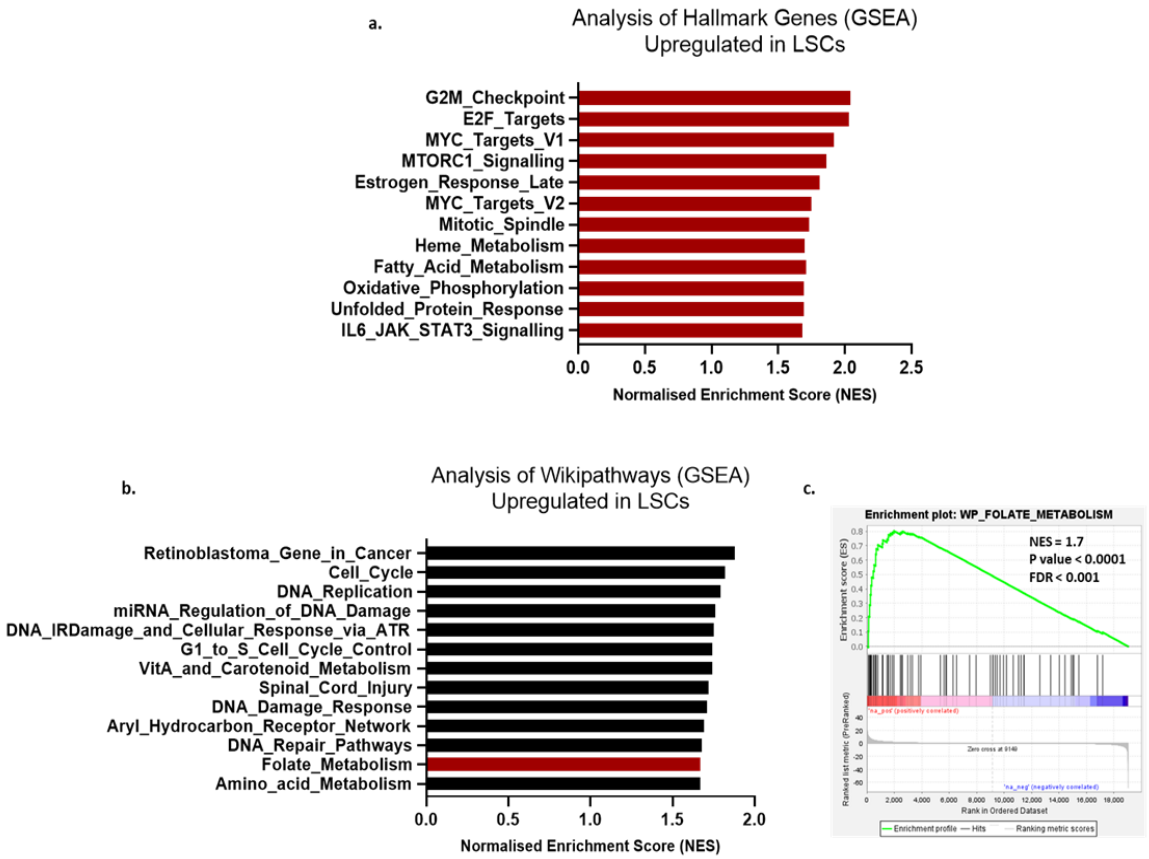

Figure 3-1: Folate metabolism is transcriptionally upregulated in LSCs. Gene set enrichment analysis (GSEA) of significantly differentially expressed genes in CML $CD34^+$ $CD38^-$ cells (LSCs) compared to normal counterparts (HSCs) using a publicly available dataset (E-MTAB-2581). N=3 CML patients and N=3 healthy donors. GSEA hallmarks represent specific well-defined biological states or processes (**a**), while wikipathways represent canonical pathways (**b**) upregulated in LSCs. GSEA plot showing enrichment of folate metabolism in LSCs compared to HSCs (**c**). Genes were classified as significantly differentially expressed when $p<0.05$ and $\log_2$Fold Change (FC) ≥ abs (0.5). NES: normalised enrichment score, FDR: false discovery rate. Data analysis performed by Mr. Daniele Sarnello.

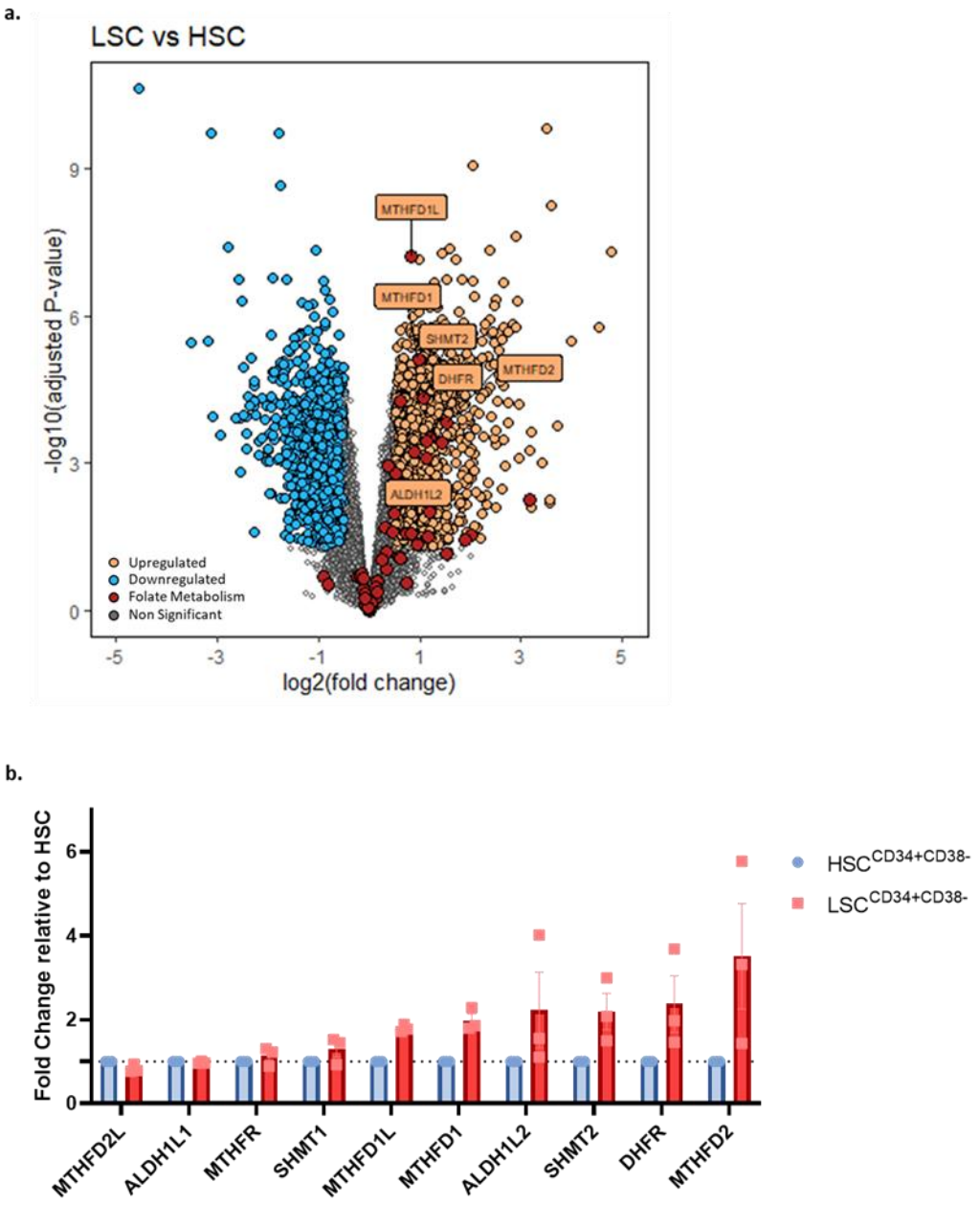

Figure 3-2: Folate metabolism associated genes, particularly those linked to the mitochondrial arm of the pathway, are upregulated in LSCs. Fold change of transcriptional data of LSCs versus HSCs. Upregulated genes are in orange, downregulated in blue, non-significant in grey, and folate metabolism associated genes in red. Plot includes names of folate genes that are significantly upregulated in LSCs compared to HSCs. Genes were classified as significantly differentially expressed when $p<0.05$ and $\log_2FC \geq$ abs (0.5). Plot generated by Mr Daniele Sarnello (**a**). Fold change of expression of folate metabolism associated genes plotted in ascending order relative to HSCs (**b**).

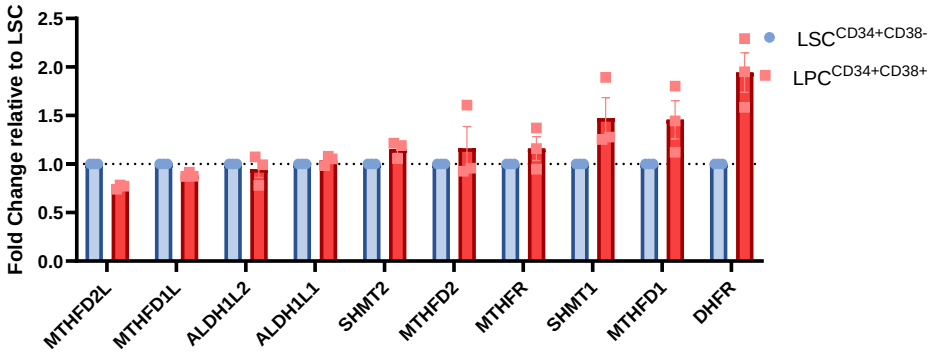

Figure 3-3: Expression of folate metabolism genes remains unchanged in more differentiated CML cells. Fold change of expression of folate metabolism associated genes in leukaemic progenitor cells $CD34^{+}CD38^{+}$ (LPCs) compared to LSCs. Genes were classified as significantly differentially expressed when $p<0.05$ and $\log_2FC \geq$ abs (0.5).

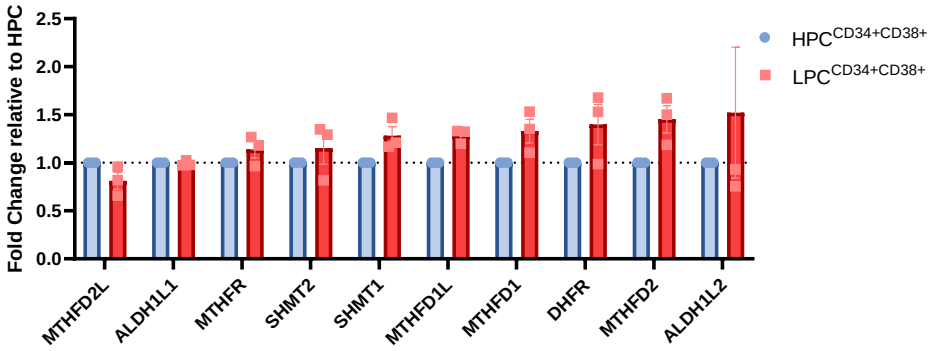

Figure 3-4: Expression of 1C metabolism associated genes is similar between LPCs and HPCs. Fold change of folate metabolism genes in LPCs compared to normal progenitor cells (HPCs). Genes were classified as significantly differentially expressed when $p<0.05$ and $\log_2FC \geq$ abs (0.5).

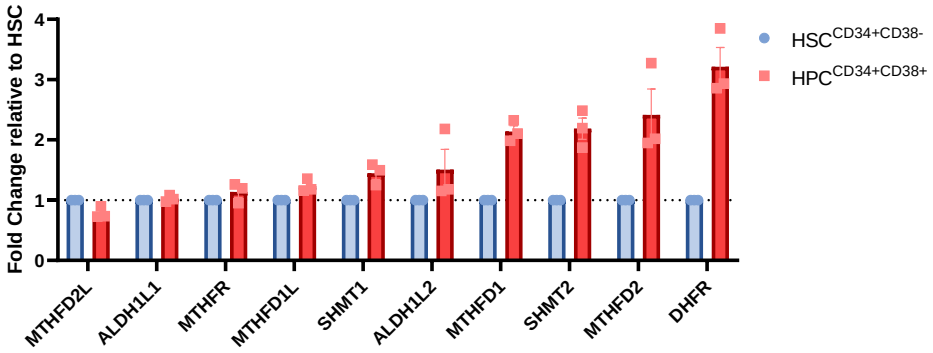

Figure 3-5: 1C metabolism associated genes are upregulated in HPCs compared to HSCs. Fold change of folate metabolism genes in normal progenitor cells (HPCs) compared to HSCs. Genes were classified as significantly differentially expressed when $p<0.05$ and $\log_2FC \geq$ abs (0.5).

3.3 Effect of imatinib on expression of folate metabolism genes

Following our initial observations regarding expression of 1C metabolism associated genes in LSCs and LPCs, we wondered if expression of these genes is altered following TKI treatment. As we previously mentioned, LSCs were found to maintain their viability using BCR-ABL independent survival signals when treated with imatinib[63]. Thus, we conducted a computational analysis of two separate microarray datasets (GSE48294, E-MTAB-2594), where CML $CD34^+$ stem cell enriched progenitor cells were treated with 2μM of imatinib for 24hr and 96hr, and 5μM of imatinib for 7 days respectively.

Following a 24h incubation with imatinib, *DHFR* (log_2FC=-0.59), *MTHFD1* (log_2FC=-0.79) and *MTHFD1L* (log_2FC=-1.23) were significantly downregulated (**Figure** 3-6**a**). *MTHFD1* (log_2FC=-1.66) and *MTHFD1L* (log_2FC=-1.01) followed the same trend after a 96h incubation with imatinib. Furthermore, there was a significant decrease of *SHMT1* (log_2FC=-1.04) and *SHMT2* (log_2FC=-0.66) expression at the 96h timepoint. Interestingly, *DHFR* (log_2FC=-0.24) and *MTHFD2* (log_2FC=-0.20) were downregulated, but this was not statistically significant. Surprisingly, a 7-day treatment with 5μM imatinib did not lead to significant downregulation of folate metabolism genes, apart from *DHFR* (log_2FC=-0.5) (**Figure** 3-6**b**). *SHMT2* (log_2FC=-0.06) and *SHMT1* (log_2FC=-0.033) experienced the least change in expression upon a prolonged treatment with imatinib.

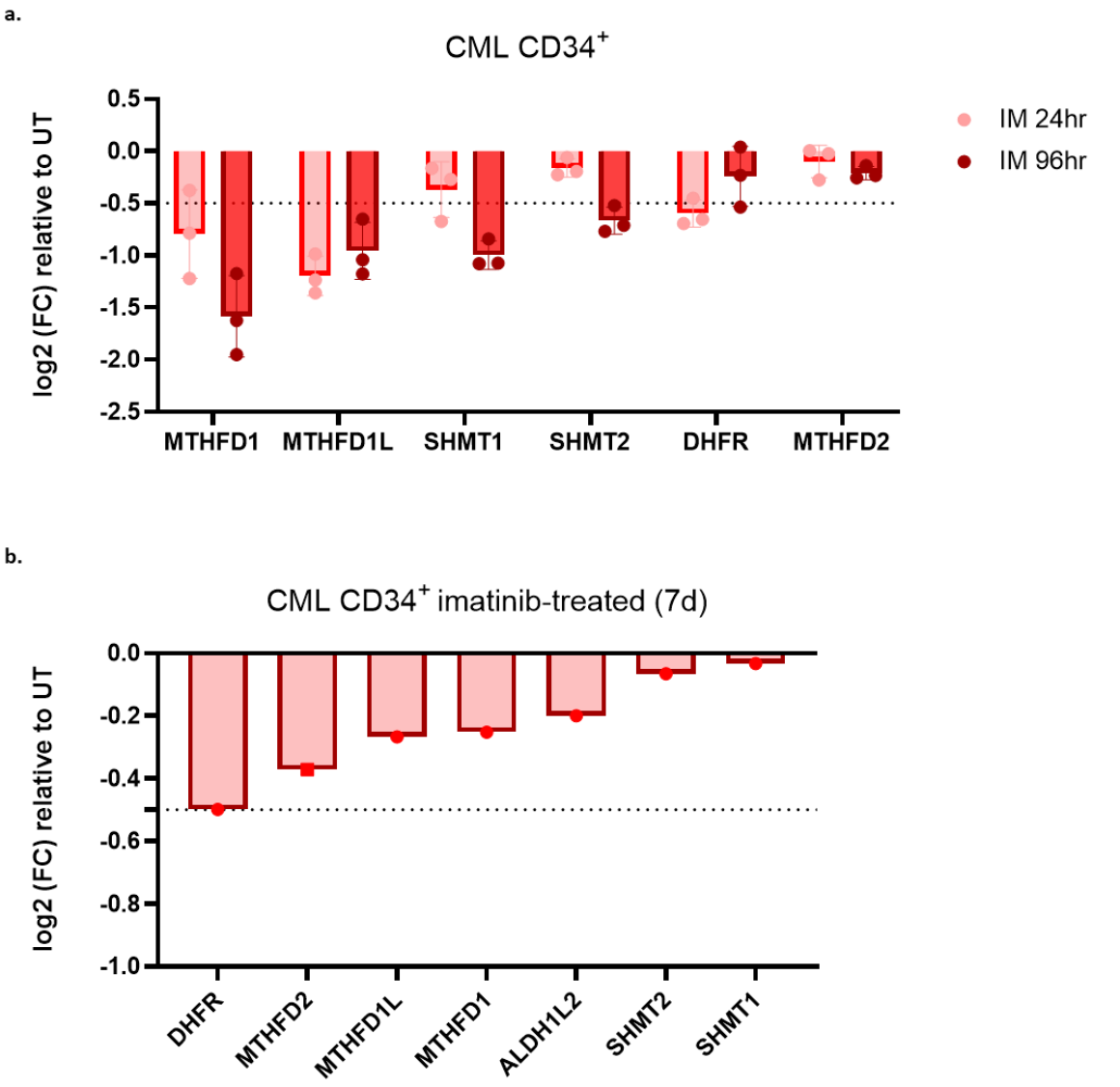

Figure 3-6: Effect of imatinib treatment in expression of folate metabolism genes. Bioinformatic analysis of publicly available microarray dataset containing patient-derived CML CD34⁺ samples (N=3) cultured in 2μM imatinib for 24hr and 96hr. GEO Accession: GSE48294. Data analysis was conducted by Mr Daniele Sarnello. Genes were classified as significantly differentially expressed when $p<0.05$ and $\log_2FC \geq$ abs (0.5). Logarithmic fold change of folate metabolism genes following a 24h or 96h treatment with 2μM imatinib (IM) relative to untreated (UT) cells (**a**) Bioinformatic analysis of publicly available microarray dataset containing patient-derived CML CD34⁺ samples (N=5) treated with 5μM imatinib for 7days. Accession: E-MTAB-2594. Data analysis was conducted by Dr Zuzana Brabcova. Genes were classified as significantly differentially expressed when $p<0.05$ and $\log_2FC \geq$ abs (0.5). Logarithmic fold change of folate metabolism genes following incubation with 5μM imatinib for 7 days. (**b**)

3.4 1C metabolism activity is upregulated in CML CD34$^+$ cells

Given the significant upregulation in expression of folate metabolism genes in LSCs compared to HSCs, we decided to investigate 1C metabolism activity in CML cells and compare it to normal counterparts. Thus, CD34$^+$ conditioned media was collected (culturing and media collection were conducted by Dr Amy Dawson), and then formate exchange rate and media concentration were assessed through GC-MS. As we previously described, the rate of 1C production exceeds the 1C demand of cancer cells, leading to excess formate production which is released from cells and tissues[89, 162]. This excess formate production and release from rapidly proliferating cells is known as formate overflow. Therefore, formate measurement is a good indicator of 1C metabolism activity.

CML CD34$^+$ had a significantly higher formate exchange rate when compared to normal counterparts (**Figure** 3-7**a**). Furthermore, CML CD34$^+$ conditioned media had a higher formate concentration, namely 0.7mM compared to 0.4mM in normal CD34$^+$ conditioned media. Overall, these data suggest that CML CD34$^+$ cells have upregulated folate metabolism activity when compared to normal CD34$^+$ cells.

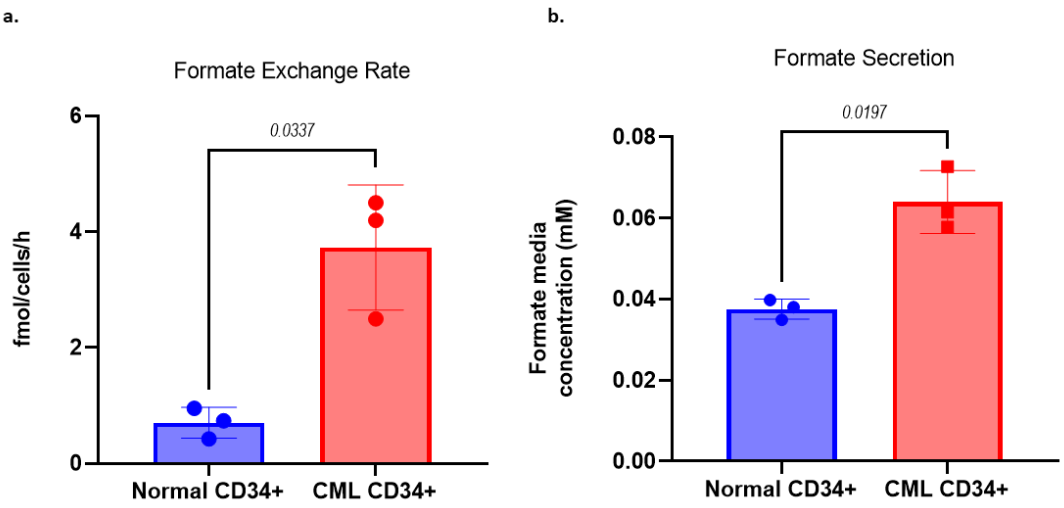

Figure 3-7: CML CD34⁺ cells have a higher folate metabolism activity when compared to normal counterparts. Graphs representing absolute formate exchange rate (**a**) and formate secretion (**b**) in CD34⁺ conditioned media following 48hr culture. Data analysis conducted by Dr Alexei Vazquez. Data representative of mean ± SD, n=3 individual patient samples. P-values were calculated with an unpaired t-test with Welch's correction.

3.5 Inhibition of folate metabolism exhibits an antiproliferative effect on CML cells

3.5.1 Blood cancer cell lines show high sensitivity to MTX

To further investigate whether 1C metabolism can be a metabolic vulnerability for CML cells, we sought tumour types with a particular sensitivity to folate pathway inhibition. We analysed publicly available data on MTX sensitivity in a wide range of different cancer cell lines (https://www.cancerrxgene.org/). All haematological cancer cell lines demonstrated high sensitivity to the DHFR inhibitor, with IC_{50} values lower compared to solid tumour cell lines (**Figure** 3-8). As expected, ALL cell lines showed the highest sensitivity to MTX (IC_{50}=0.07μM). MTX is used as frontline treatment in B-ALL and frequently used in T-ALL. Of note, CML cell lines demonstrated the second highest sensitivity to MTX (IC_{50}=0.22μM), implying that they are sensitive to inhibition of 1C metabolism. These results underpin the idea that 1C metabolism can be a metabolic vulnerability for CML cells.

3.5.2 Loss of SHMT2 leads to cell cycle arrest in K562 cells

To assess the impact of specific inhibition of folate metabolism in CML cells, we generated a K562 SHMT2 KO cell line (**Figure** 3-9**a**). As we previously described, *SHMT2* (log_2FC=1.06), *DHFR* (log_2FC=1.18) and *MTHFD2* (log_2FC=1.53) displayed the highest upregulation in LSCs when compared to normal counterparts (**Figure** 3-2**b**). Out of those three top hits, we decided to assess the impact of loss of SHMT2 in CML cells primarily for two reasons. Firstly, traditional antifolates already show high affinity for DHFR, thus making targeting other enzymes of the pathway an appealing approach. Secondly, and most importantly, because of the introduction of the small molecule inhibitor SHIN1, that represses the activity of SHMT1/2[163]. We reasoned that SHMT2 KO cells would be a good comparison to SHIN1 treated cells.

We firstly confirmed that the SHMT2 KO cell line was functional, by assessing the formate exchange rate. SHMT2 catalyses the first mitochondrial reaction of the pathway. Loss of the enzyme is expected to lead to blockage of the mitochondrial arm and subsequently, reduce the formate released out of the cells. Indeed, SHMT2 KO cells showed reduced formate exchange rate and

formate media concentration (0.0033mM) (**Figure** 3-9**b&c**). It is also worth noting that SHMT2 KO cells were maintained in culture with a HT supplement, to overcome the blockage of purine and pyrimidine biosynthesis caused by 1C metabolism inhibition. Supplement was removed prior to any experimental procedures.

Besides this, loss of SHMT2 resulted in significant decrease in cell growth when compared to control cells (**Figure** 3-10**a**). HT supplementation was sufficient to partially rescue growth of SHMT2 KO cells, however growth was not restored to control cells' level. Furthermore, PI staining, revealed that SHMT2 KO cells were characterised by a block in the S phase and reduction of cells entering the G2/M phase (**Figure** 3-10**b**). PI is a DNA stain; therefore, it binds to DNA in proportion to the amount of DNA present in the cell, giving an indication of the cell phase the cells are at. Furthermore, staining with apoptotic markers 7-AAD and annexin V demonstrated that loss of SHMT2 is mainly cytostatic and does not induce significant cell death (**Figure** 3-10**c**).

Collectively, these findings suggest that loss of SHMT2 leads to decreased cell growth due to cell cycle arrest without any significant effect on programmed cell death.

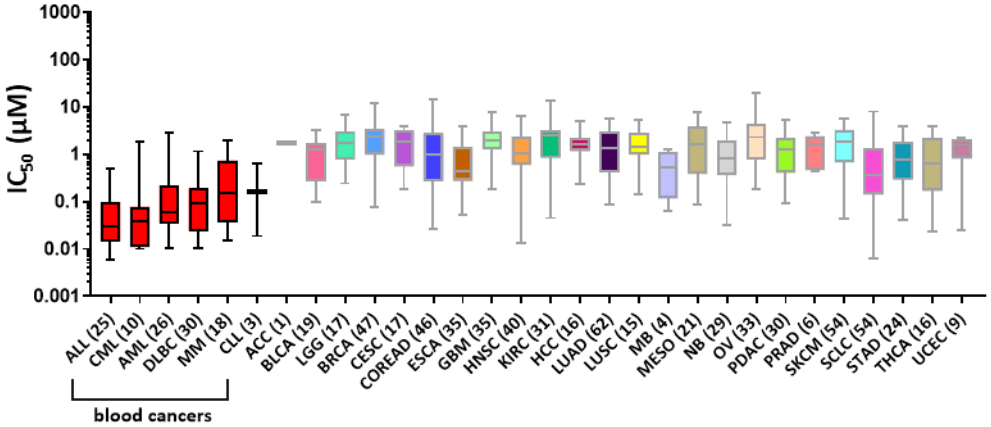

Figure 3-8: Haematological cell lines show high sensitivity to MTX. IC_{50} values for methotrexate across several cell lines as obtained by the publicly available database Genomics of Drug Sensitivity in Cancer (https://www.cancerrxgene.org/). Number in parenthesis represents number of cell lines analysed per each cancer type. ALL, acute lymphoblastic leukaemia; AML, acute myeloid leukaemia; CLL, chronic lymphoblastic leukaemia; CML, chronic myeloid leukaemia; DLBC, diffuse large B-cell lymphoma; MM, multiple myeloma; ACC, adrenocortical carcinoma; BLCA, bladder urothelial carcinoma; LGG, brain lower grade glioma; BRCA, breast invasive carcinoma; CESC, cervical squamous cell carcinoma and endocervical adenocarcinoma; COREAD, colon and rectum adenocarcinoma; ESCA, oesophageal carcinoma; GBM, glioblastoma multiforme; HNSC, head and neck squamous cell carcinoma; KIRC, kidney real clear cell carcinoma; HCC, hepatocellular carcinoma; LUAD, lung adenocarcinoma; LUSC, lung squamous cell carcinoma; MB, medulloblastoma; MESO, mesothelioma; NB, neuroblastoma; OV, ovarian serous cystadenocarcinoma; PDAC, pancreatic adenocarcinoma; PRAD, prostate adenocarcinoma; SKCM, skin cutaneous melanoma; SCLC, small cell lung carcinoma; STAD, stomach adenocarcinoma; THCA, thyroid carcinoma; UCEC, uterine corpus endometrial carcinoma.

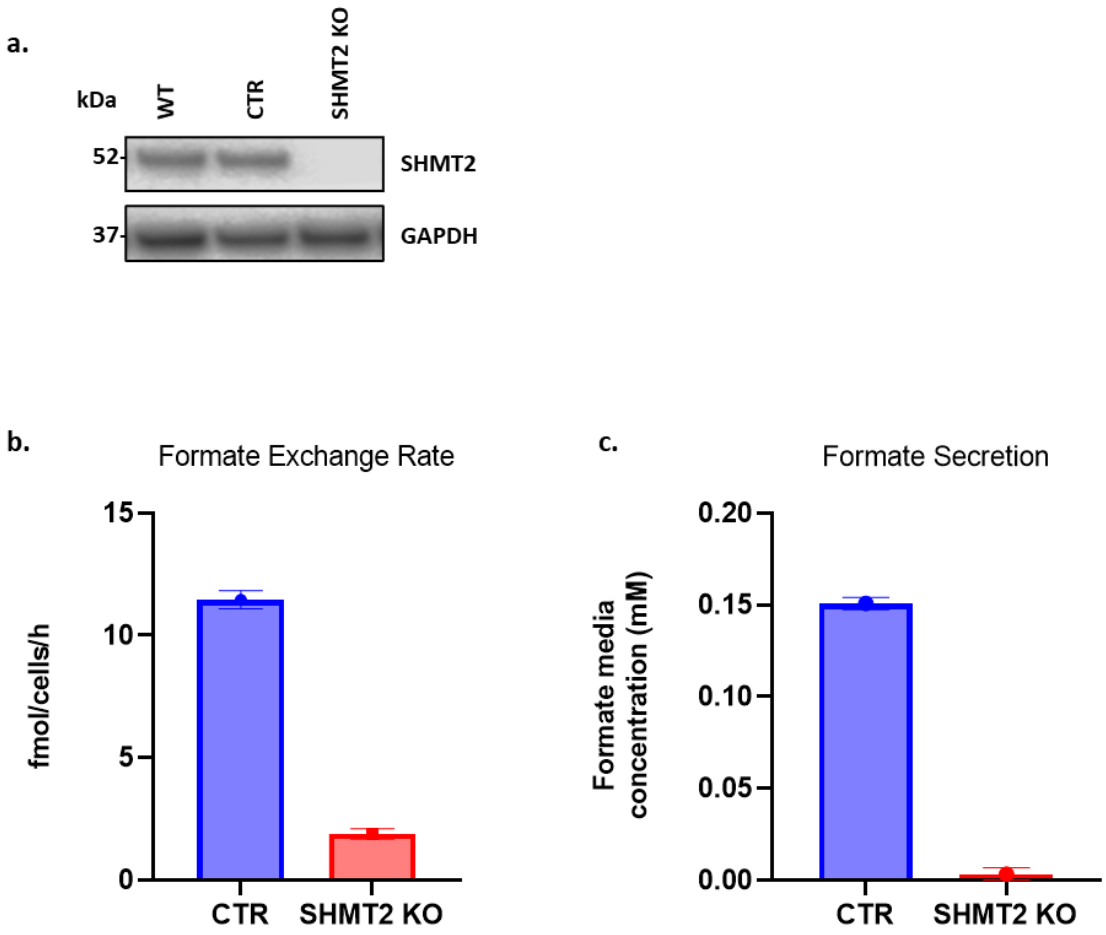

Figure 3-9: Generation of a functional K562 SHMT2 KO cell line. Immunoblot analysis showing deletion of SHMT2 in K562 cells. CTR refers to vector control cells (**a**). Formate exchange rate (**b**) and formate secretion (**c**) in K562 SHMT2 deficient cells. Data analysis conducted by Dr Alexei Vazquez. Data plotted as mean +/- SEM of triplicate wells, n=1 independent experiment.

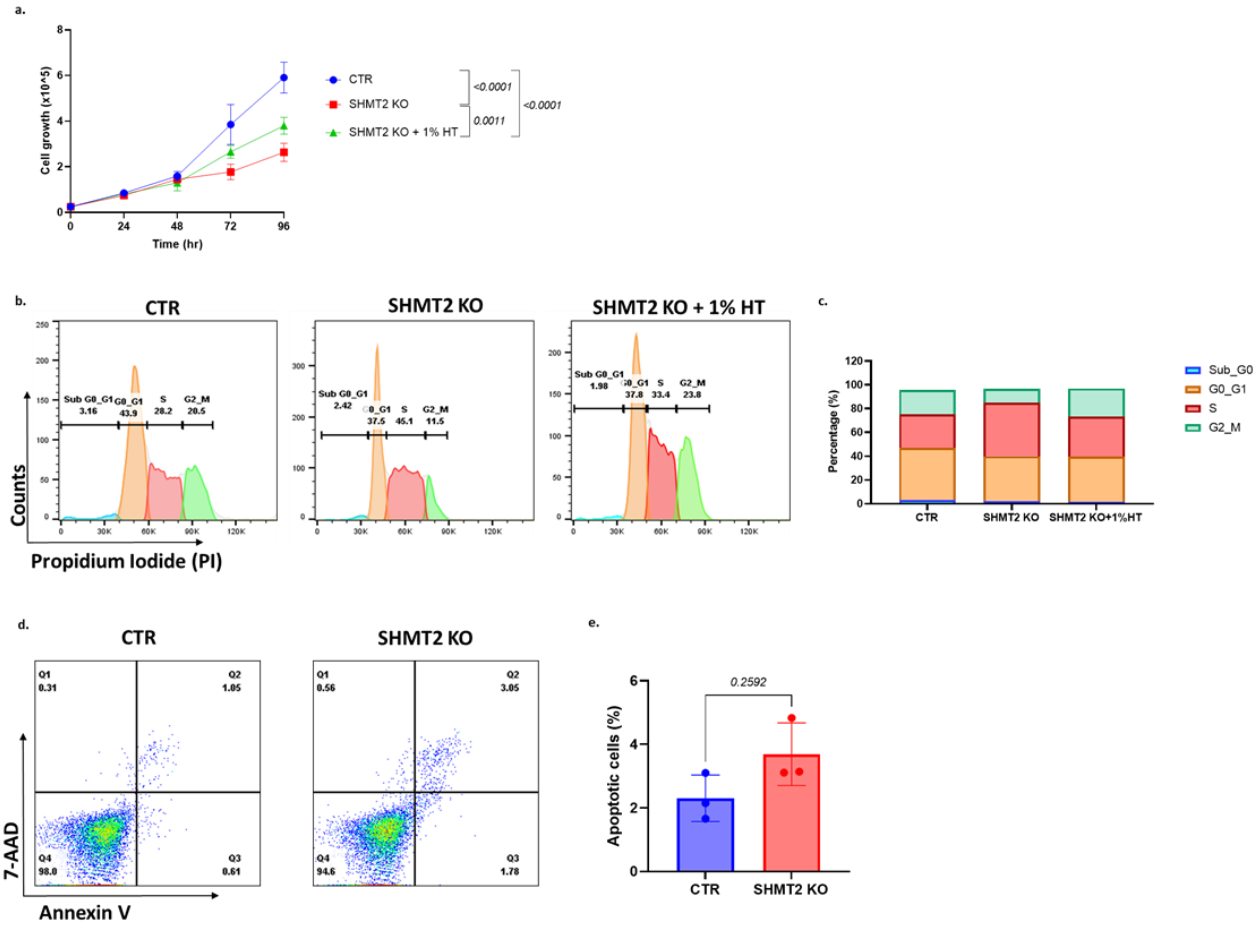

Figure 3-10: Genetic inhibition of 1C metabolism has an antiproliferative effect on CML K562 cells. Growth curves of K562 control, SHTM2 KO and SHMT2 KO supplemented with 1% hypoxanthine and thymidine supplement (HT) (**a**). Flow cytometry plots of K562 control, SHMT2 KO and SHMT2 KO +1% HT showing staining with propidium iodide (PI) to assess the effect of SHMT2 loss on cell cycle. SHMT2 KO were left without the HT supplement for 72hr prior to staining (**b**). Percentage of cell cycle stages in K562 control, SHMT2 KO and SHMT2 KO +1% HT cells (**c**). Flow cytometry plots of K562 control and SHMT2 KO stained with apoptotic markers 7-AAD and annexin V (AV) (**d**). Percentage of apoptotic cells ($AV^+7\text{-}AAD^-$ & $AV^+7\text{-}AAD^+$) in control and SHMT2 KO cells. SHMT2 KO were left without the HT supplement for 72hr prior to staining (**e**). Data were plotted as mean +/- S.D. of n=3 independent experiments for (**a**) and (**c**). N=1 independent experiments for (**b**). P-values were calculated with a two-way ANOVA with Sidak's multiple comparisons test for (**a**) and a paired t-test for (**c**). P-values displayed in (**a**) represent probability values with regards to the 96h timepoint, however, similar values were obtained for the 72h timepoint.

3.5.3 Loss of SHMT2 in CML cells impairs xenograft formation

After establishing an antiproliferative effect of folate metabolism inhibition in CML cells *in vitro*, we decided to investigate the impact of loss of 1C metabolism on tumourigenesis in an *in vivo* setting. We took advantage of another CML cell line, KCL22, which has the capacity to form extramedullary tumours when transplanted via tail vein injection into immunocompromised mice. In our lab we have established a KCL22 luciferase expressing cell line that is suitable for *in vivo* bioimaging.

Firstly, we generated a KCL22 luciferase^{+} SHMT2 KO cell line (**Figure** 3-11**a**). Following validation of the KO, we transplanted 4 million control and SHMT2 KO cells into NRGW^{41} immunocompromised mice via tail vein injection and monitored mice for 15 weeks (**Figure** 3-11**b**) 30 minutes following transplant, mice were injected with luciferin to confirm successful transplant of KCL22 cells (**Figure** 3-11**c**). Loss of SHMT2 impaired KCL22 tumour xenograft formation and resulted in significantly extended survival of mice when compared to mice transplanted with control cells (**Figure** 3-12**a**). Furthermore, tumour burden at experimental endpoint (high tumour burden or 15 weeks days post transplantation) was significantly reduced in mice transplanted with KCL22 SHMT2 KO cells (**Figure** 3-12**b**).

Overall, these data suggest that genetic inhibition of 1C metabolism through loss of SHMT2 leads to reduced ability of tumour formation of CML cells, which confirms the antiproliferative effect on CML cell lines that we observed *in vitro*.

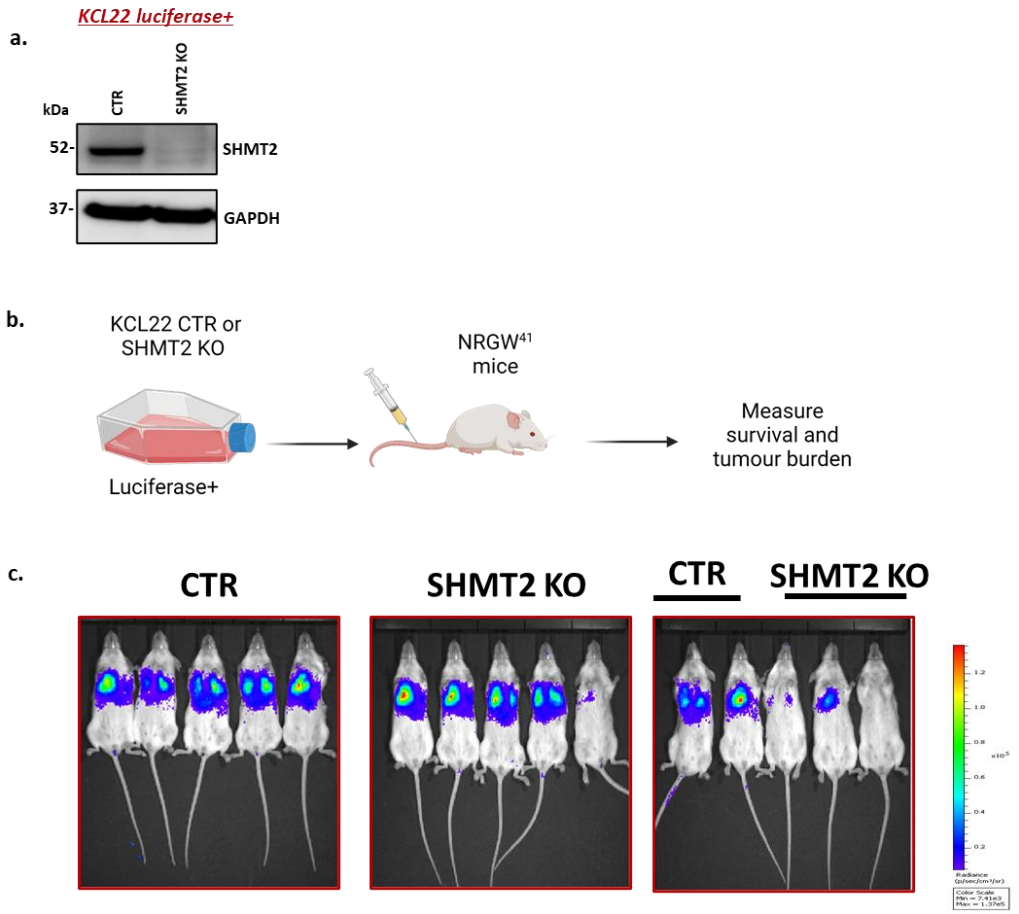

Figure 3-11: SHMT2 deficient cells impair xenograft capacity of CML cells. Immunoblot analysis showing deletion of SHMT2 in KCL22 luciferase expressing cells (**a**) Schematic representation of control and SHMT2 KO luciferase expressing cells transplanted in NRGW[41] female mice via tail vein injection (**b**) IVIS (*In Vivo* Imaging System) images of mice transplanted with control and SHMT2 KO luciferase expressing cells (**c**) N=7 mice transplanted with control cells, n=8 mice transplanted with SHMT2 KO cells.

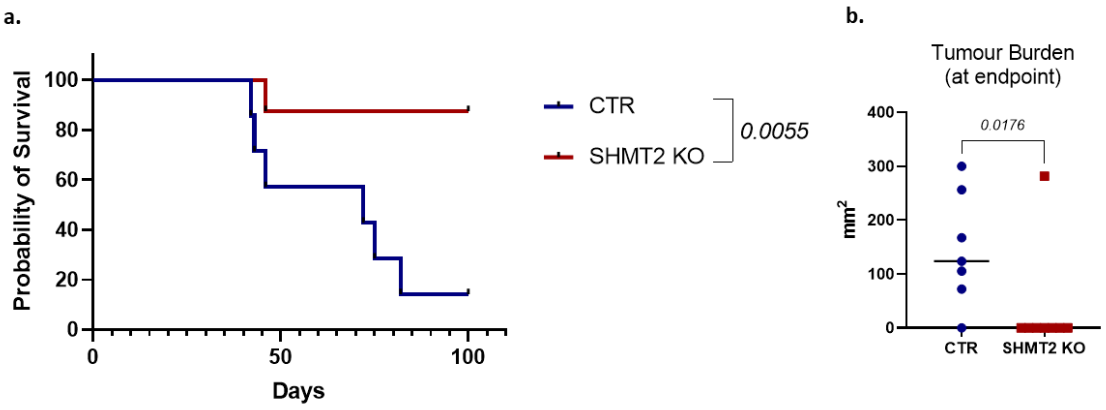

Figure 3-12: SHMT2 deficient CML cells have impaired xenograft capacity resulting in extended survival of NRGW^{41} mice. Kaplan-Meier analysis comparing survival of mice transplanted with KCL22 control and SHMT2 KO cells over 100 days (**a**). Burden of extramedullary tumours harvested from each mouse at experimental end point (**b**). In (**a**) p values were calculated using log-rank (Mantel-Cox) test. In (b) p values were calculated with a Mann-Whitney test.

3.6 Inhibition of 1C metabolism leads to blockage of *de novo* purine synthesis in CML cells

To further investigate the effect of inhibition of 1C metabolism in CML cells, we decided to use a metabolomic approach and assess metabolic changes following inhibition of the pathway. As the SHIN1 inhibitor that represses the activity of SHMT1/2 was available, we decided to include the inhibitor in our studies to assess whether observed results would be consistent using either of the two approaches. At the same time, as one of the main products of folate metabolism is nucleotide biosynthesis, we included formate supplementation in cells where 1C metabolism had been inhibited, as one of our conditions. Formate provides 1C units independently of SHMT1/2 activity, therefore it can bypass the blockage caused by SHMT1/2 inhibition and support reconstitution of purine and thymidylate synthesis by alleviating the 10-formyl THF pool (**Figure** 3-13**a**). For interpretation of our results, we defined a "rescue" by formate supplementation when there was no statistical difference between untreated/control cells and SHIN1-treated or SHMT2 KO plus formate. A "partial rescue" by formate was defined as a statistically significant difference between SHIN1-treated and SHMT2 KO cells and SHIN1-treated and SHMT2 KO cells plus formate, but there was still statistical difference between untreated/control and SHIN1-treated and SHMT2 KO cells plus formate.

As expected, both genetic and pharmacological inhibition of 1C metabolism led to a significant increase in serine levels and a significant decrease in glycine levels (**Figure** 3-13**b&c**). Furthermore, formate supplementation was not sufficient to rescue these changes and caused an even further decrease regarding glycine levels. Glycine is needed for purine synthesis, by supplementing formate to reconstitute purine biosynthesis more glycine is being used, thus the further decrease in glycine levels (**Figure** 3-14).

When evaluating the impact of folate metabolism inhibition on *de novo* purine synthesis, we observed a significant decrease in most purine metabolite levels, namely ADP, ATP, GMP and GTP (**Figure** 3-14). Similar trend was observed for AMP and GDP; however, this was not statistically significant. Formate supplementation was sufficient to rescue purine biosynthesis, reinforcing the idea that it can provide 1C units independently from SHMT1/2. In addition, we

observed a trend of decreased ribose-5-phosphate and increased levels of glutamine and aspartate. Ribose-5-phosphate is linked to glycolysis and pentose phosphate pathway. Reduction of this metabolite might suggest a blockage in glycolysis upon 1C metabolism inhibition, something we will discuss further in the next section (**3.7**). Lastly, we observed a significant increase of the purine precursor and AMPK activator AICAR. AICAR is the final intermediate in the *de novo* purine biosynthesis pathway, and its conversion to inosine monophosphate (IMP) requires 10-formyl-THF. Formate supplementation returned AICAR levels to untreated/control levels.

Interestingly, genetic or pharmacological inhibition of 1C metabolism did not result in any changes in pyrimidine levels (**Figure** 3-15), suggesting that at least at the 24h timepoint the most prominent effect is on purine biosynthesis.

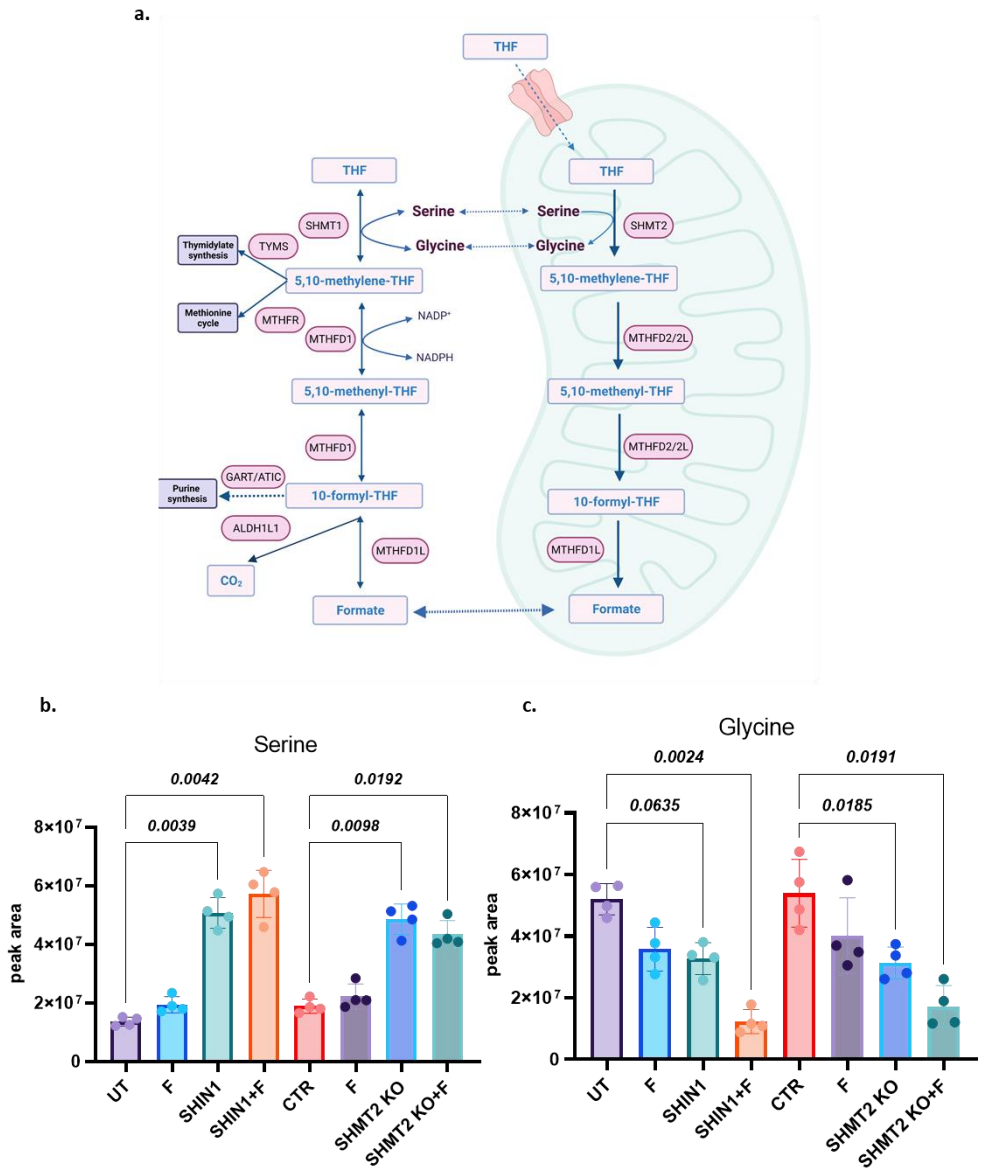

Figure 3-13: Inhibition of folate metabolism leads to serine accumulation and glycine reduction. Graphical representation of folate metabolism (**a**). Representative graphs of peak areas of serine (**b**) and glycine (**c**) in K562 treated with 1mM formate, 2.5µM of SHIN1 or a combination of both, in control cells +/- 1mM formate and in SHMT2 KO cells +/- 1mM formate. After a 24h incubation, intracellular metabolites were extracted, and samples were analysed by LC-MS. Data were plotted as mean +/- S.D. of n=4 independent experiments. P-values were calculated with a paired one-way ANOVA with Geisser-Greenhouse correction and Sidak's multiple comparisons test.

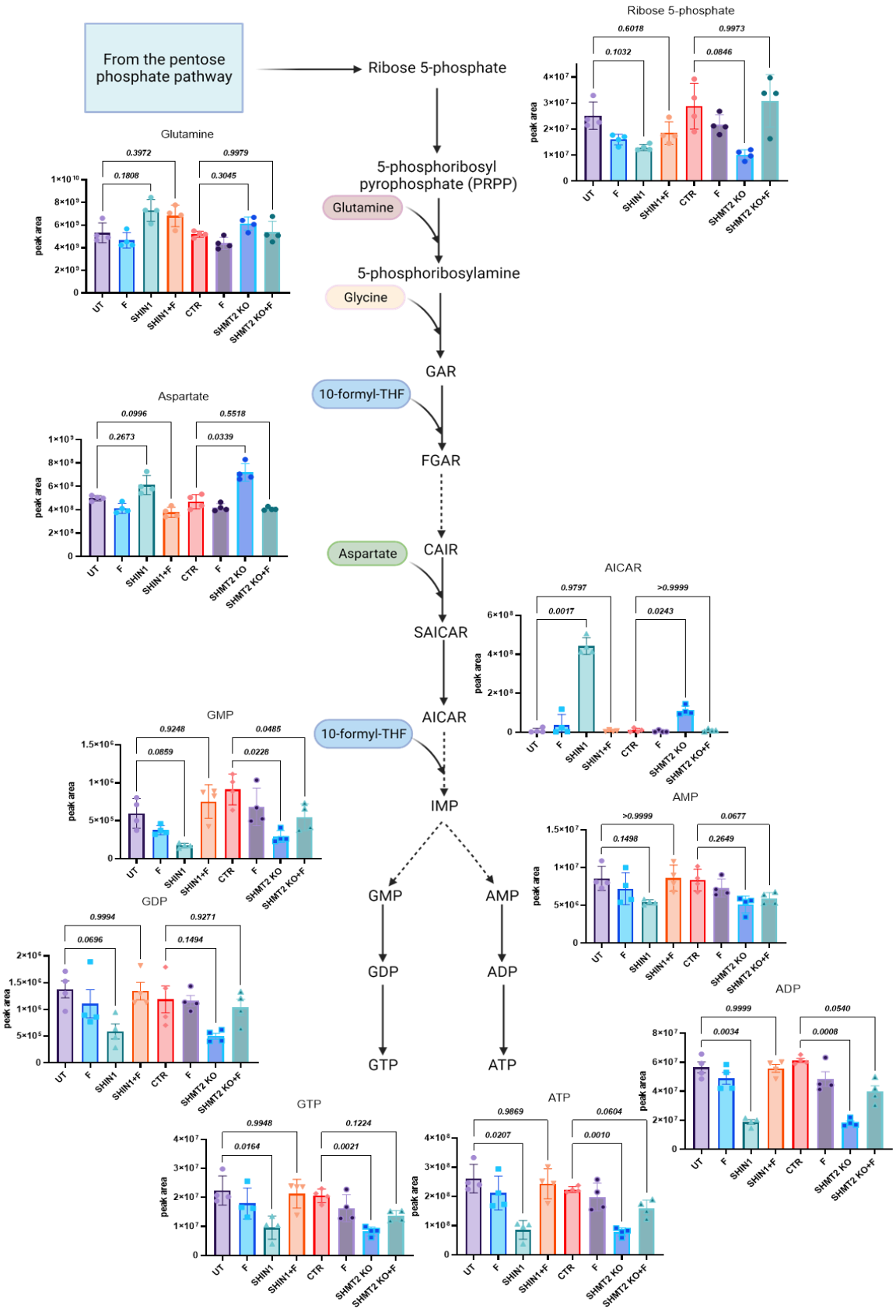

Figure 3-14: Inhibition of the folate pathway leads to reduction of purine biosynthesis. Representative graphs of peak areas of purines in K562 cells treated with 1mM formate, 2.5µM of SHIN1 or a combination of both, in control cells +/- 1mM formate and in SHMT2 KO cells +/- 1mM formate. After a 24h incubation, intracellular metabolites were extracted, and samples were analysed by LC-MS. Data were plotted as mean +/- S.D. of n=4 independent experiments. P-values were calculated with a paired one-way ANOVA with Geisser-Greenhouse correction and Sidak's multiple comparisons test.

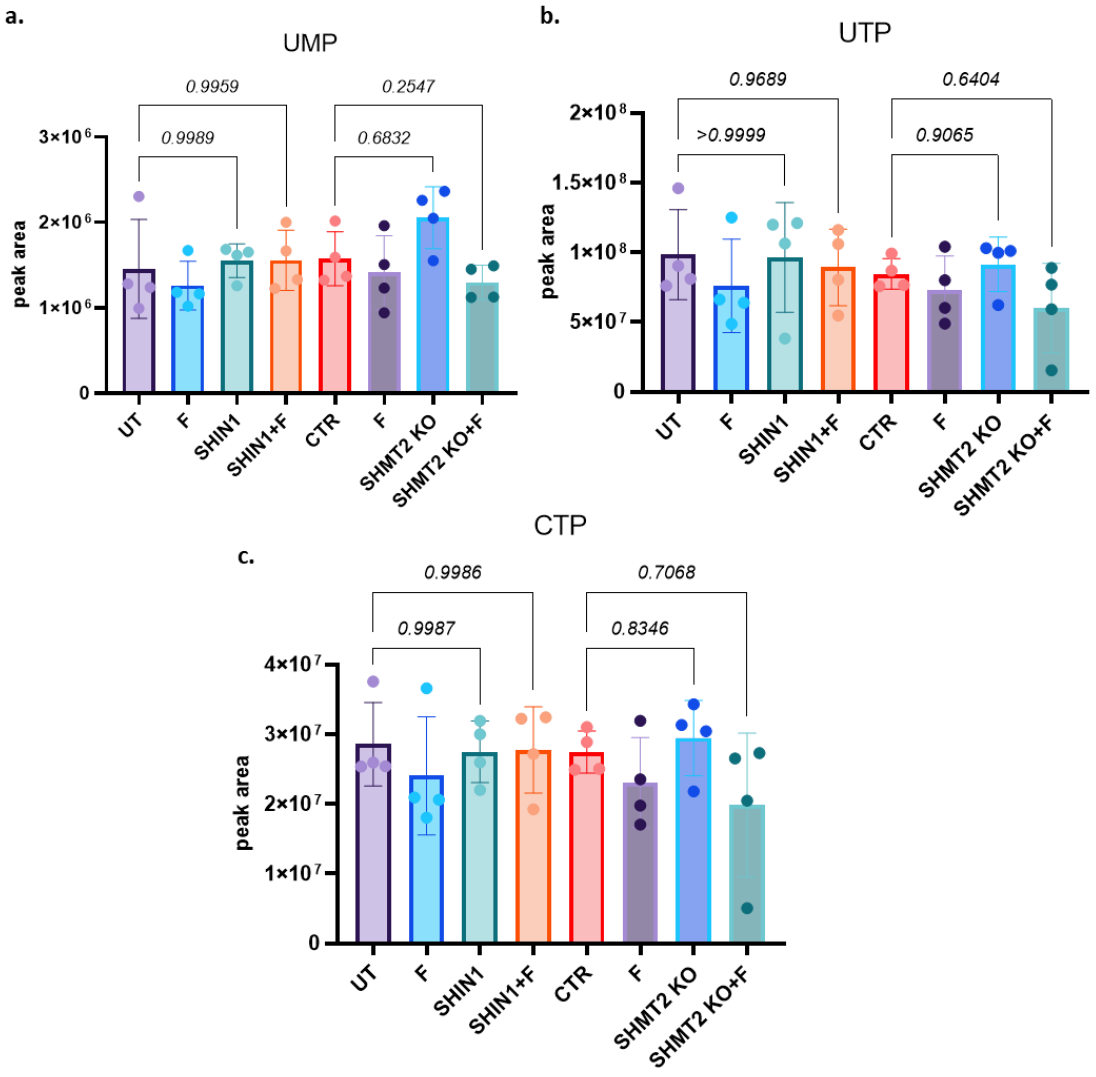

Figure 3-15: Inhibition of folate metabolism does not alter pyrimidine levels. Representative graphs of peak areas of pyramidines in K562 cells treated with 1mM formate, 2.5μM of SHIN1 or a combination of both, in control cells +/- 1mM formate and in SHMT2 KO cells +/- 1mM formate. After a 24h incubation, intracellular metabolites were extracted, and samples were analysed by LC-MS. Data were plotted as mean +/- S.D. of n=4 independent experiments. P-values were calculated with a paired one-way ANOVA with Geisser-Greenhouse correction and Sidak's multiple comparisons test.

3.7 Folate metabolism inhibition leads to glycolysis impairment in CML cells

Following the observed trend of decreased ribose 5-phosphate levels, we wondered if inhibition of folate metabolism has any impact on other metabolites related to glycolysis (**Figure** 3-16). We observed an almost 3-fold increase in the levels of glucose in SHIN1-treated and SHMT2 KO cells when compared to untreated/control cells. However, this was statistically significant only in the case of SHMT2 KO cells. Furthermore, glucose uptake was significantly decreased in SHMT2 KO cells and a similar, but non-significant trend was observed for SHIN1-treated cells (**Figure** 3-17**a**) These data suggest that SHIN1-treated and SHMT2 KO cells use significantly less glucose when compared to untreated/control cells. Interestingly, purine reconstitution through formate supplementation was sufficient to restore glucose uptake and glucose intracellular levels. In addition, pentose phosphate pathway (PPP) intermediate sedoheptulose 7-phosphate was significantly reduced upon either pharmacological or genetic inhibition of 1C metabolism (**Figure** 3-17). Formate supplementation could fully restore levels of sedoheptulose 7-phosphate in SHIN1-treated cells, but only partially do so in SHMT2 KO cells. Furthermore, we observed a trend of decreased glucose-6 phosphate and fructose 1,6-biphosphate, two important glycolysis intermediates.

Besides this, we observed a trend of increased phosphoenolpyruvate (PEP) levels when 1C metabolism was inhibited. PEP is converted into pyruvate through an irreversible reaction. Therefore, we hypothesised that due to increased PEP levels, there should be less pyruvate production. Indeed, we observed a trend of decreased pyruvate levels. Furthermore, there was a significant decrease in lactate levels, which was rescued by formate supplementation. In support of this, we discovered significantly less lactate secretion in media of SHMT2 KO or SHIN1-treated cells (**Figure** 3-17**b**). Formate addition restored lactate secretion.

To further investigate the effect of folate metabolism inhibition on glycolysis of K562 cells, we took advantage of the Seahorse XFe96 analyser (Agilent), where we measured ECAR during a Glyco Stress Test assay (**Figure** 3-17**c**). Even though we observed a trend of decreased glycolysis and glycolytic capacity upon genetic or pharmacological inhibition of 1C metabolism, this was not statistically

significant (**Figure** 3-17**d&e**). Interestingly, formate supplementation was not sufficient to rescue the decreased trend of the glycolytic capacity.

Given the repetitive effect we saw on glycolysis, we decided to investigate whether folate pathway inhibition has any effect on OXPHOS. For this, we measured OCR during a Mito Stress Tess assay. Nevertheless, we did not detect any significant changes upon inhibition of folate metabolism, suggesting that the inhibition of the pathway has an effect on glycolysis when it comes to CML cells.

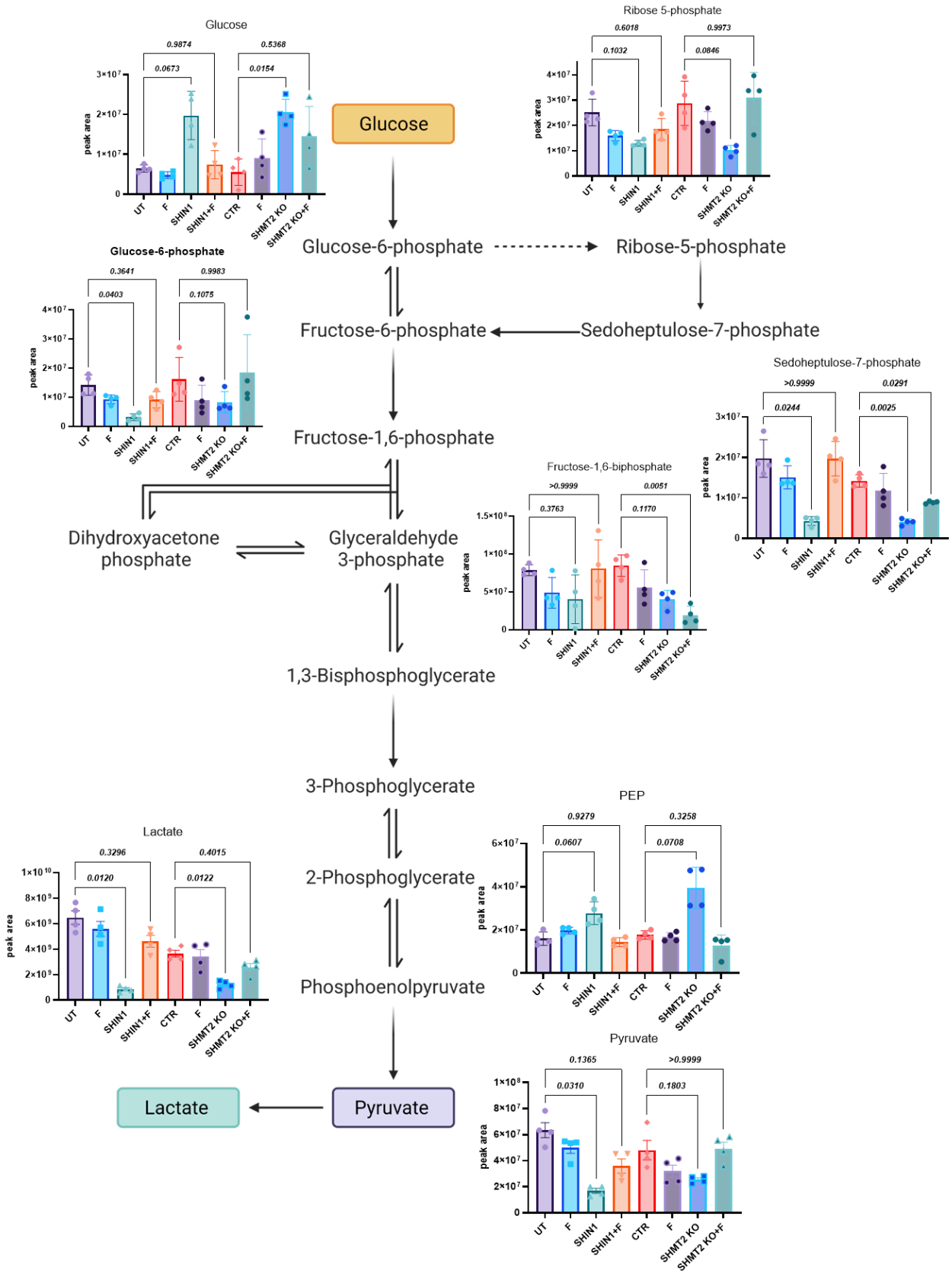

Figure 3-16: Folate metabolism inhibition leads to impairment of glycolysis in K562 cells. Representative graphs of peak areas of metabolites associated with glycolysis in K562 cells treated with 1mM formate, 2.5μM of SHIN1 or a combination of both, in control cells +/- 1mM formate and in SHMT2 KO cells +/- 1mM formate. After a 24h incubation, intracellular metabolites were extracted, and samples were analysed by LC-MS. Data were plotted as mean +/- S.D. of n=4 independent experiments. P-values were calculated with a paired one-way ANOVA with Geisser-Greenhouse correction and Sidak's multiple comparisons test.

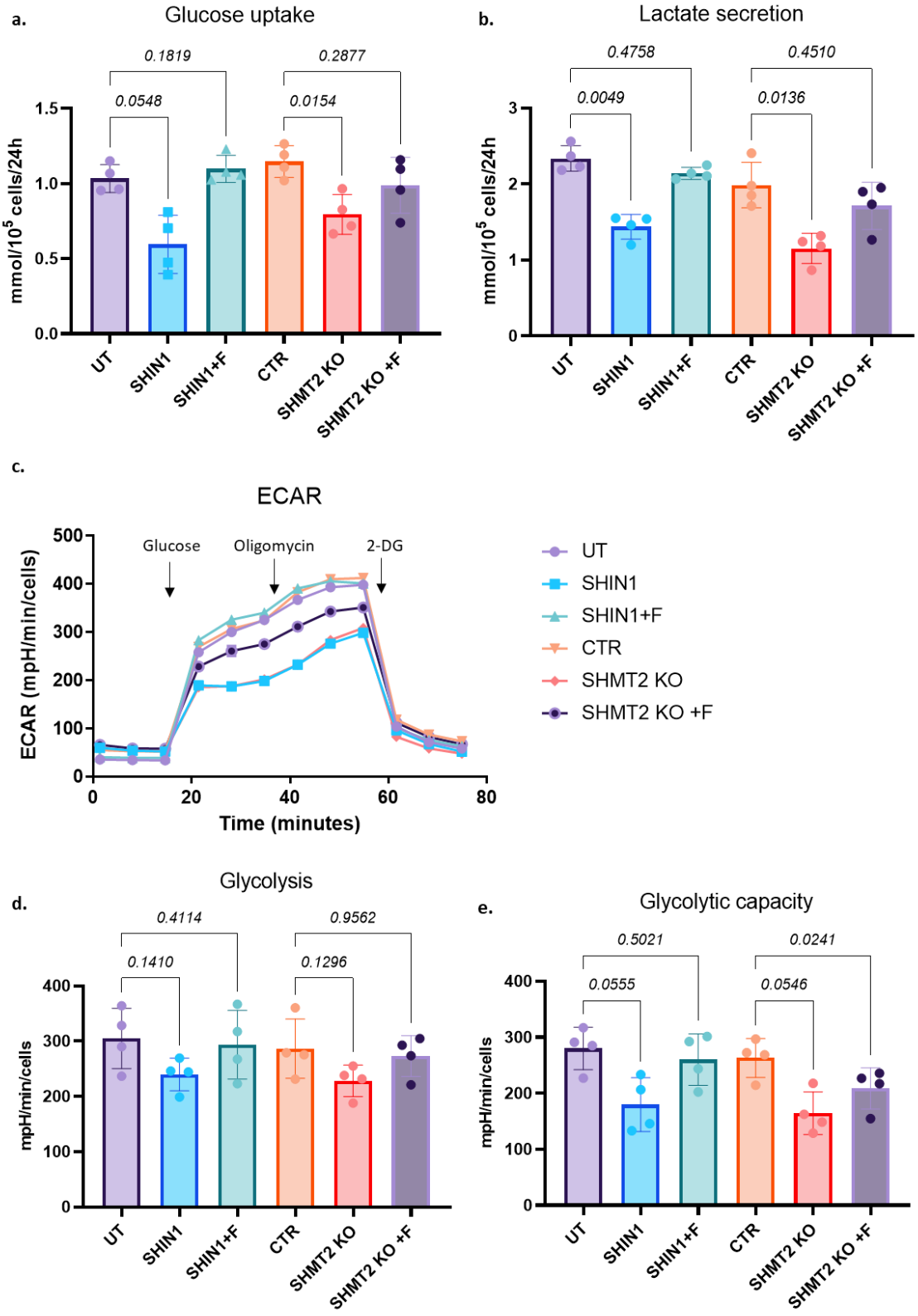

Figure 3-17: Folate metabolism inhibition leads to impairment of glycolysis in K562 cells. Quantitative analysis of glucose (**a**) and lactate (**b**) in the media of K562 cells following a 24h treatment with 2.5µM SHIN1 or a combination of SHIN1 with 1mM formate, ctr cells, SHMT2 KO cells +/- 1mM formate. Representative Glyco stress ECAR (extracellular acidification rate) profile (**c**). Basal glycolysis (**d**) and maximal glycolytic capacity (**e**) of K562 cells following a 24h treatment with 2.5µM SHIN1 or a combination of SHIN1 with 1mM formate, ctr cells, SHMT2 KO cells +/- 1mM formate. Data were plotted as mean +/- S.D. of n=4 independent experiments. P-values were calculated with a paired one-way ANOVA with Geisser-Greenhouse correction and Sidak's multiple comparisons test.

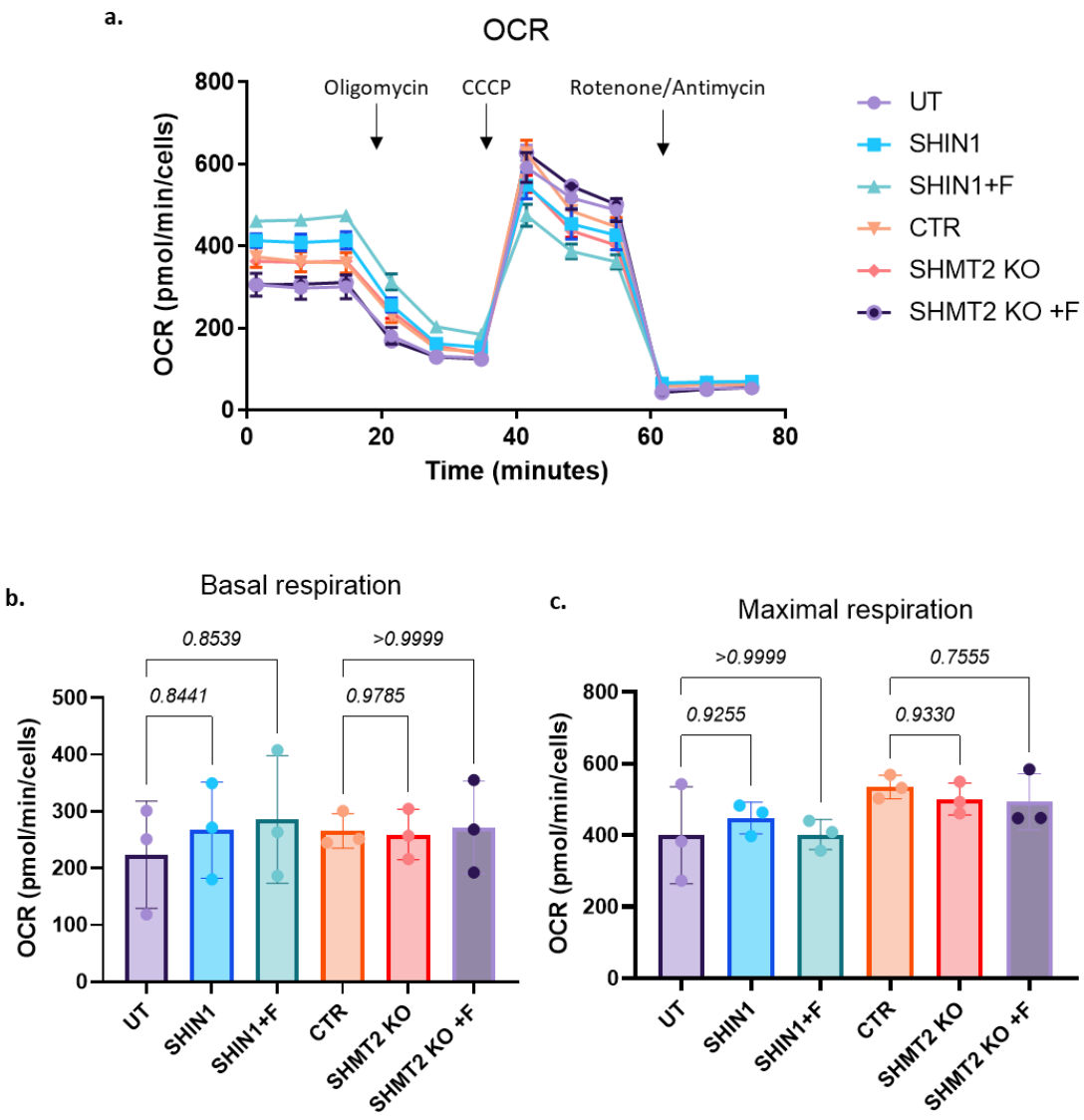

Figure 3-18: Folate metabolism inhibition does not have significant effect on OXPHOS. Representative Mito stress OCR (oxygen consumption rate) profile (**a**). Basal respiration (**b**) and maximal respiration (**c**) of K562 cells following a 24h treatment with 2.5μM SHIN1 or a combination of SHIN1 with 1mM formate, ctr cells, SHMT2 KO cells +/- 1mM formate. Data were plotted as mean +/- S.D. of n=3 independent experiments. P-values were calculated with a paired one-way ANOVA with Geisser-Greenhouse correction and Sidak's multiple comparisons test.

3.8 Discussion

Folate metabolism and its role in CML is a new area of investigation, therefore, in this chapter, our first aim was to assess expression of folate associated genes in LSCs. Using publicly available data we demonstrated that folate pathway is significantly enriched in LSCs versus HSCs (**Figure** 3-1**b&c**). Furthermore, we determined the genes that confer this enrichment are mostly folate associated genes involved in reactions in the mitochondrial arm of the pathway (**Figure** 3-2**b**). These findings are in agreement with current literature demonstrating that folate metabolism mitochondrial enzymes SHMT2 and MTHFD2 are amongst the most consistently overexpressed metabolic enzymes in cancer[84, 133]. It also supports the concept that most cancer cells produce 1C units exclusively in the mitochondria and then those 1C units are transported to the mitochondria through formate. It is also worth noting that *ALDH1L2* was found to be upregulated in LSCs compared to normal counterparts. ALDH1L2 catalyses the full oxidation of 10-formyl-THF to CO_2. This reaction is accompanied by mitochondrial NADPH production, linking folate metabolism to redox homeostasis.

In addition, we discovered that LPCs have similar expression levels of folate metabolism genes as LSCs (**Figure** 3-3). Whether these cells have also similar activity to LSCs remains to be discovered. Furthermore, when comparing expression of folate metabolism genes between LPCs and HPCs, to our surprise, we uncovered that expression levels are very similar between these two populations (**Figure** 3-4). This prompted us to hypothesise that folate metabolism genes get upregulated during normal cell fate decisions (HSCs → HPCs). Indeed, we found that folate metabolism associated genes were significantly upregulated in HPCs compared to HSCs, suggesting that 1C metabolism might be more important for more differentiated normal cells rather than stem cells (**Figure** 3-5). Given that folate genes are significantly upregulated in LSCs compared to HSCs and LPCs display similar expression with normal counterparts, these data suggest that folate metabolism might be a metabolic vulnerability for LSCs. This could open a potential therapeutic window, as LSCs are insensitive to TKI treatment. However, more data, especially regarding the activity of the pathway in these stem and progenitor cell populations will be needed to support this.

Furthermore, using two other publicly available microarray datasets (GSE48294, E-MTAB-2594) we investigated the effect of imatinib treatment on expression of 1C metabolism genes in CML $CD34^+$ cells. First dataset revealed that 24h treatment with 2μM imatinib resulted in a significant downregulation of *MTHD1*, *MTHFD1L* and *DHFR* expression, while a longer treatment (96h) resulted in downregulation of other two genes, namely *SHMT2* and *SHMT1* (**Figure** 3-6**a**). Surprisingly, the second dataset revealed that a 7-days treatment with 5μM imatinib did not result in significant changes on expression of folate genes, apart from one exception, *DHFR* (**Figure** 3-6**b**). It is possible that prolonged treatment with imatinib impacts folate metabolism activity, however, the pathway might not be completely inhibited through TKI treatment. It would also be informative to examine the expression of folate associated enzymes and folate metabolism activity upon imatinib treatment in the CML $CD34^+CD38^-$ population, which seems to be the one that confers leukaemia persistence.

This general upregulation of 1C metabolism associated enzymes correlated with increased activity of the pathway in CML $CD34^+$ compared to normal counterparts (**Figure** 3-7). Formate exchange rate and media concentration were significantly higher in CML $CD34^+$ compared to normal $CD34^+$ cells. As we mentioned above, comparing formate exchange rate in CML $CD34^+$ $CD38^-$ cells with CML $CD34^+$ cells could indicate whether the activity of the pathway is higher in LSCs.

Furthermore, we also assessed sensitivity of CML cell lines to traditional antifolate MTX comparing them to a range of other cancer cell lines (**Figure** 3-8). Publicly available data revealed that CML cell lines have the second highest sensitivity to MTX, only after ALL cell lines, where MTX is routinely used. This further reinforced the idea that folate metabolism could be a metabolic vulnerability for leukaemic cells.

Following all these findings that hinted on an important role of folate metabolism in CML cells, we generated a K562 SHMT2 KO cell line. We found that loss of SHMT2 had an antiproliferative effect leading on reduced growth, cell cycle arrest on the S phase, but no significant effect on apoptosis (**Figure** 3-10). It is worth mentioning that reconstitution of purine synthesis (through hypoxanthine supplementation) and thymidylate synthesis (through thymidine

supplementation) was sufficient to rescue the antiproliferative effect of SHMT2 loss.

Given the antiproliferative effect of 1C metabolism inhibition in K562 cells, we investigated the effect of loss of SHMT2 on the engraftment capacity of leukaemic cells. For this we exploited the fact that KCL22 cells can form extramedullary tumours when transplanted via tail vein injection into immunocompromised mice. We generated a KCL22 luciferase^{+} SHMT2 KO cell line and transplanted control and SHMT2 KO cells in NRGW[41] mice. We discovered that SHMT2 loss impairs engraftment capacity of KCL22 cells and results in significantly extended survival of mice compared to mice transplanted with control cells (**Figure** 3-11;**Figure** 3-12). Furthermore, we observed a significantly reduced tumour burden in mice transplanted with SHMT2 KO cells at the experimental endpoint (**Figure** 3-12**b)**. Most of the mice transplanted with KCL22 SHMT2 KO cells did not harvest any tumours, suggesting that loss of SHMT2 inhibits tumourigenesis. Interestingly, Ducker and colleagues demonstrated that HCT-116 colon cancer cells engineered with mitochondrial 1C enzyme deletions can form xenograft tumours, by generating cytosolic 1C units from serine via the enzyme SHMT1[89]. However, in our setting it seems that KCL22 SHMT2 KO cells cannot compensate for the loss of the mitochondrial arm of the folate pathway by upregulating the cyosolic one. In addition, formate, methyl-THF, purines, and pyrimidines are present in the plasma of mice, and, metabolically, could fulfil the 1C-unit demands of KCL22 SHMT2 KO cells. Nevertheless, none of these mechanisms was not sufficient to compensate for the loss of SHMT2 in KCL22 cells. The lack of rescue highlights the absolute dependence of growing cells *in vivo* on intrinsic 1C metabolism and the potential for its therapeutic targeting. Of note, as we previously mentioned, cells rendered genetically defective in mitochondrial folate metabolism are glycine auxotrophs, completely relying on glycine uptake. While some solid tumour cell lines can uptake glycine effectively, diffuse large B-cell lymphoma cells cannot. This makes them vulnerable to 1C metabolism inhibition even in the presence of exogenous formate[164].Thus, it is possible that glycine deficiency due to SHMT2 loss may play a role *in vivo* and prevent KCL22 SHMT2 KO from xenograft formation.

Lastly, in this chapter, we investigated the metabolic changes upon genetic and pharmacological inhibition of folate metabolism. Metabolomic analysis

confirmed that both SHMT2 loss and SHIN1 treatment resulted in impairment of *de novo* purine synthesis with a significant decrease of adenine and guanine nucleotides (**Figure** 3-14). Interestingly, this decrease was accompanied by a significant increase in the purine precursor AICAR. AICAR, as we are going to describe in the next chapter, has received a lot of interest as it is an AMP mimetic and can bind directly to AMPK resulting in its activation. It is also worth noting that formate supplementation was sufficient to restore purine synthesis. As we previously discussed, formate can bypass the SHMT1/2 blockage by donating 1C units and restore purine synthesis. Interestingly, neither genetic nor pharmacological inhibition of folate metabolism resulted in decrease in pyrimidine synthesis (**Figure** 3-15). This suggests that the antiproliferative effect of inhibition of folate metabolism is mainly due to impairment of purine biosynthesis.

Besides this, folate metabolism inhibition resulted in impairment of glycolysis (**Figure** 3-16**;Figure** 3-17). We observed a decrease in glucose uptake accompanied by an increase in intracellular glucose. Furthermore, we observed a decrease in lactate production and lactate secretion. In addition, several glycolysis intermediates were downregulated. We also noticed a strong trend of decreased glycolysis and decreased glycolytic capacity through ECAR measurements. Of note, formate supplementation was sufficient to restore glycolysis. Given that restoring purine biosynthesis rescues glycolysis, the decrease in glycolysis could be the consequence of a general inhibition of cellular proliferation. On the other hand, inhibition of the folate pathway did not have any significant effect on OXPHOS (**Figure** 3-18).

3.9 Summary

To summarise, in this chapter we described that folate metabolism genes, and particularly the ones involved in mitochondrial reactions, are upregulated in LSCs compared to HSCs. We demonstrated that expression remains unchanged when LSCs differentiate towards LPCs. We also showed that a 7-days imatinib treatment does not have significant impact on expression of folate associated genes. Furthermore, we showed that 1C metabolism activity is significantly upregulated in CML $CD34^+$ cells compared to normal counterparts and that CML cell lines display high sensitivity to MTX.

We also demonstrated that genetic inhibition of the pathway has an antiproliferative effect on K562 cells by inducing cell cycle arrest at the S phase. In addition, we showed that the antiproliferative effect can be rescued by the addition of hypoxanthine and thymidine. We demonstrated that loss of SHMT2 impairs xenograft capacity of KCL22 cells and leads to extended survival of mice compared to mice transplanted with control cells. Lastly, we showed that inhibition of folate metabolism results in impairment of purine synthesis and glycolysis with no effect in pyrimidine synthesis and OXPHOS. These changes could be rescued by the addition of formate.

Chapter 4 Inhibition of 1C metabolism causes a cascade of signalling changes in CML cells

4.1 Introduction

In the previous chapter we described that genetic or pharmacological inhibition of 1C metabolism results in a blockage of *de novo* purine synthesis and accumulation of the purine synthesis intermediate AICAR.

As previously mentioned, AICAR-dependent AMPK activation has been linked to the cytotoxic effects of antifolates[98, 119]. Furthermore, it has been described that AICAR treatment has a cytotoxic effect on CML cells, including imatinib-resistant cells, which correlated with autophagy induction. Interestingly, the same work describes that the cytotoxic effect of AICAR is AMPK-independent[165].

AMPK is a master regulator of cell metabolism (**Figure** 4-1). It is a heterotrimeric complex consisting of a catalytic α subunit and two regulatory subunits ß and γ. Interestingly, humans possess multiple isoforms for each subunit; there are two isoforms for the α subunit, two ß-subunits and three γ-subunits, potentially creating 12 different AMPK complexes.

Upon energetic deprivation, AMPK gets phosphorylated/activated and phosphorylates specific enzymes to increase the catabolic activity of the cell in order to increase ATP generation and decrease ATP consumption. On the other hand, it suppressed the anabolic activity of the cell through the modulation of the master regulator of growth mTOR. AMPK activation leads to the inhibition of mTOR complex 1 (mTORC1) by two independent mechanisms: the activation of the negative regulator tuberous sclerosis complex 2 (TSC2), and the inhibition of the mTORC1 subunit RAPTOR. Lower mTORC1 activity leads to decreased cell growth and decreased protein synthesis[166].

The role of AMPK in tumourigenesis has been ambiguous. Faubert *et al*. demonstrated that loss of AMPKα1 cooperates with MYC to accelerate lymphomagenesis, supporting a metabolic tumour suppressor function of AMPK[167]. Furthermore, additional evidence supporting a tumour suppressor role of AMPK is derived from studies with metformin. Metformin displays an AMPK-

dependent anti-neoplastic response and it has been shown to delay tumour progression[168]. As mentioned previously, metformin can also synergize with MTX to improve response to traditional antifolates, highlighting the tumour suppressor role of AMPK. Nevertheless, Saito and colleagues described that AMPK activation promotes AML with a translocation between the mixed lineage leukemia (MLL) and AF9 genes (producing MLL-AF9) and protects LICs from metabolic stress in the BM niche[169].

Therefore, in the chapter, we aimed to delineate how inhibition of 1C metabolism impacts cellular homeostasis, possibly by activating AMPK and its downstream effectors. We also investigated how these changes impact CML cells phenotypically, with focus on changes in expression of maturation markers in leukaemic cell lines (K562, THP1 and MOLM13 cells) and patient-derived CML $CD34^+$ cells.

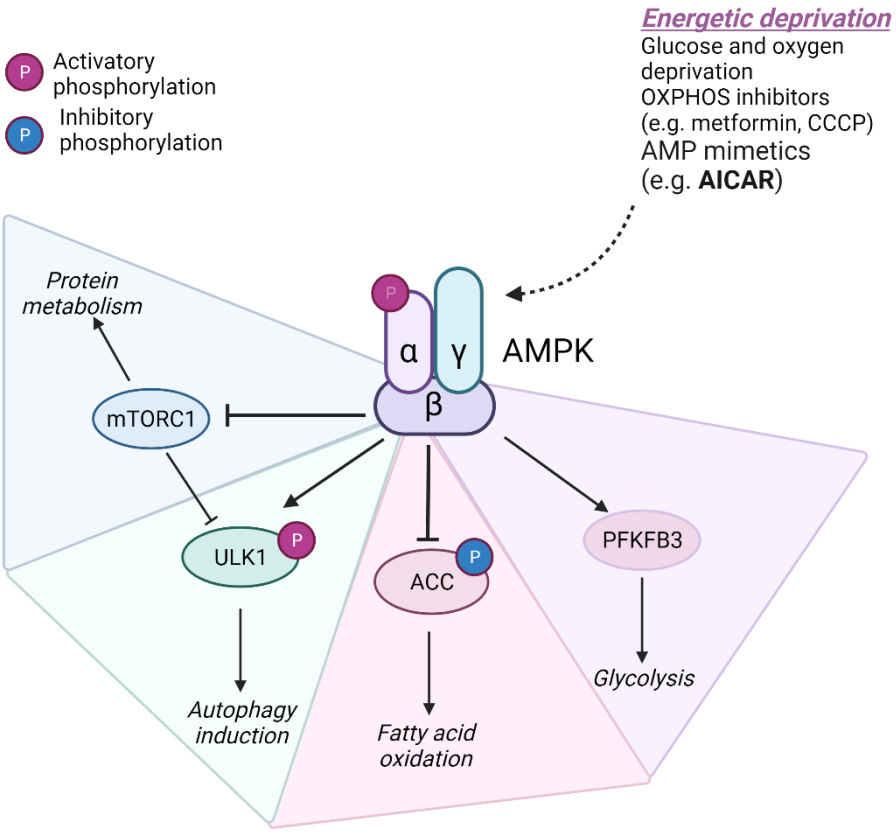

Figure 4-1: AMPK, master regulator of cell metabolism. Under low energy conditions, the AMP-activated protein kinase (AMPK) complex gets activated and phosphorylates key targets to rewire cellular metabolism. mTORC1, mechanistic target of rapamycin complex 1; ULK1, unc-51 like autophagy activating kinase; ACC, acetyl-CoA carboxylase; PFKB3, 6-phosphofructo-2-kinase/fructose-2,6-biphosphatase 3.

4.2 Folate metabolism inhibition induces AMPK signalling

To investigate the effect of 1C metabolism inhibition on AMPK signalling, K562 cells were treated with the SHIN1 dual inhibitor for 24h. Furthermore, K562 *SHMT2 KO* were cultured without HT supplement for the same time length. Formate supplementation was used to assess whether reconstitution of purine synthesis could suppress activation of AMPK, similarly to what was observed with accumulation of AICAR, which was formate dependent. Additionally, AICAR treatment was used as a positive control of AMPK activation.

This revealed that both pharmacological and genetic inhibition of 1C metabolism induced AMPK phosphorylation on Thr-172 (**Figure** 4-2). AMPK-dependent phosphorylation of ACC and ULK1 was also observed. Similar results were obtained with AICAR treatment, however there was no significant additive effect when combining 1C metabolism inhibition with AICAR treatment. Formate supplementation was sufficient to suppress activation of AMPK signalling. Simultaneously, folate metabolism inhibition suppressed mTORC1 activity, which was measured by the phosphorylation of the ribosomal protein S6. Dephosphorylation of S6 was rescued by the addition of formate, while AICAR had a more subtle effect on mTORC1 activity. It is worth noting that inhibition of 1C metabolism increased the overall levels of ULK1, suggesting that there might be a transcriptional upregulation on the mRNA level (further discussed in **4.3.2**)(**Figure** 4-2). From these results it can be concluded that pharmacological and genetic inhibition of folate metabolism leads to activation of AMPK signalling and this is dependent on purine synthesis, as formate supplementation can reverse such effect.

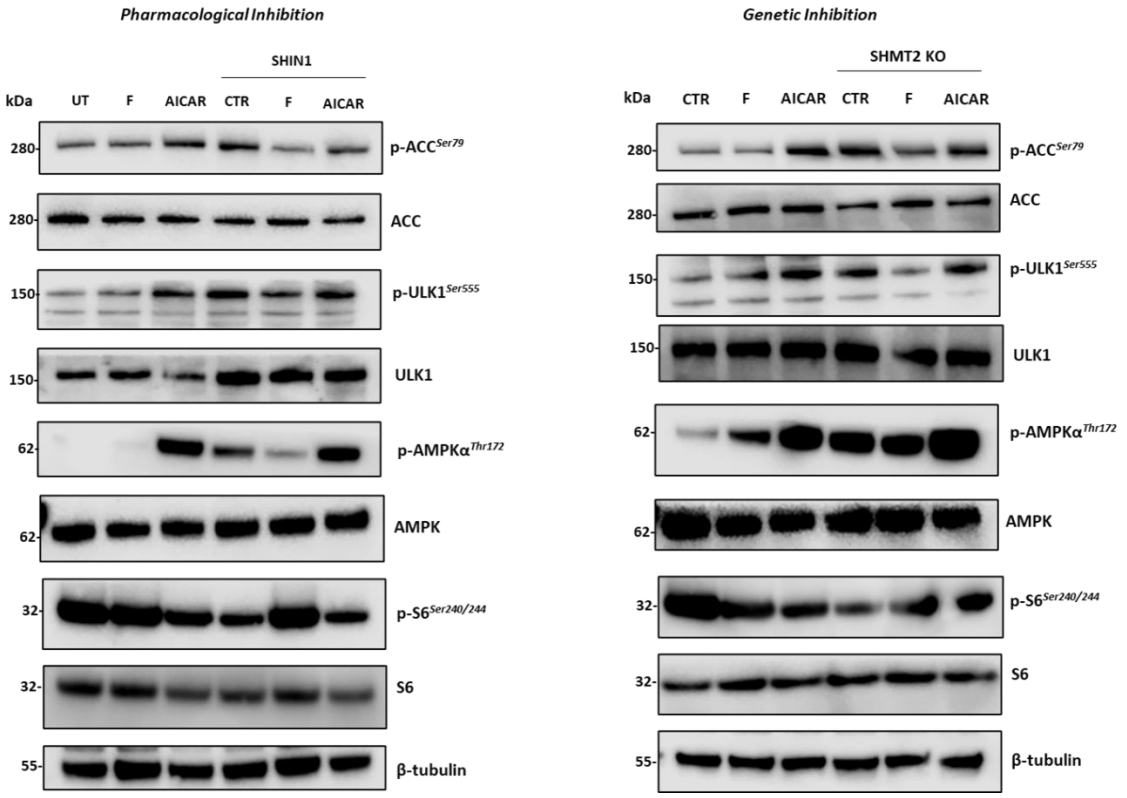

Figure 4-2: 1C metabolism inhibition induces activation of AMPK signalling. Representative western blots showing AMPK signalling markers in K562 cells following pharmacological (SHIN1; 2.5μM) or genetic inhibition of 1C metabolism. AICAR (1mM) treatment was used as a positive control of AMPK activation. All treatments were carried out for 24h.Notations: F denotes 1mM formate supplementation. β -tubulin was used a loading control. Representative of n=3 independent experiments.

4.3 1C metabolism inhibition leads to autophagy induction

4.3.1 Folate metabolism inhibition leads to induction of autophagy markers

As mentioned previously, AMPK activation promotes the catabolic activity of the cell for subsequent ATP generation. One of such pathways is autophagy, which we have previously discussed in relation to its crucial role in normal haematopoiesis and how it serves as a potential target to sensitise LSCs to TKI therapy[32, 67]. Thus, after describing activation of AMPK signalling and activating phosphorylation of ULK1, a kinase that drives initiation of autophagy, following folate metabolism inhibition, we aimed to address the effect on autophagy induction.

We uncovered that both pharmacological and genetic 1C metabolism inhibition promoted the ULK1-dependent phosphorylation of ATG13, which forms a complex with ULK1 and other proteins to initiate autophagy. Interestingly, AICAR treatment did not induce phosphorylation of ATG13. Whereas formate supplementation was sufficient to suppress the induced phosphorylation on ATG13 (**Figure** 4-3**a**).

To further assess autophagy flux, we used two well-known autophagy markers, namely (microtubule associated protein 1 light chain 3) LC3 and p62 (also known as sequestosome-1, SQSTM1). There are three human LC3 isoforms (LC3A, LC3B and LC3B) that undergo posttranslational modifications during autophagy. Cytosolic LC3-I gets conjugated to phosphatidylethanolamine to form LC3-II which is recruited to autophagosomal membranes. LC3-II is later cleaved from autophagosomal membranes and gets internalised in the autophagosome. p62 is an autophagy cargo receptor which interacts with LC3-II to deliver cargo to the autophagosome. When the autophagosome gets fused with the lysosome to form autolysosomes, sequestered intra-autophagosomal components are degraded by lysosomal hydrolases, including LC3-II and p62. When assessing these two markers (**Figure** 4-3**a**), inconclusive results were obtained, where both AICAR and pharmacological or genetic inhibition of 1C metabolism resulted in accumulation of p62. Such accumulation could suggest either a blockage in

autophagy flux (inhibition of p62degradation) or alternatively, transcriptional upregulation of the *SQSTM1* gene. With regards to LC3, SHIN1 treatment caused a decrease of both LC3-I and LC3-II, whereas there was an accumulation of LC3-II in K562 *SHMT2 KO* cells, pointing to an increase in autophagy.

To understand wherever changes in LC3 and p62 were an outcome of the accumulation of autophagosomes due to block in autophagy flux, or a result of elevated autophagic activity, we decided to use the lysosomal inhibitor hydroxychloroquine (HCQ), which blocks the fusion of the autophagosome with the lysosome. We treated K562 cells with HCQ, SHIN1 or a combination of both for 8h and we assessed p62 and LC3 levels. As expected, HCQ treatment caused an accumulation of LC3-II compared to untreated cells. Furthermore, combination of SHIN1 with HCQ caused a further increase in LC3-II accumulation (**Figure** 4-3**b**). These data strongly suggest that inhibition of folate metabolism leads to an increase in autophagic activity. As for p62, we did not observe any accumulation in SHIN1 treated K562, but this might be due to the shorter timepoint used in this experiment. However, to get a better understanding of the effect of 1C metabolism on autophagy, we decided to investigate transcriptional changes in *SQSTM1* and other autophagy related genes.

4.3.2 Inhibition of 1C metabolism results in increased expression of autophagy related genes

To investigate transcriptional changes on autophagy related genes, K562 cells were treated with SHIN1 for 24h. As before, formate supplementation was used to see whether reconstitution of the purine pool could suppress any changes caused by folate metabolism inhibition. AICAR was used to assess whether changes could be attributed to AMPK signalling activation. Autophagy related genes (*SQSTM1, ULK1, ATG5* and *ATG7)* expression was assessed via qPCR**.** **Figure** 4-3**a&b** demonstrates that folate metabolism inhibition or AICAR treatment induces p62 at protein level, which was also confirmed at transcriptional level, where *SQSTM1* exhibited a significant upregulation compared to untreated cells (**Figure** 4-4). Reconstitution of *de novo* purine synthesis via formate supplementation was sufficient to bring gene levels to that of the control cells. This significant upregulation of the gene encoding p62, reinforced the idea that upregulation of p62 on protein level was not due to

autophagy blockage on the autophagosome level, but it was a result of transcriptional upregulation of *SQSTM1*. This could indicate p62 involvement in other pathways in addition to autophagy.

Similar to *SQSTM1*, SHIN1 or AICAR treatment induced a significant increase in expression of *ULK1* compared to untreated cells. SHIN1-induced overexpression of *ULK1* was rescued by formate supplementation. Furthermore, pharmacological inhibition of 1C metabolism significantly upregulated the expression of autophagy related genes 5 and 7 (*ATG5* and *ATG7*). Interestingly, reconstitution of purine synthesis, did not rescue the SHIN1-mediated effect on expression of *ATG5,* and, as for *ATG7*, did just partially reduce it. This inability to completely suppress the effect of SHIN1 treatment could be attributed to the significant increase in expression of all four autophagy related genes following treatment with formate as a single agent (**Figure** 4-4). On protein level, formate did not increase the levels of ULK1 and p62 (**Figure** 4-2 & **Figure** 4-3**a**), potentially because of counterbalancing posttranslational modifications. AICAR treatment was sufficient to cause upregulation of *ATG5* and *ATG7,* similarly to SHIN1 treatment, suggesting that the effect of 1C metabolism inhibition on autophagy might be AMPK-dependent.

Overall, the data presented so far demonstrate that 1C metabolism inhibition leads to AMPK activation and autophagy induction. These signalling changes might be a result of suppressed purine synthesis and accumulation of the AMPK activator, AICAR.

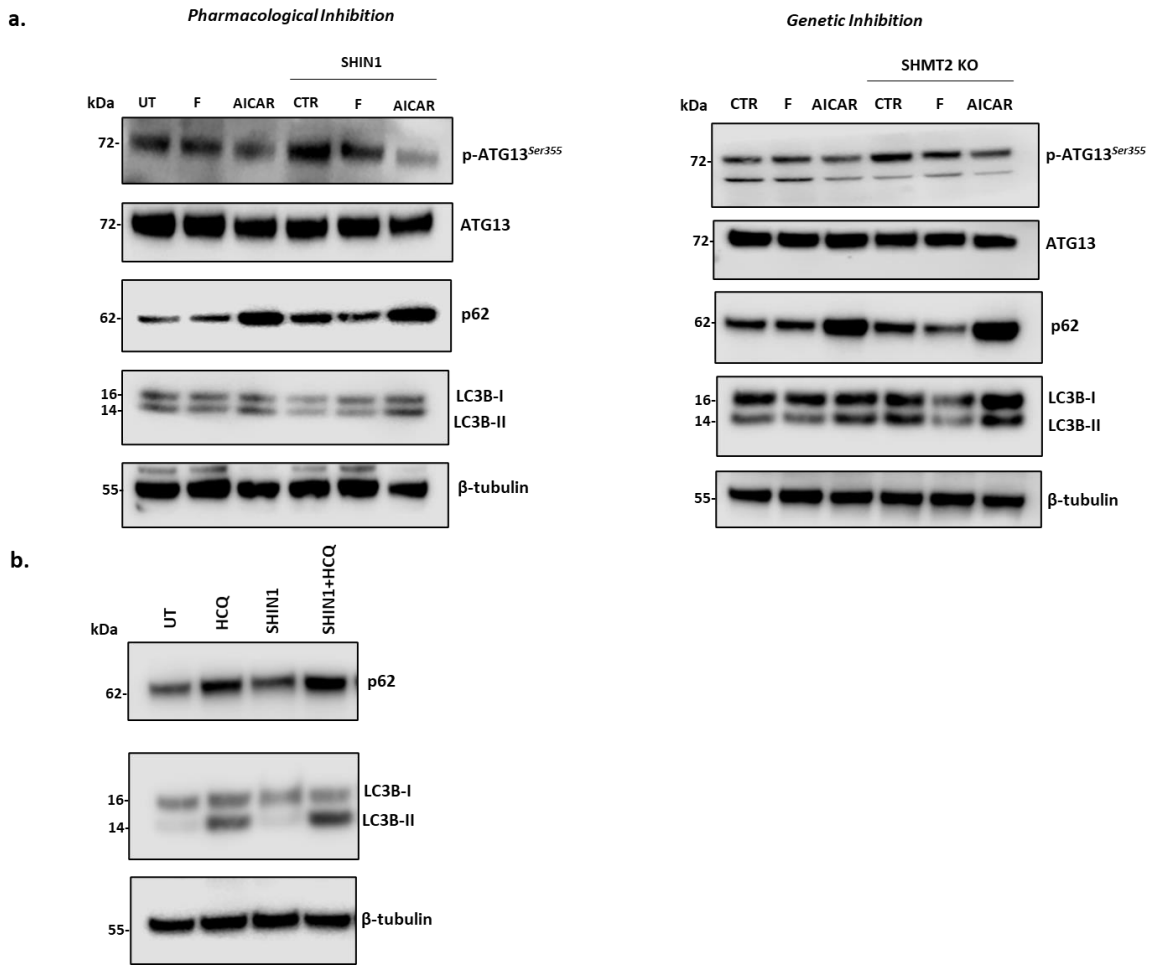

Figure 4-3: 1C metabolism inhibition induces autophagy. Representative western blots showing changes in autophagy markers upon a 24h pharmacological or genetic inhibition of folate metabolism (**a**). Western blot analysis showing changes in autophagy markers in K562 cells exposed to 5μM HCQ (hydroxychloroquine), 2.5μM SHIN1 or a combination of both for 8h.β -tubulin was used a loading control. Representative of n=3 independent experiments.

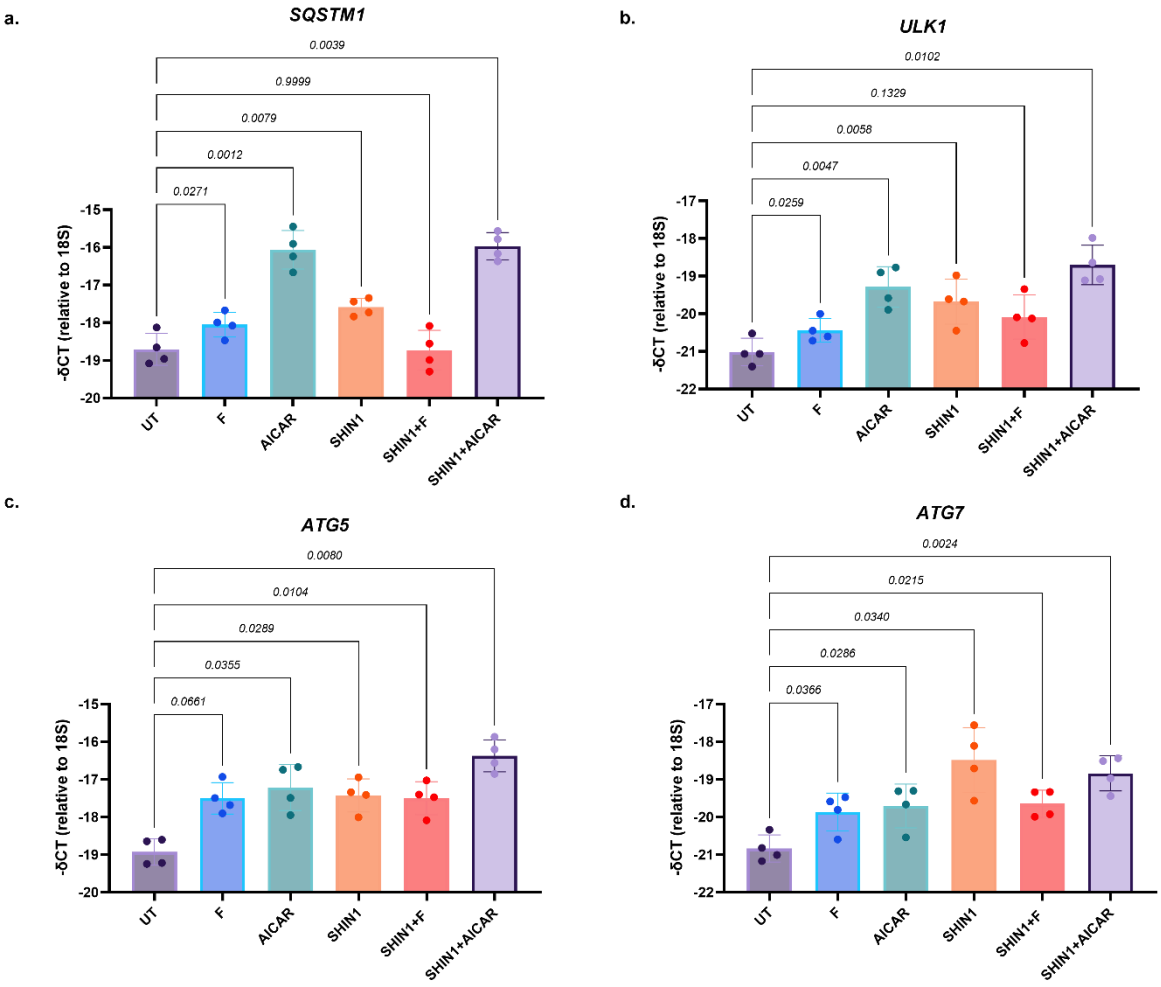

Figure 4-4: Upregulation of autophagy related genes upon inhibition of 1C metabolism. RT-PCR analysis of autophagy related genes *SQSTM1* (**a**), *ULK1* (**b**), *ATG5* (**c**) and *ATG7* (**d**) following a 24h treatment with 1mM formate (F), 1mM AICAR ,2.5µM SHIN1, or a combination of SHIN1 and F, or SHIN1 and AICAR. *18S* was used as internal amplification control. Data were plotted as mean +/- S.D. of n=4 independent experiments. P-values were calculated with a paired one-way ANOVA with Geisser-Greenhouse correction and Dunnett's multiple comparisons test.

4.4 Inhibition of 1C metabolism drives expression of erythropoiesis markers

4.4.1 Folate metabolism inhibition leads to enhanced expression of erythropoietic markers in K562 cells

Following either pharmacological or genetic inhibition of folate metabolism, cell pellets appeared to have a stronger red colour than untreated or control cells respectively, suggesting an increase in erythroid maturation which would cause a higher haemoglobin content and consequently, the appearance of a red pellet (**Figure** 4-5**a**). K562 cell line has been proposed as a useful *in vitro* model to study erythropoiesis, as these cells undergo erythroid differentiation when treated with a variety of compounds like erythropoietin and haemin[36]. Furthermore, as we have previously mentioned, autophagy and mitophagy play an important role during erythropoiesis, as they regulate the clearance of organelles like mitochondria and ribosomes[35]. Thus, we aimed to investigate whether this phenotypic change in colour would correlate with changes in expression of erythroid maturation markers. For this, we utilised two well-known erythroid markers, CD71 and glycophorinA (GlyA). CD71, also known as a transferrin receptor protein 1 (TfR1) is a transmembrane glycoprotein necessary for iron import inside the cell, while GlyA is a sialoglycoprotein found in the membrane of erythrocytes[170].

Assessment of the levels of CD71 and GlyA in SHMT2 deficient cells, revealed that loss of SHMT2 resulted in a 10-fold increase in the percentage of $CD71^{+}GlyA^{+}$ cells compared to control cells (**Figure** 4-5**b**). Additionally, 72h treatment with the SHIN1 inhibitor resulted in a 3-fold increase in the percentage of $CD71^{+}GlyA^{+}$ cells compared to untreated cells (**Figure** 4-5**c &d**). Purine synthesis reconstitution with the supplementation of formate was sufficient to suppress the increase in levels of CD71 and GlyA and bring back the percentage of $CD71^{+}GlyA^{+}$ to the level of the untreated cells. The AMPK-activator, AICAR, displayed a similar significant increase of the percentage of $CD71^{+}GlyA^{+}$ cells, implying that the increase in expression of erythroid differentiation markers could be AMPK-dependent. Of note, combination of SHIN1 and AICAR did not confer any further increase on the expression of CD71 and GlyA when compared to either SHIN1 or AICAR single treatments.

4.4.2 SHIN1 treatment induces erythroid maturation in patient-derived CML CD34$^+$ cells

To further investigate our hypothesis that folate metabolism inhibition promotes differentiation of more clinically relevant CML cells, we turned out attention to patient-derived CML CD34$^+$ cells. CML CD34$^+$ cells are cultured in serum-free media (SFM) media, supplemented with physiological concentrations of growth factors and cytokines to prevent rapid differentiation, and loss of primitive HSC markers *in vitro*. Therefore, we decided to supplement the SFM media with low units of EPO (3U/ml) to sensitise cells to erythroid differentiation[171].

CML CD34$^+$ cells were treated with the SHIN1 inhibitor for 72h and erythroid markers CD71 and GlyA were evaluated using flow cytometry. Inhibition of 1C metabolism led to a significant 3-fold increase in CD71$^+$GlyA$^+$ cells compared to untreated cells (**Figure** 4-6). A high concentration of EPO (10U/ml) was used as a positive control and demonstrated similar trend to SHIN1. Formate supplementation, similar to previous experiments in K562 cells, was sufficient to reverse the increase in expression of erythroid markers. Overall, in both K562 and CML CD34$^+$ cells, SHIN1 treatment resulted in significantly increased levels of erythroid maturation markers that could be reversed by the addition of formate, indicating that the phenotype might be dependent on purines' availability.

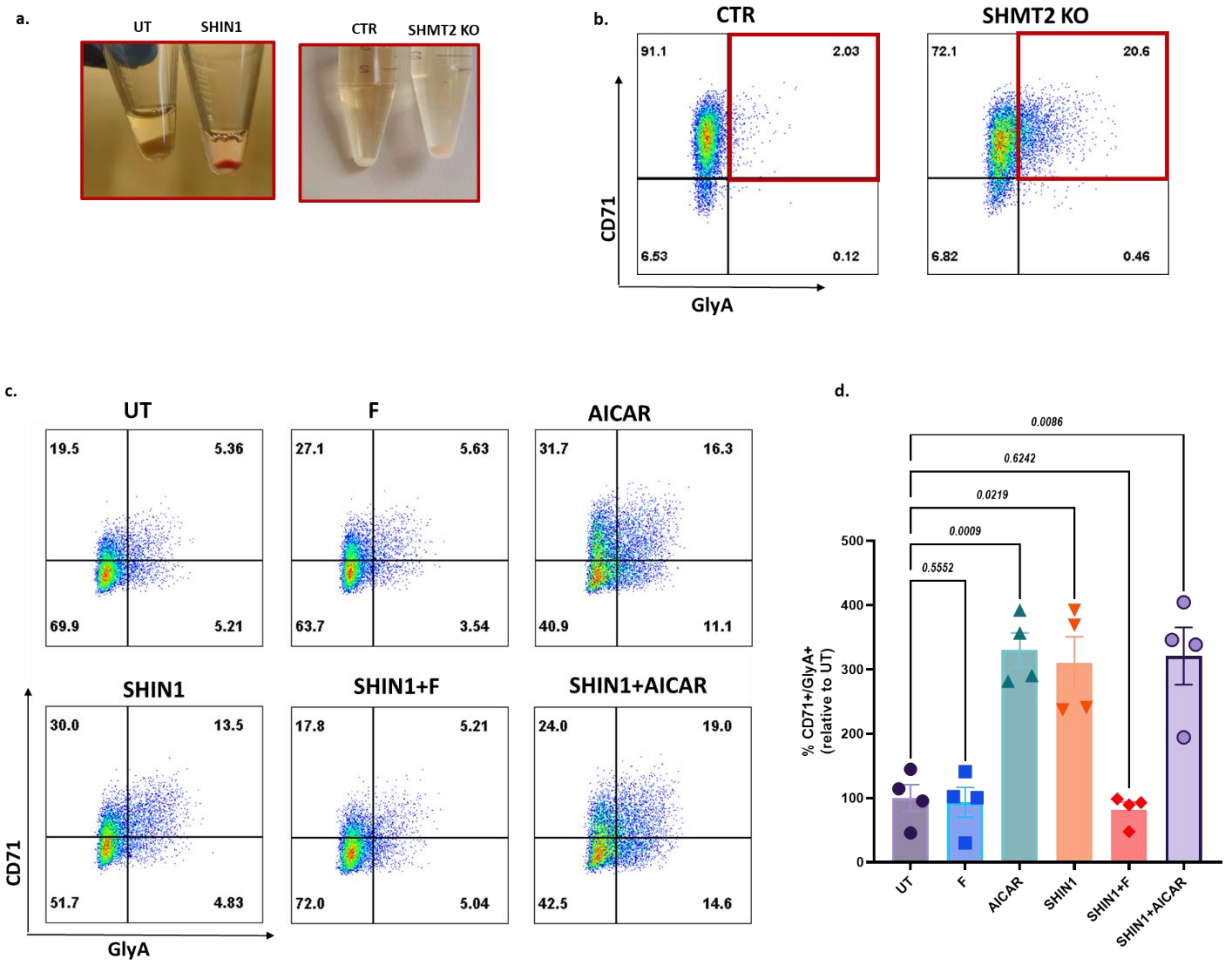

Figure 4-5: Inhibition of folate metabolism leads to an increased expression of erythropoiesis markers. Representative pictures of cell pellets in untreated (UT) and SHIN1 treated cells and vector CTR and *SHMT2* deficient cells (**a**). Flow cytometry plots showing expression of erythroid markers CD71 and Glycophorin A (GlyA) in CTR and SHMT2 deficient cells; n=1 independent experiments (**b**). Representative flow cytometry plots of levels of erythroid markers CD71 and GlyA in K562 cells following 72hr treatment using 1mM formate, 1mM AICAR, 2.5μM SHIN1 or a combination of SHIN1 with either formate or AICAR (**c**). Percentage of $CD71^{+}GlyA^{+}$ cells relative to untreated following 72hr treatment with 1mM formate, 1mM AICAR, 2.5μM SHIN1 or a combination of SHIN1 with either formate or AICAR (**d**). Data were plotted as mean +/- S.D. of n=4 independent experiments. P-values were calculated with a paired one-way ANOVA with Geisser-Greenhouse correction and Dunnett's multiple comparisons test.

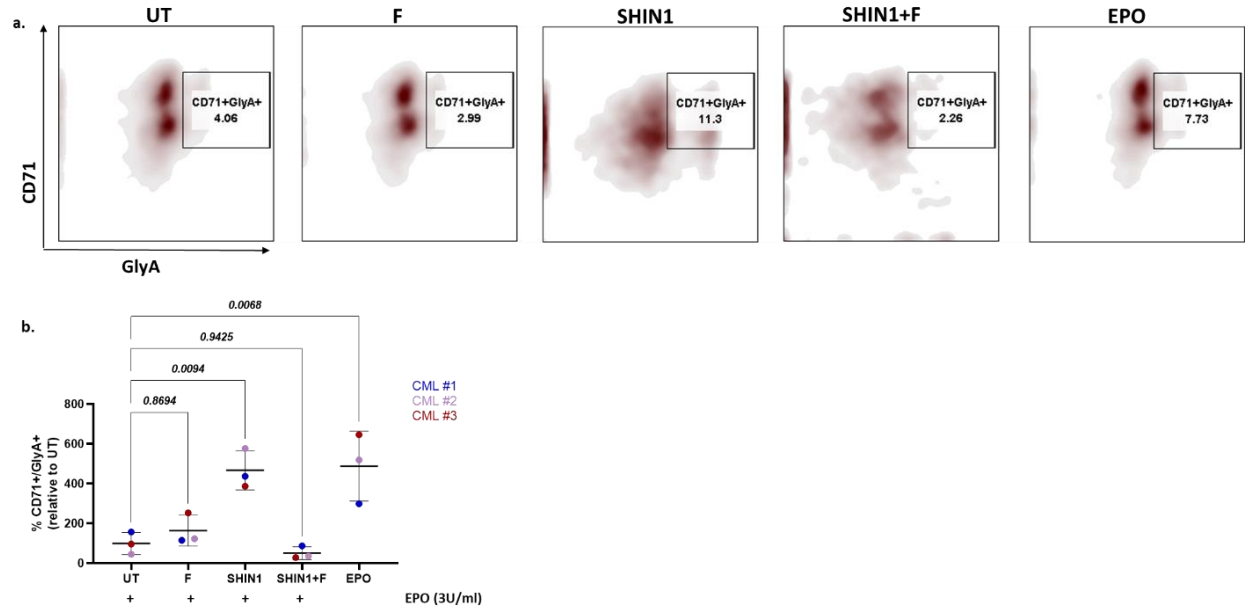

Figure 4-6: SHIN1 treatment drives an increase in erythroid markers' expression in CML CD34$^+$ cells. Representative plots showing % of CD71$^+$GlyA$^+$ CML CD34$^+$ cells treated for 72hr with 1mM formate, 2.5μM SHIN1, a combination of both or 10U/ml erythropoietin (EPO) (**a**). Percentage of CD71$^+$GlyA$^+$ cells relative to untreated following a 72h-treatment 72hr with 1mM formate, 2.5μM SHIN1, a combination of both or 10U/ml erythropoietin (EPO) (**b**). n=3 CML samples. Mean +/- SD were calculated with a paired one-way ANOVA with Geisser-Greenhouse correction and Dunnett's multiple comparisons test.

4.5 Folate metabolism inhibition promotes expression of myeloid marker CD11b in AML cell lines

Given the effect that SHIN1 treatment on erythroid markers CD71 and GlyA in K562 cells and primary CML $CD34^+$ when supplemented with low levels of EPO, we wondered whether 1C metabolism inhibition could promote specifically erythroid maturation of leukaemic cells, or overall differentiation of immature leukaemic cells. Therefore, we decided to carry out a similar experiment with two monocytic AML cell lines, THP1 and MOLM13. These cell line express monocytic surface markers like CD11b, where increase in CD11b expression correlates with differentiation into myeloid lineage. THP1 cells can differentiate into fully matured macrophages when exposed to phorbol-12-myristate-13-acetate (PMA). Pikman and colleagues demonstrated that knockdown of *MTHFD2* in MOLM13 cells resulted in increased expression of CD11b and myeloid maturation[172].

We treated both cell lines with the SHIN1 inhibitor for 72h and examined CD11b expression by flow cytometry. This revealed that in the two cell lines there was a significant increase in CD11b expression, namely around 90% in THP1 cells and 60% in MOLM13 cells (**Figure** 4-7). Furthermore, formate supplementation was sufficient to suppress the increase in CD11b and retrieve its expression to comparative level of untreated cells.

These data suggest that inhibition of folate metabolism induces differentiation of immature cells and can relieve the blockage that keeps cells in an undifferentiated state.

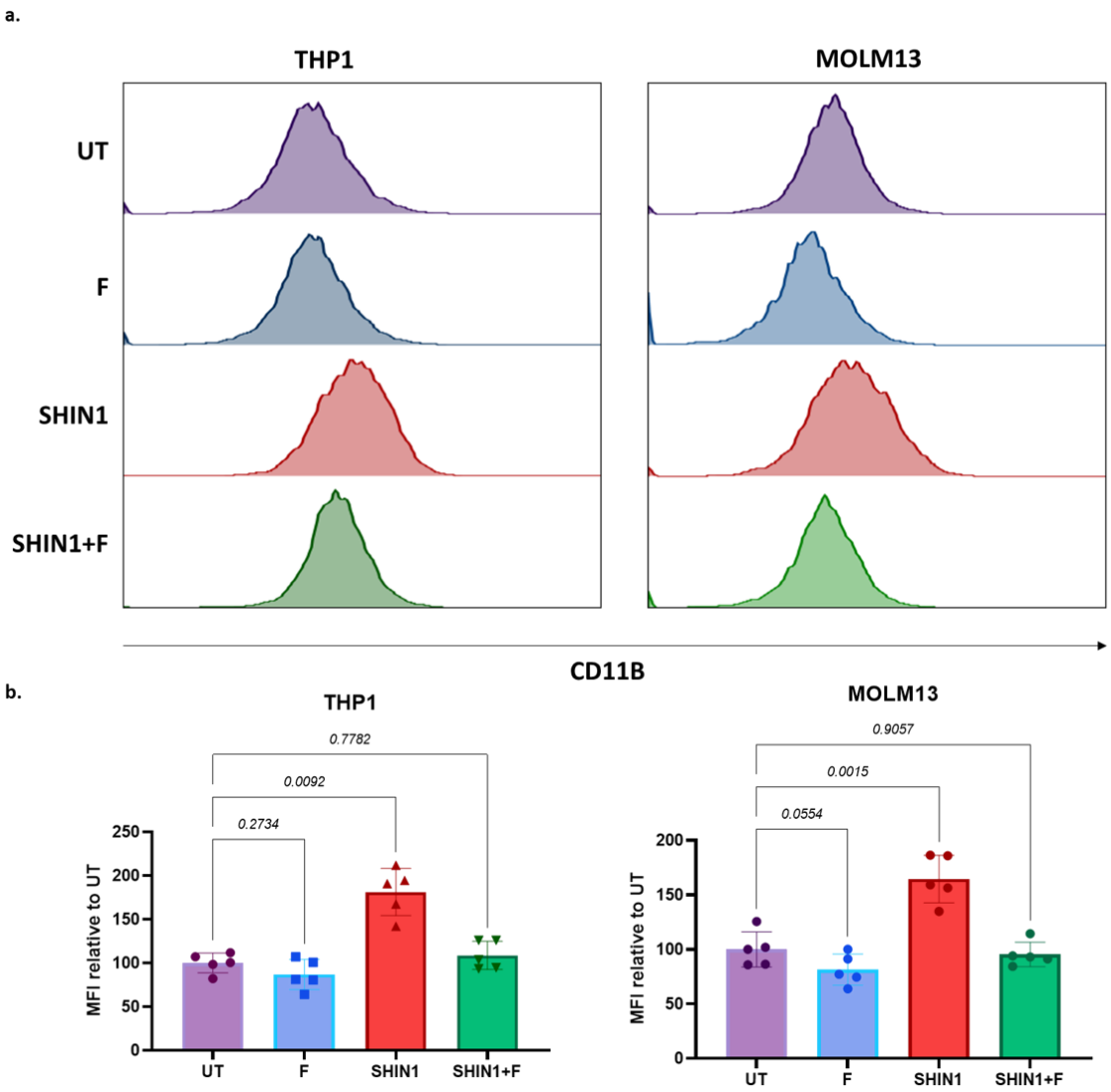

Figure 4-7: SHIN1 treatment induces an increase in myeloid maturation marker CD11b in AML cell lines. Representative FACS plots showing CD11b expression in THP1 and MOLM13 cell lines following a 72h treatment with 1mM formate, 2.5μM SHIN1 or a combination of both (**a**). Mean fluorescence intensity (MFI) of CD11b expression in THP1 and MOLM13 cell lines following a 72h treatment with 1mM formate, 2.5μM SHIN1 or a combination of both (**b**). Data were plotted as mean +/- S.D. of n=5 independent experiments. P-values were calculated with a paired one-way ANOVA with Geisser-Greenhouse correction and Dunnett's multiple comparisons test.

4.6 Discussion

In this chapter we described the effect inhibition of folate metabolism has on signalling pathways, autophagy and differentiation of CML cells. In the previous chapter we revealed that both pharmacological (using SHIN1 dual inhibitor) and genetic (loss of SHMT2) inhibition of the pathway resulted in accumulation of AICAR, an intermediate of *de novo* purine synthesis and a direct activator of AMPK (**Figure** 4-1). Indeed, it this chapter we observed that both SHIN1 treatment and loss of SHMT2 led to AMPK activation, measured by phosphorylation of AMPKα on the conserved residue Thr-172 (**Figure** 4-2). As we previously mentioned, AMPK is a master regulator of cellular metabolism and upon energy stress it gets activated to promote the catabolic activity of the cell to promote ATP production and inhibit anabolic processes that consume ATP. As expected, pharmacological and genetic inhibition led to phosphorylation of ACC and ULK1 on serine residues that are directly phosphorylated by AMPK. Furthermore, we also observed suppression of mTORC1 activity, observed by a decrease of phosphorylation of the ribosomal protein S6. Similarly to AMPK, mTOR is a critical growth regulator in animals and controls anabolic and catabolic processes in response to nutrients and nutrient-induced signals, like insulin[173]. As we previously mentioned, mTOR suppression is critical for the maintenance of HSCs through ROS repression.

It is worth mentioning that formate supplementation and ultimately, purine synthesis reconstitution was sufficient to reverse AMPK signalling activation. This suggests that AMPK signalling activation upon folate metabolism inhibition is a result of suppression of *de novo* purine synthesis. To reinforce this, SHIN1 and SHMT2 KO led to similar effects on AMPK signalling as AICAR treatment alone, indicating that the effect might be dependent on the build-up of this purine precursor. Interestingly, we did not observe any additive effect when combining 1C metabolism inhibition with AICAR, potentially due to saturation of AMPK activation through this route. It is important to note that we did not observe any differences between SHIN1-mediated dual inhibition of SHMT1/2 and SHMT2 loss with regards to AMPK activation, even though SHIN1 targets both cytosolic and mitochondrial compartment leading to complete inhibition of the pathway, whereas loss of SHMT2 leaves intact the cytosolic arm.

As both AMPK and mTOR have a direct effect on autophagy, where activation of AMPK and inhibition of mTOR lead to autophagy induction, we decided to assess the effect of 1C metabolism inhibition on autophagy. Autophagy is considered a double-edged sword in cancer, as in early tumourigenesis it can act as a tumour suppressor by degrading potentially harmful agents or damaged organelles, whereas it can turn out to be beneficial for tumour cell viability in advanced stages of tumourigenesis by protecting them from stressful microenvironments. In CML, autophagy is thought to protect LSCs from TKI-treatment, where genetic or pharmacological inhibition of autophagy can sensitise LSCs to traditional TKIs[65-67].

To get a better understanding of the autophagic flux upon inhibition of folate metabolism, we examined expression of two well-known autophagy markers, p62 and LC3. Surprisingly, we observed accumulation of p62 in AICAR or SHIN1 treated cells and in SHMT2 KO cells, which could suggest a blockage of the autophagy flux leading to accumulations of autophagosomes (**Figure** 4-3**a**). Furthermore, results on LC3B-II were inconclusive, therefore we decided to carry to treat K562 cells with the lysosomal inhibitor, HCQ, SHIN1 or a combination of both to get a better understanding of the autophagic flux. We revealed that combination of SHIN1 with HCQ caused a further accumulation of LC3-II compared to HCQ alone, indicating an increased autophagic flux (**Figure** 4-3**b**).

On a transcriptional level, we showed that SHIN1 and AICAR treatment caused a significant upregulation of *SQSTM1* expression, which would explain p62 accumulation on protein level (**Figure** 4-4). Apart from its role in autophagy as a cargo receptor, p62 is implicated in activation of nuclear factor kappa-light-chain-enhancer of activated B cells (NF-κB), the stress responsive transcription factor nuclear factor erythroid 2-related factor 2 (NRF2). It would be interesting to characterise whether p62 accumulation following 1C metabolism inhibition leads to NRF2 activation, as NRF2 has been found to regulate HSC quiescence and maintenance[174]. Furthermore, a similar trend was observed for other three autophagy markers, namely *ULK1*, *ATG5* and *ATG7*, which were found to be upregulated transcriptionally following SHIN1 or AICAR treatment. It is worth mentioning that formate supplementation was sufficient to rescue *SQSTM1* and *ATG7* upregulation, partially rescue *ULK1* overexpression and did not have any effect on *ATG5*. However, formate as single treatment induced expression of all

four genes transcriptionally, something that did not translate to the protein level for p62 and ULK1 (**Figure** 4-2**; Figure** 4-3**a**). Overall, these data suggest that 1C metabolism inhibition leads to autophagy induction in an AMPK-dependent manner.

Furthermore, we reported that folate metabolism inhibition leads to increased levels of erythroid maturation markers (CD71 and GlyA) in K562 cells and in primary CML $CD34^+$ cells when cultured with low levels of EPO (**Figure** 4-5;**Figure** 4-6**)**. Additionally, a similar phenotype was observed in THP1 and MOLM13 monocytic cells that were driven towards myeloid differentiation, assessed by expression of CD11b surface marker (**Figure** 4-7). On all occasions, purine synthesis reconstitution through formate supplementation was sufficient to suppress expression of differentiation markers and bring back expression to the level of untreated cells. AICAR treatment demonstrated very similar effect on erythroid markers in K562 cells, suggesting that the effect might be AMPK-dependent, something that we will further explore in the next chapter.

Nevertheless, the fact that 1C metabolism inhibition can promote differentiation of leukaemic cells might be of clinical interest. As we have mentioned, persistent TKI-insensitive LSCs are in a quiescent state. Thus, pushing them out of this undifferentiated state can potentially sensitise them to TKI therapy. In the previous chapter we showed that CML $CD34^+CD38^-$ have upregulated folate metabolism. Taken together, these data suggest that even though LSCs are not highly proliferative, they experience upregulation of 1C metabolism and upon inhibition of the pathway those cells might be forced to differentiate.

Undifferentiated leukaemic cells also present a challenge also in AML, which is characterised by blockage of cell differentiation and accumulation of immature cells. Furthermore, AML treatment remains a challenge, where current available therapies offer moderate success. Thus, identifying metabolic vulnerabilities of AML cells that can promote terminal differentiation of those cells might open new therapeutic windows. Our data on THP1 and MOLM13 are in agreement with the data presented by Pikman and colleagues, where authors describe that knockdown of *MTHFD2* promotes differentiation of MOLM13 cells. Additionally, they suggest that FLT3-ITD mutations are a biomarker of response to MTHFD2

suppression, something that might need to be considered for potential therapeutic purposes[172].

4.7 Summary

Overall, we showed that both pharmacological and genetic inhibition of folate metabolism result in AMPK signalling activation and autophagy induction. Besides this, we demonstrated that inhibition of the pathway leads to expression of maturation markers, either erythroid in the case of K562 cells and CML $CD34^+$ challenged with EPO, or myeloid in the case of AML cell lines THP1 and MOLM13.

Furthermore, we showed that this cascade of signalling and phenotypic changes could be reversed with the supplementation of formate, suggesting that these changes were a result of the suppression of the *de novo* purine synthesis and the build-up of the purine intermediate and AMPK activator, AICAR.

Chapter 5 1C metabolism, mitochondrial homeostasis, and cellular differentiation

5.1 Introduction

As we described in the previous chapter, inhibition of 1C metabolism leads to AMPK activation and autophagy induction. Furthermore, it promotes expression of differentiation markers, potentially promoting terminal differentiation of immature leukaemic cells.

Mitochondrial dynamics and homeostasis play a central role when it comes to differentiation of HSCs. As we previously mentioned, elevated ROS is one of the principal drivers of differentiation. ROS is a common by-product of mitochondrial respiration, linking mitochondrial function to HSCs homeostasis. Additionally, mitophagy is necessary for terminal differentiation of erythrocytes. With regards to AMPK, it has been known for over two decades to impact mitochondrial biogenesis, mostly through PGC-1α, a master transcriptional regulator of mitochondrial biogenesis[175]. Furthermore, extensive work from the Shaw lab has shown that AMPK, following energetic stress, rapidly induces mitochondrial fission and mitophagy[157, 176].

All this evidence and the fact that half of folate metabolism reactions take place in the mitochondria prompted us to investigate the impact of 1C metabolism inhibition on mitochondrial homeostasis. More specifically we assessed mitochondrial ROS, membrane potential and mass, as well as markers of mitochondrial fission, fusion and mitophagy.

Furthermore, we wanted to get a better understanding on the differentiation phenotype that we previously described and whether it was dependent on AMPK activation. As we have mentioned, there is evidence of a role of autophagy/mitophagy in differentiation, therefore we wanted to investigate whether the differentiation is dependent on the autophagy process, and whether this is dependent on AMPK activation.

5.2 1C metabolism inhibition affects mitochondrial homeostasis

5.2.1 SHIN1 treatment induces changes in mitochondrial ROS, mass, and membrane potential

To assess changes in various mitochondrial parameters, K562 cells were treated with the SHIN1 for 72h and stained with relevant mitochondrial dyes. As before, formate supplementation was used to assess whether any changes caused by inhibition of 1C metabolism were dependent on purine synthesis and AICAR was used as a positive control for AMPK activation.

ROS accumulation positively correlates with differentiation of stem cells, therefore we hypothesised that SHIN1 treatment would lead to accumulation of ROS and increased oxidative stress. Surprisingly, SHIN1 treatment resulted in a significant decrease of mitochondrial ROS (**Figure** 5-1**b**). Purine synthesis reconstitution was sufficient to rescue the SHIN1-mediated decrease of ROS, while AICAR treatment did not show any significant effect. To further validate that the increase in erythroid maturation markers in SHIN1-treated K562 cells was not due to ROS accumulation, we treated K562 cells with a combination of SHIN1 and NAC. NAC is a precursor of cysteine and glutathione and is considered as an important antioxidant. NAC supplementation could only marginally reduce the significant increase in expression of erythroid markers CD71 and GlyA, implying that erythroid maturation in the context of 1C metabolism suppression is not ROS-dependent (**Figure** 5-2**b**).

Mitochondrial mass was measured using the fluorescent dye Mitotracker Green (MTG). As displayed by the representative histograms (**Figure** 5-1**c**), SHIN1 or AICAR treatment resulted in a modest increase of mitochondrial mass, however this was not statistically significant. As inhibition of 1C metabolism induces autophagy and potentially mitophagy, we were expecting that SHIN1 treatment might have caused a decrease of mitochondrial mass, something that we did not detect using the MTG dye.

To assess mitochondrial membrane potential, we used the membrane-permeant JC-1 dye. JC-1 dye exhibits potential-dependent accumulation in mitochondria, indicated by a green fluorescence emission for the monomeric form of the

probe, which shifts to red with a concentration-dependent formation of red fluorescent J-aggregates (**Figure** 5-1**e**). Consequently, mitochondrial depolarisation is indicated by a decrease in the red/green fluorescence intensity ratio, as seen when using the mitochondrial uncoupler CCCP (**Figure** 5-1**f**). Interestingly, both SHIN1 and AICAR treatment resulted in mitochondrial hyperpolarisation, as measured by the increase in ration of JC-1 aggregates/JC-1 monomers. Interestingly, it has been shown that autophagy inducers like rapamycin or low serum growth conditions induce hyperpolarisation of the mitochondrial membrane[177]. Mitochondrial potential was brought to levels of untreated cells with the addition of formate.

Taken together these data show that inhibition of folate metabolism leads to decreased mitochondrial ROS, a modest increase in mitochondrial mass and hyperpolarization of mitochondrial membrane.

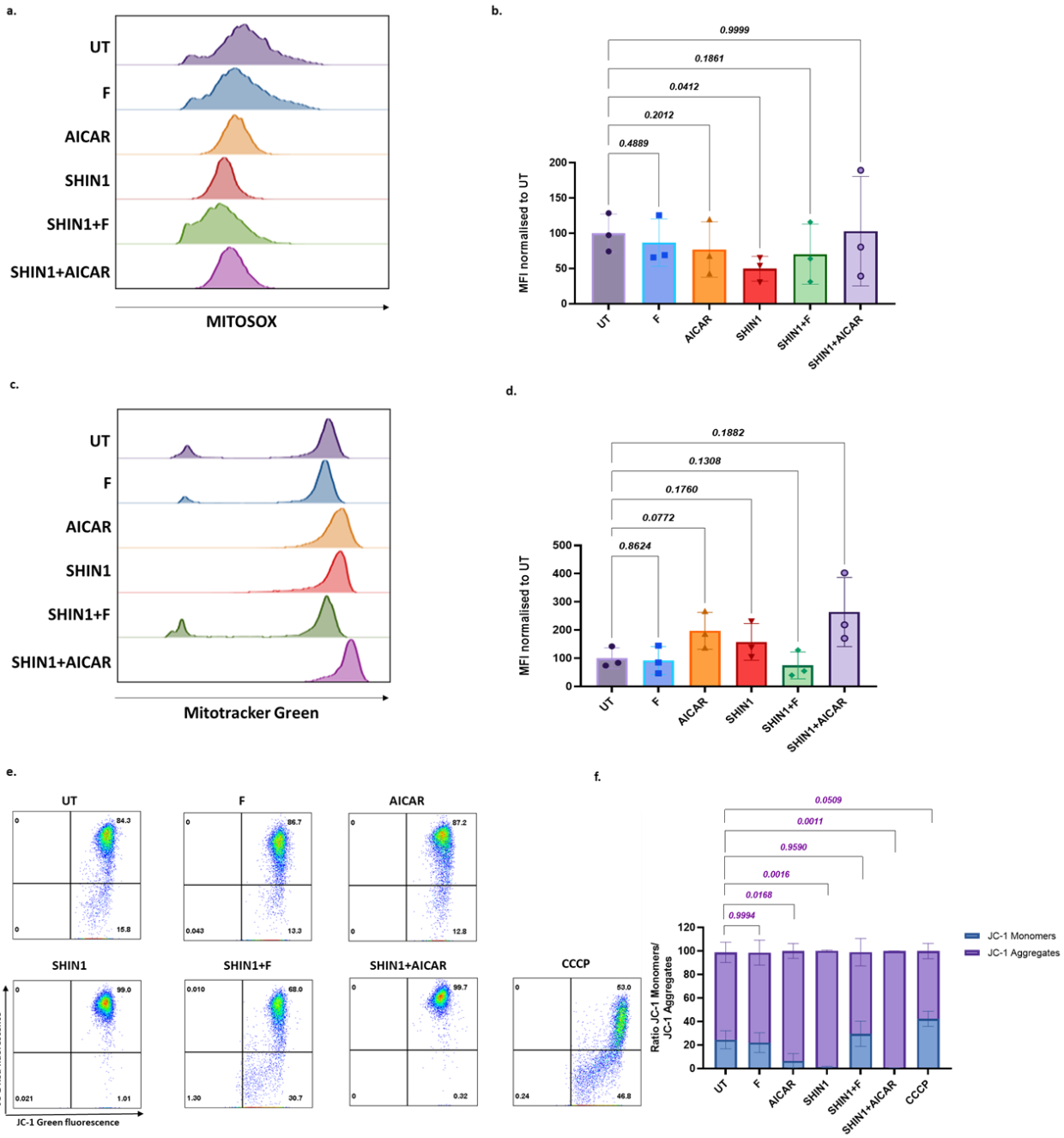

Figure 5-1: Inhibition of folate metabolism leads to changes in mitochondrial homeostasis. Representative flow cytometry plots of K562 cells showing measurements of mitochondrial ROS (MitoSOX) following 72h treatment with 1mM formate (F), 1mM AICAR, 2.5μM SHIN1, a combination of SHIN1 and F, or SHIN1 and AICAR (**a**). Graph showing mean fluorescence intensity (MFI) of MitoSOX stained cells following 72h treatment with 1mM F, 1mM AICAR, 2.5μM SHIN1, a combination of SHIN1 and F, or SHIN1 and AICAR (**b**). Representative flow cytometry plots of K562 cells showing measurements of mitochondrial mass (Mitotracker Green; MTG) following 72h treatment with 1mM F, 1mM AICAR, 2.5μM SHIN1, a combination of SHIN1 and F, or SHIN1 and AICAR (**c**). Graph showing mean fluorescence intensity (MFI) of MTG stained cells following 72h treatment with 1mM F, 1mM AICAR, 2.5μM SHIN1, a combination of SHIN1 and F, or SHIN1 and AICAR (**d**). Representative flow cytometry plots of K562 cells showing measurements of mitochondrial membrane potential using JC-1 staining following 72h treatment with 1mM F, 1mM AICAR, 2.5μM SHIN1, or a combination of SHIN1 and F, or SHIN1 and AICAR. Carbonyl cyanide m-chlorophenyl hydrazone (CCCP) was used as a positive control (**e**). Graphs representing the ratio of JC-1 monomers to JC-1 aggregates following 72h treatment with 1mM F, 1mM AICAR, 2.5μM SHIN1, a combination of SHIN1 and F, or SHIN1 and AICAR (**f**). Flow cytometry plots are representative of one of three independent experiments. Data were plotted as mean +/- S.D. of n=3 independent experiments. P-values were calculated with a paired one-way ANOVA with Geisser-Greenhouse correction and Dunnett's multiple comparisons test for (**b**) and (**d**). P-values

were calculated with a two-way ANOVA with Sidak's multiple comparisons test for (**f**). P-values displayed on (**f**) represent probability values with regards to JC-1 aggregates.

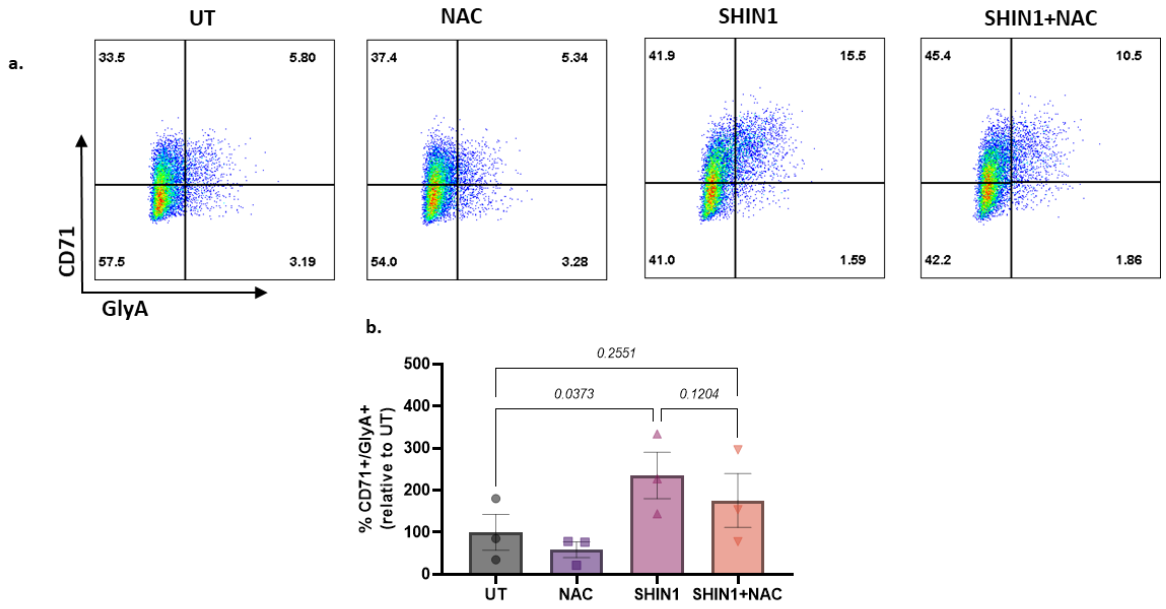

Figure 5-2: NAC treatment partially rescues the SHIN1-induced increased expression of erythroid maturation markers. Representative flow cytometry plots showing expression of erythroid maturation markers CD71 and GlyA in K562 cells following a 72h treatment with 300μM N-acetylcysteine (NAC), 2.5μM SHIN1 or a combination of both (**a**). Percentage of $CD71^{+}GlyA^{+}$ cells relative to untreated following 72hr treatment with 300μM NAC, 2.5μM SHIN1 or a combination of both (**b**). Data were plotted as mean +/- S.D. of n=3 independent experiments. P-values were calculated with a paired one-way ANOVA with Geisser-Greenhouse correction and Dunnett's multiple comparisons test.

5.2.2 SHIN1 treatment causes mitochondrial translocation of DRP1

Decrease in mitochondrial ROS and increase in mitochondrial membrane potential are characteristics of mitochondrial fragmentation/fission. Furthermore, AMPK activation following energy stress leads to mitochondrial fission. A critical protein involved in mitochondrial fission is the conserved dynamin-related protein 1 (DRP1). DRP1 gets recruited to the mitochondria by mitochondrial receptors like FIS1 (mitochondrial fission 1 protein) and MFF (mitochondrial fission factor) to initiate fragmentation. Thus, we decided to investigate the effect of SHIN1 treatment on DRP1 localisation.

To do so, mitochondrial-enriched fractions were isolated from K562 cells following a 24h treatment with the SHIN1 inhibitor. Inhibition of folate metabolism led to accumulation of DRP1 in the mitochondrial-enriched fraction (**Figure** 5-3**a**). Interestingly, there was accumulation of oligomerised DRP1, a necessary step for mitochondrial fission. This accumulation was rescued by formate supplementation. We also asked whether folate metabolism inhibition had any effect on mitochondrial fusion. Mitofusin 1 and 2 (MFN1 and MFN2) can initiate the interaction of mitochondria with each other. Furthermore, it has been reported that mitophagy can induce degradation of MFN2[178]. However, no changes were observed regarding MFN2 expression in the mitochondrial-enriched fractions of SHIN1-treated K562 (**Figure** 5-3**b).** Nonetheless, this does not exclude that SHIN1 might have an effect on MFN1, the other redundant mitofusin that can functionally replace MFN2.

5.2.3 Folate metabolism inhibition leads to accumulation of the mitophagy receptor NIX

There is a close interplay between mitochondrial fragmentation and mitophagy. Fragmented mitochondrial can be eliminated by mitophagic sequestration and subsequent lysosomal degradation. Mitochondrial depolarisation initiates Parkin-mediated mitophagy by inducing PINK1 kinase stabilisation in the mitochondrial outer membrane. Two other important mitochondrial receptors that initiate mitophagy are the BCL2 interacting protein 3 (BNIP3) and its homologue the BCL2 interacting protein 3 like (BNIP3L/NIX). BNIP3 and NIX directly interact with LC3-II at associated phagophore membranes and target mitochondria to

autophagosomes for degradation. Both are transcriptionally regulated by (hypoxia-inducible factors) HIFs; however, they display tissue specific expression, with NIX being strongly expressed in haematopoietic tissues. Besides this, as we have previously mentioned, NIX is a key regulator of erythroid maturation by promoting mitochondrial clearance from maturing reticulocytes[34]. Furthermore, it has been described that NIX initiates mitochondrial fission via DRP1 and drives epidermal differentiation[179]. Therefore, we decided to investigate what happens to BNIP3 and NIX upon inhibition of folate metabolism.

BNIP3 expression was not altered following a 24h treatment with SHIN1 (**Figure** 5-4**a**). On the other hand, *NIX* expression was significantly upregulated following inhibition of folate metabolism, while formate supplementation was sufficient to rescue this upregulation (**Figure** 5-4**b**). On protein level, mitochondrial isolation revealed accumulation of NIX in the mitochondrial-enriched fraction of K562 (**Figure** 5-4**c**). Purine synthesis reconstitution was sufficient to supress NIX accumulation. Furthermore, accumulation of LC3-II was observed in the mitochondrial-enriched fractions of SHIN1 treated K562. Overall, SHIN1 treatment resulted in accumulation of the mitochondrial mitophagy receptor NIX and mitochondrial accumulation of LC3-II, hinting at mitophagy induction following folate metabolism inhibition.

5.2.4 Translocation of DRP1 and accumulation of NIX in the mitochondria of SHIN1- treated cells is partially AMPK-dependent

As we previously pointed out, Toyama and colleagues demonstrated that ETC inhibition activates AMPK, and this leads to rapid mitochondrial fragmentation through DRP1 translocation to the mitochondria. Besides this, they showed that AMPK translocated to the mitochondria and directly phosphorylates MFF. Interestingly, they showed that direct pharmacological activation of AMPK with AICAR was sufficient to promote mitochondrial fission even in the absence of ETC stressors[157]. Furthermore, the same group recently described that ULK1, in an AMPK-dependent manner, phosphorylates Parkin to initiate mitophagy[176].

Given the DRP1 and NIX accumulation in mitochondria of SHIN1-treated K562 following inhibition of 1C metabolism, we wondered whether these effects were

AMPK-dependent. To answer this, we firstly asked if folate metabolism inhibition would cause AMPK accumulation to the mitochondria of K562 cells. However, we did not observe any significant accumulation of either phosphorylated AMPK on Thr172 or AMPK on the mitochondrial-enriched fraction of SHIN1-treated K562 (**Figure** 5-5**a**). Nevertheless, this did not rule out that AMPK activation could still be responsible for DRP1 and NIX accumulation. To better answer this, we generated an AMPKα1α2 KO. As we mentioned previously, in humans there are two isoforms of the catalytic subunit α, therefore we decided to deplete both isoforms to ensure that AMPK did not have any catalytic activity. Indeed, following AMPKα1α2 KO we did not detect any phosphorylation on AMPK at residue Thr172 and no ULK1 phosphorylation by AMPK on Ser555 was detected, implying that AMPK had completely lost its catalytic activity (**Figure** 5-5**b**).

After validating that the AMPKα1α2 KO cell line had lost its catalytic activity, KO cells were treated with the SHIN1 inhibitor for 24h followed by mitochondrial isolation. Depletion of AMPKα1α2 was sufficient to partially suppress DRP1 accumulation in the mitochondrial-enriched fraction of SHIN1-treated cells (**Figure** 5-5**c**). With regards to NIX accumulation following inhibition of folate metabolism, there seemed to be a reduction in NIX in the mitochondrial fraction of AMPKα1α2 KO K562 treated with SHIN1 compared to control cells treated with the inhibitor (**Figure** 5-5**d**). Besides this, SHIN1 treatment did not promote accumulation of LC3-II in AMPKα1α2 KO cells. However, it is worth pointing out that the reduction in NIX accumulation was not as remarkable as the reduction in DRP1 accumulation. It is worth mentioning that deletion of AMPKα1α2 resulted in increased NIX and LC3-II accumulation compared to mitochondrial fractions of untreated K562 cells, suggesting of an AMPK-independent mechanism of NIX-mediated mitophagy induction.

Overall, in this part we have shown that folate metabolism inhibition through SHIN1 treatment leads to a significant decrease of mitochondrial ROS, hyperpolarisation of the mitochondrial membrane, DRP1 translocation to the mitochondria and accumulation of the mitophagy receptor NIX. DRP1 translocation and accumulation of NIX seem to be partially dependent on AMPK. These data suggest that folate metabolism inhibition alters mitochondrial homeostasis.

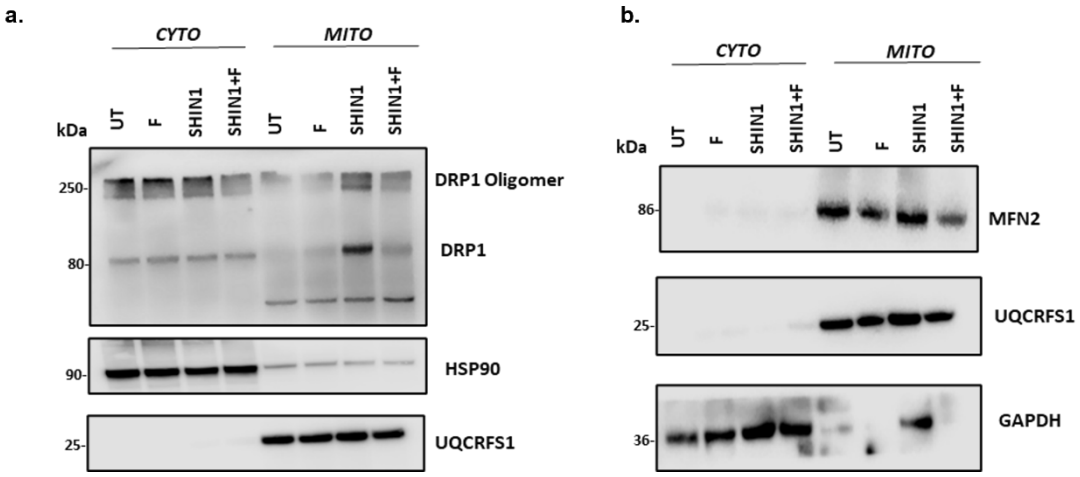

Figure 5-3: Inhibition of folate metabolism leads mitochondrial translocation of DRP1. Immunoblots of cytoplasmic and mitochondrial-enriched fraction of K562 cells following treatment with 1mM formate, 2.5μM SHIN1 or a combination of both for 24h showing DRP1 (**a**) and MFN2 (**b**) protein levels. In (**a**) HSP90 and in (**b**) GAPDH were used as a loading control for the cytosolic-enriched fraction, while UQCRFS1 was used as a loading control for the mitochondrial-enriched fraction. n=3 independent experiments for (**a**). n=1 independent experiment for (**b**).

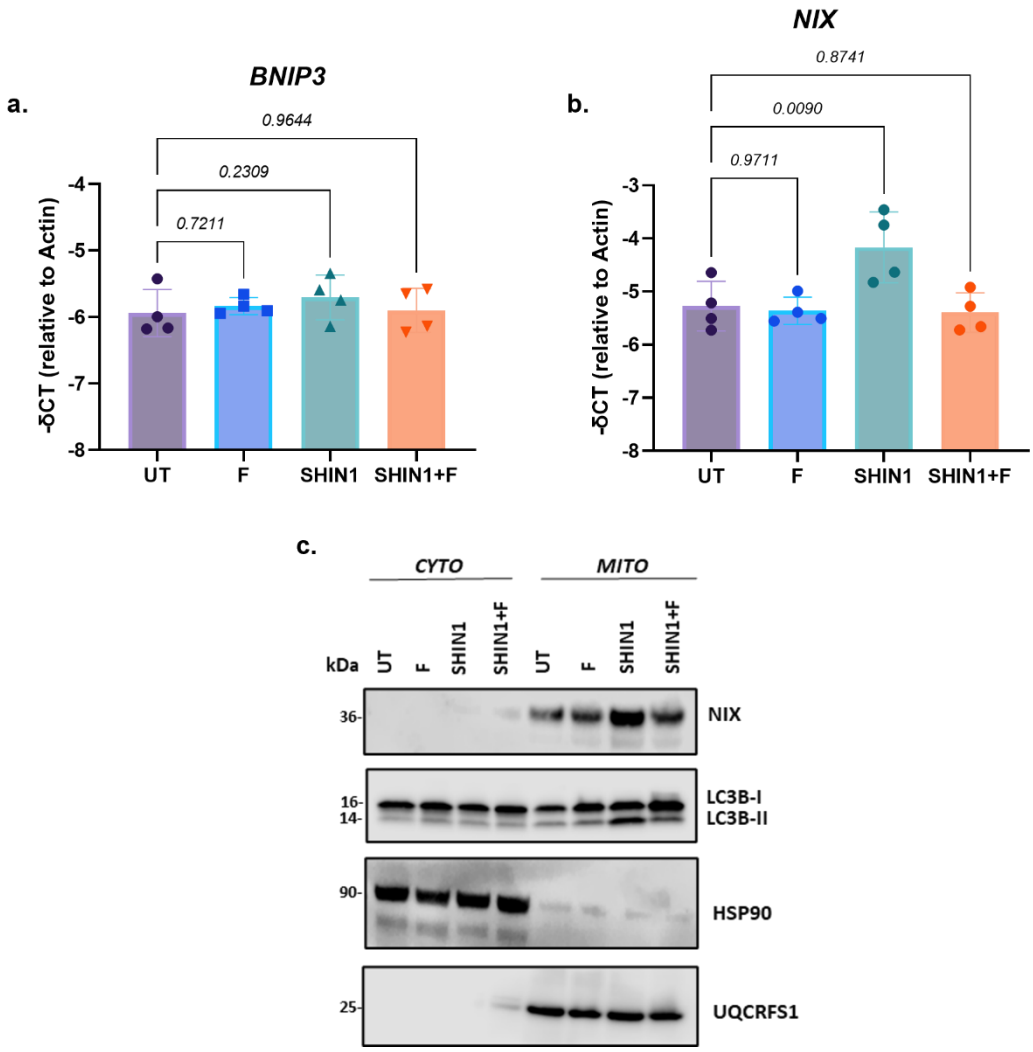

Figure 5-4: Folate metabolism inhibition leads to upregulation of mitophagy receptor NIX on transcriptional and protein level. RT-PCR analysis of mitophagy related genes *BNIP3* (**a**), and *NIX* (**b**), following a 24h treatment with 1mM formate, 2.5μM SHIN1, or a combination of SHIN1 and F. *ACTIN* was used as internal amplification control. Immunoblots of cytoplasmic and mitochondrial-enriched fraction of K562 cells following treatment with 1mM formate, 2.5μM SHIN1 or a combination of both for 24h showing changes in protein levels of mitophagy markers (**c**). HSP90 was used as a loading control for the cytosolic-enriched fraction, while UQCRFS1 was used as a loading control for the mitochondrial-enriched fraction. n=4 independent experiments for (**a**) and (**b**). n=3 independent experiments for (**c**). P-values were calculated with a paired one-way ANOVA with Geisser-Greenhouse correction and Dunnett's multiple comparisons test.

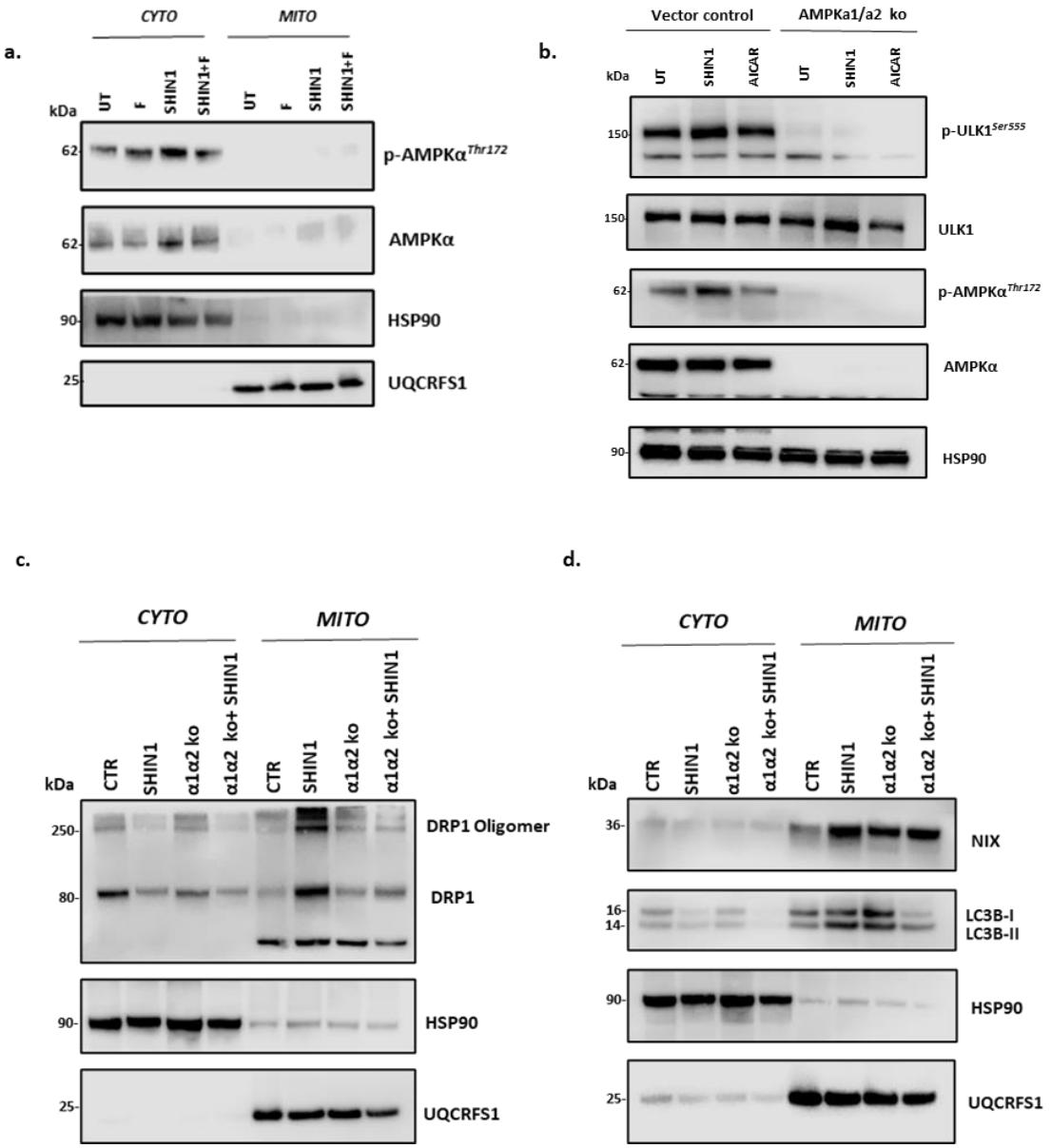

Figure 5-5: Translocation of DRP1 and accumulation of NIX in the mitochondria of SHIN1-treated cells is partially AMPK-dependent. AMPK and p-AMPK protein levels in cytoplasmic and mitochondrial-enriched fraction of K562 cells following treatment with 1mM formate, 2.5μM SHIN1 or a combination of both for 24h (**a**). Validation of AMPKα1α2 KO in K562 cells (**b**). Immunoblots of cytoplasmic and mitochondrial-enriched fraction of K562 control or AMPKα1α2 KO cells following treatment with, 2.5μM SHIN1 for 24h showing DRP1 (**c**) and mitophagy markers (**d**). HSP90 was used as a loading control for the cytosolic-enriched fraction, while UQCRFS1 was used as a loading control for the mitochondrial-enriched fraction. n=1 independent experiment for (**a**). n=2 independent experiment for (**b, c, d**).

5.3 Increased levels of erythroid maturation markers following SHIN1 treatment is AMPK-independent but autophagy-dependent

5.3.1 Increase of CD71 and GlyA levels following inhibition of folate metabolism is AMPK-independent

Following the generation of the AMPKα1α2 KO K562 cell line, we decided to investigate whether the erythroid maturation phenotype we had observed with folate metabolism inhibition was AMPK-dependent. As we demonstrated, AICAR, a direct activator of AMPK, had a similar effect in erythroid markers, significantly increasing their expression compared to untreated cells. Therefore, we hypothesised that the differentiation phenotype would be AMPK-dependent.

To our surprise, the percentage of $CD71^+$ $GlyA^+$ was not different in SHIN1-treated control cells compared to AMPKα1α2 KO treated cells (**Figure** 5-6**b**). The same was observed for AICAR-treated cells, where we even saw an increased trend of percentage of $CD71^+$ $GlyA^+$ in SHIN1-treated AMPKα1α2 KO K562 cells when compared to SHIN1-treated control cells. Those data strongly suggest that increase of expression of erythroid differentiation markers following folate metabolism inhibition is AMPK-independent. Furthermore, we demonstrated that AICAR-induced differentiation is not due to AMPK activation, but potentially happens through an independent route.

5.3.2 SHIN1 drives autophagy induction in *AMPKα1α2* depleted cells, and this drives SHIN1-dependent differentiation

Given the surprising results we obtained with regards to expression of erythroid maturation markers in AMPKα1α2 KO K562 treated with SHIN1, we questioned whether folate metabolism inhibition could still induce autophagy through mTOR-suppression in AMPKα1α2 KO cells. Till that point we believed that the autophagy induction we had observed in K562 cells where 1C metabolism was inhibited was driven by AMPK-dependent phosphorylation of ULK1 on Ser555 and AMPK-dependent suppression of mTORC1. Nevertheless, SHIN1 treatment resulted in reduced phosphorylation of mTOR via the PI3 kinase/Akt signalling pathway on residue Ser2448, both in control and AMPKα1α2 KO K562 cells (**Figure** 5-7**a**). Additionally, even though we did not observe any decrease of the

mTOR-dependent phosphorylation of ULK1 on Ser757 in SHIN1-treated control cell, there was a decreased phosphorylation of this specific residue on AMPKα1α2 KO SHIN1-treated cells. Dephosphorylation of the ribosomal protein S6 was observed in both control and AMPKα1α2 KO K562 upon inhibition of folate metabolism. Similarly, LC3-II accumulation was detected following folate metabolism inhibition in both cell lines. Surprisingly, there was reduction of p62 in AMPKα1α2 KO cells treated with the dual inhibitor, even though we previously reported that inhibition of 1C metabolism in wild-type K562 cells resulted in transcriptional upregulation of *SQSTM1*.Overall, these data suggest that inhibition of folate metabolism can still lead to suppression of mTORC1 and induction of autophagy even when AMPK has lost its catalytic activity. Interestingly, AICAR seemed to have a lesser effect compared to SHIN1 both in control cells and AMPKα1α2 KO cells, especially regarding phosphorylation of mTOR and S6.

Furthermore, as we observed autophagy induction in an AMPK-independent manner following folate metabolism inhibition, we decided to investigate whether autophagy inhibition would reverse the SHIN1-dependent differentiation phenotype we observed in AMPKα1α2 KO cells. To test this, we used HCQ and MRT403 to block the autophagic flux. As described previously, HCQ blocks the fusion of the autophagosome with the lysosome, while MRT403 is a recently developed inhibitor of the kinase activity of ULK1[67]. Treatment with the MRT403 inhibitor was sufficient to reverse the increase in expression of erythroid markers CD71 and GlyA caused by SHIN1 treatment and bring the percentage of $CD71^{+}GlyA^{+}$ cells back to the level of either untreated control or AMPKα1α2 KO cells (**Figure** 5-7**c**). HCQ demonstrated a similar trend, even though treatment with the lysosomal inhibitor was not sufficient to completely reverse SHIN1-dependent differentiation.

These results further support that inhibition of folate metabolism is driving autophagy through both AMPK activation and mTORC1 suppression, and in the absence of the catalytic activity of AMPK, suppression of mTORC1 is sufficient to induce autophagy and differentiation. To reinforce that SHIN1-mediated suppression of mTORC1 signalling drives differentiation of CML cells, we decided to test whether mTORC1 suppression, using the well-known mTORC1 inhibitor, rapamycin, would result in increased expression of CD71 and GlyA. Rapamycin

was sufficient to induce a significant increase in the percentage of $CD71^{+}GlyA^{+}$ cells, to the same extend as SHIN1 treatment (**Figure** 5-8**b**), indicating that SHIN1-induced differentiation is a result of suppression of MTORC1 activity. It is worth noting, that combination of SHIN1 with rapamycin resulted in an increased in levels of erythroid markers CD71 and GlyA, compared to SHIN1 treatment alone, although this was not statistically significant.

Overall, these data suggest that inhibition of folate metabolism increases expression of erythroid maturation markers through MTORC1 suppression and autophagy induction in an AMPK-independent manner.

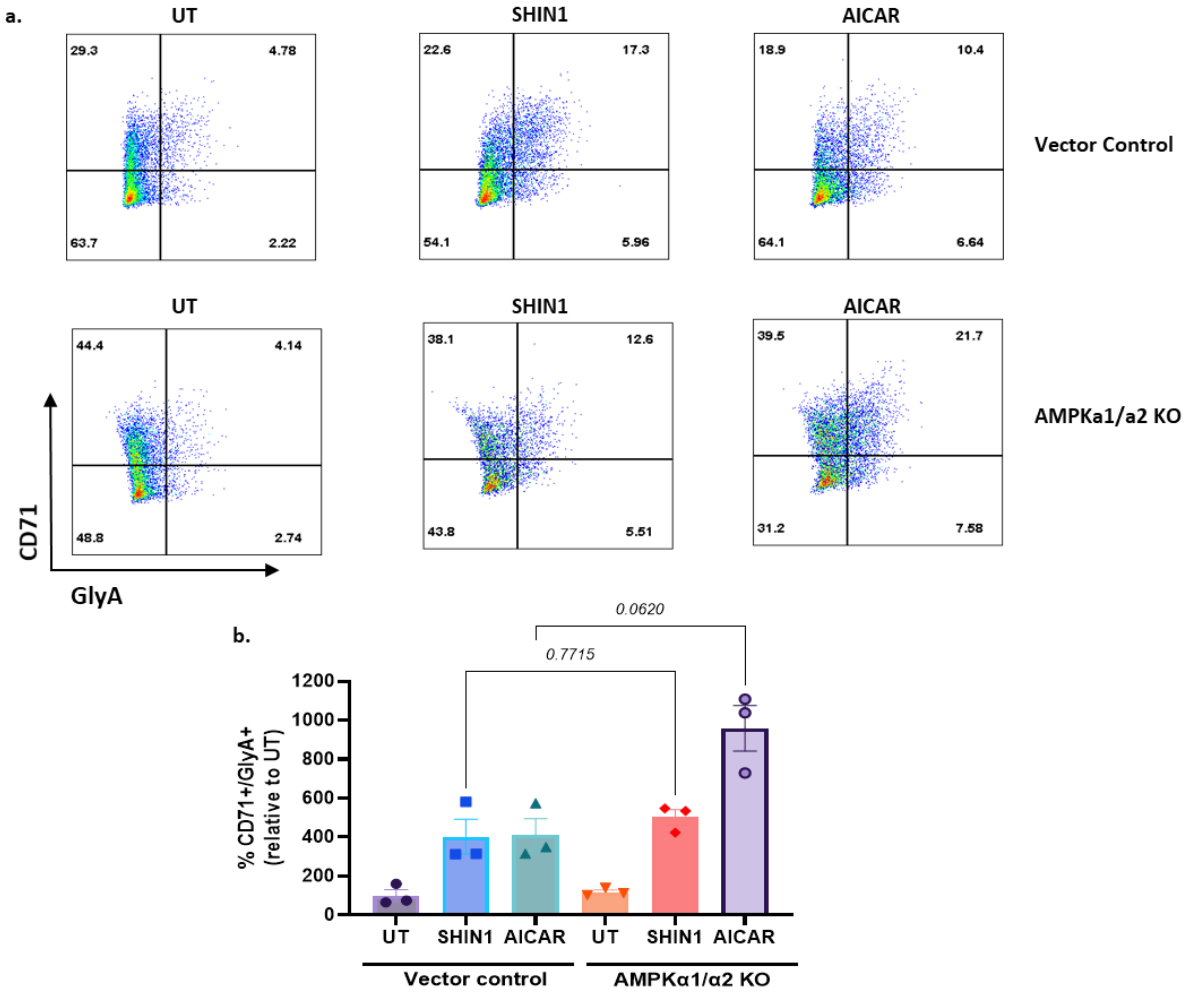

Figure 5-6: Increased expression of erythroid maturation markers following SHIN1 treatment is AMPK-independent. Representative flow cytometry plots showing expression of erythroid markers CD71 and GlyA in K562 control and AMPKα1α2 KO cells following 72hr treatment with either 2.5μM SHIN1 or 1mM AICAR (**a**). Percentage of $CD71^{+}$ $GlyA^{+}$ cells relative to untreated vector control or AMPKα1α2 KO K562 cells following a 72h treatment with either 2.5μM SHIN1 or 1mM AICAR (**b**). n=3 independent experiments. P-values were calculated with a paired one-way ANOVA with Geisser-Greenhouse correction and Dunnett's multiple comparisons test.

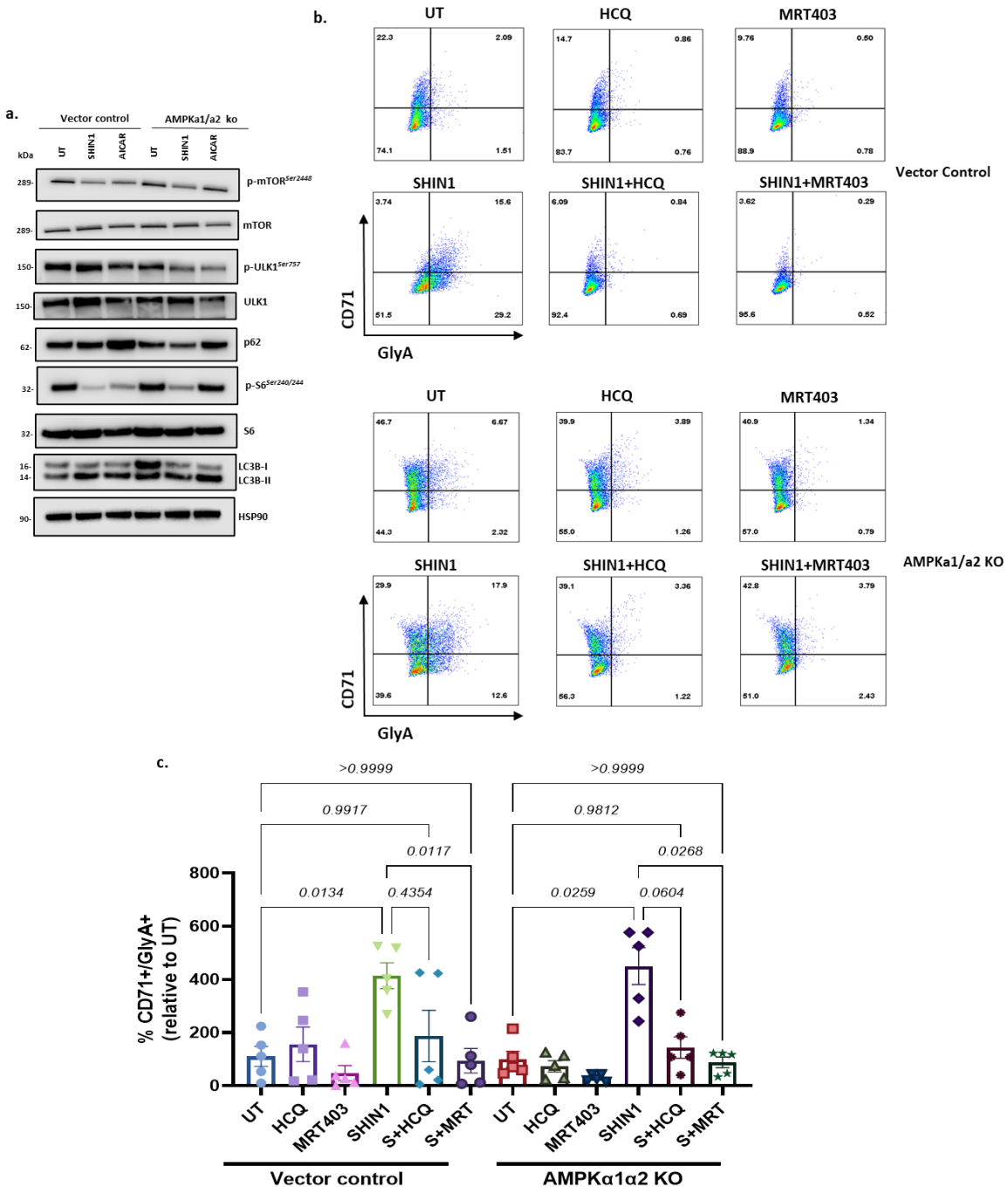

Figure 5-7: SHIN1 drives autophagy induction in AMPKα1α2 KO cells and blockage of autophagy can reverse SHIN1-dependent expression of erythroid maturation markers in AMPKα1α2 KO *K562*. Representative western blots showing mTOR and autophagy markers in control and AMPKα1α2 KO cells treated with 2.5μM SHIN1 and 1mM AICAR for 24hr (**a**). Representative flow cytometry plots depicting control and AMPKα1α2 KO K562 cells treated for 72hr with 5μM hydroxychloroquine (HCQ), 3μM MRT403, 2.5μM SHIN1 or a combination of either SHIN1 with HCQ or SHIN1 with MRT403 (**b**). Percentage of $CD71^{+}$ $GlyA^{+}$ relative to untreated control or AMPKα1α2 KO cells following a 72h treatment with 5μM HCQ, 3μM MRT403, 2.5μM SHIN1 or a combination of either SHIN1 with HCQ or SHIN1 with MRT403 (**c**). n=3 independent experiments for (**a**) and n=5 independent experiments for (**c**). P-values were calculated with a paired one-way ANOVA with Geisser-Greenhouse correction and Dunnett's multiple comparisons test.

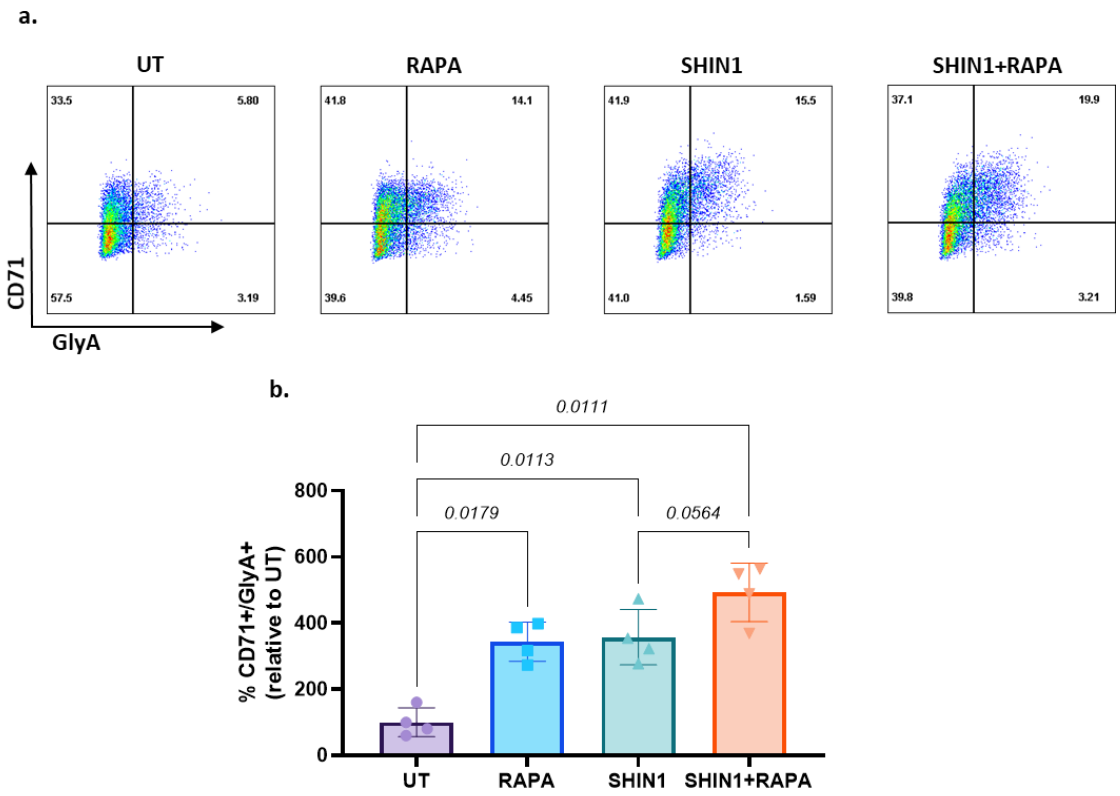

Figure 5-8: Suppression of mTORC1 can induce expression of erythroid maturation markers. Representative flow cytometry plots showing expression of erythroid maturation markers CD71 and GlyA in K562 cells following a 72h treatment with 10nM rapamycin (RAPA), 2.5μM SHIN1 or a combination of both (**a**). Percentage of $CD71^{+}GlyA^{+}$ cells relative to untreated following 72hr treatment with 10nM RAPA, 2.5μM SHIN1 or a combination of both (**b**). Data were plotted as mean +/- S.D. of n=4 independent experiments. P-values were calculated with a paired one-way ANOVA with Geisser-Greenhouse correction and Dunnett's multiple comparisons test.

5.3.3 SHIN1 is not sufficient to drive differentiation in autophagy deficient cells

To further validate that SHIN1-driven differentiation in K562 cells is autophagy-dependent we decided to use both a genetic and pharmacological approach to block autophagy flux and assess expression levels of the erythroid maturation markers CD71 and GlyA. In this way, we could eliminate the possibility that reversal of differentiation phenotype in AMPKα1α2 KO cells was a drug-related effect and not a result of autophagy inhibition.

A previous PhD student in our lab had generated two K562 cell lines where autophagy was compromised, namely a ULK1 KO and an ATG7 KO cell line (**Figure** 5-9**a**). We, therefore, treated vector control K562 cells with MRT403, SHIN1 and a combination of both for 72hr and assessed levels of differentiation markers CD71 and GlyA. At the same time, levels of the two differentiation markers were assessed in ULK1 KO or ATG7 KO cells treated with SHIN1. Similar to what was described in **Figure** 5-7**c**, MRT403 was able to suppress the SHIN1-driven increase in percentage of $CD71^+$ $GlyA^+$ in control K562 cells (**Figure** 5-9**c**). At the same time, SHIN1 was not able to drive the increase in levels of CD71 and GlyA when ULK1 or ATG7 was depleted, with the increase in percentage of $CD71^+$ $GlyA^+$ in SHIN1-treated ULK1 KO or ATG7 KO cells not being significant. However, it is worth mentioning that loss of ULK1 or ATG7 was not sufficient to completely reverse expression of the two maturation markers, as there was no statistical difference between SHIN1-treated vector control cells and SHIN1-treated ULK1 KO and ATG7 KO cells. These results further validate that induction of autophagy through inhibition of folate metabolism is necessary for differentiation of CML cells.

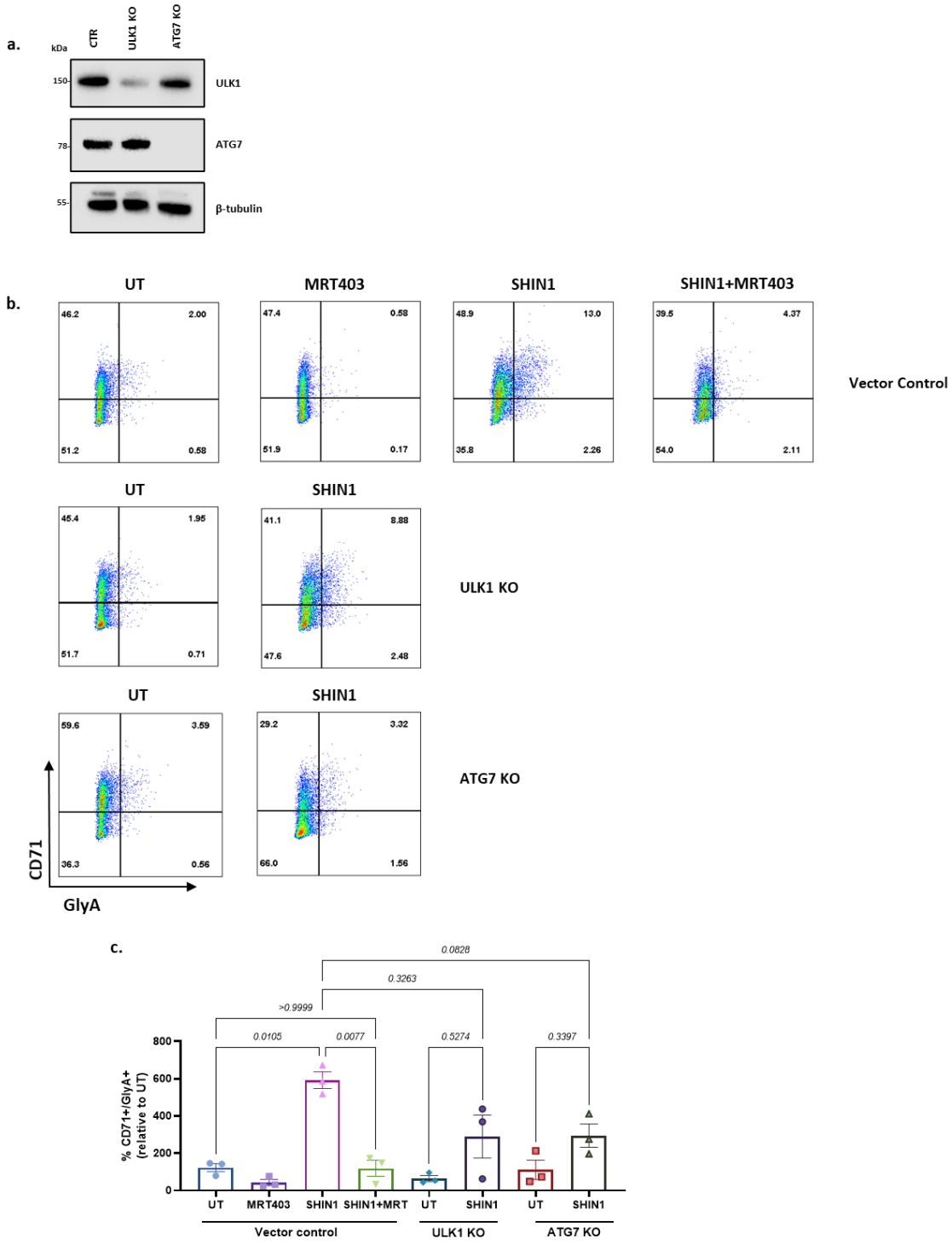

Figure 5-9: SHIN1 cannot induce increase in levels of erythroid maturation markers in autophagy deficient cells. Immunoblots showing expression of ULK1 and ATG7 in ULK1 KO and ATG7 KO cell lines compared to vector control K562 cells (**a**). Representative flow cytometry plots depicting vector control k562 cells treated 3μM MRT403, 2.5μM SHIN1, a combination of both; ULK1 KO cells treated with SHIN1 and ATG7 KO cells treated with SHIN1 for 72h (**b**). Percentage of $CD71^{+}$ $GlyA^{+}$ relative to untreated following a 72h treatment with 3μM MRT403, 2.5μM SHIN1, a combination of both for control K562 cells, SHIN1 treatment for either ULK1 KO or ATG7 KO cell lines (**c**). n=1 independent experiments for (**a**) and n=3 independent experiments for (**c**). P-values were calculated with a paired one-way ANOVA with Geisser-Greenhouse correction and Dunnett's multiple comparisons test.

5.4 AICAR likely to be driving differentiation through suppression of pyrimidine biosynthesis

Following the results described so far, we hypothesised that pharmacological inhibition of folate metabolism results in differentiation of CML cells via MTORC1 suppression and autophagy induction. Furthermore, we demonstrated that SHIN1-induced differentiation is AMPK independent. To our surprise, AICAR treatment was also sufficient to induce increased expression of erythroid maturation markers in AMPKα1α2 KO K562 cells (**Figure** 5-6**b**). However, it had a lesser effect in mTORC1 signalling and autophagy induction compared to SHIN1 (**Figure** 5-7**a**), suggesting that its effect on mTORC1 and autophagy is mediated through activation of AMPK.

To get a better understanding on how AICAR induces differentiation of CML cells, K562 cells were treated with AICAR, SHIN1 or a combination of both for 24h. Following the 24h incubation, intracellular metabolites were extracted, and samples were analysed by LC-MS (**Figure** 5-10). We observed that, unlike SHIN1, AICAR did not have any effect on adenine (AMP, ADP, ATP) and guanine (GMP, GDP, GTP) nucleotides (**Figure** 5-10**a-f**). Furthermore, AICAR led to a significant reduction of pyrimidine biosynthesis (**Figure** 5-10**g-j**). Of note, UMP, UTP and CTP were significantly reduced following AICAR treatment, while SHIN1 did not have any effect on pyrimidines. Interestingly, Dembitz and colleagues demonstrated that AICAR, through perturbation of pyrimidine biosynthesis, caused increased expression of myeloid marker CD11b in the AML cell line U937[182]. Such effect on the *de novo* pyrimidine synthesis could explain why AICAR can cause increase of erythroid maturation markers in K562 even in the absence of the catalytic subunits of AMPK (**Figure** 5-6**b**).

These results indicate that the AICAR-induced differentiation is likely to be due to perturbation of pyrimidine synthesis and not because of AMPK activation.

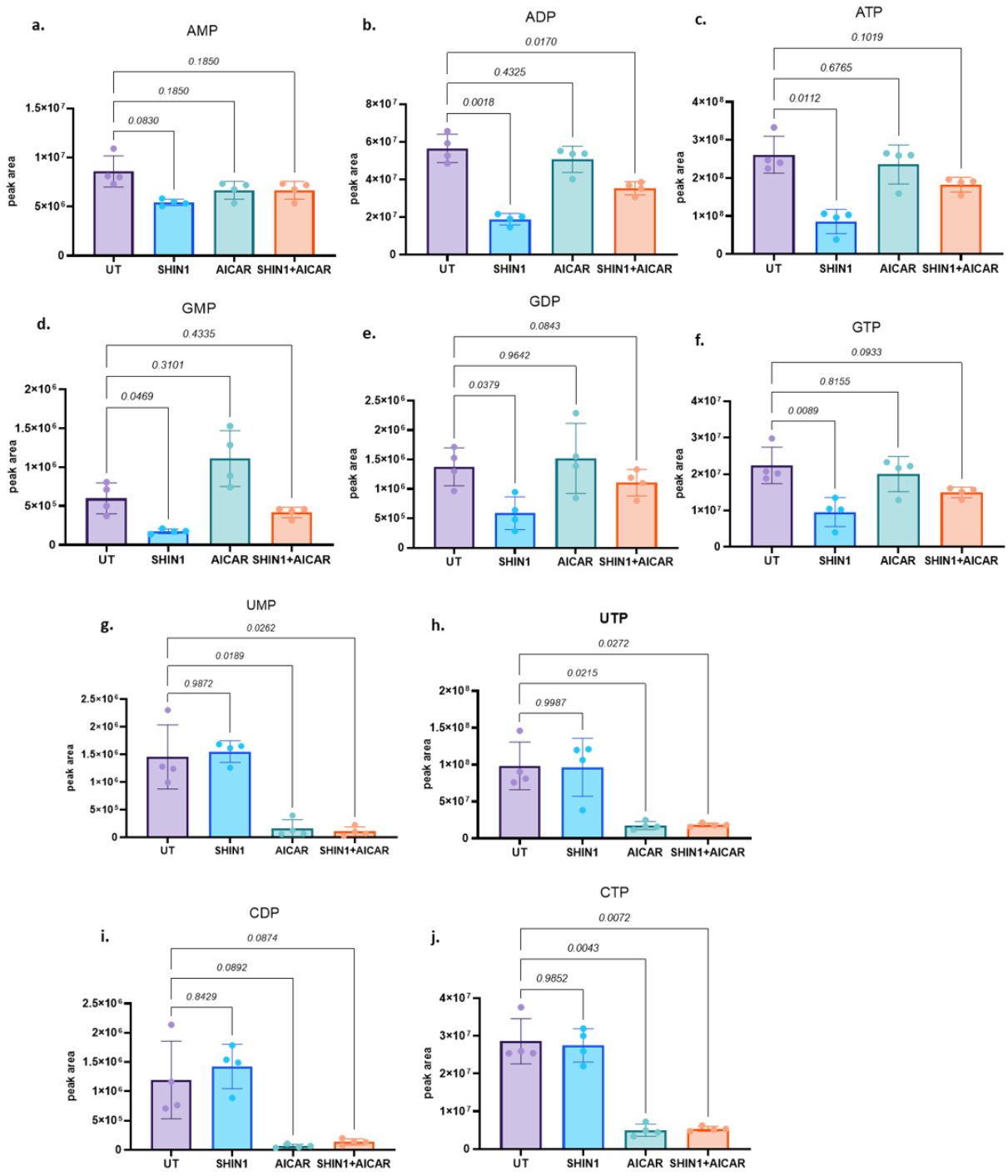

Figure 5-10: AICAR affects pyrimidine biosynthesis, while it has no effect on *de novo* purine synthesis. Representative graphs of peak areas of purines (**a-f**) and pyrimidines (**g-j**) in K562 cells following a treatment with 2.5μM SHIN1, 1mM AICAR or a combination of both. After a 24h incubation, intracellular metabolites were extracted, and samples analysed by LC-MS. Data were plotted as mean +/- S.D. of n=4 independent experiments. P-values were calculated with a paired one-way ANOVA with Geisser-Greenhouse correction and Dunnett's multiple comparisons test.

5.5 Discussion

In this chapter we described the link between folate metabolism, mitochondrial homeostasis, AMPK, and cellular differentiation. We showed that inhibition of 1C metabolism using the SHIN1 dual inhibitor causes a significant decrease of mitochondrial ROS (**Figure** 5-1**b**). These results were surprising, as we were expecting to see an increase in ROS given the positive correlation of ROS and differentiation of HSCs. However, not only SHIN1 mediated decrease of mitochondrial ROS, but treatment with the antioxidant NAC could not completely rescue the increase in percentage of $CD71^{+}$ $GlyA^{+}$ cells caused by folate metabolism inhibition, although a slight non-significant decrease was observed (**Figure** 5-2**b**).

As we mentioned in the previous chapter, SHIN1 treatment leads to upregulation of p62 both at transcriptional and protein level. p62 can activate transcriptional regulator NRF2 by direct interaction with the E3 ubiquitin ligase adaptor protein KEAP1, which leads to its proteasomal degradation. KEAP1 gets sequestered by p62, leading to increased NRF2 signalling. NRF2 plays a crucial role in antioxidant response by promoting the expression of genes whose proteins are involved in the detoxification and elimination of reactive oxidants. It is possible that folate metabolism inhibition results in NRF2 activation through p62 upregulation. This would explain the decreased in mitochondrial ROS following a 72h treatment with SHIN1. It would be interesting to examine ROS levels in earlier timepoints. Furthermore, it would be worth checking the expression of common NRF2 target genes such as NAD(P)H dehydrogenase 1 (NQO1) or glutamate—cysteine ligase catalytic subunit (GCLC).

It is also worth mentioning that formate supplementation was sufficient to restore mitochondrial ROS. AICAR treatment did not confer any significant changes.

With regards to mitochondrial mass, we used the mitochondrial dye MitoTracker green, that links to thiol group in the mitochondria regardless of their membrane potential. SHIN1 did not confer any significant changes regarding mitochondrial mass (**Figure** 5-1**d**). Surprisingly, there was a trend of increased mitochondrial mass in cells treated with either AICAR, SHIN1 or a combination of both. This

came as a surprise, as we are expecting that because of the autophagy induction we previously described due to folate metabolism inhibition, there would be a reduction of mitochondrial mass. However, it is possible that an earlier timepoint might have been more optimal to assess for mitophagy induction. Besides this, it has been described that AMPK activation leads to mitochondrial fragmentation, mitophagy and at a later timepoint to mitochondrial biogenesis through PGC-1α. Regarding mitochondrial membrane potential, we revealed hyperpolarisation of the mitochondrial membrane in SHIN1 or AICAR-treated cells (**Figure** 5-1Error! Reference source not found.**c**). Membrane potential was brought to levels of untreated cells with the supplementation of formate. Interestingly, it has been shown that autophagy inducers like rapamycin or low serum growth conditions induce hyperpolarisation of the mitochondrial membrane, which would fit with the autophagy induction following folate metabolism inhibition.

Hyperpolarisation of mitochondrial membrane and reduced mitochondrial ROS are common outcomes of mitochondrial fragmentation. Mitochondrial fragmentation is dependent on DRP1 translocation to the mitochondria. Indeed, we discovered accumulation of DRP1 in the mitochondrial-enriched fraction of K562 cells treated with the SHIN1 inhibitor. Furthermore, we noticed accumulation of DRP1 oligomers in the SHIN1-treated mitochondrial fractions (**Figure** 5-3**a**). Oligomerisation of DRP1 is an important step of mitochondrial fission. It is worth mentioning that purine synthesis reconstitution through formate supplementation was able to reverse DRP1 accumulation in the mitochondrial-enriched fraction of SHIN1-treated cells.

To further prove mitochondrial fission, it would be useful to image mitochondria of SHIN1-treated cells and see whether DRP1 co-localises in their mitochondrial membrane. Additionally, it would be informative to assess any changes in mitochondrial shape and size following folate pathway inhibition, which would suggest enhanced mitochondrial fragmentation. A challenge with K562 and leukaemic cells in general is their small size, and the fact that most of their surface area is occupied by their nucleus, making it difficult to image. The same issued applies for detection of mitochondrial degradation through mitophagy. As we described, inhibition of folate metabolism leads to upregulation of the mitophagy receptor NIX in both transcriptional and protein level (**Figure** 5-4**b,**

c). Furthermore, LC3-II accumulation in mitochondria isolated from K562 cells following SHIN1 treatment was observed. LC3-II binds to NIX to initiate mitophagy. Accumulation of LC3-II and NIX hints towards induction of mitochondrial degradation.

Interestingly, even though we did not identify significant AMPK translocation to the mitochondria of SHIN1-treated cells, depletion of AMPKα1α2 partially rescued accumulation of DRP1 and NIX, indicating that at least, partially, the effect of SHIN1 on mitochondria fragmentation and degradation can be AMPK-dependent. Nevertheless, these data suggest that inhibition of 1C metabolism through SHIN1 treatment influences mitochondrial homeostasis.

Applying the AMPKα1α2 KO K562 cell line we generated, we decided to investigate whether the increase in expression of erythroid maturation markers following 1C metabolism inhibition was AMPK-dependent. What we had described in the previous chapter is that folate metabolism inhibition induces expression of erythroid differentiation markers CD71 and GlyA. Similar results were obtained when cells were treated with the AMPK activator and purine synthesis intermediate, AICAR. Furthermore, formate supplementation was sufficient to rescue the changes in expression of erythroid markers. We, therefore, hypothesised that this phenotype caused by folate metabolism inhibition is AMPK-dependent through blockage of *de novo* purine synthesis.

Surprisingly, SHIN1-treated AMPKα1α2 KO K562 cells displayed similar percentage of $CD71^{+}GlyA^{+}$ cells as control cells treated with the inhibitor (**Figure** 5-6**b**)**.** Similar results were obtained with AICAR treatment of control and AMPKα1α2 KO cells, suggesting that the effect of SHIN1 and AICAR is AMPK-independent. In the previous chapter, we demonstrated that apart from AMPK activation, inhibition of folate metabolism led to mTORC1 suppression and autophagy induction. Thus, we speculated that SHIN1 could still induce autophagy through mTORC1 suppression in AMPKα1α2 KO cells. We addressed this hypothesis as we demonstrated that SHIN1 is still capable of suppressing mTORC1 activity (SHIN1 caused decrease of mTOR, mTOR-dependent ULK1 and S6 phosphorylation) and induced autophagy (increase in LC3-II and decrease in p62 levels) (**Figure** 5-7**a**). Interestingly, two studies published in 2017 demonstrated that MTX, PTX or lometrexol (LTX)-induced blockage of purine

synthesis, leads to suppression of MTOR signalling[180, 181]. Furthermore, Hoxhaj and colleagues described that mTORC1 senses changes in intracellular adenylates and, although, this is dependent on the TSC complex, it is independent from AMPK. Similarly to our findings, they demonstrated that inhibition of purine synthesis through MTX and LTX could still suppress MTORC1 signalling in AMPKα1α2 KO mouse embryonic fibroblasts (MEFs)[181]. It would be informative to examine whether reconstitution of *de novo* purine synthesis through formate, adenine or guanine supplementation would rescue the SHIN1-driven suppression of mTORC1 in AMPKα1α2 KO K562. With regards to levels of erythroid markers, the mTORC1 inhibitor and autophagy inducer, rapamycin, showed a significant increase in levels of erythroid markers CD71 and GlyA. In addition, combination of SHIN1 with rapamycin displayed increase in percentage of $CD71^{+}GlyA^{+}$ cells compared to SHIN1 treatment alone, although this was not statistically significant (**Figure** 5-8**b**).

Given that mTORC1 suppression ultimately leads to promotion of autophagy and the observation that SHIN1 was able to induce autophagy in AMPKα1α2 KO K562 we then decided to investigate whether autophagy suppression would reverse the increase in expression of differentiation markers. Indeed, autophagy suppression using MRT403 was sufficient to reverse the increase in CD71 and GlyA expression in both control and AMPKα1α2 KO cells (**Figure** 5-7**c**). HCQ treatment demonstrated a similar trend; however, it could not completely reverse the increase in CD71 and GlyA levels. Furthermore, SHIN1 was not sufficient to drive differentiation in ULK1 KO or ATG7 KO cells (**Figure** 5-9**b**). It should be noted that SHIN1 treatment demonstrated a trend of increased levels of erythroid maturation markers in autophagy deficient cells, although this was not statistically significant. In the case of ULK1 KO cells, the functionally redundant ULK2 is still present, while MRT403 inhibits the kinase activity of both ULK1 and ULK2. Additionally, several studies have reported the existence of an ATG5/ATG7-independent alternative of autophagy, that could explain why ATG7 KO K562 cells can still enhance the expression of maturation markers when treated with the SHIN1 dual inhibitor, even though this increase is not significant[183].

Lastly, in an attempt to get a better understanding on how AICAR drives differentiation in AMPKα1α2 KO K562 cells, we revealed that AICAR treatment

leads to impairment of *de novo* pyrimidine synthesis (**Figure** 5-10). While AICAR did not have any effect on adenine (AMP, ADP, ATP) and guanine (GMP, GDP, GTP) nucleotides (**Figure** 5-10**a-f**), it significantly reduced UMP, UTP and CTP levels (**Figure** 5-10**g-j**). We previously showed that SHIN1 leads to suppression of purine biosynthesis, a phenotype that is likely linked to mTORC1 inactivation. The fact that AICAR does not have any effect on purine nucleotides, might explain why it cannot suppress mTORC1 activity to the same extend as SHIN1. Its effect on mTORC1 is likely a result of activation of AMPK signalling, thus loss of AMPKα1α2 dampens its effect. Interestingly, Dembitz and colleagues demonstrated that AICAR, through perturbation of pyrimidine biosynthesis, caused increased expression of myeloid marker CD11b in the AML cell line U937[182]. It is possible that AICAR can cause increase of erythroid maturation markers in K562 even in the absence of the catalytic subunits of AMPK through impairment of *de novo* pyrimidine synthesis (**Figure** 5-6**b**).These results indicate that the AICAR-induced differentiation is due to perturbation of pyrimidine synthesis and not because of AMPK activation.

Overall, the data described on this chapter indicate that the differentiation driven by the inhibition of folate metabolism is a result of mTORC1 suppresion, autophagy induction, but not AMPK activation.

5.6 Summary

In this chapter we demonstrated that inhibition of folate metabolism disrupts mitochondrial homeostasis by reducing mitochondrial ROS, hyperpolarisation of the mitochondrial membrane, accumulation of the mitochondrial fission related protein DRP1 and the mitophagy receptor NIX. Furthermore, we revealed that that DRP1 and NIX accumulation was partially dependent on AMPK activity.

We also uncovered that SHIN1 is capable of inducing mTOR suppression and autophagy induction even when the catalytic activity of AMPK is depleted, suggesting that that inhibition of folate metabolism can lead to autophagy induction in an AMPK-independent manner. Lastly, we described that increase in expression of erythroid markers CD71 and GlyA following inhibition of 1C metabolism is dependent on autophagy.

Chapter 6 SHIN1 treatment impairs proliferation and short-term colony formation capacity of patient-derived CML CD34$^+$ cells

6.1 Introduction

Following our observations in K562 cells, in this chapter, we decided to turn our focus on the impact of folate metabolism inhibition through SHIN1 treatment in CML CD34$^+$ cells.

We previously described that enzymes involved in 1C metabolism are overexpressed in CML LSCs compared to HSCs. Furthermore, we showed that traditional TKI therapy, such as imatinib treatment, does not fully suppress expression of those enzymes, implying that deregulated folate metabolism activity persists following imatinib treatment. In addition, we demonstrated that the activity of the pathway is significantly increased in CML CD34$^+$ cells, measured by the increase in formate exchange rate and formate media concentration of those cells compared to normal counterparts. Besides this, we described that inhibition of the folate metabolism leads to cell cycle arrest and inhibition of proliferation in K562 cells.

Thus, we decided to investigate how SHIN1 treatment affects proliferation, apoptosis and short-term colony formation capacity of patient-derived CML CD34$^+$ cells. Of clinical relevance, we assessed whether combination of SHIN1 with imatinib treatment would further potentiate the anti-proliferative effect of imatinib. At the same time, we also assessed the effect of SHIN1 treatment in CD34$^+$ samples derived from surplus cells collected from femoral head BM, surgically removed from patients undergoing hip replacement. These cells will be referred as normal CD34$^+$ cells.

6.2 SHIN1 treatment impairs cell proliferation of CML $CD34^+$ cells

To assess proliferation of CML $CD34^+$ cells following SHIN1 treatment, $CD34^+$ cells were cultured in Plasmax supplemented with physiological growth factors and stained with cell trace violet (CTV) prior to being treated with the inhibitor. Following a 72h treatment, CTV staining was assessed via flow cytometry. Cell division 0 to 3 (D0-D3) were measured as a dilution of the fluorescent intensity of the CTV dye.

In line with our cell line data, SHIN1 treatment significantly decreased $CD34^+$ cell division and enriched for the undivided (D0) $CD34^+$ population, compared to untreated cells (**Figure** 6-1**b**). SHIN1 did not result in any significant change in cell death compared to untreated cells (**Figure** 6-1**c**). These data support the idea that SHIN1 has a cytostatic effect at least regarding CML cells. Surprisingly, formate supplementation did not prevent the cytostatic effect of SHIN1. It did cause a slight decrease of undivided cells and a slight increase of cells in D2 division, but these changes were not statistically significant. Furthermore, when comparing SHIN1 with imatinib, SHIN1 showed a similar cytostatic effect as the well-known TKI. (**Figure** 6-2**b**). In addition, SHIN1 did not enhance the cytostatic effect of imatinib. Imatinib did not significantly increase the number of annexin V^+ cells (**Figure** 6-2**c**). A short-term combination treatment of SHIN1 with imatinib did not lead to any change in programmed cell death compared to untreated cells or imatinib and SHIN1 treatment alone.

6.3 SHIN1 reduces the short-term colony formation capacity of CML CD34$^+$ cells

To further understand the effect of inhibition of folate metabolism in stem and progenitor CML cells, we assessed expression of markers CD34 and CD133 following a 72h treatment with either formate, SHIN1, imatinib or a combination of either SHIN1 with formate or SHIN1 with imatinib. While percentage of CD34$^+$CD133$^+$ increased from 5% in untreated cells to 10% in SHIN1-treated cells or imatinib-treated cells (**Figure** 6-3**b & d**), this increase was not statistically significant. Formate supplementation did not have any effect on the percentage of CD34$^+$CD133$^+$. Furthermore, combination of SHIN1 with imatinib demonstrated a trend toward increased expression of both stem cell markers when compared to single treatment of either SHIN1 or imatinib. These data fit with our observation that SHIN1 is cytostatic and enriches for the undivided CML CD34$^+$ cells. Furthermore, as mentioned previously, a number of studies have described that imatinib targets more differentiated cells, which have potentially lost the CD34 marker, while it is less efficient in targeting primitive CML cells. As SHIN1 demonstrated a similar increase in the percentage of CD34$^+$CD133$^+$ CML cells, we wondered how this would affect the CFC potential of primitive CML cells.

Following a 72h treatment with either formate, SHIN1, imatinib or a combination of SHIN1 with formate or imatinib, CD34$^+$ cells were placed in a semi-solid media to assess proliferation and differentiation into colonies in response to cytokine stimulation. Colonies were manually counted after 13-14 days. We observed that SHIN1 treatment led to a 50% reduction of the CFC of progenitor CML cells (**Figure** 6-4**a&b**). Similarly to what we have described so far, formate addition was not sufficient to rescue the effect of SHIN1. Imatinib had a comparable effect to SHIN1, however, this was not statistically significant. Interestingly, SHIN1 treatment sensitised cells to imatinib, as there was a further reduction of 25-30% of the counted colonies compared to imatinib alone, when combining both treatments together. Notably, neither drug, alone nor in a combination, had a significant effect on the CFC capacity of normal CD34$^+$ cells (**Figure** 6-4**c**).

Overall, these data suggest that inhibition of folate metabolism has an effect on primitive patient-derived cells by inhibiting their proliferation and reducing their

CFC capacity. Of clinical interest, SHIN1 treatment is capable of sensitising CML cells to imatinib, with no significant effect to normal $CD34^+$ cells.

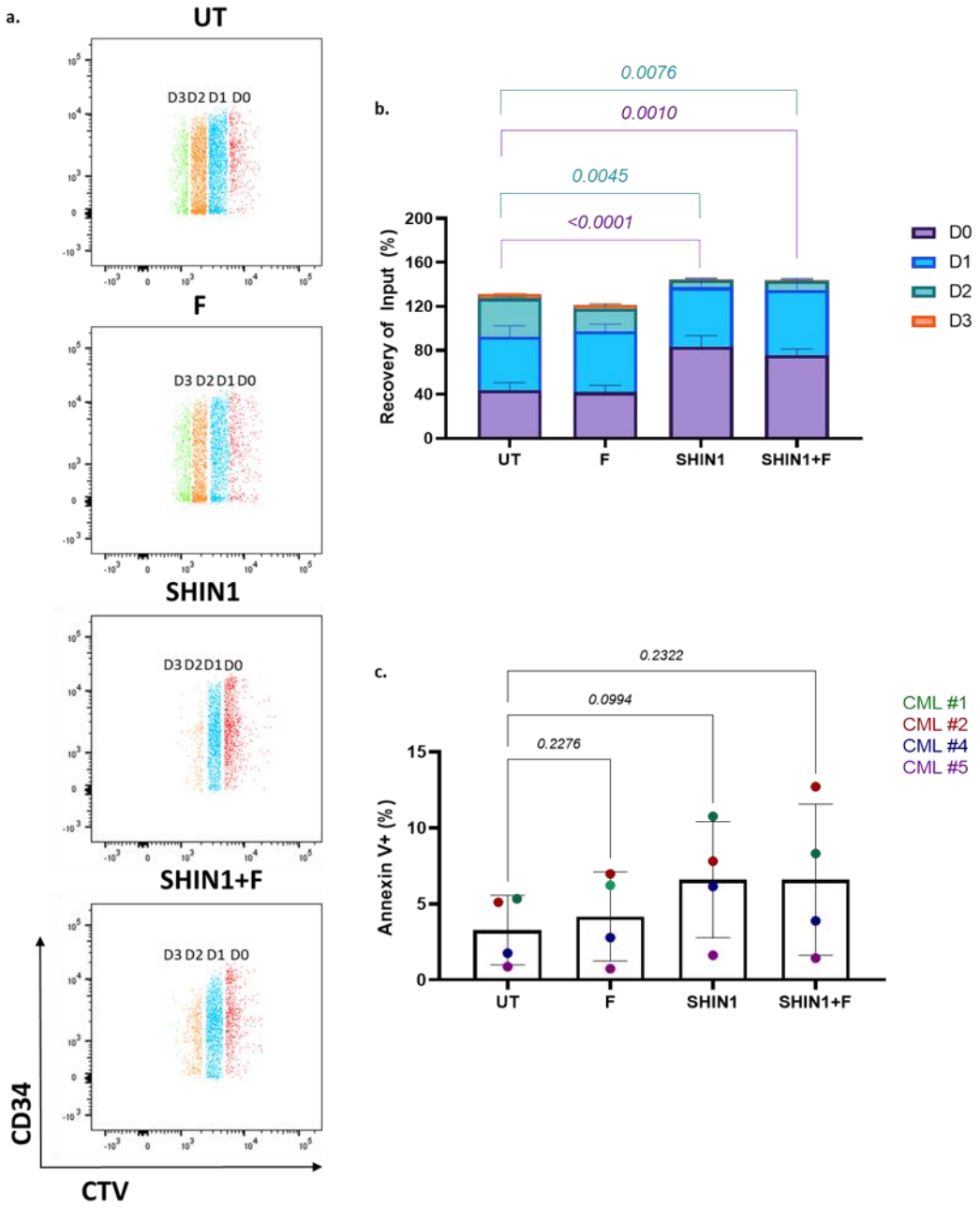

Figure 6-1: SHIN1 treatment leads to enrichment of undivided CML CD34⁺ cells but does not induce cell death. Representative flow cytometry plot outlining CTV gating of CML CD34⁺ cells treated with 1mM formate, 2.5μM SHIN1 or a combination of both for 72hr (**a**). CTV tracked proliferation of CD34⁺ cells treated with 1mM formate, 2.5μM SHIN1 or a combination of both reported as recovery of input (%), where input represents number of input cells (**b**). D0 represents undivided cells, D1-D3 number of divisions measured as dilution of the fluorescence intensity of the CTV dye. Annexin V staining of CML CD34⁺ cells cultured in the presence of 1mM formate, 2.5μM SHIN1 or a combination of both for 72hr (**c**). Data representative of mean ± SD, n=4 individual patient samples. P-values were calculated with a two-way ANOVA with Sidak's multiple comparisons test for (**b**), where p-values represent probability values with regards to D0 and D2. P-values were calculated with a paired one-way ANOVA with Geisser-Greenhouse correction and Dunnett's multiple comparisons test for (**c**).

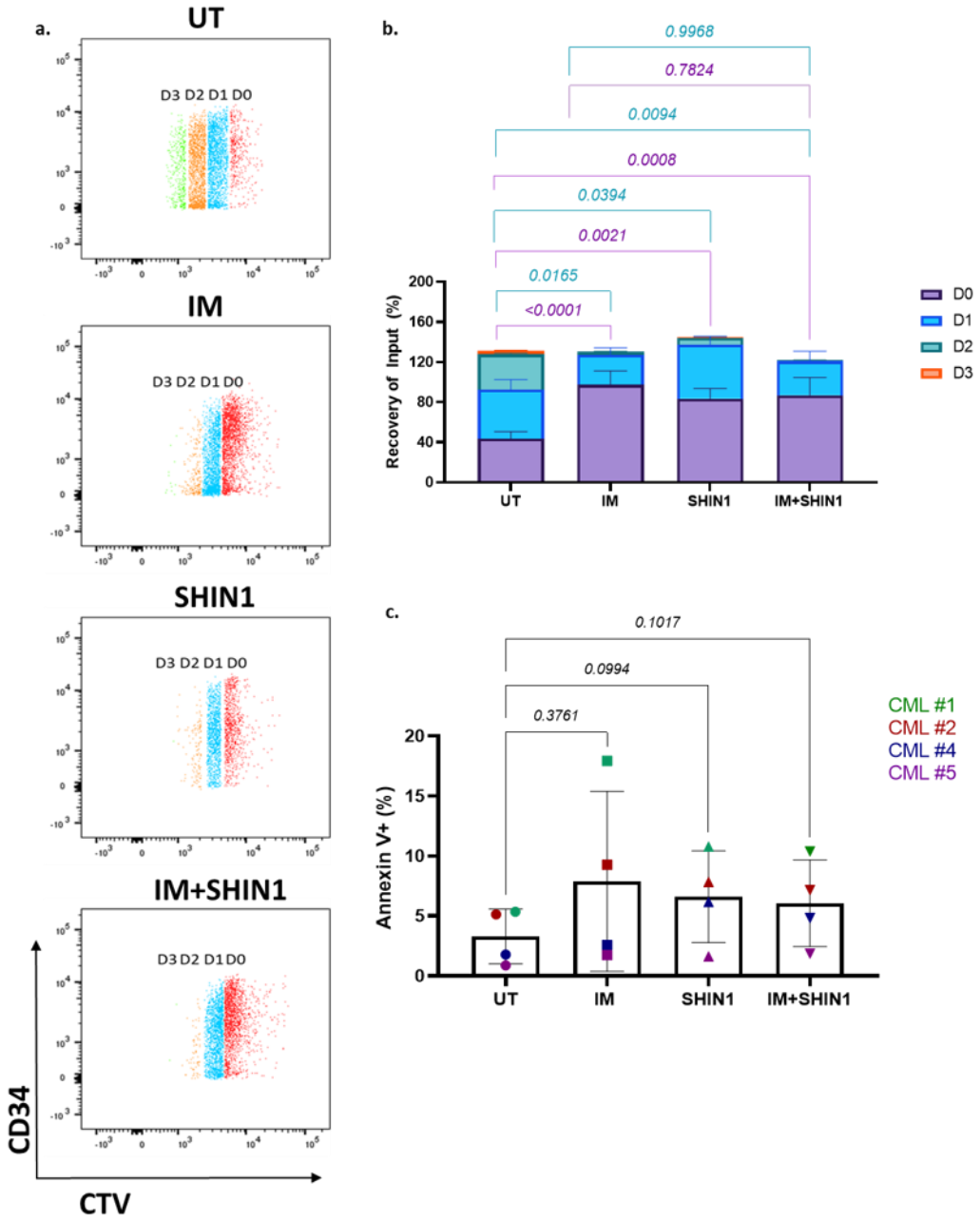

Figure 6-2: SHIN1 treatment exhibits a similar antiproliferative effect to imatinib in CML CD34⁺ cells. Representative FACS plot outlining CTV gating of CML CD34⁺ cells treated with 2μM imatinib (IM) 2.5μM SHIN1 or a combination of both for 72hr (**a**). CTV tracked proliferation of CD34⁺ cells treated with 2μM imatinib, 2.5μM SHIN1 or a combination of both reported as recovery of input (%), where input represents number of input cells (**b**). Annexin V staining of CML CD34⁺ cells cultured in the presence of 2μM imatinib, 2.5μM SHIN1 or a combination of both for 72hr (**c**). Data representative of mean ± SD, n=4 individual patient samples. P-values were calculated with a two-way ANOVA with Sidak's multiple comparisons test for (**b**), where p-values represent probability values with regards to D0 and D2. P-values were calculated with a paired one-way ANOVA with Geisser-Greenhouse correction and Dunnett's multiple comparisons test for (**c**).

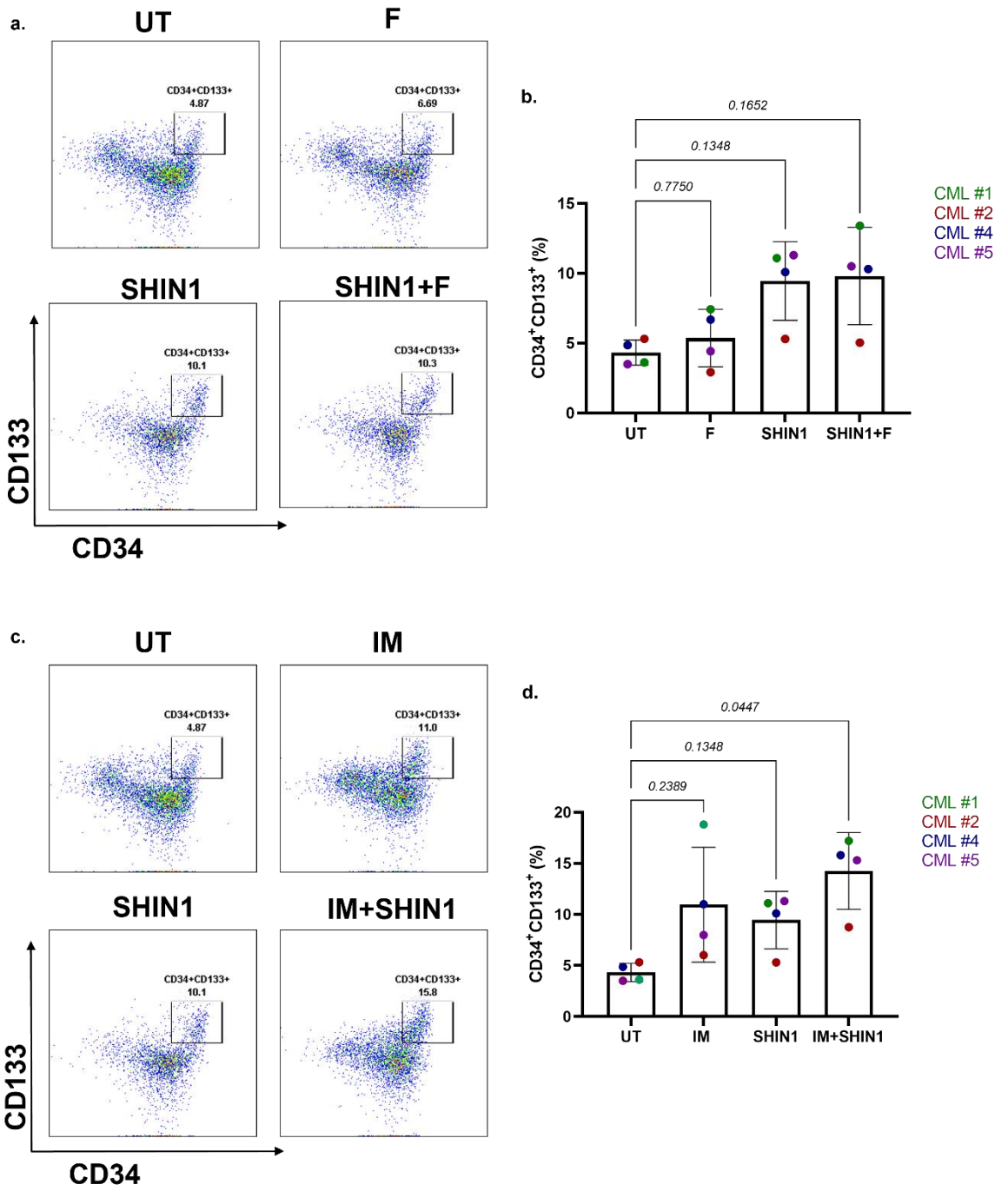

Figure 6-3: SHIN1, similarly to imatinib, leads to a trend of increased proportion of CD34⁺CD133⁺ cells. Flow cytometry plots showing expression levels of CD34 and CD133 stem cell markers following 72h treatment with 1mM formate, 2.5μM SHIN1 or a combination of both (**a**). Graphs showing percentage of CD34⁺CD133⁺ cells following 72h treatment with 1mM formate, 2.5μM SHIN1 or a combination of both (**b**) Flow cytometry plots showing expression levels of CD34 and CD133 stem cell markers following 72h treatment with 2μM imatinib, 2.5μM SHIN1 or a combination of both (**c**). Graphs showing percentage of CD34⁺CD133⁺ cells following 72h treatment with 2μM imatinib, 2.5μM SHIN1 or a combination of both. Data representative of mean ± SD, n=4 individual patient samples. P-values were calculated with a paired one-way ANOVA with Geisser-Greenhouse correction and Dunnett's multiple comparisons test.

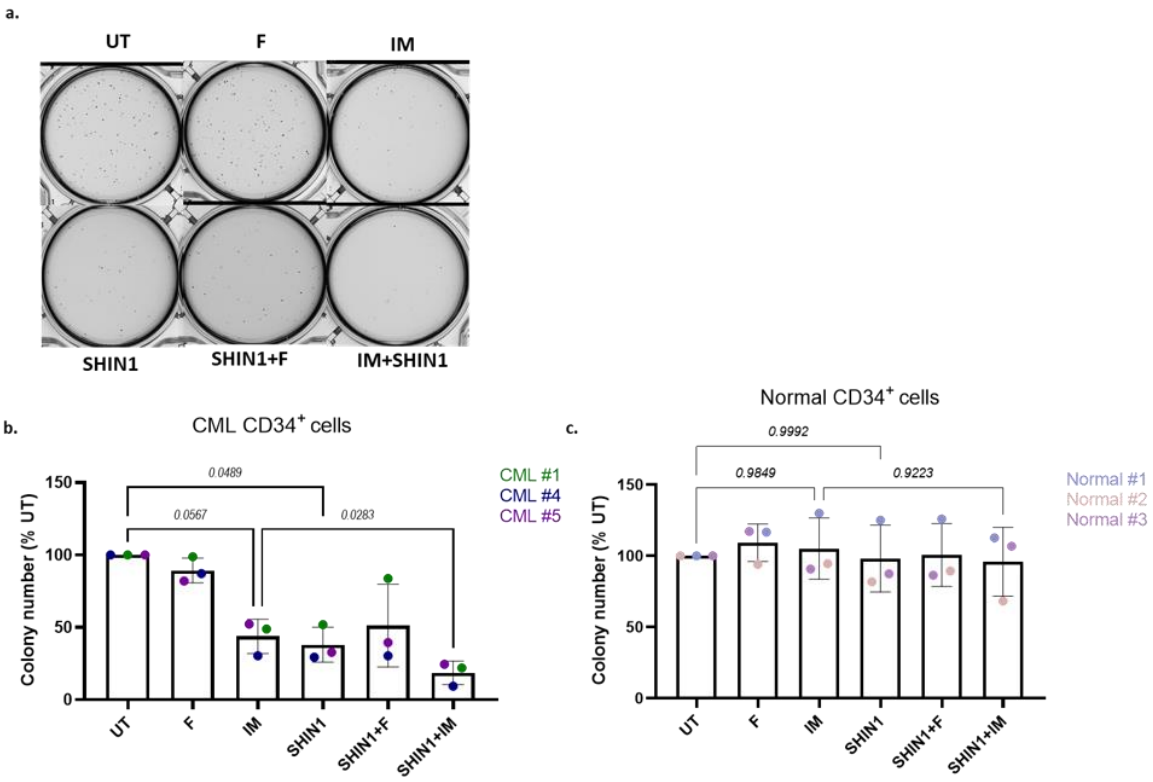

Figure 6-4: SHIN1 impairs colony formation capacity of patient-derived stem and progenitor CML cells. Representative pictures of CML colonies following a 72h treatment with formate, imatinib, SHIN1, a combination of SHIN1 with formate or a combination of SHIN1 and imatinib (**a**). Colony number of CML CD34$^+$ relative to UT following a 72h treatment with formate, imatinib, SHIN1, a combination of SHIN1 with formate or a combination of SHIN1 and imatinib (**b**). Colony number of normal CD34$^+$ relative to UT following a 72h treatment with formate, imatinib, SHIN1, a combination of SHIN1 with formate or a combination of SHIN1 and imatinib (**c**). n=3 individual patient samples. P-values were calculated with a paired one-way ANOVA with Dunnett's multiple comparisons test.

6.4 Discussion

In this chapter, we assessed the effect of inhibition of 1C metabolism in stem and progenitor CML cells. What we discovered is that SHIN1 treatment has an antiproliferative effect on CML CD34$^+$ cells and leads to a significant increase in undivided cells, with no apparent effect on cell death (**Figure** 6-1**b & c**). Surprisingly, formate supplementation was not sufficient to rescue the antiproliferative effect of SHIN1. In K562, reconstitution of purine and thymidylate synthesis with HT supplement was sufficient to rescue growth (**Figure** 3-10**a**). CML CD34$^+$ were cultured in the physiological relevant media Plasmax, that better recapitulates the nutritional environment of a tumour[158]. However, when cells were cultured in SFM, that mainly consists of IMDM, and it is historically the media of choice to culture primary samples, formate was able to partially rescue cell growth (**Figure** 6-5). Notably, formate and hypoxanthine are present in Plasmax, while they are not present in other commercial media. SHIN1 did not have any significant effect on cell growth in Plasmax compared to untreated cells (**Figure** 6-5), which could be potentially attributed to the presence of formate and hypoxanthine in the media. Formate, by donating 1C units independently of SHMT1/2 activity can reconstitute purine and thymidylate synthesis and bypass the blockage caused by SHIN1, as we have demonstrated throughout this thesis. However, as we mentioned, SHIN1 was capable of impairing cell division of CML CD34$^+$ cells (**Figure** 6-1**b**), suggesting that exogenous formate or hypoxanthine is not sufficient to rescue proliferation. Recent work from the Vousden lab demonstrated that A549 (lung adenocarcinoma cell line) cells can access exogenous formate for purine synthesis when cultured in Plasmax[184]. As it was previously mentioned, inhibition of SHMT1/2 results in reduction of glycine levels. Glycine through the glycine cleavage system contributes to glutathione production. In the same work from the Vousden lab it was also described that in Plasmax serine is rewired into glutathione synthesis[184]. In addition, formate supplementation not only does not rescue glycine levels, but it decreases them even further due to incorporation in purine synthesis. This could explain why formate supplementation is not sufficient to rescue SHIN1-mediated changes in Plasmax. Therefore, it would be interesting to see if glycine or a combination of formate and glycine can reverse SHIN1-mediated changes in CML CD34$^+$ cells. It has been shown that genetic or

pharmacological inhibition of 1C metabolism leads to impairment of T-cell proliferation. In that context, formate alone cannot rescue cell growth, while a combination of formate with glycine is sufficient to reverse the effect of 1C metabolism inhibition on cell growth[185].

Imatinib, the well-known TKI, had a very similar antiproliferative effect on CML $CD34^+$ cells, causing an enrichment of undivided cells (**Figure** 6-2**b**) However, we did not notice any additive effect when combining both treatments together. Of note, neither drug, alone, nor in combination resulted in significant levels of programmed cell death (**Figure** 6-2**c**).

It is worth mentioning that both treatments alone, or in combination led to a trend of increased percentage of $CD34^+CD133^+$ cells. Both surface markers are described in literature as markers of HSCs. Imatinib has been reported to target more differentiated cells and to be incapable of targeting primitive CML cells. It is possible that also SHIN1 can target more efficiently differentiated cells, or that even though it enriches for $CD34^+CD133^+$ cells, these cells are not functional. To get a better insight into this an attractive experiment would be the long-term culture-initiating cell (LTC-IC) assay. During the LTC-IC assay, CD34+ CML cells are treated with the treatment of choice, and then are placed in a liquid culture for 5 weeks before placement in semisolid medium. This method ensures selective measurement of the functional capacity of long-term LSCs to initiate and sustain haematopoiesis *in vitro*. Short-term progenitor cells lose their colony-forming potential during the 5 weeks in liquid culture. As SHIN1 is not suitable for *in vivo* studies, another option would be to treat CML $CD34^+$ cells *in vitro* and then transplant them into sublethally irradiated immunodeficient mice to assess their engraftment capacity.

However, we demonstrated that SHIN1 impairs short-term colony formation ability of CML $CD34^+$ cells and it sensitises cells to imatinib (**Figure** 6-4**b**). Once more, addition of formate was incapable of rescuing the effect of SHIN1 treatment. Besides this, we also showed that neither SHIN1, imatinib or a combination of both, had a significant effect on the differentiation capacity of normal $CD34^+$ cells (**Figure** 6-4**c**). This latest finding is of a particular clinical interest, as it has been reported that MTX leads to bone marrow suppression[131]. The possibility that SHIN1 might not have a deleterious effect on normal

haematopoietic cells, implies that it might be a better and more selective inhibitor by avoiding the adverse effects of traditional antifolates.

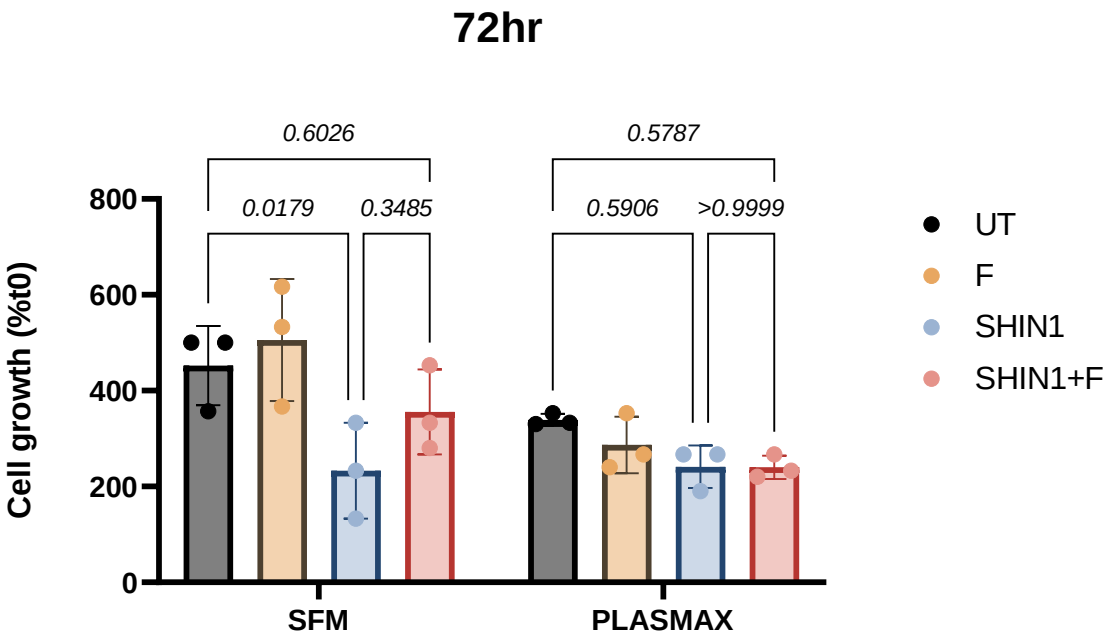

Figure 6-5: Plasmax alters growth of CML CD34⁺ cells. Graph depicting percentage of cell growth relative to t0 of CML CD34⁺ cells following a 72h treatment with 1mM formate, 2.5μM SHIN1 or a combination of both when cultured in either SFM media or Plasmax (**a**). Data representative of mean ± SD, n=4 individual patient samples. P-values were calculated with a two-way ANOVA with Sidak's multiple comparisons test.

6.5 Summary

To sum up, in this chapter we demonstrated that SHIN1 impairs proliferation of primitive CML cells. We showed that formate supplementation is not sufficient to rescue the antiproliferative effect of SHIN1.

Furthermore, we described that inhibition of 1C metabolism leads to decreased colony formation ability of CML $CD34^+$ cells and combination of SHIN1 with imatinib can sensitise cells to the traditional TKI. We also described that SHIN1 does not affect CFC capacity of normal primitive cells, affirming a potential therapeutic window.

Chapter 7 Conclusions and future perspectives

Collectively, this thesis has presented previously unrecognised role of folate metabolism in CML as a model of LSC-driven haematological malignancies (**Figure** 7-1). Herein, we will discuss our findings with regards to current literature, explore future directions, limitations and potential implications of this study.

7.1 Folate metabolism and LSCs

Previous work from our lab has demonstrated that LSCs have high metabolic activity due to increased mitochondrial mass and increased OXPHOS when compared to normal HSCs[75]. Furthermore, the same work demonstrated that, compared to normal HSCs, CML LSCs display an increased oxidative anaplerotic metabolism that supports aspartate biosynthesis. Several recent studies have highlighted that mitochondrial respiration is necessary for aspartate biosynthesis in cancer cells[71, 72]. Aspartate contributes directly to purine and pyrimidine synthesis, therefore to nucleotide biosynthesis. Additionally, it has been shown that when disrupting the ETC-linked generation of ATP via OXPHOS, cancer cells can still survive as long as the ETC-linked TCA cycle function is intact[74]. This indicates that glycolysis alone can support the energetic needs of the cell, while mitochondrial respiration is likely necessary for aspartate synthesis that, ultimately, contributes to nucleotide synthesis and can maintain proliferation of the cancer cells. With regards to CML LSCs, it would be informative to investigate whether mitochondrial respiration is upregulated to support aspartate biosynthesis and its link to nucleotide synthesis. If so, nucleotide synthesis would then be exposed as a targetable vulnerability for LSCs.

Folate metabolism plays a crucial role in nucleotide biosynthesis, energy homeostasis and redox defence[84]. 10-formyl-THF gets incorporated into purine and pyrimidine precursors. Furthermore, folate metabolism has been demonstrated to be a metabolic vulnerability in various malignancies, including several haematological cancers[164, 172, 186]. Indeed, we found folate metabolism associated genes to be upregulated in LSCs ($CD34^+CD38^-$) compared to normal counterparts. Furthermore, we discovered that folate metabolism activity measured by formate exchange rate is significantly upregulated in CML $CD34^+$

cells compared to normal $CD34^+$ cells. The $CD34^+$ cell population is stem cell enriched, but it also contains more differentiated cells that express CD38. It would be interested to assess the activity of the pathway in $CD34^+CD38^-$ and compare it to more differentiated LPCs ($CD34^+CD38^+$). Transcriptionally, expression of folate metabolism genes was found to be similar in LSCs and LPCs, suggesting that folate metabolism activity is also likely to be similar in these two populations.

Of clinical relevance, analysis of publicly available microarray data of CML $CD34^+$ cells treated with imatinib revealed that expression of folate metabolism genes does not significantly change following imatinib treatment, implying that the activity of the pathway might not be significantly impaired upon TKI therapy. Research has shown that imatinib, despite complete inhibition of BCR-ABL kinase, cannot target LSCs that seem to persist in a BCR-ABL independent way[64]. Thus,it can be hypothesised that the folate pathway might be a metabolic vulnerability for this population and its inhibition might sensitise cells to imatinib, however this requires further investigation.

Another topic of interest would be to assess the impact of TKI therapy on mitochondrial respiration and nucleotide synthesis. Of note, one study using CML cell lines described that imatinib treatment resulted in a reduction in glycolysis and a compensatory increase in oxidative metabolism in CML cells[187]. Flis and colleagues demonstrated that increased expression of ETC genes in CML LSCs compared to normal counterparts is not reverted following imatinib treatment[188]. Lastly, work from our lab revealed that tigecycline, by inhibiting mitochondrial protein synthesis and impairing ETC, can sensitise LSCs to imatinib *in vitro* and *in vivo*[75]. All these findings hint that imatinib is not able to fully inhibit mitochondrial respiration and DNA and RNA synthesis, reinforcing the idea that folate metabolism inhibition might sensitise cells to imatinib treatment due to blockage of nucleotide biosynthesis.

7.2 Inhibition of folate metabolism has an antiproliferative effect on CML cells *in vitro* and *in vivo*

To further understand the role of folate metabolism in CML cells, we generated a K562 SHMT2 KO cell line. We found that genetic inhibition of the mitochondrial arm of the pathway led to decreased cell growth and cell cycle arrest in the S phase, while we did not observe any significant effect on programmed cell death. Interestingly, HT supplementation and ultimately reconstitution of nucleotide synthesis, partially rescued the antiproliferative effect of SHMT2 loss. Furthermore, loss of SHMT2 significantly impaired the KCL22 tumour xenograft formation. It resulted in significantly extended survival of mice when compared to mice transplanted with control cells and significantly reduced tumour burden. It should be noted that most of the mice transplanted with KCL22 SHMT2 KO cells did not form any tumours, suggesting that loss of SHMT2 prevents tumourigenesis.

Our *in vivo* findings support that genetic inhibition of mitochondrial folate metabolism is sufficient to inhibit tumourigenesis. On the contrary, genetic disruption of mitochondrial 1C metabolism has been shown to result in partial tumour growth inhibition in a HCT-116 xenograft model[89]. This is attributed to compensation of loss of the mitochondrial arm of the pathway by upregulation of the cytosolic arm. Interestingly, circulating formate, purines, and pyrimidines, which could fulfil the 1C-unit demands of KCL22 SHMT2 KO cells, were not sufficient to compensate for the loss of SHMT2. This highlights the absolute dependence of growing CML cells *in vivo* on intrinsic 1C metabolism and the potential for folate metabolism therapeutic targeting.

It should be noted that NRGW[41] mice transplanted with KCL22 cell, do not develop CML. While transplantation of KCL22 SHMT2 KO gave insight into the importance of 1C metabolism in tumour formation, it is not informative about the impact of inhibition of the pathway following leukaemia development. A commonly used mouse model to study leukaemogenesis *in vivo* is the SCLtTA/BCR-ABL double transgenic model (DTG). In this model, transactivator protein tTA is under the control of the 3' enhancer of the murine stem cell leukaemia (SCL) gene and crossed with a TRE-BCR-ABL mouse to generate

SCLtTA/BCR-ABL DTG mouse[189]. However, another limitation to study the impact of 1C metabolism inhibition *in vivo* is that SHIN1 is not suitable for such studies due to rapid clearance, highlighting the need of developing new specific folate metabolism inhibitors that could be used *in vivo*.

7.3 Inhibition of folate metabolism causes a cascade of signalling changes in CML cells

Metabolic analysis of K562 cells following either genetic or pharmacological inhibition of 1C metabolism led to significant reduction of purine biosynthesis, with no significant effect on *de novo* pyrimidine synthesis. Furthermore, formate supplementation was sufficient to restore purine biosynthesis. Formate provides 1C units independently of SHMT1/2 activity, therefore it can bypass the blockage caused by SHMT1/2 inhibition and support reconstitution of purine synthesis by alleviating the 10-formyl THF pool. Another important 1C metabolism product necessary for purine synthesis is glycine. Inhibition of mitochondrial folate metabolism makes cells glycine auxotrophs. Formate supplementation cannot restore glycine levels. García-Cañaveras *et al*. showed that exogenous formate is sufficient to restore purine synthesis and proliferation defects in T-ALL cell lines[186]. Nevertheless, Ducker *et al*. demonstrated that diffuse large B-cell lymphoma cells require glycine for purine synthesis and cell growth. They showed that even though formate rescues folate 1C levels, it cannot rescue purine synthesis[164]. Furthermore, Pikman and colleagues revealed that suppression of MTHFD2 in AML cell lines increases glycine dependence, and formate addition cannot rescue cell growth[172]. Throughout our work formate supplementation was sufficient to rescue most of the changes caused by inhibition of the folate pathway, suggesting that in CML, at least in cell culture, lack of 1C units for nucleotide synthesis seems to be the primary deficiency. How this would translate *in vivo* and whether glycine is a limiting factor in CML tumour models remains to be revealed.

Due to blockage of purine biosynthesis, AICAR, a purine intermediate and AMPK activator was significantly upregulated following inhibition of 1C metabolism. AICAR links metabolism with cellular signalling through AMPK. Indeed, we observed AMPK activation, mTOR suppression and autophagy induction following inhibition of 1C metabolism. These results support literature that suggests that

MTX treatment causes accumulation of AICAR and AMPK activation in breast and prostate cancer cell lines[115]. Furthermore, induction of AMPK through MTX is thought to be linked with the anti-proliferative effects of MTX[115-117].

Furthermore, inhibition of folate metabolism resulted in changes in mitochondrial homeostasis. Inhibition of the pathway resulted in reduction of mitochondrial ROS, hyperpolarisation of the mitochondrial membrane, accumulation of the mitochondrial fission related protein, DRP1 and mitophagy receptor, NIX in the mitochondrial-enriched fraction of the cells. It should be noted that, although DRP1 and NIX accumulation indicate induction of mitochondrial fragmentation and mitophagy, application of more robust techniques (such as advanced mitochondrial imaging) is required to reach more conclusive results. Nevertheless, AMPK activation has been previously linked to mitochondrial fragmentation and mitophagy[166]. Furthermore, depletion of AMPKα1α2 partially rescued accumulation of DRP1 and NIX, indicating that at least, partially, the effect of 1C metabolism inhibition on mitochondria fragmentation and degradation might be AMPK-dependent.

7.4 Inhibition of 1C metabolism leads to differentiation of CML cells

Phenotypically, we observed that following genetic or pharmacological inhibition of folate metabolism, cell pellets appeared to have a stronger red colour than untreated or control cells respectively, suggesting an increase in erythroid maturation. Flow cytometry assessment of levels of erythroid maturation markers CD71 and GlyA, validated that inhibition of 1C metabolism results in a significant increase in percentage of $CD71^{+}GlyA^{+}$ cells compared to untreated/control K562 cells. Furthermore, similar results were obtained following pharmacological SHMT1/2 inhibition in CML $CD34^{+}$ cells when cultured with low levels of EPO. Notably, formate supplementation was sufficient to rescue levels of erythroid maturation markers. Similarly, SHIN1 treatment resulted in promotion of myeloid maturation of AML cell lines, measured through CD11b levels. Pikman and colleagues demonstrated that suppression of MTHFD2 resulted in increased levels of CD11b in MOLM14, THP1 and U939 AML cell lines[172]. Maturation of CML cells might have clinical implications. As described, imatinib therapy cannot effectively eliminate quiescent, undifferentiated LSCs,

thus finding novel ways to promote differentiation of LSCs can sensitise them to TKI treatment.

Interestingly, we uncovered that maturation of CML cells following SHIN1 treatment was not dependent on AMPK activity. Furthermore, we demonstrated that mTOR inhibition and autophagy induction following 1C-unit depletion persists even in K562 AMPKα1α2 KO cells. In addition, increased levels of erythroid maturation markers following SHIN1 treatment were reversed following pharmacological or genetic inhibition of autophagy. This suggested that differentiation in the context of 1C metabolism inhibition is AMPK-independent, but autophagy-dependent. In support of our findings, two recent studies have described that a series of antifolates result in mTOR suppression through impairment of purine synthesis[180, 181]. Hoxhaj and colleagues described that mTORC1 senses changes in intracellular adenylates in an AMPK-independent manner. Furthermore, they show that in mouse embryonic fibroblasts purine biosynthesis suppression can inhibit mTOR signalling in the absence of AMPKα1α2[181]. Thus, it would be important to assess whether adenine or guanine can prevent inhibit differentiation, mTOR suppression and autophagy induction in AMPKα1α2 KO cells following 1C metabolism inhibition. We have seen that formate supplementation in wild type K562 cells is sufficient to rescue mTOR inhibition and suppress differentiation. If this is due to purine synthesis restoration, then adenine/guanine or even formate supplementation should be able to provide similar findings in AMPKα1α2 KO cells. If this is the case, we can conclude that the changes elicited following 1C metabolism inhibition are attributed to impairment of *de novo* purine synthesis. Our results indicate that AICAR on one side, and purines on the other control AMPK, mTOR and autophagy in CML cells.

7.5 Folate metabolism has an antiproliferative role CML $CD34^+$ cells

Consistently to what we observed in K562 cells *in vitro* and KCL22 cells *in vivo*, pharmacological inhibition of 1C metabolism in CML $CD34^+$ cells resulted in impaired cell proliferation and short-term CFC potential. In addition, SHIN1 treatment did not have any effect on the CFC potential of normal $CD34^+$ cells. Interestingly, SHIN1 treatment sensitised cells to imatinib, as there was a further

reduction of the counted colonies compared to imatinib alone, when combining both treatments together. However, unlike what we have described so far, formate supplementation was not sufficient to rescue any of the SHIN1-meidated effects. To carry out the experiments mentioned above, CML $CD34^+$ cells were cultured in Plasmax supplemented with physiological growth factors. Interestingly, unlike other commercial media, formate is present in Plasmax. In principle, the presence of exogenous formate should dampen the effect of SHIN1. However, SHIN1 treatment significantly decreased $CD34^+$ cell division and led to a 50% reduction of the CFC of progenitor CML cells even though exogenous formate was present. It is possible that in SFM media, where formate is absent, SHIN1 might have an even stronger effect in CML $CD34^+$ cells. In support of this, cell growth of $CD34^+$ cells was significantly impaired when treated with the SHIN1 inhibitor in SFM media, while it did not change in Plasmax media. Recent work from the Vousden lab demonstrated that A549 cells can access exogenous formate for purine synthesis when cultured in Plasmax[184]. However, authors demonstrate that extracellular formate does not influence the contribution of extracellular serine in purine synthesis. This could explain why SHIN1 has an antiproliferative effect on Plasmax even with exogenous formate present. Furthermore, the same work displayed that hypoxanthine salvage pathway is a major contributor of purines when cells are cultured in Plasmax. Of note, they demonstrated that when limiting serine availability, cells increased extracellular hypoxanthine uptake, sparing available serine for other pathways such as glutathione production. SHIN1 blocks the serine to glycine production and likely the contribution of glycine to the glutathione pool. These findings suggest that serine and 1C metabolism is potentially rewired in other processes apart from nucleotide synthesis in this culture media. If supplementation with glycine would rescue the antiproliferative effect of SHIN1 in CML $CD34^+$ remains to be discovered.

Lastly, it would be worth investigating the effect of SHIN1 treatment in LSCs. We did observe a trend of increased percentage of $CD34^+CD133^+$ cells. It is possible that SHIN1 enriches for $CD34^+CD133^+$ cells, however, these cells might not be fully functional. An LTC-IC assay would provide some insights into the matter. Furthermore, as SHIN1 is not suitable for *in vivo* studies, another option would be to treat CML $CD34^+$ cells *in vitro* and then transplant them into sublethally

irradiated immunodeficient mice to assess their engraftment capacity. Such experiments would improve our understanding of the effect of SHIN1 inhibition in LSCs.

7.6 Additional remarks

This investigation would not have been feasible without the access to primary patient-derived samples and as such without the collaboration with the NHS biorepository department and access to the Paul O' Gorman research centre bio-bank. Collection and isolation of primary cells is linked to significant challenges related to ethics, consent, and health service collaboration. However, primary samples provide an invaluable pre-clinical resource. In this thesis, combining CML cell lines, primary samples, and *in vivo* models we have demonstrated how folate metabolism might be a metabolic vulnerability for LSCs and sensitise this population to traditional therapeutic approaches.

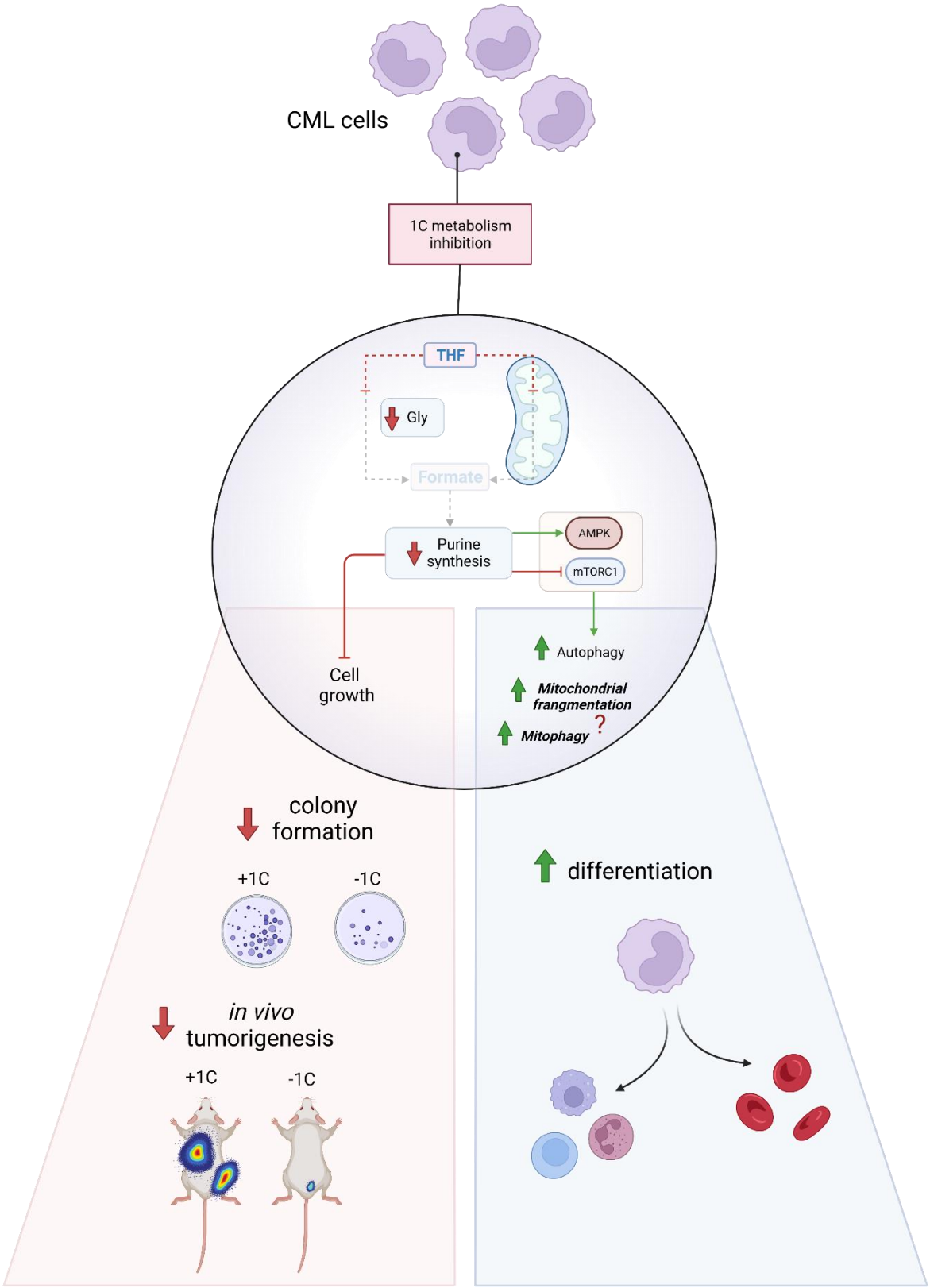

Figure 7-1: Impact of inhibition of folate metabolism in CML cells.
Generated with BioRender.com.

List of References

1. Quesenberry, P.J. and G.A. Colvin, *Hematopoietic stem cells, progenitor cells, and cytokines.* Williams Hematology, 2001. **338**: p. 153-174.
2. Till, J.E. and E.A. McCulloch, *A direct measurement of the radiation sensitivity of normal mouse bone marrow cells.* Radiation research, 1961. **14**(2): p. 213-222.
3. Siminovitch, L., E.A. McCulloch, and J.E. Till, *The distribution of colony-forming cells among spleen colonies.* 1963.
4. Becker, A.J., E.A. McCulloch, and J.E. Till, *Cytological demonstration of the clonal nature of spleen colonies derived from transplanted mouse marrow cells.* 1963.
5. Wilson, A., et al., *Hematopoietic stem cells reversibly switch from dormancy to self-renewal during homeostasis and repair.* Cell, 2008. **135**(6): p. 1118-1129.
6. Cabezas-Wallscheid, N., et al., *Identification of regulatory networks in HSCs and their immediate progeny via integrated proteome, transcriptome, and DNA methylome analysis.* Cell stem cell, 2014. **15**(4): p. 507-522.
7. Pietras, E.M., et al., *Functionally distinct subsets of lineage-biased multipotent progenitors control blood production in normal and regenerative conditions.* Cell stem cell, 2015. **17**(1): p. 35-46.
8. Cheng, H., Z. Zheng, and T. Cheng, *New paradigms on hematopoietic stem cell differentiation.* Protein & cell, 2020. **11**(1): p. 34-44.
9. Pronk, C.J., et al., *Elucidation of the phenotypic, functional, and molecular topography of a myeloerythroid progenitor cell hierarchy.* Cell stem cell, 2007. **1**(4): p. 428-442.
10. Paul, F., et al., *Transcriptional heterogeneity and lineage commitment in myeloid progenitors.* Cell, 2015. **163**(7): p. 1663-1677.
11. Haas, S., et al., *Inflammation-induced emergency megakaryopoiesis driven by hematopoietic stem cell-like megakaryocyte progenitors.* Cell stem cell, 2015. **17**(4): p. 422-434.
12. Velten, L., et al., *Human haematopoietic stem cell lineage commitment is a continuous process.* Nature cell biology, 2017. **19**(4): p. 271-281.
13. Krause, D.S., et al., *CD34: structure, biology, and clinical utility [see comments].* 1996.
14. Baum, C.M., et al., *Isolation of a candidate human hematopoietic stem-cell population.* Proceedings of the National Academy of Sciences, 1992. **89**(7): p. 2804-2808.
15. Malavasi, F., et al., *Evolution and function of the ADP ribosyl cyclase/CD38 gene family in physiology and pathology.* Physiological reviews, 2008. **88**(3): p. 841-886.
16. Hao, Q.-L., et al., *Extended long-term culture reveals a highly quiescent and primitive human hematopoietic progenitor population.* 1996.
17. Wisniewski, D., et al., *Further phenotypic characterization of the primitive lineage− CD34+ CD38− CD90+ CD45RA− hematopoietic stem cell/progenitor cell sub-population isolated from cord blood, mobilized peripheral blood and patients with chronic myelogenous leukemia.* Blood cancer journal, 2011. **1**(9): p. e36-e36.
18. Jang, Y.-Y. and S.J. Sharkis, *A low level of reactive oxygen species selects for primitive hematopoietic stem cells that may reside in the low-*

oxygenic niche. Blood, The Journal of the American Society of Hematology, 2007. **110**(8): p. 3056-3063.
19. Bigarella, C.L., R. Liang, and S. Ghaffari, *Stem cells and the impact of ROS signaling*. Development, 2014. **141**(22): p. 4206-4218.
20. Ito, K. and T. Suda, *Metabolic requirements for the maintenance of self-renewing stem cells*. Nature reviews Molecular cell biology, 2014. **15**(4): p. 243-256.
21. Takubo, K., et al., *Regulation of the HIF-1a level is essential for hematopoietic stem cells*. Cell stem cell, 2010. **7**(3): p. 391-402.
22. Simsek, T., et al., *The distinct metabolic profile of hematopoietic stem cells reflects their location in a hypoxic niche*. Cell stem cell, 2010. **7**(3): p. 380-390.
23. Vannini, N., et al., *Specification of haematopoietic stem cell fate via modulation of mitochondrial activity*. Nature communications, 2016. **7**(1): p. 1-9.
24. Inoki, K., M.N. Corradetti, and K.-L. Guan, *Dysregulation of the TSC-mTOR pathway in human disease*. Nature genetics, 2005. **37**(1): p. 19-24.
25. Schieke, S.M., et al., *The mammalian target of rapamycin (mTOR) pathway regulates mitochondrial oxygen consumption and oxidative capacity*. Journal of Biological Chemistry, 2006. **281**(37): p. 27643-27652.
26. Chen, C., et al., *TSC–mTOR maintains quiescence and function of hematopoietic stem cells by repressing mitochondrial biogenesis and reactive oxygen species*. The Journal of experimental medicine, 2008. **205**(10): p. 2397-2408.
27. Rimmelé, P., et al., *Mitochondrial metabolism in hematopoietic stem cells requires functional FOXO 3*. EMBO reports, 2015. **16**(9): p. 1164-1176.
28. Miyamoto, K., et al., *Foxo3a is essential for maintenance of the hematopoietic stem cell pool*. Cell stem cell, 2007. **1**(1): p. 101-112.
29. Ansó, E., et al., *The mitochondrial respiratory chain is essential for haematopoietic stem cell function*. Nature cell biology, 2017. **19**(6): p. 614-625.
30. He, C. and D.J. Klionsky, *Regulation mechanisms and signaling pathways of autophagy*. Annual review of genetics, 2009. **43**: p. 67-93.
31. Mortensen, M., et al., *The autophagy protein Atg7 is essential for hematopoietic stem cell maintenance*. Journal of Experimental Medicine, 2011. **208**(3): p. 455-467.
32. Ho, T.T., et al., *Autophagy maintains the metabolism and function of young and old stem cells*. Nature, 2017. **543**(7644): p. 205-210.
33. Ito, K., et al., *Self-renewal of a purified Tie2+ hematopoietic stem cell population relies on mitochondrial clearance*. Science, 2016. **354**(6316): p. 1156-1160.
34. Sandoval, H., et al., *Essential role for Nix in autophagic maturation of erythroid cells*. Nature, 2008. **454**(7201): p. 232-235.
35. Kundu, M., et al., *Ulk1 plays a critical role in the autophagic clearance of mitochondria and ribosomes during reticulocyte maturation*. Blood, The Journal of the American Society of Hematology, 2008. **112**(4): p. 1493-1502.
36. Rutherford, T., J. Clegg, and D. Weatherall, *K562 human leukaemic cells synthesise embryonic haemoglobin in response to haemin*. Nature, 1979. **280**(5718): p. 164-165.

37. Jørgensen, H. and T. Holyoake, *Characterization of cancer stem cells in chronic myeloid leukaemia.* Biochemical Society Transactions, 2007. **35**(5): p. 1347-1351.
38. Frazer, R., A.E. Irvine, and M.F. McMullin, *Chronic myeloid leukaemia in the 21st century.* The Ulster medical journal, 2007. **76**(1): p. 8.
39. O'hare, T., et al., *Pushing the limits of targeted therapy in chronic myeloid leukaemia.* Nature reviews Cancer, 2012. **12**(8): p. 513-526.
40. Savona, M. and M. Talpaz, *Getting to the stem of chronic myeloid leukaemia.* Nature reviews cancer, 2008. **8**(5): p. 341-350.
41. Höglund, M., F. Sandin, and B. Simonsson, *Epidemiology of chronic myeloid leukaemia: an update.* Annals of hematology, 2015. **94**(2): p. 241-247.
42. Apperley, J.F., *Chronic myeloid leukaemia.* The Lancet, 2015. **385**(9976): p. 1447-1459.
43. Pendergast, A.M., et al., *BCR-ABL-induced oncogenesis is mediated by direct interaction with the SH2 domain of the GRB-2 adaptor protein.* Cell, 1993. **75**(1): p. 175-185.
44. Cilloni, D. and G. Saglio, *Molecular pathways: Bcr-abl.* Clinical Cancer Research, 2012. **18**(4): p. 930-937.
45. O'Hare, T., et al., *Targeting the BCR-ABL signaling pathway in therapy-resistant Philadelphia chromosome-positive leukemia.* Clinical Cancer Research, 2011. **17**(2): p. 212-221.
46. Skorski, T., et al., *Phosphatidylinositol-3 kinase activity is regulated by BCR/ABL and is required for the growth of Philadelphia chromosome-positive cells.* 1995.
47. Markova, B., et al., *Novel pathway in Bcr-Abl signal transduction involves Akt-independent, PLC-γ1-driven activation of mTOR/p70S6-kinase pathway.* Oncogene, 2010. **29**(5): p. 739-751.
48. Naka, K., et al., *TGF-β–FOXO signalling maintains leukaemia-initiating cells in chronic myeloid leukaemia.* Nature, 2010. **463**(7281): p. 676-680.
49. Hoelbl, A., et al., *Stat5 is indispensable for the maintenance of bcr/abl-positive leukaemia.* EMBO molecular medicine, 2010. **2**(3): p. 98-110.
50. Sawyers, C.L., W. Callahan, and O.N. Witte, *Dominant negative MYC blocks transformation by ABL oncogenes.* Cell, 1992. **70**(6): p. 901-910.
51. Druker, B.J., et al., *Effects of a selective inhibitor of the Abl tyrosine kinase on the growth of Bcr–Abl positive cells.* Nature medicine, 1996. **2**(5): p. 561-566.
52. Buchdunger, E., et al., *Inhibition of the Abl protein-tyrosine kinase in vitro and in vivo by a 2-phenylaminopyrimidine derivative.* Cancer research, 1996. **56**(1): p. 100-104.
53. O'Brien, S.G., et al., *Imatinib compared with interferon and low-dose cytarabine for newly diagnosed chronic-phase chronic myeloid leukemia.* New England Journal of Medicine, 2003. **348**(11): p. 994-1004.
54. Mughal, T.I., et al., *Chronic myeloid leukemia: reminiscences and dreams.* Haematologica, 2016. **101**(5): p. 541.
55. Mahon, F.-X., et al., *Discontinuation of imatinib in patients with chronic myeloid leukaemia who have maintained complete molecular remission for at least 2 years: the prospective, multicentre Stop Imatinib (STIM) trial.* The lancet oncology, 2010. **11**(11): p. 1029-1035.
56. Rea, D., et al., *Discontinuation of dasatinib or nilotinib in chronic myeloid leukemia: interim analysis of the STOP 2G-TKI study.* Blood, The Journal of the American Society of Hematology, 2017. **129**(7): p. 846-854.

57. Fialkow, P.J., R.J. Jacobson, and T. Papayannopoulou, *Chronic myelocytic leukemia: clonal origin in a stem cell common to the granulocyte, erythrocyte, platelet and monocyte/macrophage.* The American journal of medicine, 1977. **63**(1): p. 125-130.
58. Takahashi, N., et al., *Lineage involvement of stem cells bearing the philadelphia chromosome in chronic myeloid leukemia in the chronic phase as shown by a combination of fluorescence-activated cell sorting and fluorescence in situ hybridization.* Blood, The Journal of the American Society of Hematology, 1998. **92**(12): p. 4758-4763.
59. Huntly, B.J., et al., *MOZ-TIF2, but not BCR-ABL, confers properties of leukemic stem cells to committed murine hematopoietic progenitors.* Cancer cell, 2004. **6**(6): p. 587-596.
60. Holyoake, T., et al., *Isolation of a highly quiescent subpopulation of primitive leukemic cells in chronic myeloid leukemia.* Blood, The Journal of the American Society of Hematology, 1999. **94**(6): p. 2056-2064.
61. Bhatia, R., et al., *Persistence of malignant hematopoietic progenitors in chronic myelogenous leukemia patients in complete cytogenetic remission following imatinib mesylate treatment.* Blood, 2003. **101**(12): p. 4701-4707.
62. Chomel, J.-C., et al., *Leukemic stem cell persistence in chronic myeloid leukemia patients with sustained undetectable molecular residual disease.* Blood, The Journal of the American Society of Hematology, 2011. **118**(13): p. 3657-3660.
63. Corbin, A.S., et al., *Human chronic myeloid leukemia stem cells are insensitive to imatinib despite inhibition of BCR-ABL activity.* The Journal of clinical investigation, 2011. **121**(1): p. 396-409.
64. Hamilton, A., et al., *Chronic myeloid leukemia stem cells are not dependent on Bcr-Abl kinase activity for their survival.* Blood, The Journal of the American Society of Hematology, 2012. **119**(6): p. 1501-1510.
65. Bellodi, C., et al., *Targeting autophagy potentiates tyrosine kinase inhibitor–induced cell death in Philadelphia chromosome–positive cells, including primary CML stem cells.* The Journal of clinical investigation, 2009. **119**(5): p. 1109-1123.
66. Baquero, P., et al., *Targeting quiescent leukemic stem cells using second generation autophagy inhibitors.* Leukemia, 2019. **33**(4): p. 981-994.
67. Ianniciello, A., et al., *ULK1 inhibition promotes oxidative stress–induced differentiation and sensitizes leukemic stem cells to targeted therapy.* Science Translational Medicine, 2021. **13**(613): p. eabd5016.
68. Giustacchini, A., et al., *Single-cell transcriptomics uncovers distinct molecular signatures of stem cells in chronic myeloid leukemia.* Nature medicine, 2017. **23**(6): p. 692-702.
69. Warburg, O., *On the origin of cancer cells.* Science, 1956. **123**(3191): p. 309-314.
70. Vander Heiden, M.G., L.C. Cantley, and C.B. Thompson, *Understanding the Warburg effect: the metabolic requirements of cell proliferation.* science, 2009. **324**(5930): p. 1029-1033.
71. Birsoy, K., et al., *An essential role of the mitochondrial electron transport chain in cell proliferation is to enable aspartate synthesis.* Cell, 2015. **162**(3): p. 540-551.
72. Sullivan, L.B., et al., *Supporting aspartate biosynthesis is an essential function of respiration in proliferating cells.* Cell, 2015. **162**(3): p. 552-563.

73. Krall, A.S., et al., *Asparagine couples mitochondrial respiration to ATF4 activity and tumor growth*. Cell Metabolism, 2021. **33**(5): p. 1013-1026. e6.
74. Martínez-Reyes, I., et al., *Mitochondrial ubiquinol oxidation is necessary for tumour growth*. Nature, 2020. **585**(7824): p. 288-292.
75. Kuntz, E.M., et al., *Targeting mitochondrial oxidative phosphorylation eradicates therapy-resistant chronic myeloid leukemia stem cells*. Nature medicine, 2017. **23**(10): p. 1234-1240.
76. Abraham, A., et al., *SIRT1 regulates metabolism and leukemogenic potential in CML stem cells*. The Journal of clinical investigation, 2019. **129**(7): p. 2685-2701.
77. Li, L., et al., *Activation of p53 by SIRT1 inhibition enhances elimination of CML leukemia stem cells in combination with imatinib*. Cancer cell, 2012. **21**(2): p. 266-281.
78. Smithells, R.W., S. Sheppard, and C.J. Schorah, *Vitamin dificiencies and neural tube defects*. Archives of Disease in Childhood, 1976. **51**(12): p. 944-950.
79. Beaudin, A.E. and P.J. Stover, *Insights into metabolic mechanisms underlying folate-responsive neural tube defects: a minireview*. Birth Defects Research Part A: Clinical and Molecular Teratology, 2009. **85**(4): p. 274-284.
80. Hibbard, B.M., *The role of folio acid in pregnancy, with particular reference to anaemia, abruption and abortion*. Journal of Obstetrics and Gynaecology of the British Commonwealth, 1964. **71**: p. 529-542.
81. Farber, S., et al., *Temporary remissions in acute leukemia in children produced by folic acid antagonist, 4-aminopteroyl-glutamic acid (aminopterin)*. New England Journal of Medicine, 1948. **238**(23): p. 787-793.
82. Morscher, R.J., et al., *Mitochondrial translation requires folate-dependent tRNA methylation*. Nature, 2018. **554**(7690): p. 128-132.
83. Nilsson, R., V. Nicolaidou, and C. Koufaris, *Mitochondrial MTHFD isozymes display distinct expression, regulation, and association with cancer*. Gene, 2019. **716**: p. 144032.
84. Ducker, G.S. and J.D. Rabinowitz, *One-carbon metabolism in health and disease*. Cell metabolism, 2017. **25**(1): p. 27-42.
85. Pietzke, M., J. Meiser, and A. Vazquez, *Formate metabolism in health and disease*. Molecular Metabolism, 2020. **33**: p. 23-37.
86. Tibbetts, A.S. and D.R. Appling, *Compartmentalization of Mammalian folate-mediated one-carbon metabolism*. Annual review of nutrition, 2010. **30**: p. 57-81.
87. Gregory III, J.F., et al., *Primed, constant infusion with [2H3] serine allows in vivo kinetic measurement of serine turnover, homocysteine remethylation, and transsulfuration processes in human one-carbon metabolism*. The American journal of clinical nutrition, 2000. **72**(6): p. 1535-1541.
88. Herbig, K., et al., *Cytoplasmic serine hydroxymethyltransferase mediates competition between folate-dependent deoxyribonucleotide andS-adenosylmethionine biosyntheses*. Journal of Biological Chemistry, 2002. **277**(41): p. 38381-38389.
89. Ducker, G.S., et al., *Reversal of Cytosolic One-Carbon Flux Compensates for Loss of the Mitochondrial Folate Pathway*. Cell Metabolism, 2016. **23**(6): p. 1140-1153.

90. Meiser, J., et al., *Serine one-carbon catabolism with formate overflow.* Science advances, 2016. **2**(10): p. e1601273.
91. Patel, H., E. Di Pietro, and R.E. MacKenzie, *Mammalian fibroblasts lacking mitochondrial NAD+-dependent methylenetetrahydrofolate dehydrogenase-cyclohydrolase are glycine auxotrophs.* Journal of Biological Chemistry, 2003. **278**(21): p. 19436-19441.
92. Labuschagne, C.F., et al., *Serine, but not glycine, supports one-carbon metabolism and proliferation of cancer cells.* Cell Rep, 2014. **7**(4): p. 1248-58.
93. Lewis, C.A., et al., *Tracing compartmentalized NADPH metabolism in the cytosol and mitochondria of mammalian cells.* Molecular cell, 2014. **55**(2): p. 253-263.
94. Fan, J., et al., *Quantitative flux analysis reveals folate-dependent NADPH production.* Nature, 2014. **510**(7504): p. 298-302.
95. Zheng, Y., et al., *Mitochondrial one-carbon pathway supports cytosolic folate integrity in cancer cells.* Cell, 2018. **175**(6): p. 1546-1560. e17.
96. Bao, X.R., et al., *Mitochondrial dysfunction remodels one-carbon metabolism in human cells.* elife, 2016. **5**: p. e10575.
97. Meiser, J., et al., *Increased formate overflow is a hallmark of oxidative cancer.* Nature Communications, 2018. **9**(1): p. 1-12.
98. Oizel, K., et al., *Formate induces a metabolic switch in nucleotide and energy metabolism.* Cell Death & Disease, 2020. **11**(5): p. 1-14.
99. Tait-Mulder, J., et al., *The conversion of formate into purines stimulates mTORC1 leading to CAD-dependent activation of pyrimidine synthesis.* Cancer & Metabolism, 2020. **8**(1).
100. Yang, L., et al., *Serine catabolism feeds NADH when respiration is impaired.* Cell metabolism, 2020. **31**(4): p. 809-821. e6.
101. Gravel, S.-P., et al., *Serine deprivation enhances antineoplastic activity of biguanides.* Cancer research, 2014. **74**(24): p. 7521-7533.
102. Diehl, F.F., et al., *Cellular redox state constrains serine synthesis and nucleotide production to impact cell proliferation.* Nature metabolism, 2019. **1**(9): p. 861-867.
103. Chen, L., et al., *NADPH production by the oxidative pentose-phosphate pathway supports folate metabolism.* Nature metabolism, 2019. **1**(3): p. 404-415.
104. Ye, J., et al., *Serine catabolism regulates mitochondrial redox control during hypoxia.* Cancer Discov, 2014. **4**(12): p. 1406-17.
105. Piskounova, E., et al., *Oxidative stress inhibits distant metastasis by human melanoma cells.* Nature, 2015. **527**(7577): p. 186-191.
106. Balsa, E., et al., *Defective NADPH production in mitochondrial disease complex I causes inflammation and cell death.* Nature Communications, 2020. **11**(1): p. 1-12.
107. Krupenko, N.I., et al., *ALDH1L2 is the mitochondrial homolog of 10-formyltetrahydrofolate dehydrogenase.* Journal of Biological Chemistry, 2010. **285**(30): p. 23056-23063.
108. Izbicka, E., et al., *Distinct mechanistic activity profile of pralatrexate in comparison to other antifolates in in vitro and in vivo models of human cancers.* Cancer chemotherapy and pharmacology, 2009. **64**(5): p. 993-999.
109. Ferreri, A., et al., *A multicenter study of treatment of primary CNS lymphoma.* Neurology, 2002. **58**(10): p. 1513-1520.

110. Batchelor, T., et al., *Treatment of primary CNS lymphoma with methotrexate and deferred radiotherapy: a report of NABTT 96-07.* Journal of Clinical Oncology, 2003. **21**(6): p. 1044-1049.
111. Chabner, B.A., et al., *Polyglutamation of methotrexate. Is methotrexate a prodrug?* The Journal of clinical investigation, 1985. **76**(3): p. 907-912.
112. Allegra, C.J., et al., *Inhibition of phosphoribosylaminoimidazolecarboxamide transformylase by methotrexate and dihydrofolic acid polyglutamates.* Proceedings of the National Academy of Sciences, 1985. **82**(15): p. 4881-4885.
113. Gorlick, R., et al., *Intrinsic and acquired resistance to methotrexate in acute leukemia.* New England Journal of Medicine, 1996. **335**(14): p. 1041-1048.
114. Kool, M., et al., *MRP3, an organic anion transporter able to transport anti-cancer drugs.* Proceedings of the National Academy of Sciences, 1999. **96**(12): p. 6914-6919.
115. Tedeschi, P.M., et al., *Quantification of folate metabolism using transient metabolic flux analysis.* Cancer & metabolism, 2015. **3**(1): p. 1-14.
116. Fodor, T., et al., *Combined treatment of MCF-7 cells with AICAR and methotrexate, arrests cell cycle and reverses Warburg metabolism through AMP-activated protein kinase (AMPK) and FOXO1.* PLoS One, 2016. **11**(2): p. e0150232.
117. Pirkmajer, S., et al., *Methotrexate promotes glucose uptake and lipid oxidation in skeletal muscle via AMPK activation.* Diabetes, 2015. **64**(2): p. 360-369.
118. Sengupta, T.K., et al., *Cytotoxic effect of 5-aminoimidazole-4-carboxamide-1-β-4-ribofuranoside (AICAR) on childhood acute lymphoblastic leukemia (ALL) cells: implication for targeted therapy.* Molecular cancer, 2007. **6**(1): p. 1-12.
119. Beckers, A., et al., *Methotrexate enhances the antianabolic and antiproliferative effects of 5-aminoimidazole-4-carboxamide riboside.* 2006.
120. Kuznetsov, J.N., et al., *AMPK and Akt determine apoptotic cell death following perturbations of one-carbon metabolism by regulating ER stress in acute lymphoblastic leukemia.* Mol Cancer Ther, 2011. **10**(3): p. 437-47.
121. Teachey, D.T., et al., *mTOR inhibitors are synergistic with methotrexate: an effective combination to treat acute lymphoblastic leukemia.* Blood, The Journal of the American Society of Hematology, 2008. **112**(5): p. 2020-2023.
122. Papadopoli, D.J., et al., *Methotrexate elicits pro-respiratory and anti-growth effects by promoting AMPK signaling.* Scientific Reports, 2020. **10**(1): p. 1-9.
123. Corominas-Faja, B., et al., *Metabolomic fingerprint reveals that metformin impairs one-carbon metabolism in a manner similar to the antifolate class of chemotherapy drugs.* Aging (Albany NY), 2012. **4**(7): p. 480.
124. Kanarek, N., et al., *Histidine catabolism is a major determinant of methotrexate sensitivity.* Nature, 2018. **559**(7715): p. 632-636.
125. Borsi, J.D. and P.J. Moe, *Systemic clearance of methotrexate in the prognosis of acute lymphoblastic leukemia in children.* Cancer, 1987. **60**(12): p. 3020-3024.

126. Treon, S. and B. Chabner, *Concepts in use of high-dose methotrexate therapy.* Clinical chemistry, 1996. **42**(8): p. 1322-1329.
127. Skärby, T.C., et al., *High leucovorin doses during high-dose methotrexate treatment may reduce the cure rate in childhood acute lymphoblastic leukemia.* Leukemia, 2006. **20**(11): p. 1955-1962.
128. Sterba, J., et al., *Pretreatment plasma folate modulates the pharmacodynamic effect of high-dose methotrexate in children with acute lymphoblastic leukemia and non-Hodgkin lymphoma:"folate overrescue" concept revisited.* Clinical chemistry, 2006. **52**(4): p. 692-700.
129. Howard, S.C., et al., *Preventing and managing toxicities of high-dose methotrexate.* The oncologist, 2016. **21**(12): p. 1471.
130. Flombaum, C.D. and P.A. Meyers, *High-dose leucovorin as sole therapy for methotrexate toxicity.* Journal of clinical oncology, 1999. **17**(5): p. 1589-1589.
131. Takami, M., et al., *Severe complications after high-dose methotrexate treatment.* Acta Oncologica, 1995. **34**(5): p. 611-612.
132. Hoekstra, M., et al., *Factors associated with toxicity, final dose, and efficacy of methotrexate in patients with rheumatoid arthritis.* Annals of the Rheumatic Diseases, 2003. **62**(5): p. 423-426.
133. Nilsson, R., et al., *Metabolic enzyme expression highlights a key role for MTHFD2 and the mitochondrial folate pathway in cancer.* Nature Communications, 2014. **5**(1): p. 1-10.
134. Fabre, I., G. Fabre, and I.D. Goldman, *Polyglutamylation, an important element in methotrexate cytotoxicity and selectivity in tumor versus murine granulocytic progenitor cells in vitro.* Cancer research, 1984. **44**(8): p. 3190-3195.
135. Poser, R.G., F.M. Sirotnak, and P.L. Chello, *Differential synthesis of methotrexate polyglutamates in normal proliferative and neoplastic mouse tissues in vivo*. 1981, AACR.
136. Schrøder, H., *Methotrexate kinetics in myeloid bone marrow cells and peripheral neutrophils.* Cancer chemotherapy and pharmacology, 1987. **19**(1): p. 42-46.
137. Bosson, G., *Reduced folate carrier: biochemistry and molecular biology of the normal and methotrexate-resistant cell.* British journal of biomedical science, 2003. **60**(2): p. 117-129.
138. Barredo, J. and R.G. Moran, *Determinants of antifolate cytotoxicity: folylpolyglutamate synthetase activity during cellular proliferation and development.* Mol Pharmacol, 1992. **42**(4): p. 687-94.
139. Pizzorno, G., et al., *Impaired polyglutamylation of methotrexate as a cause of resistance in CCRF-CEM cells after short-term, high-dose treatment with this drug.* Cancer Research, 1988. **48**(8): p. 2149-2155.
140. Chabner, B.A. and T.G. Roberts, *Chemotherapy and the war on cancer.* Nature Reviews Cancer, 2005. **5**(1): p. 65-72.
141. Lin, J.T., et al., *Basis for natural resistance to methotrexate in human acute non-lymphocytic leukemia.* Leukemia research, 1991. **15**(12): p. 1191-1196.
142. de Jonge-Peeters, S.D., et al., *ABC transporter expression in hematopoietic stem cells and the role in AML drug resistance.* Critical reviews in oncology/hematology, 2007. **62**(3): p. 214-226.
143. De Grouw, E., et al., *Preferential expression of a high number of ATP binding cassette transporters in both normal and leukemic CD34+ CD38− cells.* Leukemia, 2006. **20**(4): p. 750-754.

144. Rots, M.G., et al., *Role of folylpolyglutamate synthetase and folylpolyglutamate hydrolase in methotrexate accumulation and polyglutamylation in childhood leukemia.* Blood, The Journal of the American Society of Hematology, 1999. **93**(5): p. 1677-1683.
145. Göker, E., et al., *Acute monocytic leukemia: A myeloid leukemia subset that may be sensitive to methotrexate.* Leukemia, 1995. **9**(2): p. 274.
146. Argiris, A., et al., *Increased methotrexate polyglutamylation in acute megakaryocytic leukemia (M7) compared to other subtypes of acute myelocytic leukemia.* Leukemia, 1997. **11**(6): p. 886-889.
147. Rots, M.G., et al., *A possible role for methotrexate in the treatment of childhood acute myeloid leukaemia, in particular for acute monocytic leukaemia.* Eur J Cancer, 2001. **37**(4): p. 492-8.
148. Sirotnak, F., et al., *A new analogue of 10-deazaaminopterin with markedly enhanced curative effects against human tumor xenografts in mice.* Cancer chemotherapy and pharmacology, 1998. **42**(4): p. 313-318.
149. Kinahan, C., et al., *The anti-tumor activity of pralatrexate (PDX) correlates with the expression of RFC and DHFR mRNA in preclinical models of multiple myeloma.* Oncotarget, 2020. **11**(18): p. 1576.
150. Ramirez, J., et al., *Pemetrexed acts as an antimyeloma agent by provoking cell cycle blockade and apoptosis.* Leukemia, 2007. **21**(4): p. 797-804.
151. Vazquez, A., P.M. Tedeschi, and J.R. Bertino, *Overexpression of the mitochondrial folate and glycine–serine pathway: a new determinant of methotrexate selectivity in tumors.* Cancer research, 2013. **73**(2): p. 478-482.
152. García-Cañaveras, J.C., et al., *SHMT inhibition is effective and synergizes with methotrexate in T-cell acute lymphoblastic leukemia.* Leukemia, 2020: p. 1-12.
153. Pikman, Y., et al., *Targeting serine hydroxymethyltransferases 1 and 2 for T-cell acute lymphoblastic leukemia therapy.* 2020.
154. Ducker, G.S., et al., *Human SHMT inhibitors reveal defective glycine import as a targetable metabolic vulnerability of diffuse large B-cell lymphoma.* Proceedings of the National Academy of Sciences, 2017. **114**(43): p. 11404-11409.
155. Scaletti, E., et al., *Structural basis of inhibition of the human serine hydroxymethyltransferase SHMT 2 by antifolate drugs.* FEBS letters, 2019. **593**(14): p. 1863-1873.
156. Pikman, Y., et al., *Targeting MTHFD2 in acute myeloid leukemia.* Journal of Experimental Medicine, 2016. **213**(7): p. 1285-1306.
157. Toyama, E.Q., et al., *AMP-activated protein kinase mediates mitochondrial fission in response to energy stress.* Science, 2016. **351**(6270): p. 275-281.
158. Voorde, J.V., et al., *Improving the metabolic fidelity of cancer models with a physiological cell culture medium.* Science advances, 2019. **5**(1): p. eaau7314.
159. O'Prey, J., et al., *Application of CRISPR/Cas9 to autophagy research.* Methods in enzymology, 2017. **588**: p. 79-108.
160. Meiser, J., et al., *Serine one-carbon catabolism with formate overflow.* Science Advances, 2016. **2**(10): p. e1601273.
161. Miller, P.H., et al., *Analysis of parameters that affect human hematopoietic cell outputs in mutant c-kit-immunodeficient mice.* Experimental hematology, 2017. **48**: p. 41-49.

162. Meiser, J., et al., *Serine one-carbon catabolism with formate overflow.* 2016.
163. Ducker, G.S., et al., *Human SHMT inhibitors reveal defective glycine import as a targetable metabolic vulnerability of diffuse large B-cell lymphoma.* 2017.
164. Ducker, G.S., et al., *Human SHMT inhibitors reveal defective glycine import as a targetable metabolic vulnerability of diffuse large B-cell lymphoma.* Proceedings of the National Academy of Sciences, 2017. **114**(43): p. 11404-11409.
165. Robert, G., et al., *Acadesine kills chronic myelogenous leukemia (CML) cells through PKC-dependent induction of autophagic cell death.* PloS one, 2009. **4**(11): p. e7889.
166. Herzig, S. and R.J. Shaw, *AMPK: guardian of metabolism and mitochondrial homeostasis.* Nature reviews Molecular cell biology, 2018. **19**(2): p. 121-135.
167. Faubert, B., et al., *AMPK is a negative regulator of the Warburg effect and suppresses tumor growth in vivo.* Cell metabolism, 2013. **17**(1): p. 113-124.
168. Buzzai, M., et al., *Systemic treatment with the antidiabetic drug metformin selectively impairs p53-deficient tumor cell growth.* Cancer research, 2007. **67**(14): p. 6745-6752.
169. Saito, Y., et al., *AMPK protects leukemia-initiating cells in myeloid leukemias from metabolic stress in the bone marrow.* Cell stem cell, 2015. **17**(5): p. 585-596.
170. Chen, K., et al., *Resolving the distinct stages in erythroid differentiation based on dynamic changes in membrane protein expression during erythropoiesis.* Proceedings of the National Academy of Sciences, 2009. **106**(41): p. 17413-17418.
171. Oburoglu, L., et al., *Glucose and glutamine metabolism regulate human hematopoietic stem cell lineage specification.* Cell stem cell, 2014. **15**(2): p. 169-184.
172. Pikman, Y., et al., *Targeting MTHFD2 in acute myeloid leukemia.* Journal of Experimental Medicine, 2016. **213**(7): p. 1285-1306.
173. Sabatini, D.M., *Twenty-five years of mTOR: Uncovering the link from nutrients to growth.* Proceedings of the National Academy of Sciences, 2017. **114**(45): p. 11818-11825.
174. Tsai, J.J., et al., *Nrf2 regulates haematopoietic stem cell function.* Nature cell biology, 2013. **15**(3): p. 309-316.
175. Cantó, C., et al., *Interdependence of AMPK and SIRT1 for metabolic adaptation to fasting and exercise in skeletal muscle.* Cell metabolism, 2010. **11**(3): p. 213-219.
176. Hung, C.-M., et al., *AMPK/ULK1-mediated phosphorylation of Parkin ACT domain mediates an early step in mitophagy.* Science Advances, 2021. **7**(15): p. eabg4544.
177. Warnes, G., *Flow cytometric assays for the study of autophagy.* Methods, 2015. **82**: p. 21-28.
178. Benischke, A.-S., et al., *Activation of mitophagy leads to decline in Mfn2 and loss of mitochondrial mass in Fuchs endothelial corneal dystrophy.* Scientific reports, 2017. **7**(1): p. 1-11.
179. Simpson, C.L., et al., *NIX initiates mitochondrial fragmentation via DRP1 to drive epidermal differentiation.* Cell reports, 2021. **34**(5): p. 108689.

180. Emmanuel, N., et al., *Purine nucleotide availability regulates mTORC1 activity through the Rheb GTPase*. Cell reports, 2017. **19**(13): p. 2665-2680.
181. Hoxhaj, G., et al., *The mTORC1 signaling network senses changes in cellular purine nucleotide levels*. Cell reports, 2017. **21**(5): p. 1331-1346.
182. Dembitz, V., et al., *The ribonucleoside AICAr induces differentiation of myeloid leukemia by activating the ATR/Chk1 via pyrimidine depletion*. Journal of Biological Chemistry, 2019. **294**(42): p. 15257-15270.
183. Nishida, Y., et al., *Discovery of Atg5/Atg7-independent alternative macroautophagy*. Nature, 2009. **461**(7264): p. 654-658.
184. Hennequart, M., et al., *The impact of physiological metabolite levels on serine uptake, synthesis and utilization in cancer cells*. Nature communications, 2021. **12**(1): p. 1-10.
185. Ma, E.H., et al., *Serine is an essential metabolite for effector T cell expansion*. Cell metabolism, 2017. **25**(2): p. 345-357.
186. García-Cañaveras, J.C., et al., *SHMT inhibition is effective and synergizes with methotrexate in T-cell acute lymphoblastic leukemia*. Leukemia, 2021. **35**(2): p. 377-388.
187. Klawitter, J., et al., *Time-dependent effects of imatinib in human leukaemia cells: a kinetic NMR-profiling study*. British journal of cancer, 2009. **100**(6): p. 923-931.
188. Flis, K., et al., *Chronic myeloid leukemia stem cells display alterations in expression of genes involved in oxidative phosphorylation*. Leukemia & lymphoma, 2012. **53**(12): p. 2474-2478.
189. Koschmieder, S., et al., *Inducible chronic phase of myeloid leukemia with expansion of hematopoietic stem cells in a transgenic model of BCR-ABL leukemogenesis*. Blood, 2005. **105**(1): p. 324-334.